DEVELOPING A FRAMEWORK FOR THE DESIGN OF THE MILLING AND ROUGHER CIRCUITS FOR A PLATINUM-BEARING UG2 ORE

JOHANNES JAKOBUS STEYN

Thesis Presented for the Degree of
DOCTOR OF PHILOSOPHY

Department of Chemical Engineering
UNIVERSITY OF CAPE TOWN

August 2012

SYNOPSIS

In the western limb of the Bushveld Igneous Complex, platinum is mined predominantly from two reefs – Merensky and UG2. Most of the platinum group minerals (PGM's) in Merensky ore are associated with base metal sulphides (BMS), and thus Merensky concentrators will usually resemble simple BMS circuits. However, the mineralogy of UG2 ore is more complicated, and thus UG2 circuits are also more complex. The UG2 reef is a chromitite layer in the critical zone of the Bushveld Igneous Complex, which results in high chromite content. Chromite causes significant complications in the downstream smelter process, and therefore chromite constraints are imposed on UG2 concentrators. A further aspect complicating the treatment of UG2 ore is that PGM's are not only associated with BMS, but ultra-fine PGM's are also locked in gangue minerals. This affects the milling and flotation characteristics of the circuits, as it is not possible to efficiently target the liberation and recovery of relatively large BMS and ultra-fine PGM's in the same circuit. As a result UG2 circuits have evolved to deal with these issues in a number of ways.

This thesis focuses on the design of milling and flotation circuits to optimise the recovery of coarse BMS (with associated PGM's) and ultra-fine PGM's contained in associated siliceous gangue minerals. In order to achieve this, UG2 circuits usually feature more than one milling and flotation stage. In the primary stage, a relatively coarse grind targets the liberation and recovery of BMS, while much finer grinds in subsequent milling stages target the liberation and recovery of PGM's locked in siliceous minerals. In recent years stirred mills have been incorporated into UG2 circuits for the liberation of fine PGM's locked in gangue. These mills grind exclusively via attrition type breakage, as opposed to the predominant impact breakage in a ball mill. The development of these multi-stage circuits to treat UG2 ore was based to a large extent on a qualitative evaluation of the ore and mineralogy, as well as by trial and error over many years of operation, rather than being built on a scientific foundation. Therefore, the aim of this project was to gain an understanding of the effect of breakage mechanism and circuit configuration on the floatability profile of a UG2 ore. This information would then be used to establish a formal design framework for the selection of mill type, and the number of milling and flotation stages to meet specified performance criteria. In order to achieve these goals, it was necessary to design a set of experiments that would investigate multiple mill-float circuits and various milling devices.

The experiments were conducted on a pilot scale with a ball mill, IsaMill and Stirred Media Detritor (SMD), together with Lonmin's flotation pilot plant. The ball mill represented a milling device in which impact breakage would predominate, using steel balls as a grinding media, whilst the IsaMill and SMD represented devices that grind exclusively via attrition, using inert grinding media. The mills and flotation cells were arranged into different mill-float configurations to test the effect of multiple milling and flotation stages on the PGM recovery of UG2 ore. The data was fitted to a kinetic model adapted from the literature to determine the floatability of the ore as a function of its treatment in the different circuits tested. Some new modelling methodologies were developed to incorporate disparate data sets into the same modelling framework.

An analysis of the performance of the different circuits showed that PGM recovery increased with an increase in the number of mill-float stages, while a single mill-float stage produced higher initial grades. On a size-by-size basis additional mill-float stages resulted in an increase in PGM recovery in all size classes, while no minimum size was detected for optimum flotation (the highest recoveries for all three circuits were achieved in the finest size fraction). A detailed analysis of the data and floatability profiles revealed the following:

(i) Multi-stage circuits minimise over-grinding, and this manifests as an improved recovery in the finest size fraction that was measured (-10μm).

(ii) Sub 10μm liberated PGM's displayed higher floatabilities than locked or partially liberated PGM's in coarser size fractions, resulting in the higher recoveries observed in this size fraction for all circuits.

(iii) Preferential liberation of PGM's was observed for this ore. This meant that stage-wise removal also favoured recovery in coarser sizes, since partially liberated PGM's were recovered before being liberated to a finer size fraction by additional milling.

(iv) Attrition breakage is more efficient than impact breakage at liberating valuables in the finest size fraction, but also more prone to over-grinding of liberated PGM-bearing BMS particles. Therefore circuits with attritioning devices are more likely to benefit from multiple mill-float stages.

(v) Impact breakage is more efficient at liberating particles from coarse size fractions – the host will usually be shattered and the valuable mineral liberated to a smaller size fraction.

(vi) In contrast, attrition breakage gradually chips away at the host particle, often achieving partial liberation of the valuable particle in a relatively coarse size fraction. Therefore, attrition breakage favours recovery in coarser sizes, as valuables are liberated in a coarser size fraction than with impact breakage. This does not indicate that attrition breakage is more efficient at liberating valuables from coarse sizes, as impact breakage will usually liberate more particles from coarse sizes, but these liberated particles are recovered in finer size fractions.

(vii) For UG2 ore, it was found that significantly higher PGE concentrate grades could be achieved with stirred mills. Results indicate that this was driven by the liberation of PGM's from BMS, since the recovery of fine, liberated PGM's would result in higher PGE grades than the recovery of PGM's associated with BMS.

From these observations and findings it was possible to construct a framework for the milling and rougher design of UG2 circuits. The information required for the design is a target size distribution, size and associations of the valuable minerals and the hardness and breakage characteristics of the ore. From this information the number and type of milling devices, as well as the number of flotation stages can be selected. The target grind for each stage is driven to a large extent by economic return-on-investment considerations, although the recovery-grind relationship of the ore can assist in making that decision. Although the work and design framework was established for UG2 ore, it can be used to design the main stream milling and rougher circuits for most ore types.

DECLARATION

I hereby certify that the work embodied in this thesis is the result of original research and has not been submitted for another degree at any other university or institution.

Johannes Jakobus Steyn
August 2012

PUBLICATIONS

Steyn, J., Knopjes, B., Goodall, C. and Harris, M.
Evaluating the effect of multiple grinding and flotation stages on flotation performance
Proceedings of the Centenary of Flotation Conference, Brisbane, Australia, 4-6 June, 2005

CONFERENCE PRESENTATIONS

Steyn, J., Harris, M., Knopjes, B. and Goodall, C.
Effect of grinding mechanism on the floatability of a UG2 platinum-bearing ore
Presented at the SAIMM Conference, Cape Town, 2009

ACKNOWLEDGEMENTS

I would like to thank the following people and institutions for their support and assistance during this project:

- Firstly my wonderful wife Sunette, for this thesis would not have been completed without her unwavering support, patience, encouragement and drive.
- My supervisor, Martin Harris, for his invaluable advice, guidance and support throughout the project.
- Lonmin Platinum, for sponsoring this project and making available the necessary resources and time to complete the work. In this regard I would like to acknowledge the support from all the managers I reported to during the project. Especially Bert Knopjes for initiating and driving the project in the early stages, and Selwyn Green for his assistance and support to finalise the thesis.
- All my colleagues at Lonmin Platinum and UCT for advice, assistance and encouragement over the years. In particular Dr Victor Ross, Dr Craig Goodall and Allen Hemphill who assisted greatly with proof reading.
- Finally, all my family and friends for their support and encouragement.

CONTENTS

LIST OF FIGURES

LIST OF TABLES

GLOSSARY

BMS

Base metal sulphides

Close Circuit Milling

A milling configuration where the coarse fraction of the classification circuit is returned to the mill

DMS

Dense medium separation

DPFC-Model

Distributed property floatability component model

EDX

Energy dispersive X-ray analysis

EFC-Model

Empirical floatability component model

Entrainment

The non-selective recovery of material to a flotation concentrate, primarily via the recovery of water

EPL

Eastern Platinum, a subsidiary of Lonmin Platinum

FCTR

Floatability characterisation test rig. A highly automated and mobile flotation pilot plant

Fractional Analysis

A method where a sample is screened into different size fractions and each fraction is assayed for metal or mineral content

HPGR

High pressure grinding roll

High Intensity Stirred Mill

Stirred mills characterised by a high energy input per unit area. These mills typically use inert grinding media such as ceramic beads or silica sand (also see IsaMill and SMD)

Hot Batch Flotation Test

A laboratory scale flotation test that is performed on a freshly taken sample of slurry from a plant or pilot plant process stream. Since the goal of such a test is to determine the flotation rate of the stream, no reagents is added.

Inert Circuits

For this project an inert circuit is defined as a mill-rougher configuration where the final mill in the circuit is a high intensity stirred mill using inert media

IsaMill

A horizontal high intensity stirred mill manufactured by Xstrata Technology (also see High Intensity Stirred Mill)

MF1

A mill and rougher configuration with one mill followed by a rougher stage

MF2

A mill and rougher configuration with two mills, each followed by a rougher stage

MF3

A mill and rougher configuration with three mills, each followed by a rougher stage

Open Circuit Milling

A milling configuration with no significant circulation stream that recycles back to the mill. Classification is either done in front of the mill, or as scalping after the mill. The scalping oversize stream is usually quite small, and therefore returned to the mill

PGE

Platinum group elements

PGM

Platinum group minerals

Preferential Breakage

A mechanism where some mineral is liberated at a faster rate than the rest of the rock. This typically results in an accumulation of this mineral in the finer sizes.

Regrind Mill

In the context of this project a regrind mill is defined as a mill in the main circuit (thus not in the cleaning circuit). A regrind mill will be fed by either the discharge of another mill or the tailings from a rougher bank.

Reverse Classification

Reverse classification occurs in a hydrocyclone when it is fed by minerals with significant densities differences. A cyclone classifies on mass, thus fine, heavy particles can report to the underflow forcing light, coarse particles to the overflow. This process is called reverse classification, and is especially detrimental if the valuable mineral is locked in the lighter minerals.

ROM Ball Mill

Run-of-mine ball mill. This is a mill that is fed by run-of-mine ore, but where the rock is not competent enough to warrant an autogenous or semi-autogenous mill. The ROM ball mill will typically have a relatively aggressive lifter profile, and the ball levels will be somewhere between a SAG mill and a traditional ball mill

ROM Ore

Run-of-mine ore

SEM

Scanning electron microscope

SMD

Stirred media detritor. A vertical high intensity stirred mill manufactured by Metso (also see High Intensity Stirred Mill)

Steel Circuits

For this project a steel circuit is defined as a mill-rougher configuration where the mill is a ball mill using steel media

Vacuum Densifier

A vacuum densifier is a hydrocyclone where the overflow discharges below the level of the spigot, thereby sucking a vacuum. The vacuum is controlled with a flapper valve below the spigot and another valve breaking the vacuum on the overflow. These are very efficient dewatering devices, and are used in the platinum industry before regrind mills.

NOMENCLATURE

Greek symbols

β	Froth stability parameter
δ	Froth drainage parameter
ε_g	Gas hold up in the froth
τ	Slurry retention time

Multiple Subscripts

ENT	Degree of entrainment or entrainability
ENT_i	Entrainability of particle class i
ENT_{size}	Entrainability of size class
k	Flotation rate constant
k_c	Flotation rate constant in the pulp zone
k_{cz}	Flotation rate constant in the collection zone
k_i	Flotation rate constant of floatability class i
k_{slow}	Flotation rate constant of slow floating material
k_{fast}	Flotation rate constant of fast floating material
K_{slow}	Approximate flotation rate constant for slow floating material in the circuit
K_{fast}	Approximate flotation rate constant for fast floating material in the circuit
$K_{i,size}$	Approximate flotation rate constant by size for floatability class i in the circuit
m	Mass
m_i	Mass of particle class i
mi,size	Mass of particle class i in each size fraction
$m_{fast,size}$	Mass of fast floating material in each size fraction
$m_{slow,size}$	Mass of slow floating material in each size fraction
p	Probability
p_f	Probability of flotation
p_c	Probability of particle–bubble collision
p_a	Probability of particle-bubble attachment
p_s	Probability that the particle-bubble combination will be stable enough to enter the concentrate

P	Floatability
P_i	Floatability of particle class i
$P_{i,size}$	Floatability by size for particle class i
$P_{fast,size}$	Floatability of fast floating particles in each size class
$P_{slow,size}$	Floatability of slow floating particles in each size class
Q	Volumetric flow rate
Q_{air}	Volumetric air flow rate into the cell
Q_{tails}	Volumetric flow rate of tails
Q_{conc}	Volumetric flow rate of concentrate
R	Recovery
R_∞	Mineral recovery at infinite time
R_c	Recovery in the pulp zone
R_f	Recovery in the froth zone
Rf,i	Froth recovery for particle class i
$R_{ent,i}$	Recovery by entrainment of size i
R_w	Water recovery
$R_{w,batch}$	Water recovery in a batch cell
V	Volume
V_{slurry}	Volume of slurry
V_f	Froth volume
x	Mass fraction
x_{slow}	Mass fraction of slow floating material
x_i	Mass fraction in floatability class i
$x_{fast,size}$	Mass fraction of fast floating material by size

Other

A	Flotation cell cross-sectional area
C	Amount of floatable material in the pulp at time t
Cf_i	Entrainment classification function for size i
d_{32}	Sauter mean diameter
d_i	Equivalent spherical bubble size
FRT	Froth residence time

S_b	bubble surface area flux 2.13
t	Time

LIST OF MINERALS AND ROCKS [1]

Anorthite

Anorthite is the calcium endmember of plagioclase feldspar. The formula of pure anorthite is $CaAl_2Si_2O_8$.

Basalt

Basalt is a common extrusive volcanic rock. By definition, basalt is defined as an aphanitic igneous rock that contains, by volume, less than 20% quartz and less than 10% feldspathoid and where at least 65% of the feldspar is in the form of plagioclase.

Braggite

Braggite is a sulphide mineral of platinum, palladium and nickel with chemical formula: (Pt, Pd, Ni)S.

Chalcopyrite

Chalcopyrite is a copper iron sulphide mineral. It has the chemical composition $CuFeS_2$.

Chlorite

The chlorites are a group of phyllosilicate minerals. Chlorites can be described by the following four endmembers based on their chemistry via substitution of the following four elements in the silicate lattice; Mg, Fe, Ni, and Mn: $(Mg_5Al)(AlSi_3)O_{10}(OH)_8$, $(Fe_5Al)(AlSi_3)O_{10}(OH)_8$, $(Ni_5Al)(AlSi_3)O_{10}(OH)_8$,$(Mn,Al)_6(Si,Al)_4O_{10}(OH)_8$

Chromite

Chromite is an iron chromium oxide: $FeCr_2O_4$. It is an oxide mineral belonging to the spinel group.

Chromitite

Chromitite is an igneous cumulate rock composed mostly of the mineral chromite.

[1] Mineral descriptions were obtained from the Wikipedia and Webmineral websites (en.wikipedia.org and webmineral.com)

Cooperite

Cooperite is a grey mineral consisting of platinum sulphide (PtS), generally in combinations with sulphides of other elements such as palladium and nickel (PdS and NiS). Its general formula is (Pt,Pd,Ni)S. It is a dimorph of braggite.

Feldspar

Feldspars ($KAlSi_3O_8$ – $NaAlSi_3O_8$ – $CaAl_2Si_2O_8$) are a group of rock-forming tectosilicate minerals which make up as much as 60% of the Earth's crust.

Feldspathoid

The feldspathoids are a group of tectosilicate minerals which resemble feldspars but have a different structure and much lower silica content.

Gabbro

Gabbro refers to a large group of dark, coarse-grained, intrusive mafic igneous rocks chemically equivalent to basalt.

Granite

Granite is a common and widely occurring type of intrusive, felsic, igneous rock. By definition, granite is an igneous rock with at least 20% quartz by volume.

Hypersthene

Hypersthene is a common rock-forming inosilicate mineral belonging to the group of orthorhombic pyroxenes. The chemical formula is $(Mg,Fe)SiO_3$.

K-feldspar

See Feldspar ($KAlSi_3O_8$)

Labradorite

Labradorite ($(Ca,Na)(Al,Si)_4O_8$), a feldspar mineral, is an intermediate to calcic member of the plagioclase series.

Laurite

Laurite is an opaque black, metallic ruthenium sulphide mineral with formula: RuS_2. It can contain osmium, rhodium, iridium, and iron substituting for the ruthenium.

Malanite

Malanite is an isometric-hexoctahedral mineral containing copper, iridium, platinum, and sulphur. The chemical formula for malanite is $Cu(Pt,Ir)_2S_4$.

Mica

The mica group of sheet silicate (phyllosilicate) minerals includes several closely related materials having highly perfect basal cleavage.

Millerite

Millerite is a nickel sulphide mineral, NiS.

Norite

Norite is a mafic intrusive igneous rock composed largely of the calcium-rich plagioclase labradorite and hypersthene with olivine.

Olivine

The mineral olivine is a magnesium iron silicate with the formula $(Mg,Fe)_2SiO_4$.

Orthopyroxene

Orthopyroxene is an orthorhombic member of the pyroxene group (see pyroxenes).

Pentlandite

Pentlandite is an iron-nickel sulphide, $(Fe,Ni)_9S_8$. Pentlandite usually has a Ni:Fe ratio of close to 1:1.

Phlogopite

Phlogopite is a yellow, greenish, or reddish-brown member of the mica family of phyllosilicates. It is also known as magnesium mica.

Plagioclase

Plagioclase is an important series of tectosilicate minerals within the feldspar family. Rather than referring to a particular mineral with a specific chemical composition, plagioclase is a solid solution series, more properly known as the plagioclase feldspar series.

Pyrite

The mineral pyrite, or iron pyrite, is an iron sulphide with the formula FeS_2. Pyrite is the most common of the sulphide minerals.

Pyroxenes

The pyroxenes are a group of important rock-forming inosilicate minerals found in many igneous and metamorphic rocks. They share a common structure consisting of single chains of silica tetrahedra and they crystallize in the monoclinic and orthorhombic systems. Pyroxenes have the general formula $XY(Si,Al)_2O_6$ (where X represents calcium, sodium, $iron^{+2}$ and magnesium and more rarely zinc, manganese and lithium. Y represents ions of smaller size, such as chromium, aluminium, $iron^{+3}$, magnesium, manganese, scandium, titanium, vanadium and even $iron^{+2}$).

Pyroxenite

Pyroxenite is an ultramafic igneous rock consisting essentially of minerals of the pyroxene group.

Pyrrhotite

Pyrrhotite is an unusual iron sulphide mineral with a variable iron content: $Fe_{(1-x)}S$ (x = 0 to 0.2).

Quartz

Quartz is the second most abundant mineral in Earth's continental crust, after feldspar. It is made up of a continuous framework of SiO_4 silicon–oxygen tetrahedra, with each oxygen atom being shared between two tetrahedra, giving an overall formula SiO_2.

Sulfarsenides

The sulfarsenide minerals are a subgroup of the sulphide minerals which include arsenic replacing sulphur as an anion in the formula.

Talc

Talc is a mineral composed of hydrated magnesium silicate with the chemical formula $H_2Mg_3(SiO_3)_4$ or $Mg_3Si_4O_{10}(OH)_2$.

CHAPTER 1
INTRODUCTION

In South Africa, platinum group elements (PGE's) are mined almost exclusively from the Bushveld Igneous Complex. Three main PGE reefs are found in the complex – Merensky, UG2 and Platreef. The Merensky reef has been exploited for more than 80 years. Mining of the UG2 reef started less than 40 years ago, but exploitation has accelerated to the point where this has now become the primary source of PGE production. Development of Platreef has only started relatively recently, although this is likely to be a source of growing importance in the future.

According to Bryson (2004), the high chromite content in UG2 ore causes considerable difficulty in the extraction of PGE's. At high concentrations the chromite spinel can accumulate in the furnace, and therefore chromite constraints are imposed on UG2 concentrators. Also, the mineralogical associations of PGE's in UG2 ore are significantly more complex than for Merensky ore. Platinum group minerals (PGM's) are not only associated with base metal sulphides (BMS), but individual platinum sulphide grains also occur in association with various gangue minerals. BMS liberate at grinds coarser than 30µm, while the individual PGM minerals only liberate below 10µm. Also, BMS flotation becomes problematic below 20µm, while PGM sulphides do not float well below 2 to 3µm. As a result, UG2 ore needs to be milled significantly finer than Merensky for efficient liberation and recovery of PGE's, at the risk of over-grinding BMS (with associated PGM's). Such fine grinds can also lead to higher chromite recoveries via entrainment.

In order to achieve good PGE recoveries under chromite constraints, UG2 circuits can be quite complex, with multiple milling and flotation stages and complex cleaning arrangements (Knights and Bryson, 2009 and Goodall, 1995). The most common configuration is the mill-float-mill-float circuit, also known as an MF2 circuit. This configuration consists of two full rougher stages, with a regrind mill between the two rougher banks. Such stage-wise removal of concentrate allows for relatively coarse BMS and fine platinum sulphide minerals to be targeted in separate circuits. In this way, over-grinding of valuable particles and chromite is minimised.

A variety of milling types and arrangements are used for the treatment of UG2 ore (Rule, 2008 and Goodall, 1995). The aim of the primary mill is to produce the coarsest size distribution that can be treated in a flotation circuit. Traditionally, the secondary milling set-up was a closed circuit ball mill, targeting a sufficiently fine grind for PGM liberation. However, recent developments in grinding and classification technology have broadened the options available for the processing of UG2 ore. For example, in the primary circuit, high pressure grinding rolls (HPGR's) provides an energy efficient alternative to rod mills and even Run-of-Mine (ROM) ball mills. In the secondary circuit, high intensity stirred mills and vacuum densifiers have been incorporated into the flow sheet. The densifiers allow for efficient liberation in an open circuit arrangement, while the stirred mills present a way to target fine particle liberation more efficiently. In general, the milling environment and breakage characteristics are important factors in presenting an optimum feed to flotation, and stirred mills provide improved control over these parameters (Pease *et al*, 2006). For example, grinding media size and composition can be used to affect the breakage characteristics, the mineral surface properties and the chemical environment of the flotation feed. For fine particle flotation these parameters can be controlled more efficiently in a stirred mill than in a ball mill.

Significant research has been conducted into the effect of the chemical environment in the mill on flotation performance, and the general consensus is that a more reducing milling environment is detrimental for flotation (Cullinan *et al*, 1999 and Johnson, 2002). The chemical environment affects the absorption of flotation chemicals to mineral surfaces. Furthermore, iron by-products from grinding media can bind to freshly liberated mineral surfaces, adversely affecting the recovery potential of some minerals. It is considered that the attritioning action in a stirred mill can significantly improve the surface of the mineral for flotation by removal of slimes coatings. Gangue slimes can coat fresh mineral surfaces, and this can be detrimental for fines flotation in particular (Grano *et al*, 1994; Pease *et al*, 2006). The breakage mechanism in the mill can also affect the relative size and degree of liberation of valuable particles, especially at very fine grind sizes. Fine particles are usually more difficult to recover by flotation, and thus are more likely to be adversely affected by slimes coatings or a reducing chemical environment. Therefore, the grinding environment and how these particles are presented to flotation can significantly affect the floatability of fine particles.

From the sections above, the design of UG2 circuits was driven to a large extent by a qualitative analysis of the mineralogy, as well as advances in technology. However, little formal research has been conducted on the optimum design and operating parameters for these circuits. Therefore, this project aims to investigate the effect of breakage mechanism and circuit configuration on the floatability profile of a UG2 ore, and from this to establish a framework for the design and equipment selection for UG2 ore in particular and complex ores in general.

Information was gathered by conducting pilot plant campaigns with a ball mill, IsaMill and stirred media detritor (SMD) in conjunction with a pilot-scale flotation circuit. The equipment was arranged into a single mill-float circuit (MF1), a two-stage circuit (mill-float-mill-float or MF2) and a three-stage circuit (mill-float-mill-float-mill-float or MF3). Overall recovery and grades, as well as size-by-size performance were evaluated for the different configurations. The primary flotation feeds were also subjected to mineralogical analysis. In order to evaluate the effect of different milling devices and circuit configurations on the behaviour of the ore, it was necessary to measure some properties of the ore. Size distribution and elemental analysis can be used to determine the high level response of the ore, but does not reveal information regarding the floatability profile. Mineralogical liberation data is a direct measure of ore properties that effect floatability, but it was not practical to do for every stream, and mineralogy does not provide quantitative floatability numbers. Therefore, in order to determine the floatability profile throughout the circuit, a kinetic model was fitted to the experimental data. In this model the floatability of the mineral is separated from froth recovery, entrainment and the hydrodynamic conditions in the cell. Due to the large number of parameters required for a robust description of the process, “hot” batch flotation tests (see glossary for description) were performed on selected streams. The kinetics of the batch flotation tests were linked to the model of the circuit to constrain the model fit and ensure that the model parameters were statistically robust. It was not possible to perform size analysis on the batch float concentrate samples owing to sample mass constraints for assay. As a result it was necessary to develop a procedure to link the unsized batch data with the size-by-size model of the circuit. Further, it was also necessary to develop a methodology to determine the contribution of entrainment in a batch flotation system.

From the floatability profile provided by the model, it was possible to evaluate the effect of the different mill types on floatability, with special attention to the breakage mechanism. The

flotation response for each size fraction in different circuits was also studied. This information was used to establish a rule-based framework for the design of the main stream milling and flotation circuits for UG2 ore. This framework could then be tested against current practices, in effect the accumulated knowledge acquired from forty years of industrial practice.

1.1 Expected outcome of this study

The primary objective of this study is to develop a conceptual methodology to determine the most efficient milling and rougher flotation design for PGE ores in particular, and complex ores in general. In order to achieve this objective, the study had to investigate the following two factors:

(i) The liberation and floatability profile in each size class being generated by different types of milling devices – in this case ball and stirred mills.
(ii) The effect of multiple milling and flotation stages on the recovery of PGE's in different size classes. This was linked to the floatability profiles being generated by the different milling devices.

1.2 Novelty

Although UG2 circuits have been designed successfully in the past, no formal design framework has been established in the literature. In particular, the role and application of new stirred milling technologies has yet to be clearly established. This project aims to establish such a framework by studying the milling environment and multiple mill-float stages.

The milling environment under which breakage occurs has been studied by various researchers in the past. Most of these studies have focussed on the chemical environment, and especially the negative impact of a reducing milling environment on flotation (Cullinan *et al*, 1999; Johnson, 2002). In addition, the coverage of mineral surfaces by either gangue or the by-products of grinding media, with specific attention to the effect this has on flotation has also been investigated. These factors will be expanded on in the Literature Review. However, there is little or no information reported in the literature on the effect of the breakage mechanism on the floatability distribution of the product particles. The kind of attrition

breakage that occurs in the energy-intensive environment of a stirred mill has the potential to present a different profile to flotation than a ball mill, where impact breakage dominates. The floatability profile generated by stirred mills will be compared to a ball mill on a size-by-size basis. Some basic mineralogy of the mill products will also be analysed to verify the conclusions from the floatability profiles.

Multiple milling and rougher flotation stages are common practice in the platinum industry. The conventional wisdom dictates that these circuits minimise over-grinding, which leads to improved rougher recoveries. Therefore, multiple grind-float circuits should improve mineral recovery in the finer size fractions. However, the effect of such circuits on other size fractions has not been examined to any great extent. It is plausible to suggest that if the floatability profile is affected by the breakage mechanism, or some other mechanism such as preferential breakage, that mineral recovery in coarser size fractions will also be affected by stage-wise flotation. Therefore, the impact of multi mill-float arrangements on mineral recovery will be investigated for fine, middling and coarse size fractions. Not only the recovery by size, but also the floatability profile and mineralogy of the flotation feeds will be studied to determine the behaviour of the mineral through the different flotation stages.

Throughout this study it is necessary to compare the floatability profiles of different milling devices and flotation configurations. In order to determine these floatability numbers, circuit results are fitted to a flotation model on a size basis, with floatability as one of the model parameters. Both the model and the procedure for fitting the data have been well established in the past (see Literature Review). A key step in the process is to generate batch flotation data on selected streams, and simultaneously fitting this batch data and the circuit data to a model. However, in this study the circuit data was generated on a size-by-size basis, while the batch flotation results were unsized. This creates difficulties when comparing the sized floatabilities of the circuit with the unsized rate constants generated for the batch data. A procedure was developed to incorporate this disparate data set into a model, in effect creating a link between sized and unsized modelling parameters. In addition, it was necessary to develop a new method to deal with entrainment by size in a batch flotation cell, using a single parameter decay function.

CHAPTER 2
LITERATURE REVIEW

The Literature Review is divided into three sections – the first being a summary of platinum-bearing South African ores in general, and the UG2 ore used in this study specifically. Next is an evaluation of circuit considerations when treating UG2 ore. Included in this section is a review of the effect of milling conditions and breakage mechanism, as well as the effect of chemistry and particle size on flotation performance. Finally, previous work on batch and continuous circuit modelling is reviewed, along with a discussion of the de-coupled kinetic model used in this study.

2.1 The Bushveld Igneous Complex

Platinum grains were discovered in South Africa near Naboomspruit (Hochreiter *et al*, 1985). Dr. Hans Merensky devised a prospecting plan, which led to the discovery of a platinum-rich reef on the farm Maandagshoek in 1924. The reef stretched over a continuous horizon, traceable for kilometre upon kilometre on strike. The reef was part of the Bushveld Igneous Complex, which contains the world's richest source of platinum group metals, chrome and vanadium, as well as vast copper, nickel, iron and tin deposits.

Platinum group elements (PGE's) are mined from three areas in the complex: the Western, Eastern and Northern Limbs. Two reefs are mined from the Western and Eastern Limbs, known as the Merensky and UG2 reefs. The well-developed infrastructure close to the Western Limb has seen this area undergo considerable exploitation. However, in recent years major developments have taken place along the Eastern Limb. The Northern Limb contains Platreef, which has seen some development in recent years, and is likely to be of growing importance in the future.

The Complex is clearly stratified into distinct layers, shown in Figure 2.1 (Hochreiter *et al*, 1985):

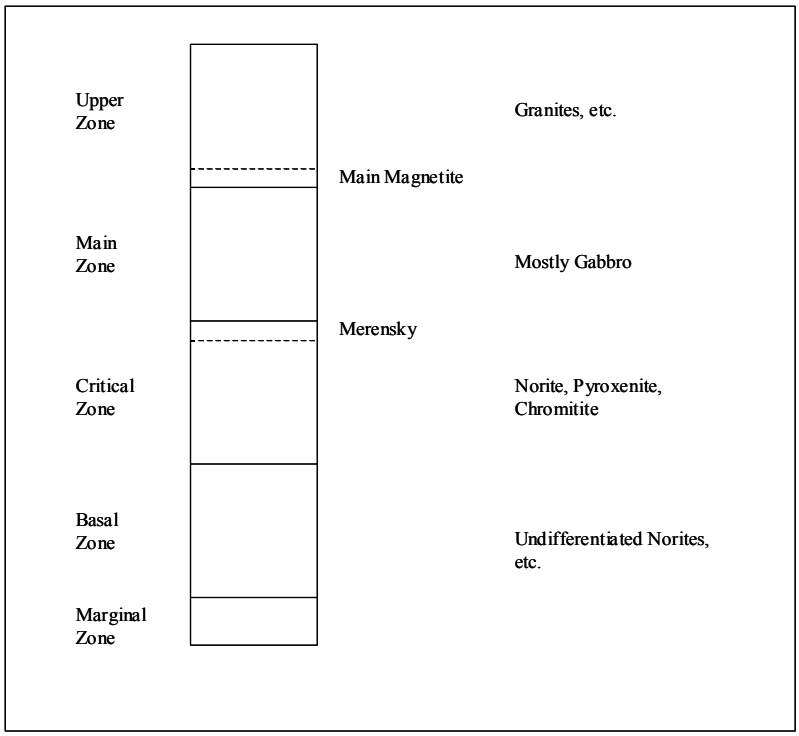

Figure 2.1 Stratigraphy of the Bushveld Complex

Most of the PGE's in the Bushveld Igneous Complex are found within the Critical Zone. Figure 2.2 shows that this zone is divided according to chromitite layers into the Upper Group, Middle Group and Lower Group (Hochreiter *et al*, 1985):

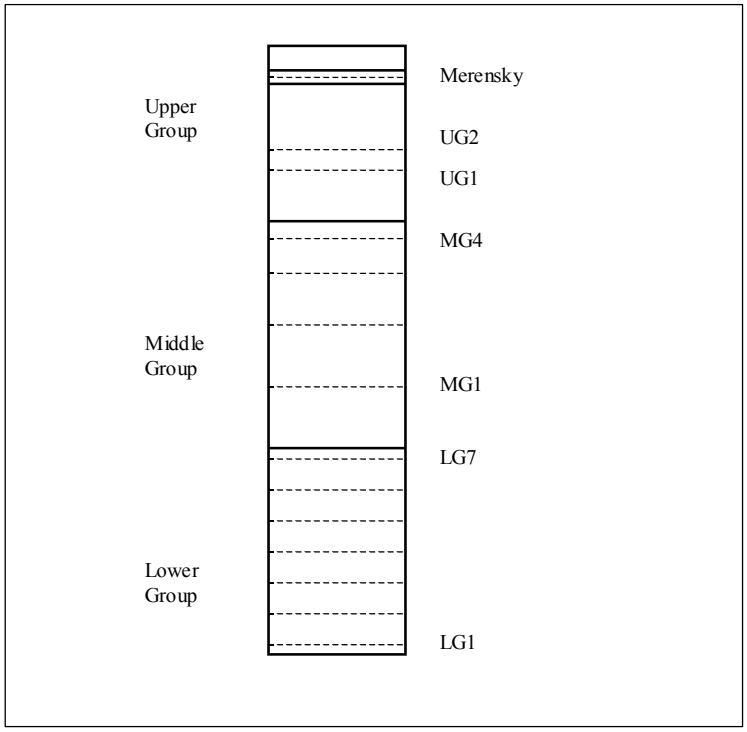

Figure 2.2 Stratigraphy of the Critical Zone

The Critical Zone hosts the two main reefs from which PGE's are mined – the Merensky reef and the UG2 reef. The Merensky Reef is situated near the top of the Critical Zone, where the chromitite layer is poorly developed. As the name suggests, the UG2 reef is the second chromitite layer in the Upper Group. According to Liddell *et al* (1985), the UG2 reef lies approximately 150 meters below the Merensky reef in the Western Bushveld complex, and is between 15 and 255 centimetres thick. The chromitite content in the UG2 reef ranges between 30% and 90%, with the balance consisting mainly of silicate gangue (typically orthopyroxene and plagioclase). Base metal sulphides (BMS) occur in trace quantities, typically on chromitite grain boundaries. Chalcopyrite, pyrrhotite and pentlandite are the main BMS occurring in the UG2 reef. PGE's in the UG2 reef are associated with these BMS, or occur as single grains. These single grain platinum group minerals (PGM's) occur on the boundary between chromitite grains, between chromite and silica gangue grains or locked in various gangue minerals.

The relative quantities of the BMS and PGM's vary significantly along the UG2 reef. BMS grain sizes typically have a mean of around 30μm, while PGE grain sizes are significantly smaller (usually less than 10μm). The PGE grade in UG2 ore ranges between 5ppm and 10ppm, with an average grade of 7ppm.

2.2 Processing of UG2 ore

2.2.1 Smelter Chrome constraints

According to Liddell *et al* (1985), processing of UG2 run-of-mine (ROM) ore follows the route of milling and flotation in a concentrator, smelting of the concentrate and subsequent refining stages. Conventional smelting of PGM concentrate is done at temperatures of between 1400^{o}C and 1700^{o}C (Knights and Bryson, 2009). However, at these temperatures chromite can build up in the furnace, as the chrome spinel is stable up to 2000^{o}C (Wesseldijk *et al*, 1999). This can result in extended downtime, either because of breakdowns or frequent furnace relining (Bryson, 2004 and Lanham, 2008). Therefore, the smelter imposes chromite constraints on UG2 concentrate; typically less than 3% (Corrans *et al*, 1982). Much of the concentrator design and operating philosophy for UG2 ore is driven by this concentrate chromite constraint.

2.2.2 Concentrator circuits

The beneficiation of PGE's from UG2 ore is complicated by the mineralogy, which necessitates the recovery of ultra-fine PGM's, as well as much coarser BMS with associated PGE's. The need to maximise PGE recovery, combined with the chromite constraint imposed by the smelter, result in complicated UG2 concentrator circuits. In particular, the need to suppress chromite recovery poses unique challenges to process engineers. The main mechanism for chromite recovery to flotation concentrate is entrainment, although it has been found that chromite can be recovered via true flotation under certain conditions, most likely as a result of association with altered silicates such as talc, which are naturally floatable (Ekmekçi *et al*, 2003). Entrainment arises from fine particles that are recovered with water to flotation concentrate (Savassi *et al*, 1998), and is mainly dependent on particle size and density. For UG2 ore, Robertson (2002) found that entrainment usually becomes insignificant above 38μm. This relatively fine particle size where entrainment becomes insignificant is related to the high density of gangue particles in UG2 ore. Therefore, concentrators treating UG2 ore would try to minimise the generation of fine chromite in order to minimise entrainment. This poses challenges, as the relatively fine BMS and ultra-fine PGE's grain sizes require fine grinding for liberation and efficient recovery.

In order to optimise PGE recovery under chromite constraints, most UG2 plants incorporate the stage-wise removal of valuable minerals. The most common configuration is a mill-float-mill-float circuit, also known as the MF2 configuration (Knights and Bryson, 2009). It consists of a primary and secondary mill, with two full flotation circuits. The advantage of such a configuration is that it allows for the removal of relatively coarse valuable particles in the primary stage, before over-grinding of chromite or valuable minerals can occur. Only in the secondary stage is a fine grind achieved, targeting fine, non-liberated PGM's. The typical primary grind is usually between 35% and 40% passing 75μm, while the secondary mill would target a grind of between 75% and 80% passing 75μm (Goodall, 1995 and Valenta, 2007).

In the rougher circuit, UG2 concentrators have been influenced by the development of large-size flotation cells. Yianatos *et al* (2006) reported that mechanical cell size has increased ten fold since the 1980's. The increase in cell size looks set to continue, with the recent

installation of flotation cells in excess of 300m^3 at Copperton Concentrator, Utah (FLSmidth, 2010). This increase in size has offered the opportunity to reduce the cost of building and operating a concentrator, as well as to increase the throughput a single concentrator stream can achieve. However, there are indications that larger flotation cells are less efficient than smaller cells. Deglon *et al* (2000) summarised the hydrodynamics and gas dispersion of a wide variety of cells in the South African platinum industry. It was found that larger cells typically operate at lower power densities and that the efficiency of mixing and solid suspension also decreases with increasing cell size.

Several cleaning configurations are used when treating UG2 ore. Most circuits have long residence times to maximise the recovery of slow floating PGM, as well as multiple cleaning stages to reduce chromite to acceptable levels (Goodall, 1995). More than one final concentrate stream is often produced; a high-grade concentrate targeting fast floating minerals and a low-grade concentrate where slow floating material is recovered. The application of column cells has been tested in UG2 cleaning circuits, but with limited success, and the use of these cells is not common at present (Lanham, 2008). However, improvements in column design and operation has revived interest in this technology, so this may change in the future.

2.2.3 Comminution

2.2.3.1 Pre-concentration

The chromite in UG2 ore has a much higher density than the siliceous rock that contains the PGM's. This presents an opportunity to reject waste material by using dense-medium separation (DMS) before the primary milling stage. The use of DMS is largely dependent on ore characteristics such as waste-to-reef ratio and the PGE content in the DMS waste stream. Where applicable, DMS can allow for wide-reef mechanised mining. The drawbacks are the loss of values to the DMS waste stream, as well as an increase in the chromite grade reporting to the primary mill[2] (Merkle and McKenzie, 2002 and Bryson, 2004). Typically, the relatively high PGM losses to the waste stream have prevented concentrators from adopting the DMS technology. The exceptions are where DMS was developed to allow for wide-reef

[2] This is a standard outcome of DMS on UG2 ore – where the light fraction is removed (silicates in this case), it will lead to a higher grade of the heavier material (chromite for UG2 ore)

mining. Optical sorting has also been investigated, but since a significant amount of PGM's are found on the reef-gangue interface, PGM losses in the discard stream have generally been found to be unacceptably high.

2.2.3.2 Reverse classification

In the past, comminution of UG2 ore was done in closed milling circuits with a hydrocyclone providing the separation (Knights and Bryson, 2009). However, hydrocyclones separate based upon size and density, and thus the density difference between chromite and the siliceous matrix minerals results in inefficient classification. Fine, dense chromite can report to the cyclone underflow at the expense of coarser silica minerals. The disadvantage is twofold: Chromite cycles through the milling circuit more times than other minerals, wasting energy in over-grinding mostly barren chromite. Secondly, valuable minerals associated with coarse siliceous minerals are displaced to the overflow, resulting in poor liberation and ultimately in PGE recovery losses (Becker *et al*, 2008).

In order to minimise reverse classification, the recent trend is to remove the hydrocyclone (Knights and Bryson, 2009). The primary mill is then operated either in open circuit or in close circuit with a scalping screen. Such circuits tend to produce a coarser overall grind, although the grind of siliceous minerals would usually be finer than when in closed circuit, resulting in better liberation of valuable minerals.

Owing to the finer grind in the secondary circuit, reverse classification is more pronounced. Several techniques have been employed to operate the secondary mills in open circuit, thus minimising reverse classification. Nel *et al* (2005) report that significant improvements were made at Impala's UG2 plant by converting the secondary mill from closed to open circuit. The open circuit classification was achieved with a two-stage cyclone configuration[3]. The observed improvement in performance was attributed to the coarser chromite and finer siliceous mineral grind that was achieved. Knights and Bryson (2009) reported that the improved dewatering efficiency of vacuum hydrocyclones ensured a high density feed to the secondary mill, which allowed the mill to run in open circuit with a single stage cyclone.

[3] Feed to the milling circuit is first processed in a cyclone. The overflow of this cyclone is treated in a second cyclone - both underflows are routed to the mill and the overflow of the second cyclone combines with mill product as flotation feed

Another alternative to the conventional hydrocyclone is the three-product cyclone, currently in development (Mainza *et al*, 2006, Becker *et al*, 2008 and Bryson, 2004). In addition to the usual underflow and overflow streams, this cyclone also produces a middling stream that usually contains the troublesome fine chromite and coarse siliceous fractions. This stream can then be treated separately to ensure optimum performance, and allows for the mill to operate in closed circuit while minimising reverse classification.

2.2.3.3 Milling circuits

According to Goodall (1995), typical primary milling circuits in older UG2 plants would include a crusher plant followed by a rod mill and/or ball mill. However, due to economic considerations newer plants employ Run-of-Mine (ROM) mills. These would include ball mills, semi-autogenous (SAG) mills and, less often, fully autogenous (FAG) mills (Rule, 2008). More recently, the high-pressure grinding roll (HPGR) technology has reached the stage where it provides another alternative in the primary comminution circuit. According to Apling and Bwalya (1997), use of an HPGR can result in enhanced levels of liberation at a coarser grind. In addition, significant energy savings can be achieved through the use of the HPGR. In view of the global rise in energy costs, it is envisaged that HPGR installations will become more prominent in the future, especially in applications with harder ore types, such as ore from the Platreef. The first HPGR application on UG2 ore was installed at Northam Platinum in 2008 (Rule, 2008).

In the past, ball mills have been used almost exclusively in the secondary milling of UG2 ore. However, recently IsaMills have been incorporated into the secondary milling circuit to produce better liberation of valuable minerals (Rule, 2008). The IsaMill is a horizontal stirred mill, with a high energy density and fine, inert grinding media. This allows for the efficient liberation of fine, valuable particles (Pease *et al*, 2006). Because of the high energy density, care must be taken not to over-grind chromite. In addition, chromite can build up in the IsaMill, causing losses in efficiency and even unplanned stoppages. Rule (2008) showed that the current solution to these issues is to separate a chromite rich stream that bypasses the IsaMill.

Stirred mills have also been included in UG2 cleaning circuits. According to Rule (2008), the use of fine grinding in the cleaning circuit has major benefits; the inert grinding environment,

high intensity attritioning and better liberation lead to improved recovery and grade. However, there is currently very little information to quantify the contribution of these factors to the performance of this technology.

2.2.3.4 Milling environment

Extensive work has been done on examining the interactions between grinding media and sulphide minerals (i.e. Iwasaki *et al*, 1983; Yelloji Rao and Natarajan, 1989; Johnson, 2002; Greet, 2008). These studies all indicate that a galvanic couple exists between sulphide minerals and steel grinding media. This increases the corrosion rate of the grinding media, and the corrosion products can affect the floatability of sulphide minerals by precipitation on the surface. According to Cullinan *et al* (1999) and Johnson (2002), the corrosion products include iron hydroxide species like $Fe(OH)_3$, FeOOH, Fe_2O_3 and Fe_3O_4. Their work investigated the difference in flotation response when using forged steel balls as opposed to high-chrome steel balls, and the results suggest that the iron debris from the more reducing forged steel environment have a significant adverse effect on flotation performance. Grano *et al* (1994) and Pease *et al* (2006) found that this effect is most pronounced on fine size fractions (Figure 2.3)[4]:

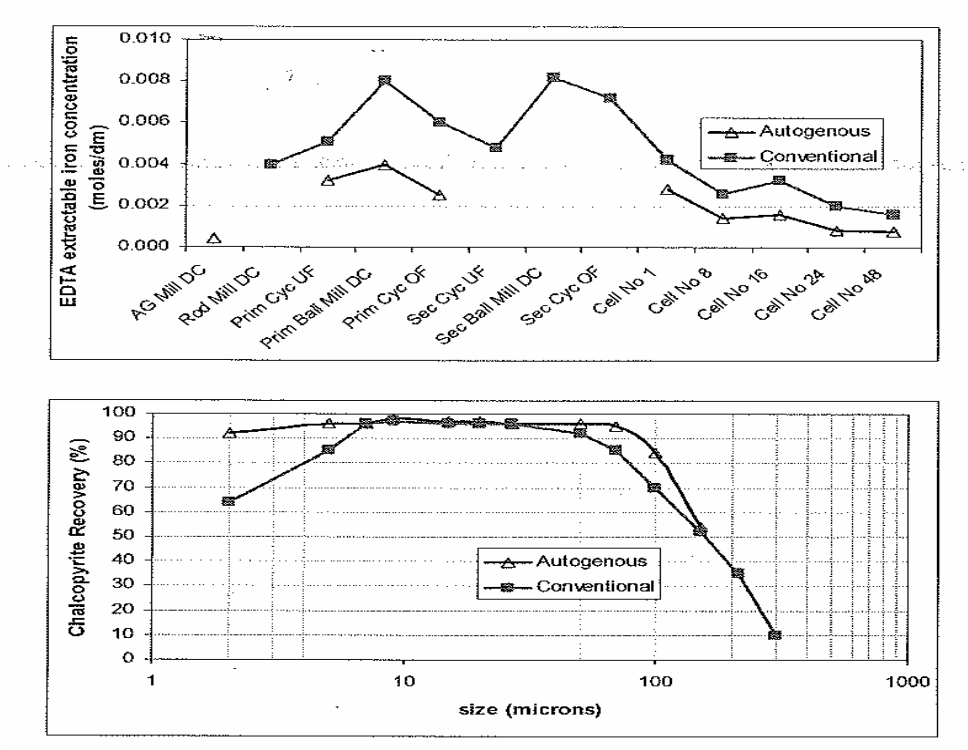

Figure 2.3 Effect of grinding media on recovery in different size classes

[4] Conventional as referred to in Figure 2.3 means milling using steel balls

Greet (2008) examined the effect on UG2 ore, and it was concluded that changing from forged steel to high-chrome steel media had a positive impact on PGM, copper and nickel metallurgical performance. This improvement was attributed to a shift in the Eh to more oxidising conditions, increasing the level of oxygen in the pulp and reducing the amount of extractable iron in solution. An optimum chrome content level was found in the grinding media, and it was speculated that more inert media types could have a deleterious effect on flotation, as the chemical environment may become too oxidising and depress platinum bearing sulphides.

2.2.3.5 Breakage characteristics

According to Hogg (1999), the principle modes of particle breakage can be classified as massive fracture (impact breakage) and attrition. Impact breakage occurs when the overall stress acting on a particle exceeds some critical value, and results in disintegration of the particle into a large number of fragments, all significantly smaller than the parent. Many researchers have measured this minimum energy for different particle types and sizes (i.e. Austin, 2002, Kapur *et al*, 1997, Tavares and King, 1998 and Vogel and Peukert, 2004). When the energy of an impact event is below the threshold for impact breakage, attrition of particles can occur. Attrition is associated with smaller applied stresses for which the critical value is only exceeded locally, i.e. at the edges (Hogg, 1999). In this mode, the original particle retains its identity but experiences a slow, continuous loss of mass. At the same time, there is a continuous production of fragments much smaller than the parent.

According to Austin (2002), particles of a given size generally have a range of strengths, thus an impact event may break some particles and not others. However, it was found that smaller particles require higher specific impact energy to produce the same degree of breakage as larger particles. That is, a smaller particle may require less force to break, but more stress is required and therefore it is more competent. Also, the statistical probability of an impact event occurring is directly related to particle size. This leads to the observation by Hogg (1999) that attrition processes become more prominent at finer sizes.

Powell *et al* (2008) hypothesized that comminution is a generic process of ore breakage in a range of modes, which can be modelled as a fundamental process. According to this model,

different equipment types impart this fundamental range of comminution processes in different ratios and intensities. Typical inputs would be particle and grinding media properties, probability of interaction between classes, mode of breakage (impact, abrasion or attrition) etc. This suggests that a ball mill would typically break particles via both impact and attrition, with the proportion of each mode being determined by factors such as ball and particle size, ball load, etc. The small media found in a stirred mill prevents impact breakage, as a single impact event would typically not carry enough energy to break a particle. However, the large number of impact events, combined with the high energy density found within these mills would result in a high level of attrition grinding.

The effect of the breakage mechanism on liberation characteristics is not well understood. Wills and Atkinson (1993) commented that most development in comminution has ignored the fact that the aim is to not merely to reduce particle size, but to liberate minerals from each other. It was also observed that when excess strain is placed upon the rock matrix, cracks appear spontaneously, move very fast and tend to ignore grain boundaries. These are the conditions prevalent in most comminution devices in the platinum industry, with the exception of the HPGR. As a result liberation of minerals is often not very selective, and probably results in significant over-grinding to achieve the desired level of liberation.

2.2.4 Flotation

2.2.4.1 Chemistry

The flotation performance of UG2 ore varies significantly from site to site. Even samples from the same area often display different kinetics (Corrans *et al*, 1982). Despite these differences, the flotation recipe for UG2 ore is similar at most sites. It was developed from a classical base metal sulphide flotation recipe, even though the BMS grades are relatively low (Valenta, 2007). Copper sulphate is usually added as activator, and thiol collectors such as xanthates are used as collectors. Natural floatable gangue such as talc is often present, and is depressed using either guar or a carboxyl-methyl cellulose depressant (CMC). Various types of frothers are used in UG2 circuits, and the balance between frother and depressant is critical in controlling PGM and chromite grades.

As was described earlier, much of UG2 flotation is focussed on reducing the chromite grade in final concentrate. Valenta (2007) found that increasing solids percentage and frother resulted in an increase in solids recovery due to entrainment. However, the increase was non-selective, and resulted in an increase in both solids and PGM recovery. An increase in depressant addition resulted in a decrease in solids recovery, without affecting PGM recovery. However, chromite grade did increase at higher depressant dosages, as floatable siliceous material is depressed over the non-floatable chromite, resulting in an increase in the relative concentration of chromite.

2.2.4.2 Effect of particle size on flotation

It has long been understood that particle size is an important parameter in the flotation process. Gaudin *et al* (1931) reported that an optimum size range exists for maximum mineral recovery, and that this size range is mineral dependent. Since then a lot of research has been conducted on the subject, with similar conclusions (i.e. Schubert and Bischofberger, 1978; Trahar, 1981; Feng and Aldrich, 1999). Of particular interest is the article by Schubert and Bischofberger (1978), who found that different turbulent conditions are needed to float fine and coarse particles, and that the simultaneous optimisation of the recovery of these particles in the same flotation cell is not possible. These findings are extremely relevant for UG2 ore, where valuable minerals occur over a wide size range from relatively coarse to ultra-fine. Therefore, most of UG2 circuit design has focussed on recovering both coarse BMS and fine PGM sulphide particles.

Trahar (1981) examined the effect of particle size on flotation recovery by analysing the following expression:

$$p_f \propto p_c . p_a . p_s \qquad (2.1)$$

where:

p_f = probability of flotation

p_c = probability of collision

p_a = probability of attachment

p_s = probability that the particle-bubble combination will be stable enough

to enter the concentrate

The probability of collision is related to physical variables such as particle and bubble diameters, densities, velocity etc. As particle size decreases the statistical probability of a collision with a bubble also decreases. It was found that the probability of adherence was inversely related to particle size, due to a combination of the contact time between particle and bubble and induction time (time taken for thinning and rupture of the water film between particle and bubble). The probability p_s is directly related to the strength of adhesion between the particle and bubble, which is directly related to contact angle and inversely related to particle size. To summarize, the decreased recovery from true flotation observed in fine size fractions are related to the following:

(a) Decreased probability of collision, because of the size of the bubbles and particles.
(b) Decreased probability of particle attachment, because of the relatively long induction time versus contact time of fine particles.
(c) Increased probability of detachment, because of smaller contact angle observed for fine particles.

Trahar (1981) also noted that entrainment is a major contributor to the recovery of fine particles, and that this can play a significant role in the behaviour of fine particles in flotation.

Another mechanism that can adversely affect fines flotation is the milling environment that was discussed in Section 2.2.3.4 (also see Figure 2.3). Surface coatings of valuable minerals by hydrophilic species will reduce flotation recovery in all size fractions, but especially for fine particles. The reason surface coatings affect fine particles more than coarse articles is probably due to their relative surface area – a lesser degree of coating is necessary to render fine particles hydrophilic. However, Pease *et al* (2006) found that fine particles (-10μm) respond well to flotation under the correct conditions. It was observed that liberation is the dominant driver in the recovery of even fine particles, and once fine particles are liberated they can be efficiently recovered by the selection of appropriate flotation conditions.

2.3 Flotation modelling

2.3.1 Modelling of a batch flotation system

As discussed by Arbiter and Harris (1962), it is widely accepted that the flotation response of floatable material in a batch system can be well described by the following equation:

$$\frac{dC}{dt} = -kC \qquad (2.2)$$

where:

t = time

C = the amount of floatable material in the pulp at time t

k = overall flotation rate constant

Integrating Equation (2.2) yields:

$$\ln \frac{C(t)}{C(0)} = -kt \qquad (2.3)$$

Recovery (R) can be expressed as follows:

$$R = \frac{C(t)}{C(0)} \qquad (2.4)$$

Substituting (2.4) into (2.3) becomes:

$$R = 1 - e^{-kt} \qquad (2.5)$$

Since it has been observed that mineral recovery in batch tests seldom reaches 100%, equation (2.5) is generally used in the following form:

$$R = R_{\infty}(1 - e^{-kt}) \qquad (2.6)$$

where R_{∞} is the mineral recovery at infinite time.

However, flotation is a selective process with material being recovered at different rates. Therefore, a single rate constant cannot account for the response of an ore comprising particles with a wide range of both size and liberation characteristics. Klimpel (1980) suggested a variation on Equation 2.6 with the rate constant describing a distribution:

$$R = R_{\infty}\left(1 - \frac{1}{kt}\left(1 - e^{-kt}\right)\right) \qquad (2.7)$$

However, the model proposed by Kelsall (1961) is the most practical when used in association with two floatability classes:

$$R = x_{slow}(1 - e^{-k_{slow}t}) + (1 - x_{slow})(1 - e^{-k_{fast}t}) \qquad (2.8)$$

where:

x_{slow} = fraction of material classified as slow floating

k_{slow} = rate constant of slow floating material

k_{fast} = rate constant of fast floating material

It is important to note that batch flotation tests are usually carried out at very shallow froth depths. Therefore, the rate constants shown in Equations 2.6, 2.7 and 2.8 relate mainly to the pulp performance (Mathe *et al*, 2000).

2.3.2 Modelling of a continuous flotation system

In a continuous flotation cell, Arbiter and Harris (1962) have shown that mineral recovery is given by the following equation:

$$R = \frac{k\tau}{k\tau + 1} \qquad (2.9)$$

where:

τ = slurry retention time

With τ being defined as:

$$\tau = \frac{V_{slurry}}{Q_{tails}} \qquad (2.10)$$

where:

V_{slurry} = volume of slurry

Q_{tails} = volumetric flow rate of tails

Equation 2.9 assumes first order kinetics and no overloading of bubbles. The rate constant in the equation is a combined rate from both the pulp and the froth phases. Various models have been derived from Equation (2.9), using a combined rate constant for the froth and pulp phases (Mankosa and Yoon, 1993; Loveday and Raghubir, 1995 and King, 1978). However, mineral recovery in a flotation cell is driven by a number of dependent and independent factors in the pulp and froth phase. Therefore, Finch and Dobby (1990) proposed a model that decouples the effects in the froth and pulp phases. The system can be visualised in the following probability network (Figure 2.4):

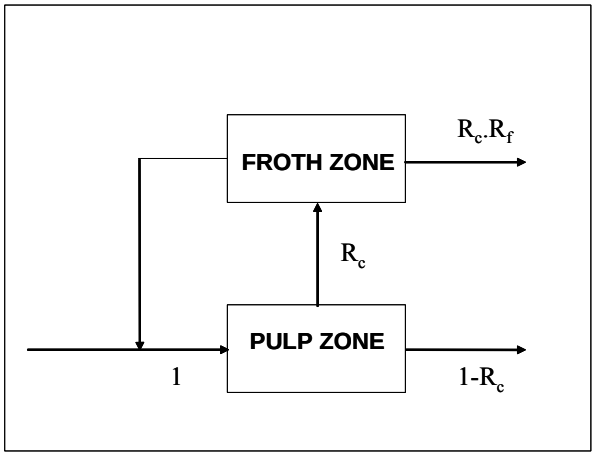

Figure 2.4 Probability network for decoupled flotation cell

where:

R_c = Recovery in the pulp zone
R_f = Recovery in the froth zone

Based on this probability network, the overall recovery can be calculated as the following:

$$R = \frac{R_c R_f}{R_c R_f + (1 - R_c)} \qquad (2.11)$$

For completely mixed conditions in the pulp, substitution of Equation 2.9 for R_c yields:

$$R = \frac{k_c \tau_c R_f}{1 + k_c \tau_c R_f} \qquad (2.12)$$

The flotation rate constant in the pulp is a function of particle variables such as particle size, degree of liberation and surface chemistry, as well as the hydrodynamics of the flotation cell. Gorain *et al* (1998a) proposed the following equation, separating particle and hydrodynamic variables:

$$k = PS_b \qquad (2.13)$$

where
P = floatability parameter
S_b = bubble surface area flux

Substitution of Equation (2.13) into Equation (2.12) yields the following equation for mineral recovery:

$$R = \frac{PS_b R_f \tau}{1 + PS_b R_f \tau} \qquad (2.14)$$

The parameters S_b, R_f and P will now be discussed in more detail, as well as a methodology to include entrainment in the equation.

2.3.2.1 Bubble surface area flux (S_b)

The bubble surface area flux (S_b) arose from the need to separate the flotation rate constant into contributions from cell hydrodynamics and particles. Gorain *et al* (1995a, 1995b and 1996) investigated the effect of impeller type, impeller speed and air flow rate on hydrodynamic variables such as bubble size, gas hold-up and superficial gas velocity. When metallurgical performance was expressed in terms of a flotation rate constant, it was found that neither bubble size, nor gas hold-up, nor superficial gas velocity could be related to the flotation rate individually. However, when these hydrodynamic variables were combined into the bubble surface area flux, a linear relationship was observed with the flotation rate constant. The bubble surface area flux is calculated from the hydrodynamic parameters in the following way:

$$S_b = \frac{6J_g}{d_{32}} \qquad (2.15)$$

where:

J_g = superficial gas velocity

d_{32} = Sauter mean diameter

The Sauter mean diameter is defined as follows:

$$d_{32} = \frac{\sum_{i=1}^{n} d_i^3}{\sum_{i=1}^{n} d_i^2} \qquad (2.16)$$

where:

d_i = equivalent spherical bubble size

n = sample size

It was found that the relationship between S_b and the rate constant also holds for individual size fractions, and that the relationship is independent of the type of impeller used. This suggests that S_b is a good measure of the hydrodynamic conditions within a flotation cell (Gorain, 1997). In a subsequent study Gorain (1998b) found that the k-S_b relationship is linear at shallow froth depths, but non-linear at deeper froths. This implies that froth recovery is playing an important role in the flotation kinetics, and further proof of the need to isolate froth recovery from the overall flotation rate constant.

In order to calculate S_b, it is necessary to determine the bubble size as well as the superficial gas velocity. Schwarz and Alexander (2006) reviewed the current methodologies used to determine these parameters. Bubble size can be measured by using the UCT bubble size analyser (Tucker *et al*, 1994). The analyser consists of a sampling system and an optical/electronic detector system. Incoming bubbles are cleaned of attached particles by the sampler before entering a capillary, where bubbles are deformed into cylinder shape. Sensors measure the length of the bubbles, and a Sauter mean bubble size is calculated. More recently, McGill University has developed another sensor to determine bubble size (Chen *et al*, 2001). Bubbles from the pulp phase are introduced into a viewing chamber, where photographs are obtained. The bubble size distribution can then be determined from image analysis techniques.

The general definition of J_g is:

$$J_g = \frac{Q_{air}}{A} \qquad (2.17)$$

where:

Q_{air} = volumetric air flow rate into the cell

A = cell cross-sectional area

Gorain *et al* (1996) used a J_g probe to measure the superficial gas velocity. The probe is based upon the rate of displacement of water from a tube by air rising from the flotation cell, after correcting for pressure differences between the points of sampling and water displacement.

2.3.2.2 Froth recovery (R_f)

Determining froth recovery is particularly problematic, mainly because of difficulty in measuring the material entering the froth phase, as well as the processes occurring within the forth phase such as bubble coalescence and particle dropback. Various researchers have devised methods to directly measure froth recovery. These methods usually involve controlled laboratory conditions, and/or specialised, sensitive equipment, which limit their use in a plant environment. However, these are valuable methodologies for researching froth recovery. Falutsu and Dobby (1989) and Contini *et al* (1988) investigated forth recovery in a modified column cell. Both found that froth recovery was inversely related to particle size, dependent on froth bias velocity and not strongly related to froth height. Vera (1995) used Contini's approach, and found that under certain conditions froth recovery is strongly dependent on froth height. Ross (1988) devised a froth-sampling lance, which collected froth to a sealed container at a particular forth height. This method can provide excellent measurements of the froth, but can be difficult to operate. Another problem is that it cannot distinguish between the contribution of floatable and entrained material in the froth.

Several indirect measurements of froth recovery have been proposed, in which froth performance is evaluated in terms of a froth recovery factor (R_f). Finch and Dobby (1990) described R_f as follows:

$$R_f = \frac{k}{k_{cz}} \qquad (2.18)$$

where

k_{cz} = collection zone flotation rate constant

Laplante *et al* (1983a and 1983b) have shown that the overall flotation rate constant decreases with an increase in froth depth, an observation that was confirmed by Mular and Musara (1991). When transformed to froth recovery, the relationship between froth depth and the overall rate constant can be used to isolate the effects of various flotation variables on froth performance. However, the relationship between froth recovery and froth depth cannot be used to determine the dominant processes within the froth or to develop a scale-up model for the froth phase.

A mechanistic froth recovery model should include froth sub-processes such as bubble coalescence, particle detachment and dropback of detached particles, as well as physical properties such as particle size and density. However, most of the froth sub-processes cannot be measured directly. The alternative is a mathematical model which uses meaningful numbers. Gorain *et al* (1998a) suggested the following model, after showing a relationship exists between froth recovery and froth residence time (FRT):

$$R_f = e^{-\beta.FRT} \qquad (2.19)$$

where:

β = a derived froth stability parameter

FRT is calculated from the following equation:

$$FRT = \frac{V_f(1-\varepsilon_g)}{Q_{conc}} \qquad (2.20)$$

where:

V_f = froth volume

Q_{conc} = concentrate flow rate

ε_g = gas hold up in the froth

2.3.2.3 Floatability (P)

Floatability describes the propensity of the mineral to form a stable attachment to a bubble (Harris, 1998). This value is influenced by the properties of the mineral particle, such as size, degree of liberation, hydrophobicity etc. The property is not amenable to any direct measurement procedure, and therefore flotation plants are often designed and operated based on lumped kinetic parameters, such as the rate constant from Equation 2.9. This parameter can be determined when the influence of the froth phase is minimised, for example the shallow froths found in a batch flotation cell. However, for simulation purposes it is usually necessary to separate the contribution of cell environment, entrainment and the froth phase

from the mineral floatability. Runge *et al* (1997) and Harris (1998) have adopted this approach to extract floatability parameters from batch data for plant simulations. This methodology will be explored in Section 2.3.2.5.

2.3.2.4 Entrainment

Particles can be recovered in a flotation cell by two distinct mechanisms. True flotation represents valuable minerals that attach to bubbles as a result of their surface properties. This mechanism represents the majority of particles recovered to flotation concentrate (Savassi *et al*, 1998). However, the separation efficiency between valuable particles and gangue depends to a large extend on the degree of entrainment of gangue particles.

Entrainment arises from fine particles that settle slowly enough to become part of the fluid phase. Since water is invariably recovered as a result of the bubble swarm rising through the pulp (Savassi *et al*, 1998), these suspended particles are recovered with the water and represent entrained material. It is a non-species specific mechanism that depends only on the size and density of the particle and the water recovery to flotation concentrate.

Johnson (1972) found that gangue recovery was directly proportional to water recovery, and proposed the following equation for recovery as a result of entrainment.

$$R_{ent,i} = Cf_i R_w \qquad (2.21)$$

where:

$R_{ent,i}$ = recovery by entrainment of size i

Cf_i = classification function for size i

R_w = water recovery

The classification function Cf_i can also be expressed as the degree of entrainment or the entrainability (ENT_i) of the ore in particle class i, and can be defined as follows:

$$ENT_i = \frac{\text{mass of entrained particles in class i reporting to concentrate}}{\text{mass of water reporting to concentrate}} \qquad (2.22)$$

The degree of entrainment shows an inverse relationship with particle size and density, since light particles are more likely to be suspended in the water, and large particles are more likely to drain back to the froth. Savassi (1998) showed that recovery via true flotation (Equation 2.14) and entrainment (Equations 2.21 and 2.22) can be combined into a single equation for a grouped class of particles with similar set of properties (particle class i):

$$R_i = \frac{P_i S_b \tau R_{f,i}(1-R_w) + R_w ENT_i}{(1+P_i S_b \tau R_{f,i})(1-R_w) + R_w ENT_i} \qquad (2.23)$$

The overall recovery can then be expressed as follows:

$$R = \sum_{i=1}^{n} m_i R_i \qquad (2.24)$$

where:

m_i = mass of particle class i in feed

n = number of particle classes

The contribution by true flotation can be seen by replacing $ENT_i = 0$ into Equation 2.23, which then reduces to Equation 2.14. The contribution by entrainment alone can be calculated by substituting $P_i = 0$ into Equation 2.23:

$$R_i = \frac{ENT_i R_w}{1 - R_w + ENT_i R_w} \qquad (2.25)$$

Savassi *et al* (1998) proposed the following empirical equation to calculate the degree of entrainment from particle size:

$$ENT_i = \frac{2}{e^{2.292\left(\frac{dp_i}{ENT_{20}}\right)^{adj}} + e^{-2.292\left(\frac{dp_i}{ENT_{20}}\right)^{adj}}} \qquad (2.26)$$

$$adj = 1 + \frac{\ln(\delta)}{e^{\frac{dp_i}{ENT_{20}}}} \qquad (2.27)$$

where:

ENT_{20} = particle size at which $ENT_i = 20\%$

δ = froth drainage parameter

According to Harris *et al* (2002), ENT represents an entrainability curve for the ore, a property that is comparable to floatability. The parameters E_{20} and δ are analogues of the properties P and R_f from Equation 2.14.

Robertson (2002) has shown that a non-floatable tracer, such as MnO_2, could be used to measure entrainability. His work confirmed that entrainability is largely size and density dependent, and that entrainability for UG2 ore becomes insignificant at particle sizes coarser than 38μm.

2.3.2.5 Determining floatability distribution

The kinetic response of a flotation feed is often used as a proxy for the floatability of the minerals in the feed. A problem arises because such lumped kinetic numbers do not separate the effect of the flotation cell, froth recovery and entrainment, and cannot be used to simulate the effect of these parameters independently. Therefore, a need exits to determine floatability independently of the cell, froth performance and degree of entrainment. According to Harris *et al* (2002), two approaches can be used to determine floatability:

A distributed property floatability component model (DPFC-Model)
An empirical floatability component model (EFC-Model)

In the DPFC-Model, the feed is divided into classes based on measurable physical properties. The flotation recovery of each class is then used to determine the floatability of that class. According to Harris *et al* (2002), several physical properties have been investigated to characterise the floatability classes. These include size distribution, mineral association, liberation and chemical surface coverage. Although size alone is usually inadequate, defining floatability according to liberation by size and/or surface coverage will likely become important in the future. However, at the present time mineralogical analysis is costly, the

mineralogy may not adequately describe floatability and the error in both mineralogical measurement and the model parameters can be relatively large. The same issues are also valid for models based upon chemical surface coverage. Therefore, the EFC-Model provides a more robust, cost-effective alternative to determine floatability.

The EFC-Model approach is based upon work done by Imaizumi and Inoue (1965), where the mass of particles in each stream is divided into different floatability components, each with a mean flotation rate constant. Lynch *et al* (1981) defined a floatability component as a set of particles that displays similar flotation kinetics under fixed operating and chemical environments. In this approach, it is assumed that floatability values are conserved through the flotation circuit, as long as no regrinding, chemical addition or oxidation occurs. Therefore, the EFC-Model approach attempts to determine the floatability distribution of the feed into a flotation circuit, and calculates the distribution in the rest of the circuit. Because of the lack of a measurable property to approximate floatability, the floatability distribution is derived by fitting a floatability-based model to a circuit that is assumed to be in steady state and with a constant feed. However, as the cells in the circuit would not be expected to operate under the same conditions, this would significantly affect the accuracy of floatability numbers. As a result, a de-coupled model such as Equation 2.23 is often used to separate the cell hydrodynamics, froth characteristics and entrainment from floatability.

This methodology requires a relatively large number of parameters, especially as it is usually necessary to divide the feed into at least three size classes. Batch flotation tests on selected streams in the circuit can add additional constraints that would allow for a robust solution to the model. These batch flotation tests are performed “hot” on samples taken from the circuit, without changing the pulp chemistry. A robust floatability distribution can be obtained by simultaneously fitting the batch tests and circuit results by using standard sum-of-error-squared minimisation techniques (Runge *et al*, 1997).

Harris *et al* (2002) concluded that the EFC-Model approach represents a highly flexible method for deriving the floatability distribution. The method has been applied to a wide range of ore types, in pilot plant and full-scale operations and over a wide size range and operating conditions. However, grade prediction with the EFC-Model approach is often not as robust, since errors in any of the component models will propagate in the grade prediction. For

reasonable gangue prediction, it is very important to develop the model by size, and to explicitly include entrainment in the model.

2.4 Summary of Literature Review

2.4.1 Processing of UG2 ore

In the Bushveld Igneous Complex, PGE's are mined mainly from the Merensky and UG2 reefs. The complex mineralogy of PGE's in the UG2 reef, combined with high chromitite contents, has necessitated the need for complex concentrator circuits. The key factors to consider when treating UG2 ore can be summarised as follows:

(a) Some PGE's are associated with BMS, which have an average grain size of around 30μm. A significant amount of research have shown that an optimum size range exists for efficient flotation, and therefore it is important not to over-grind these BMS particles

(b) Significant amounts of PGM's occur on the grain boundaries of other minerals, or are locked in gangue minerals. Since these minerals are very small (<10μm), fine grinding is necessary for liberation.

(c) Chrome can cause difficulty in the downstream processing of UG2 ore, and therefore concentrate chrome grades are usually constrained. In flotation, chromite is recovered almost exclusively via entrainment, which favours small particles. Therefore, a coarser grind would also benefit the suppression of chromite recovery.

In order to produce the coarsest possible concentrate for the BMS and chromite minerals, while still liberating fine PGM's, most UG2 concentrators utilise stage-wise removal of concentrate. The most popular configuration is the MF2 circuit, where a coarse concentrate is produced in the primary stage, while liberation and recovery of fine PGM's are targeted in the secondary stage. Since milling of UG2 ore is conducted in two stages, it is possible to exercise a lot more control over the grinding environment than in a single stage. The focus of the primary comminution stage is to reduce particle size for effective material transport. In a

ROM type UG2 mill this would entail large steel balls, which does not allow for much control of the grinding environment. However, material transport is not an issue in the secondary milling stage, and thus the focus can be placed on liberation of fine particles and the environment under which such liberation occurs. Traditionally this was done by using smaller steel balls with a higher chrome content, which would ensure a finer grind and more oxidising environment. However, high intensity stirred mills allow for the use of ultra-fine, inert grinding media in the secondary milling stage. These mills grind exclusively through attrition, and are much more efficient at liberating fine particles. Although the effect of the inert grinding environment has been investigated extensively in the past, not much research has been done on the effect of the breakage mechanism on floatability.

Since the aim of this thesis is to develop a framework for the design of the main milling and rougher circuits, it was necessary to study the effect of different milling environments and breakage mechanisms on the floatability of UG2 ore. When to present the liberated material to flotation, as well as the number of flotation stages will also be investigated. Data was generated on a pilot scale by arranging flotation cells, ball mills and stirred mills into different circuit configurations. Since it is not possible to measure floatability directly, the results were fitted to a flotation model. The floatability distributions derived from the model were then used to evaluate the effect of breakage mechanism, as well as the different circuit configurations.

2.4.2 Modelling

The EFC-Model approach was followed to determine the floatability distribution generated by the different mills. The advantage of this approach is that particle floatability is separated from the effects of the froth phase, entrainment and the hydrodynamics of the cell. The general form of the model is shown in Equation 2.23. A summary of the different modelling parameters, as well as how each was handled in this project is presented in the section that follows:

S_b

S_b, or bubble surface area flux, represents the hydrodynamics of the cell in the flotation model. S_b is calculated from the superficial gas velocity (J_g) and the mean bubble size. For

this project, J_g was calculated from Equation 2.17, using measured values for the volume of air into the cell and the cross-sectional area. The bubble size was determined using a UCT bubble sizer.

R_f

R_f, or the froth recovery, was determined from Equation 2.19. The froth residence time could be calculated for each cell, and the β parameter was model fitted.

ENT

ENT, or entrainability, is a classification function that is defined as the mass of entrained particles relative to the mass of water recovered. ENT is inversely related to particle size, and thus a single parameter exponential decay function was used to fit ENT for each size fraction. For the batch flotation results, a methodology had to be developed to incorporate the effect of entrainment into the batch flotation model.

R_w

R_w is the water recovery, which was measured for each flotation cell in the circuit.

P_i and m_i

P_i and m_i represent the floatability and floatability mass fraction for size class i. For the circuit, these values were determined by fitting data to Equation 2.23 for different size classes. In order to achieve a robust model fit, batch flotation tests were performed on selected streams, and the results fitted to Equation 2.8. However, due to constraints on the amount of concentrate that could be produced by the batch cell, the concentrates were not analysed by size class. This posed a challenge when reconciling the batch data with the circuit data, as the unsized fast and slow floating fractions for the batch tests would not necessarily reconcile with the sized fractions for the circuit. Therefore, it was necessary to develop a methodology that would allow for the reconciliation of sized and unsized floatability fractions.

To summarise, circuit and batch flotation data were fitted simultaneously to the model. S_b values for each cell were measured, R_f was determined by fitting the β parameter, ENT for each size class was determined from a single-parameter exponential decay function and R_w was measured. A methodology had to be developed to reconcile the floatability fractions of the unsized batch data with the sized circuit results. Finally, a methodology had to be developed to incorporate entrainment into the batch flotation model.

2.5 Hypotheses

The milling action, size of grinding media and chemical environment under which grinding occurs can all impact on mineral floatability. The coarse grinding media in a ball mill liberates valuable particles via impact breakage and attrition grinding, while the fine grinding media in a stirred mill will grind exclusively via attrition grinding. Therefore these mills will generate different floatability profiles, which lead to the following hypothesis:

Grinding mechanism on coarse particles:

Hogg (1999) found that impact breakage typically results in the disintegration of a particle into a large number of fragments, all significantly smaller than the parent. Therefore, it is hypothesised that the impact breakage in a ball mill will generate liberated and partially liberated material in medium to small size fractions, as coarse particles are broken apart. The ball mill should also be more efficient at the size reduction of coarse particles.

Hogg (1999) also reported that during attrition breakage the parent particle experiences a slow, continuous loss of mass while retaining its identity. Therefore the attrition grinding in a stirred mill should result in an increase in degree of liberation of coarse particles, as gangue is removed gradually. Since some of this material would have relatively small floatable surfaces, the average floatability in the parent size class should also be lower than produced by a ball mill. Thus, a stirred mill would increase the amount of floatable material in coarse fractions, but it would not be as efficient at liberating valuables from these sizes into finer size classes.

Grinding mechanism on fine particles:

It is hypothesised that a combination of media size and milling action should result in attritioning being more efficient than impact breakage at liberating particles from finer size fractions. This is because small particles require higher specific impact energies to produce the same degree of breakage as larger particles. Therefore grinding at fine sizes relies more on small, localised breakage events than massive fracture by impact. In addition, the statistical probability of an impact event occurring is directly related to particle size. Therefore, smaller media will have a better chance of interacting with a mineral particle, and small grinding media is also more likely to grind via attritioning. As a result, the over-grinding of fine, liberated particles is also more likely where attrition type grinding becomes predominant.

Grinding mechanism and gangue recovery

An inert environment and attrition grinding should also have an effect on PGM grade. Besides the floatability and recovery of PGM particles, the grade is also affected by the recovery of non-valuable gangue minerals and BMS. The non-valuable gangue is recovered predominantly via entrainment, although a significant portion can be recovered by flotation (Wiese *et al*, 2010). BMS is highly floatable, and although not classified as gangue, will nonetheless lower the PGM grade.

Since the attrition grinding action is constantly chipping off fine gangue from larger particles, the amount of floatable and non-floatable gangue in the fine size fractions would be expected to increase. Thus, it would be expected that more depressant would be required to achieve the same grade as for a feed produced by a ball mill. Attritioning would also remove fine gangue from floatable PGM minerals, which would be expected to increase the rate of recovery of PGM minerals relative to the gangue minerals.

It is therefore hypothesised that stirred mills would result in less association between PGM's and gangue. If possible to depress the gangue liberated from PGM-containing host particles, as well as the gangue removed from floatable surfaces, stirred mills would generate higher PGM grades. Therefore, in stirred mills floatable gangue is more likely to be over-milled or

depressed, while non-floatable gangue is less likely to be entrained via the brittle froths that result from higher depressant dosages.

Surface cleaning and chemical environment in the mill

The literature review suggests that the chemical environment in the mill and the surface cleaning effects of attritioning can significantly impact on particle floatability. These effects appear to be more pronounced in finer size classes. As a result, it should be possible to examine the effect of breakage mechanism on coarse sizes, while in the fine sizes it may be problematic to decouple the effect of the breakage mechanism from surface cleaning and the chemical environment.

Circuit Configuration

The different mills will each present a different floatability distribution to flotation. The work of Trahar (1981) and others has shown that an optimum size range exists for flotation, which is different for different minerals. However, Pease *et al* (2006) have shown that liberation is more important than the optimum flotation size for minerals that liberate below this size. In essence, a liberated particle, even if it is ultra-fine (sub 10μm) will typically have a higher floatability than a non-liberated particle in the optimum size range.

Therefore, it is hypothesised that a rougher regrind configuration has the potential for improved flotation recovery of valuable minerals, as the stage-wise recovery of valuables will minimise over-grinding while allowing for the liberation of fine particles. This effect is amplified by the use of stirred mills, as attrition grinding would be more likely to over-grind fine, valuable particles.

In the case of UG2 ore, PGE's occur across a wide size range, either associated with relatively coarse BMS or as single grain PGM's in the -10μm size fraction. Thus, UG2 ore should be ideally suited for rougher regrind circuits, as liberation of fine PGM particles can result in over-grinding of BMS. Stage-wise removal of floatable material will minimise over-grinding, while still allowing for liberating of PGM's.

Design Framework

It is hypothesised that the research into breakage mechanism and circuit configuration would guide the development of a design framework for the milling and rougher circuits of an UG2 ore.

CHAPTER 3
EXPERIMENTAL PROCEDURE

3.1 Introduction

Two pilot plant campaigns were conducted to investigate the effect of grinding mechanism, as well as multi-stage milling and flotation on floatability. All procedures, material, equipment and configurations will be discussed in this chapter.

In the first campaign, three mills were used to allow the configuration of three different circuits. Overall mill power and flotation residence time were kept constant between the circuits, allowing the focus to be on the effect of circuit configuration and grinding mechanism, rather than size distribution and flotation efficiency. For the second campaign, the milling power and flotation residence times were intentionally varied to evaluate circuit configuration and breakage mechanism at different size distributions. This was done by using only two mills and half the number of flotation cells as the first campaign.

3.2 First campaign

3.2.1 Ore

UG2 ore from Lonmin Platinum's Eastern Platinum (EPL) mine was used for the test work. A 30 ton sample was collected from #3 Shaft at EPL, and sent to Mintek for crushing, blending and bagging.

Ore was crushed with a jaw crusher, followed by a cone crusher in close circuit with a 6mm screen. The product was sun dried before being bagged using a rotary splitter. PGM, Cr_2O_3 and density analysis were conducted on the ore. Note that all PGM analysis in this thesis was conducted by fire assay at Mintek for combined platinum, palladium, rhodium and gold (ISO 17025 / ASD-MET-FA002). This is typically referred to as a 4E PGM analysis (4 elements). The ore characteristics are shown in Table 3.1:

Table 3.1 Ore Characteristics

PGM Grade (g/ton)	3.80
Cr_2O_3 Grade (%)	29.51
Specific Gravity	3.85

3.2.2 Pilot plant equipment

Milling

Three milling devices were used. Mill specifications are shown in Table 3.2:

Table 3.2 Milling specifications

	Primary Mill	**Secondary Mill**	**Tertiary Mill**
Device	Ball Mill	Stirred Media Detritor	IsaMill
Mill Type	Horizontal Ball Mill	Vertical Stirred Mill	Horizontal Stirred Mill
Mill Size (dm^3)	1500	1000	100
Motor (kW)	11.0	18.5	55.0
Discharge	Grate	Screen	Separator
Grinding Media	Steel Balls	Silica Sand	Ceramic Balls
Media Size (mm)	40 – 70	2 – 4	2

Flotation

The Floatability Characterization Test Rig (FCTR) at Lonmin Platinum was used for flotation test work. The FCTR was originally developed within the AMIRA P9 Project[5] in partnership with EIMCO Process Equipment Company (now FLSmidth). It is a highly instrumented flotation pilot plant with automatic sampling facilities on all streams (Rahal *et al*, 2000). Twelve 150-litre FCTR rougher cells were used, each with a 2.5kW motor. Air addition was controlled with an air rotameter.

[5] Information on the P9 Project can be found at the project web site: http://www.p9project.com

3.2.3 Circuit configuration

The equipment was arranged into circuits with one (MF1), two (MF2) and three (MF3) milling and flotation stages. Milling and flotation operating parameters were kept constant for each configuration as far as possible, in terms of overall size distribution, reagent addition, air addition and pulp densities. Therefore, it was considered that differences in performance could primarily be related to changes in the circuit configuration. Note that although the overall size distribution was kept constant (as far as possible), it does not imply that the mineral distribution by size would also be similar for the different circuits. In fact, it would be expected that stage-wise removal of PGM's should result in a coarser PGM profile. The three circuits are shown in Figures 3.1 to 3.3

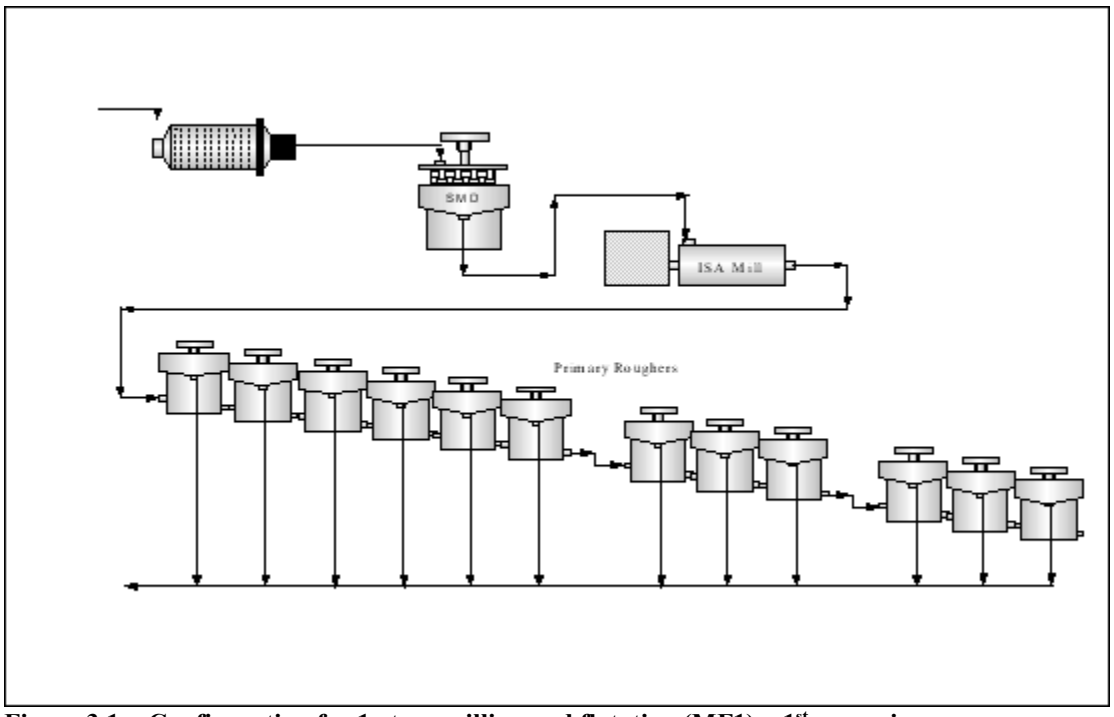

Figure 3.1 Configuration for 1-stage milling and flotation (MF1) – 1st campaign

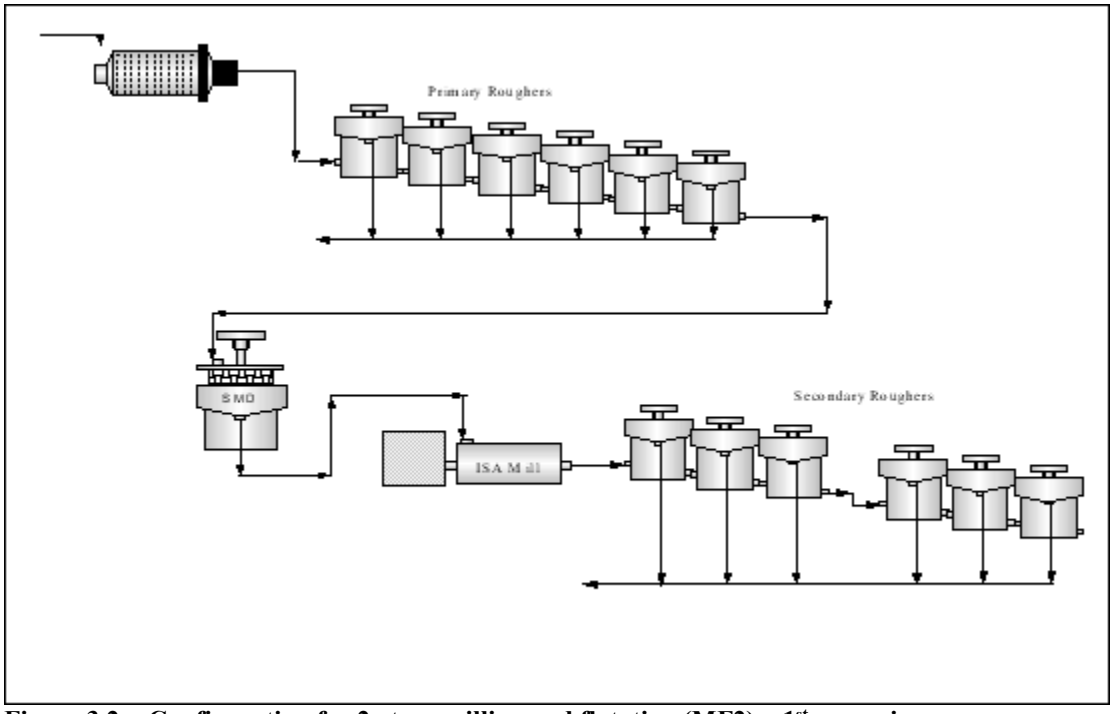

Figure 3.2 Configuration for 2-stage milling and flotation (MF2) – 1st campaign

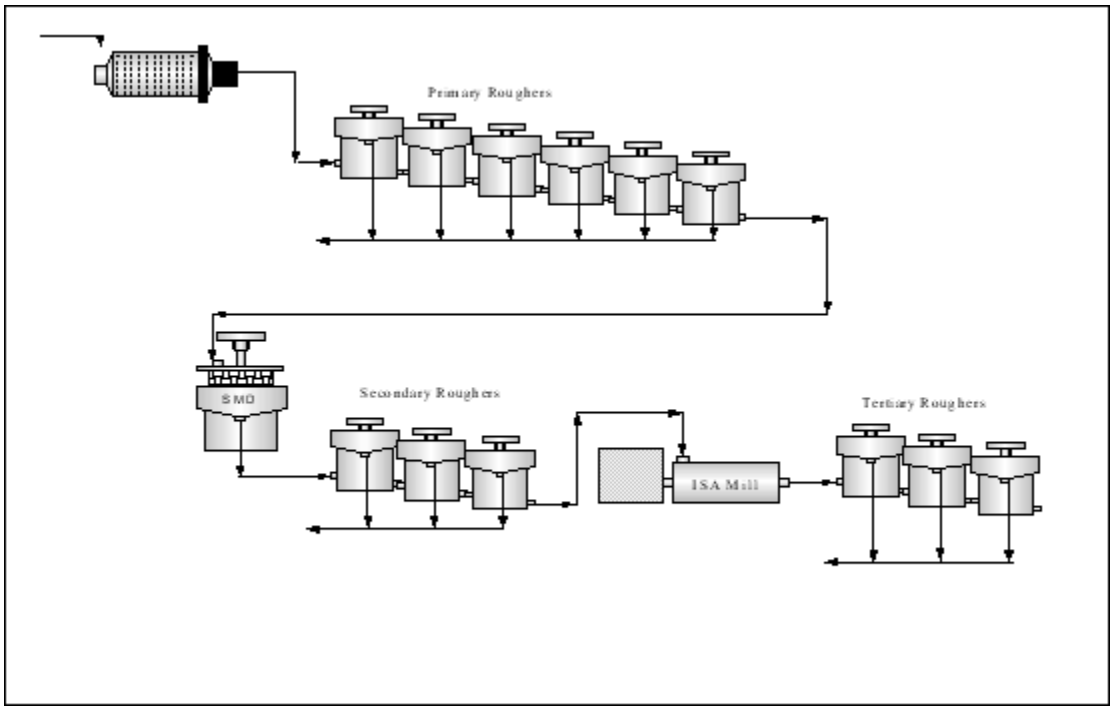

Figure 3.3 Configuration for 3-stage milling and flotation (MF3) – 1st campaign

3.2.4 Mill power

Since one of the requirements was to achieve similar final size distributions for all three circuits, it was necessary to draw the same milling power for each configuration. Mill power is shown in Table 3.3:

Table 3.3 Mill power for the three configurations

	Ball Mill Power (kW)	**SMD Power (kW)**	**IsaMill Power (kW)**
MF1 Configuration	9.5	17.2	44.3
MF2 Configuration	9.5	17.3	44.0
MF3 Configuration	9.5	17.1	43.9

3.2.5 Flotation Operating Conditions

Reagent dosing points and dosages rates are shown in Table 3.4:

Table 3.4 Reagent dosages for the MF1, MF2 and MF3 tests

Reagent	**Dosage Point**	**MF1 (g/ton)**	**MF2 (g/ton)**	**MF3 (g/ton)**
Activator ($CuSO_4$)	Ball mill discharge	50	50	50
Frother (DOW 200)	Primary Float Feed	20	20	20
Depressant (CMC type)	Primary Float Feed	70	40	40
Depressant (CMC type)	Flotation Cell 7	30	60	40
Depressant (CMC type)	Flotation Cell 10	-	-	20
Collector (SIBX)	Primary Float Feed	100	70	70
Collector (SIBX)	Flotation Cell 7	70	100	70
Collector (SIBX)	Flotation Cell 10	30	30	60

Note that overall collector and depressant dosage were the same for all three circuits, while the stage-wise addition was varied according to the size distribution at the dosage point. For

the MF2 and MF3 circuits, cells 7 and 10 correspond to the secondary and tertiary flotation feeds.

Air addition rates were kept constant for all three configurations, while small adjustments were made to froth height to ensure decent froth transport. Air addition, froth height and bubble size for each cell are shown in Table 3.5:

Table 3.5 First campaign flotation operating conditions

Cell	Air (l/min)	Froth Height (cm)			Bubble Size (mm)		
		MF1	MF2	MF3	MF1	MF2	MF3
1	150	5.8	5.6	5.5	1.0	1.1	1.2
2	150	6.3	6.0	6.2	0.9	1.1	1.1
3	160	6.0	5.9	5.8	1.0	1.0	1.2
4	180	4.7	4.5	4.1	1.1	1.1	1.0
5	180	6.1	6.1	5.9	1.2	1.1	1.2
6	180	5.9	6.0	6.0	1.1	1.2	1.2
7	150	5.8	5.8	5.8	1.1	1.0	0.9
8	155	5.7	5.8	5.7	1.0	1.1	1.1
9	160	5.6	5.6	5.4	1.1	1.2	1.1
10	155	4.9	5.0	5.1	1.0	0.9	0.9
11	150	4.8	4.9	5.0	0.9	1.0	1.1
12	155	4.8	4.9	4.9	1.0	1.0	1.1

A primary flotation feed solids content of 33% was targeted for all three configurations. No additional water was added to the circuit after the primary milling stage.

3.2.6 Sampling and analysis

Sampling

Sampling was conducted using automatic sample cutters designed to take full stream samples. An exception was the primary mill feed sample, which was collected every 15 minutes using a bucket and stopwatch. The following samples were taken:

- Primary Mill Feed
- All Mill Products
- Cells 1 - 12 Individual Concentrates
- Cells 1 - 12 Individual Tailings
- Cell 1 – 6 Combined Concentrate
- Cell 7 – 9 Combined Concentrate
- Cell 10 – 12 Combined Concentrate

Composition Analysis

All samples were analysed for PGM's and water content. Although Cr_2O_3 assays were performed, Cr_2O_3 modelling was beyond the scope of this thesis. The Cr_2O_3 grades are included in the Appendices. The grades of Cu, Ni, and S^{2-} in UG2 ore is usually below detection limits, especially in tailings samples. Therefore, no analysis was performed on these elements.

Fractional Analysis

Fractional analysis was performed on the flotation feed, tails and combined concentrate for each circuit. The following screens were used:

- 106µm
- 75µm
- 53µm
- 10µm

Each size fraction was analysed for PGM's by fire assay.

3.2.7 Batch flotation tests

Batch flotation tests were performed using a Denver batch flotation machine and a 5-litre cell on the flotation feed and tails of each flotation stage in the three configurations. The machine

was operated at 1600rpm and 40l/min air intake. No reagents or water was added during the tests. Concentrate was removed in regular 15-second intervals, and composite concentrate samples were collected at the following time intervals, as per the standard Lonmin procedure (CON_R&D_SOP_04):

- 1 minute
- 2.5 minutes
- 7.5 minutes
- 15 minutes
- 20 minutes

Due to assay mass constraints, the concentrate and final tail samples were analysed for PGM's only.

3.2.8 Mineralogy

Mineralogical analyses were done on the primary flotation feed of each circuit configuration, as well as the crushed ore sample used in all the campaigns. For each analysis, two sub-samples were used for the preparation of the polished sections, while another sub-sample was pulverised for X-Ray diffraction analysis. The following mineralogical techniques were used:

X-Ray diffraction analysis

X-ray diffraction using a Siemens D-500 diffractometer was used to investigate major variations in the mineralogy of the ore. This system gives a lower detection limit of approximately 3 to 4 volume percent of the crystalline phases present.

Scanning-electron microscopy (SEM)

SEM, coupled with energy-dispersive X-ray analysis (EDX) were used for mineral identification. An image analyser, fully integrated with the SEM and EDX systems, was used to perform automated searches for PGE minerals. The smallest PGM grains detected with this method measure approximately 0.5µm in diameter.

3.3 Second campaign

A second set of pilot plant runs was conducted following the same basic procedure as explained above. In this case two mills were used and therefore only MF1 and MF2 configurations were tested. A coarser final grind was selected for this series of tests, to broaden the size range over which the flotation performance was investigated.

3.3.1 Ore

The ore sample that was prepared for the first campaign was also used in the second campaign.

3.3.2 Pilot plant Equipment

In the second campaign, the pilot ball mill and SMD were used, along with six 150-litre rougher cells. This equipment was described in Section 3.2.2 for the first campaign.

3.3.3 Circuit configuration

The equipment was arranged into MF1 and MF2 configurations. These are shown in Figures 3.4 and 3.5:

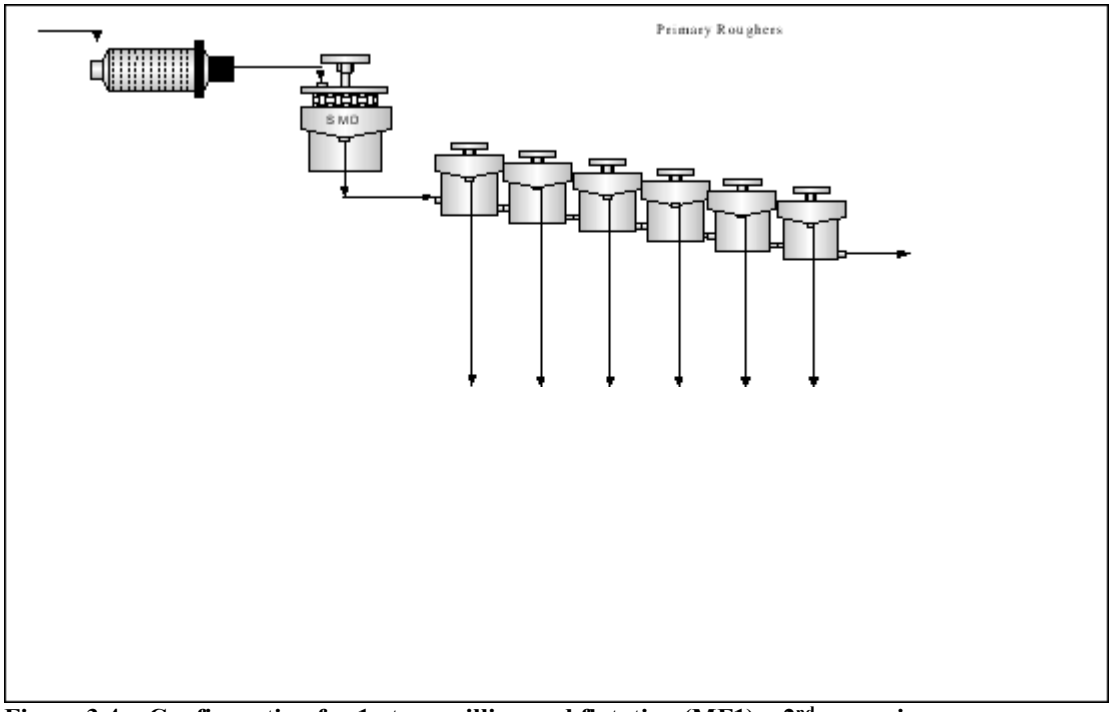

Figure 3.4 Configuration for 1-stage milling and flotation (MF1) – 2nd campaign

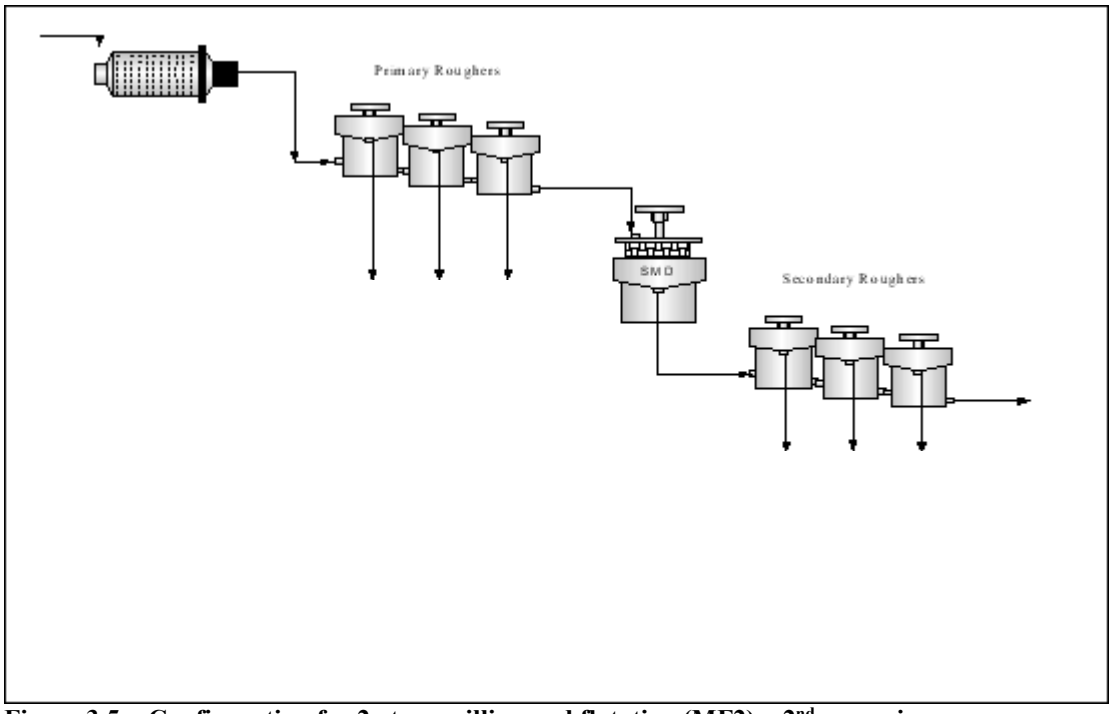

Figure 3.5 Configuration for 2-stage milling and flotation (MF2) – 2nd campaign

Milling and flotation parameters were kept constant for the two circuits.

3.3.4 Milling power

Mill power was kept constant to ensure similar final size distributions for the two circuits (Table 3.6.):

Table 3.6 Mill Power for the two configurations

	Ball Mill Power (kW)	**SMD Power (kW)**
MF1 Configuration	9.0	17.5
MF2 Configuration	9.0	17.5

3.3.5 Flotation Operating Conditions

Reagent dosing points and dosages are shown in Table 3.7:

Table 3.7 Reagent dosages for the MF1 and MF2 tests

Reagent	**Dosage Point**	**MF1 (g/ton)**	**MF2 (g/ton)**
Activator ($CuSO_4$)	Ball mill discharge	50	50
Frother (DOW 200)	Primary Float Feed	20	20
Depressant (CMC type)	Primary Float Feed	70	50
Depressant (CMC type)	Flotation Cell 4	30	50
Collector (SIBX)	Primary Float Feed	100	70
Collector (SIBX)	Flotation Cell 4	70	100

Overall collector and depressant dosages were kept the same for both circuits, although the stage-wise additions were varied according to the size distribution at the dosage point.

Other flotation operating conditions are shown in Table 3.8:

Table 3.8 Second campaign flotation operating conditions

Cell	Air (l/min)		Froth Height (cm)		Bubble Size (mm)	
	MF1	MF2	MF1	MF2	MF1	MF2
1	155	155	5.5	5.5	1.0	1.0
2	155	155	5.4	5.4	1.1	1.1
3	160	160	5.4	5.4	1.0	1.0
4	170	160	5.3	4.9	1.0	1.0
5	170	165	5.4	5.0	1.1	1.0
6	170	165	5.2	4.8	1.0	1.1

Solid content for the primary flotation feed was approximately 30%. No additional water was added to the circuit.

3.3.6 Sampling and analysis

Sampling

Samples were taken using automatic sample cutters designed to take full stream cuts. Once again the primary mill feed sample was collected using a bucket and stopwatch at 15 minutes intervals. The following samples were taken:

- Primary Mill Feed
- All Mill Products
- Cells 1 – 6 Individual Concentrates
- Cells 1 - 6 Individual Tailings
- Cells 1 – 3 Combined Concentrate
- Cells 4 – 6 Combined Concentrate

Composition and Fractional Analysis

The same elemental and fractional analyses were performed as was described for the first campaign (Section 3.2.6).

3.3.7 Batch flotation tests

The same batch flotation procedure was used as described in Section 3.2.7. Batch flotation tests were conducted on the flotation feed and tails of each flotation stage in the two configurations

3.3.8 Mineralogy

The same mineralogical analyses were performed on the feed to each primary flotation stage as described for the first campaign.

CHAPTER 4
RESULTS FROM FIRST PILOT PLANT CAMPAIGN

4.1 Introduction

Results for the first pilot plant campaign are presented in this chapter. The complete set of data for these tests can be found in Appendix A.

4.2 Milling results

The particle size distributions for the MF1, MF2 and MF3 circuits are shown in Figures 4.1 to 4.3:

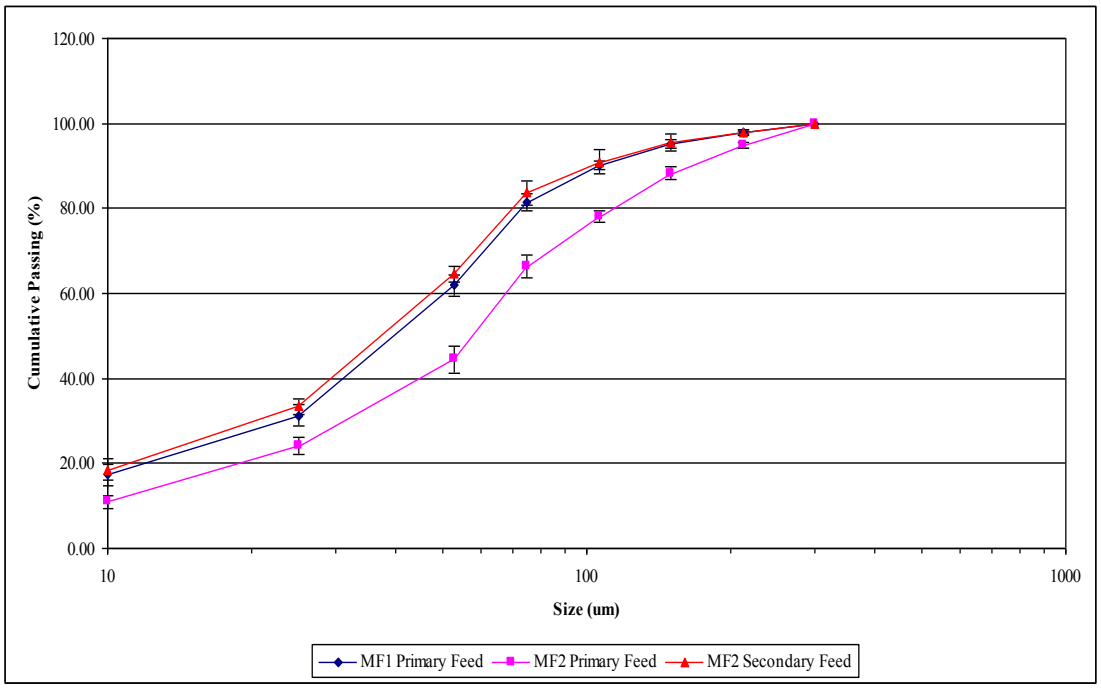

Figure 4.1 MF1 and MF2 Particle Size Distribution

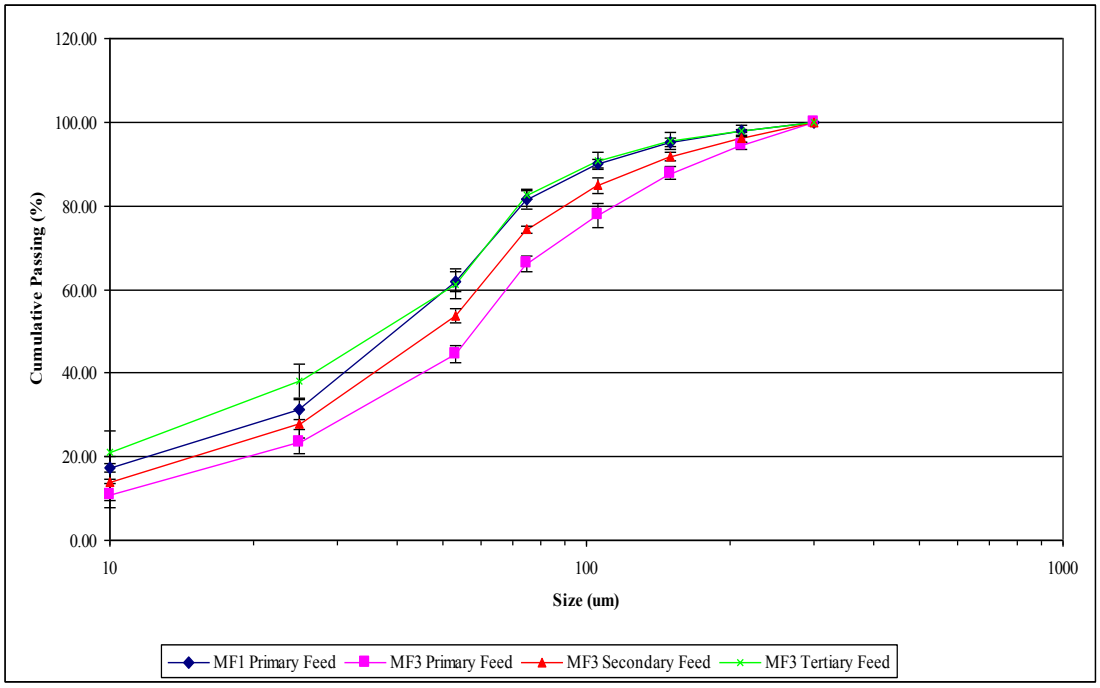

Figure 4.2 MF1 and MF3 Particle Size Distributions

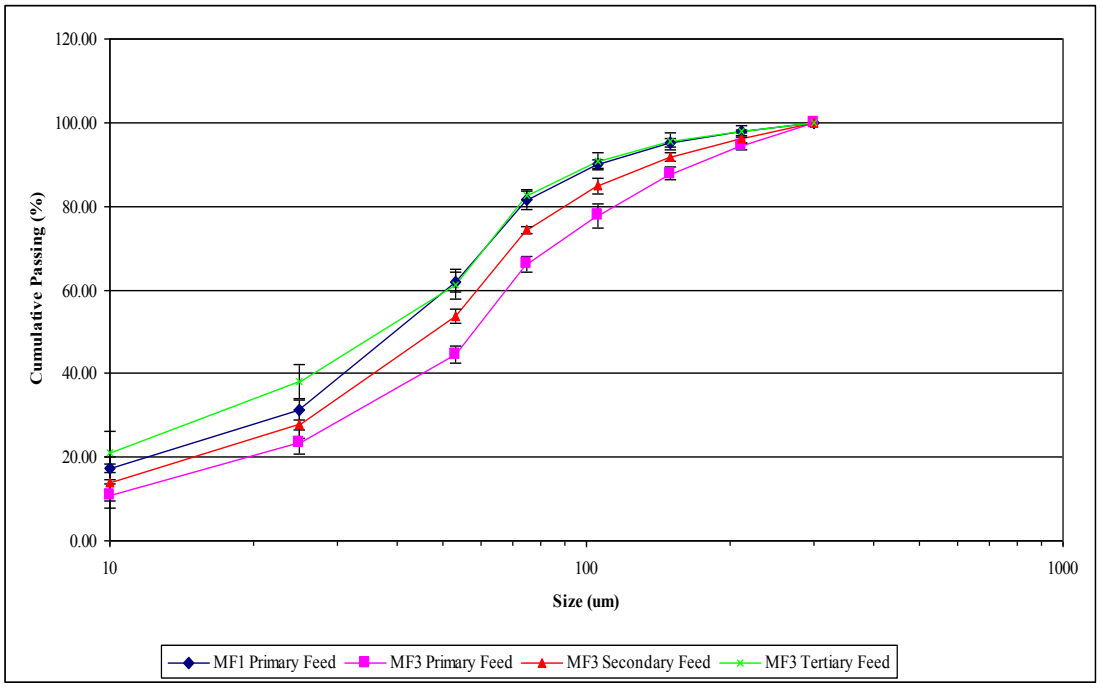

Figure 4.3 MF2 and MF3 Particle Size Distributions

The cumulative % -75µm achieved by the different milling stages are shown in Table 4.1:

Table 4.1 Cumulative % -75µm achieved by each milling stage

	MF1	MF2	MF3
Primary	**81.5**	66.4	66.2
Secondary	-	**83.6**	74.3
Tertiary	-	-	**82.8**

The particle size distributions for the three circuits (Figures 4.1 to 4.3) confirm that similar final size distributions were achieved, as was intended. Table 4.1 shows that the final stage of each configuration also produced a similar % -75µm: The primary grind for the MF1 circuit was 81.5% -75µm, compared with 83.6% in the MF2 secondary stage and 82.8% in the MF3 tertiary stage. The primary grind for the MF2 and MF3 circuits were also very close, at 66.4% and 66.2% -75µm respectively. As was mentioned in the experimental procedure, this does not imply that the PGM size distribution was also similar for the three circuits.

4.3 Mineralogy of the ore

The mineralogy of the ore sample will be discussed in this section. The mineralogy of each flotation feed will be presented in Section 4.8.

4.3.1 General mineralogy

The ore sample consists predominantly of chromite with interstitial silicates, mainly orthopyroxene, anorthite and phlogopite. These primary silicates have in places been replaced by secondary silicates like chlorite, talc, quartz, K-feldspar etc.

The BMS assemblage consists of pentlandite (often with Ni>Fe), chalcopyrite and pyrite, with minor pyrrhotite and millerite. BMS tend to be located at chromite-silicate boundaries, with grain boundaries ranging from <10µm to more than 100µm. Sulphides tend to be associated preferentially with late- and postmagmatic silicates, with areas of secondary silicate formation commonly peppered with <10µm sulphide grains, enclosed in secondary silicates.

4.3.2 PGM mineralogy

Relative proportion of PGE minerals

Based on the major elements present, each PGM grain was categorised into one of six classes of PGE minerals:

Pt,Pd,Ni,S	-	mainly braggite and cooperite
Pt,Rh,Cu,S	-	malanite
Ru,Os,Ir,S	-	laurite
PGE-As-(S)	-	sulfarsenides of Ir / Rh / Ru
Pt-Fe alloy	-	sometimes containing Pd and/or Rh
Other	-	various non-sulphide minerals

Since a relatively small number of PGE mineral grains (between 100 and 200) were examined for each polished section, it is possible that a single, large particle can skew data based solely on percent volume calculations. Therefore the proportions of PGE minerals are expressed both as percent volume and number of grains. The relative proportions of these six classes of PGE minerals are shown in Table 4.2:

Table 4.2 Relative proportion of PGE minerals in ore sample

	Volume (%)	**Number of Grains (%)**
(Pt,Pd),S	40.7	45.7
(Pt,Rh,Cu),S	24.8	22.8
(Ru,Os,Ir).S	25.2	18.2
PGE-As-(S)	3.2	5.2
Pt-Fe-alloy	2.8	0.8
Other	3.3	7.3

From Table 4.2, PGE sulphides are predominating, while small amounts of PGE sulfarsenides, Pt-Fe alloys and non-sulphide PGE minerals are also present. The PGE minerals often form composite grains with each other.

PGE grain size distributions

The equivalent circle diameter was used to determine grain sizes. Measured PGE mineral grain size distributions are showed in Table 4.3:

Table 4.3 Measured PGE mineral grain size distribution

Size (μm)	Volume (%)	Number of Grains (%)
0-2	4.0	27.0
2-4	21.2	41.5
4-6	23.5	15.7
6-8	21.0	7.8
8-10	10.5	2.3
>10	19.8	5.7

PGE mineral grains were generally smaller than 10μm, with a median of 2-4μm.

PGE mineral mode of occurrence

In terms of mode of occurrence, each grain examined was classified as follows:

Liberated grain (Lib)
Locked in BMS or at a sulphide-sulphide grain boundary (Lock BMS)
At the grain boundary of BMS with silicate and/or chromite (GB BMS-Si/Cr)
Locked in silicate or at a silicate-silicate grain boundary (Lock Si)
At the grain boundary of chromite and silicate (GB Si-Si/Cr)
Locked in chromite (Lock Cr)

The mode of occurrence is shown in Table 4.4.:

Table 4.4 PGE mineral mode of occurrence

	Volume (%)	Number of Grains (%)
Lib	4.2	2.6
Lock BMS	12.6	17.8
GB BMS-Si/Cr	35.0	36.6
Lock Si	21.0	23.2
Lock Cr	5.0	4.6
GB Si-Si/Cr	22.2	15.2

From Table 4.4, only a small percentage of PGE minerals are liberated after crushing. Approximately half the PGE minerals are associated with BMS, while the balance is locked in gangue minerals, usually secondary silicates. The PGE minerals locked in chromite is almost exclusively (Ru,Os,Ir)-S.

4.4 Mass balancing and data integrity

For each circuit configuration, mass balances were done for the following data sets: the circuit, fractional analysis and batch flotation. First the circuit mass balances were calculated, and then the fractional analysis and batch flotation data were fitted to correspond with the values that were calculated for the circuit. In order to determine the validity of the mass balances, each data set will be analysed by comparing the raw data set with the balanced values. Finally, the different raw data sets will be compared to each other to determine consistency between data sets.

4.4.1 Circuit mass balance

All flotation feed, tails and concentrate streams were sampled and analysed for PGM grade and % solids. The mass balances were done by simultaneously balancing experimental data for mass flows, PGM grades and % solids. The balanced values are compared graphically to raw data for PGM's in Figure 4.4 and for % solids in Figure 4.5:

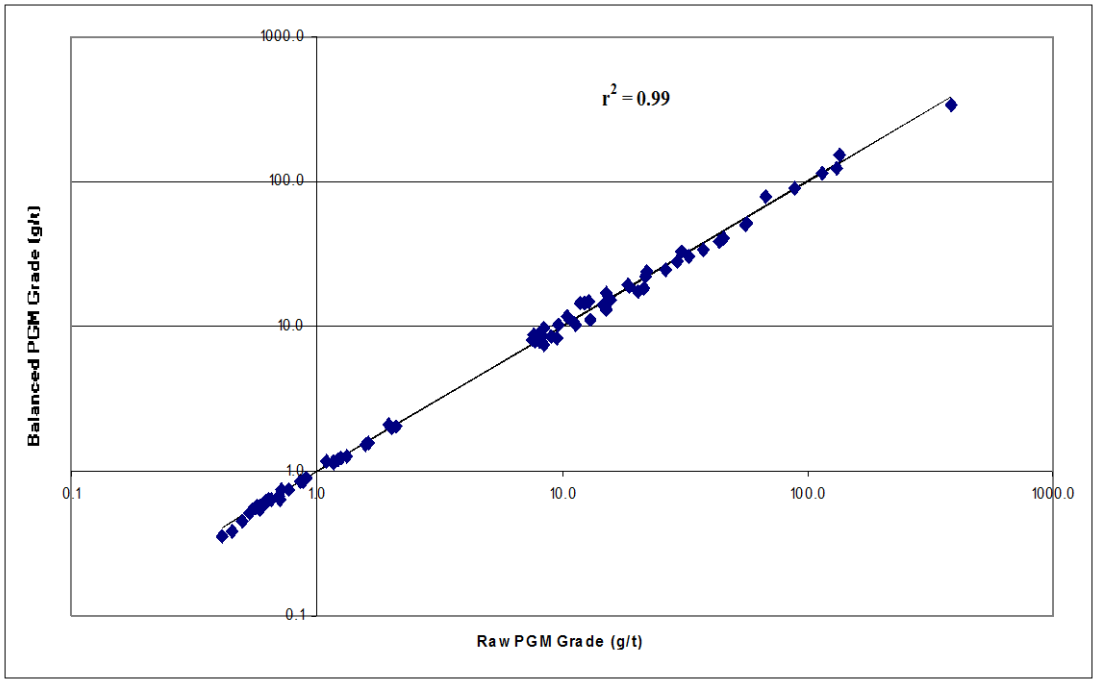

Figure 4.4 Balanced vs. Raw PGM grades for the MF1, MF2 and MF3 mass balances

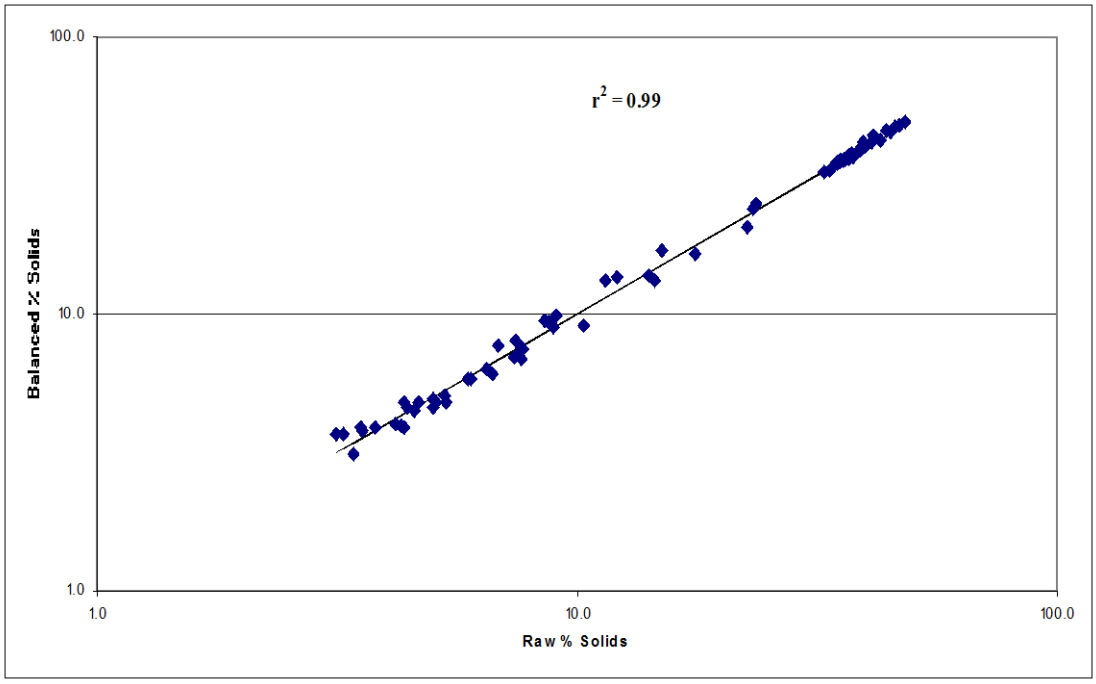

Figure 4.5 Balanced vs. Raw % solids for the MF1, MF2 and MF3 mass balances

A visual inspection of Figures 4.4 and 4.5 indicate that the raw and balanced data are in very good agreement. This indicates that no major manipulation of the data was required to obtain the mass balances. Also, fitting a 45º line through the data is an indication of how much the

raw data had to be manipulated to achieve a mass balance. For both graphs the correlation coefficient is above 0.99.

4.4.2 Fractional analysis

For fractional analysis, the mass fractions and PGM grades were adjusted simultaneously to balance the feed, tails and concentrate in each size fraction. The combined PGM grade for each stream also had to correspond with the balanced value for the circuit. The balanced PGM grades and mass percentages versus raw data for all three circuits are shown in Figures 4.6 and 4.7 respectively:

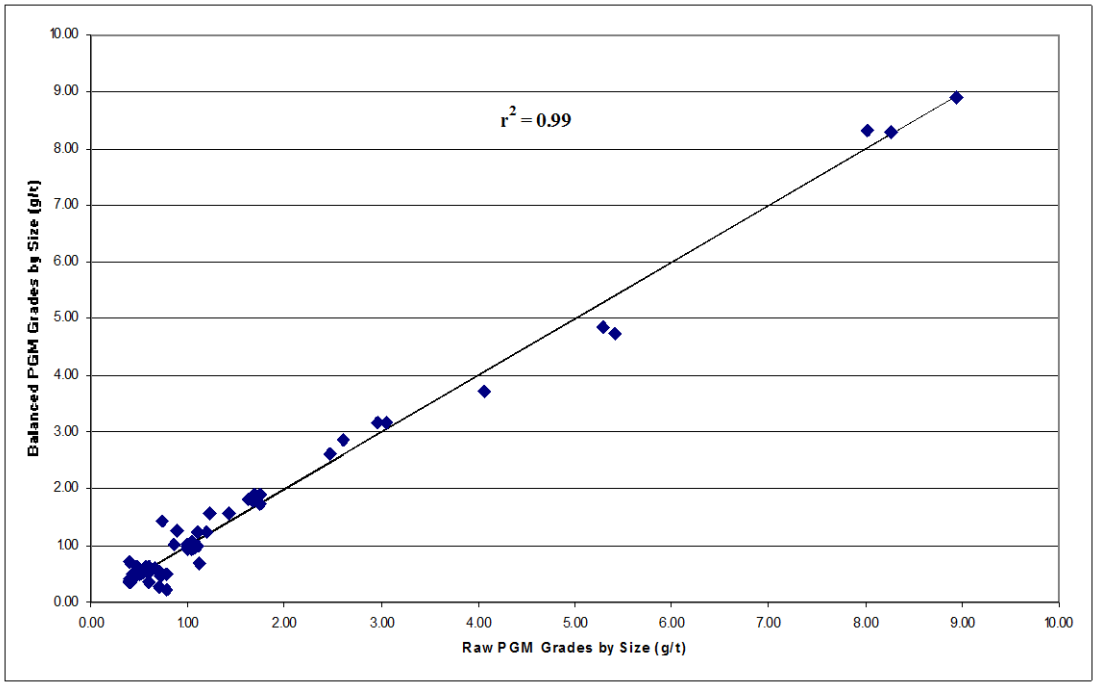

Figure 4.6 Balanced vs. Raw PGM Grades for MF1, MF2 and MF3 fractional analysis

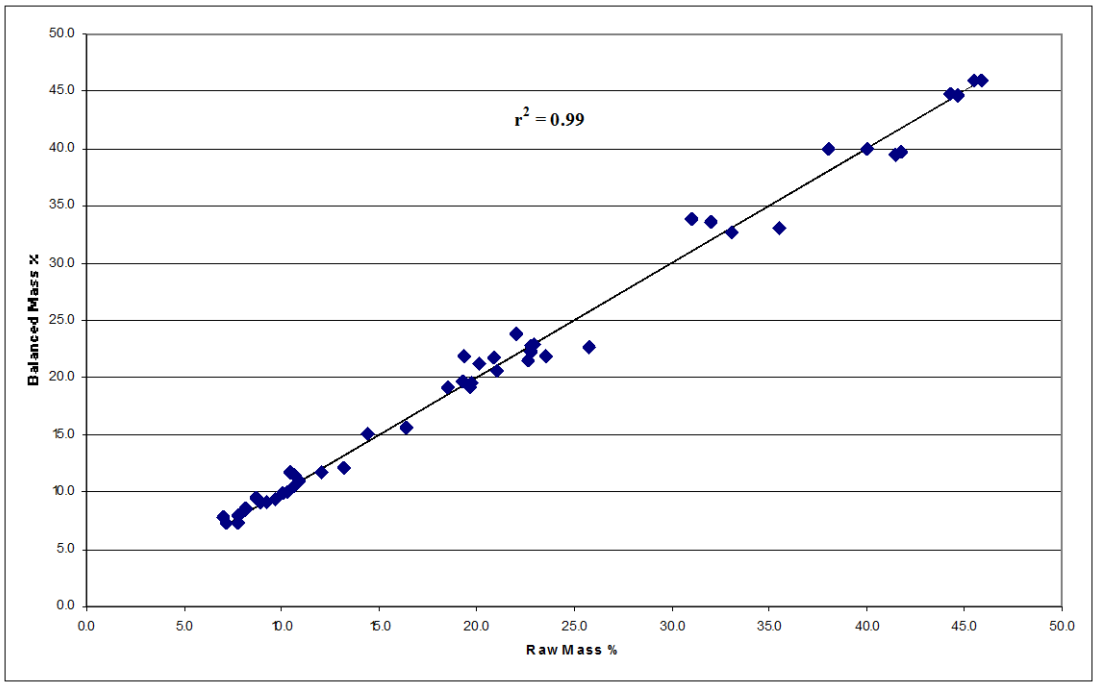

Figure 4.7 Balanced vs. Raw mass percentages for MF1, MF2 and MF3 fractional analysis

More manipulation of the raw data was required to achieve a mass balance for the fractional analysis than for the circuit balances. This was expected, since the data had to be balanced across size fractions, as well as within each data set, and there was insufficient sample to do repeat analyses. The lack of repeats, combined with the difficulties in mass balancing across size fractions resulted in the relatively large adjustments to the data. However, because of the large number of data points, the correlation between raw and balanced data is still greater than 0.99.

4.4.3 Batch flotation

For each batch flotation test, the mass and PGM grades were balanced so that the build-up grade of the stream corresponded with the value determined by the circuit balance. The balanced PGM grades and mass percentages versus raw data for all three circuits are shown in Figures 4.8 and 4.9 respectively:

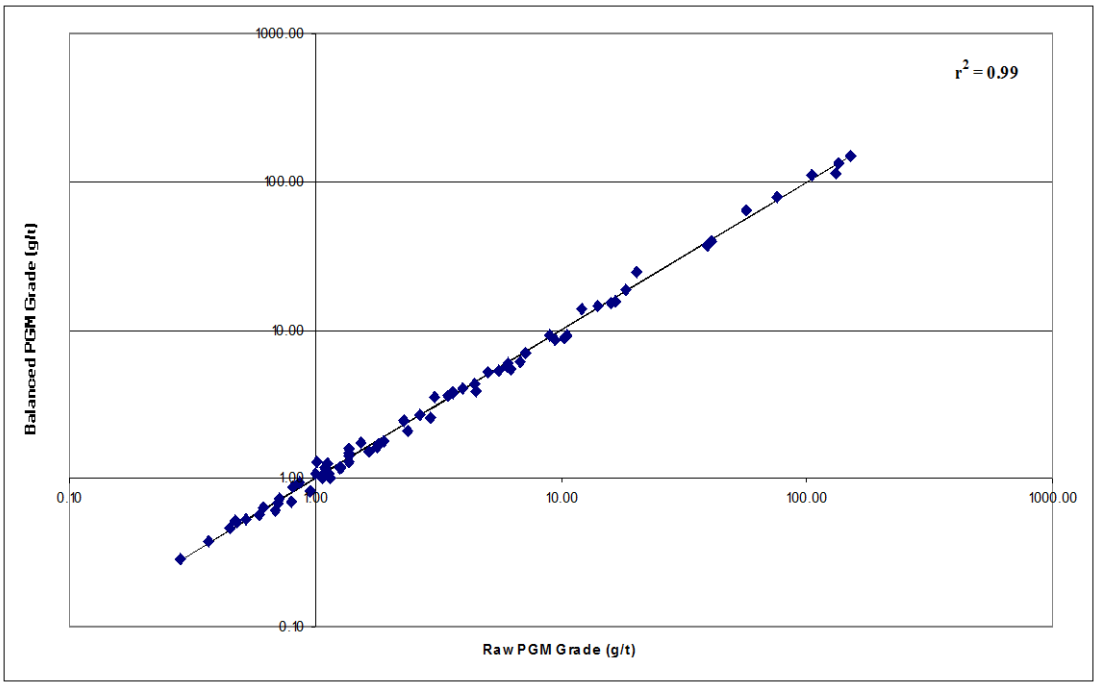

Figure 4.8 Balanced vs. Raw PGM Grades for MF1, MF2 and MF3 batch floats

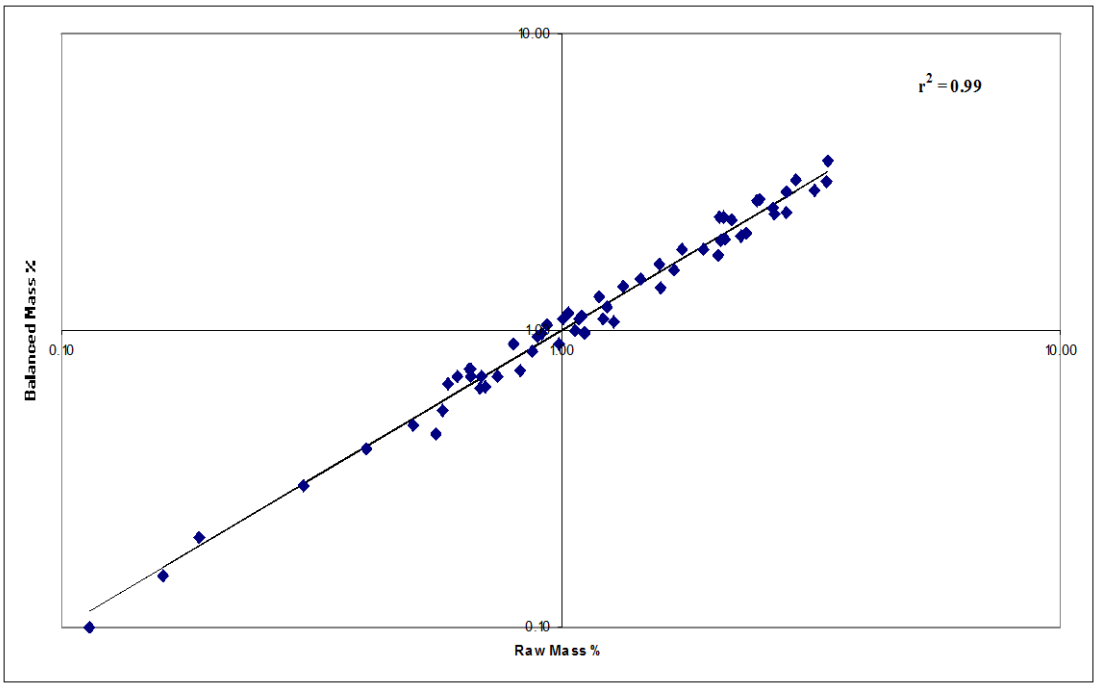

Figure 4.9 Balanced vs. Raw mass percentages for MF1, MF2 and MF3 batch floats

The graphs show that little manipulation of the raw data was required to obtain batch flotation balances that agree with the circuit. The correlation coefficient between raw and fitted data is also higher than 0.99 for both PGM grades and mass percentages.

4.4.4 Comparing feed and tails values between data sets

PGM recovery is most sensitive to feed and tail grades. Therefore, the validity of any conclusions concerning recovery will be determined by the accuracy of these values. Comparing raw data from the circuit sampling campaigns with the raw build-up head grades from the batch flotation and fractional analysis can give an indication of the consistency of these numbers. These grades for the three configurations are shown in Table 4.5:

Table 4.5 Feed and tail PGM grades (g/t) for the three configurations tested

	Raw Circuit	**Build-up from Raw Fractional**	**Build-up from Raw Batch**	**Balanced**
MF1 Primary Feed	3.75	3.91	3.80	3.75
MF1 Primary Tail	0.56	0.59	0.55	0.56
MF2 Primary Feed	3.85	3.86	3.90	3.85
MF2 Primary Tail	1.10	1.09	1.18	1.16
MF2 Secondary Feed	1.13	1.05	1.07	1.16
MF2 Secondary Tail	0.53	0.55	0.51	0.52
MF3 Primary Feed	3.80	3.95	3.77	3.80
MF3 Primary Tail	1.17	1.06	1.10	1.16
MF3 Secondary Feed	1.15	0.95	1.22	1.16
MF3 Secondary Tail	0.59	0.49	0.52	0.55
MF3 Tertiary Feed	0.51	0.46	0.54	0.55
MF3 Tertiary Tail	0.41	0.41	0.36	0.36

From Table 4.5 it can be seen that the raw data from the circuit compares favourably with the build-up values from the raw fractional analysis and batch flotation data. When considering that the circuit, batch flotation and fractional analysis samples were taken separately during the sampling campaigns, the consistency in the assays suggest that the values were representative of the plant performance.

4.5 Flotation results

The PGM recovery versus residence time curves for the three configurations are shown in Figure 4.10:

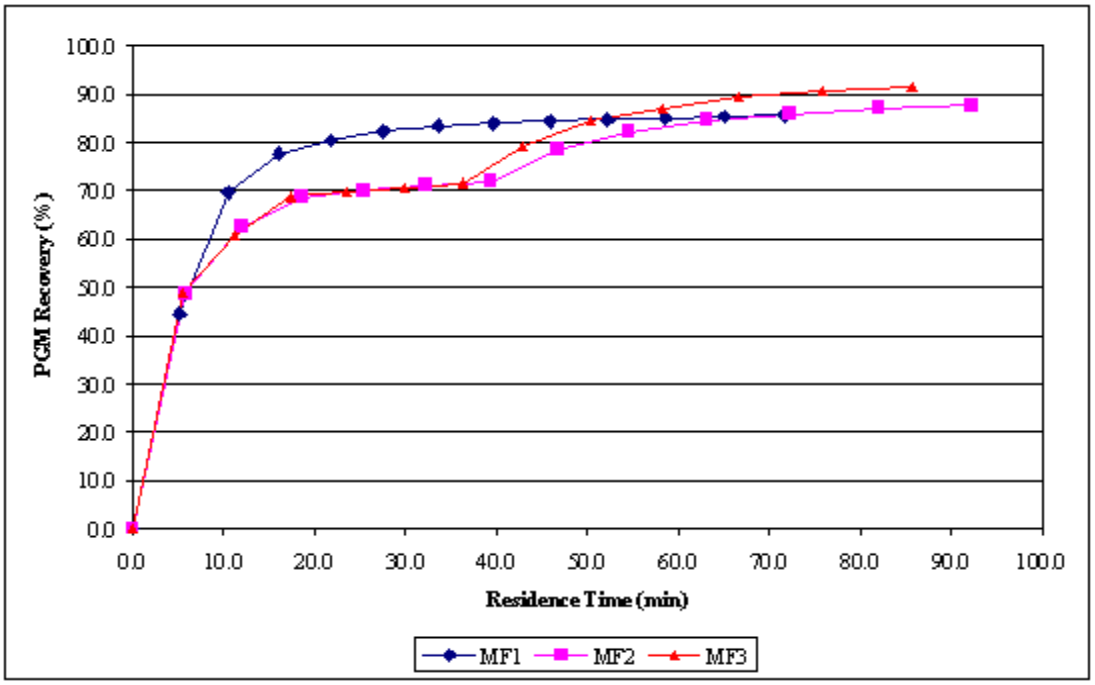

Figure 4.10 PGM Recovery vs. Residence Time curves for the MF1, MF2 and MF3 circuits

From Figure 4.10, the MF1 configuration displayed the fastest initial rate of PGM recovery. However, multiple mill-float circuits incrementally increased the flotation rate in the secondary and tertiary flotation stages. The overall outcome was that the highest final PGM recovery was achieved with the MF3 configuration, followed by the MF2 and then the MF1 configuration.

Figure 4.11 shows the PGM recovery versus PGM grade curves, while the PGM grade for each cell is displayed in Figure 4.12:

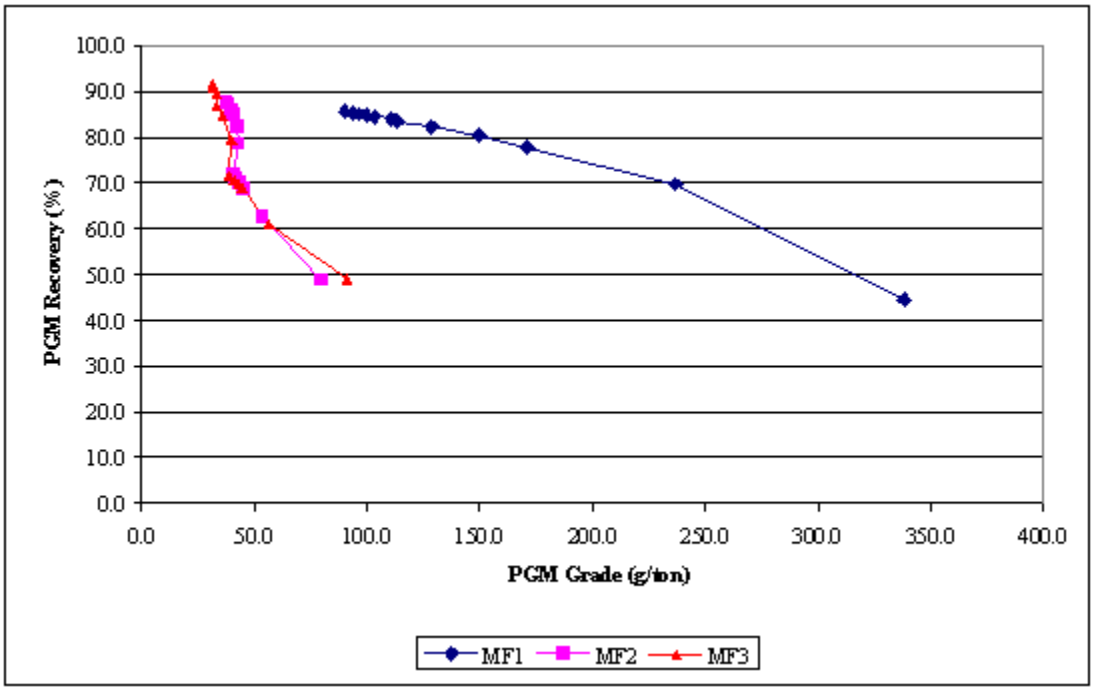

Figure 4.11 PGM Recovery vs. PGM Grade for the MF1, MF2 and MF3 configurations

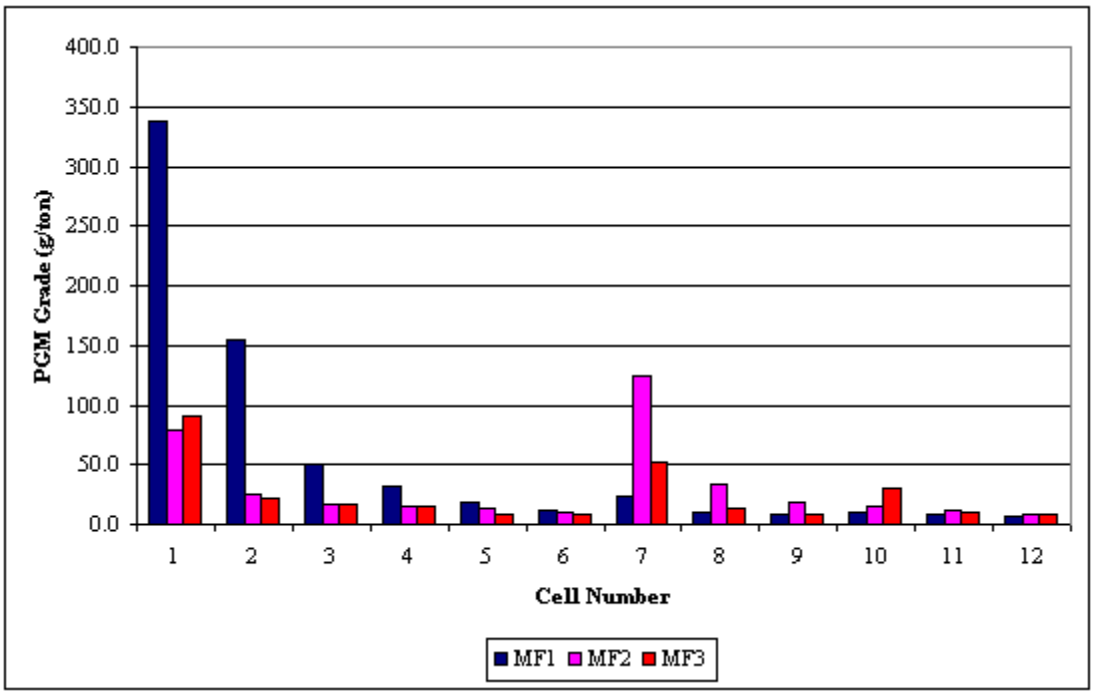

Figure 4.12 PGM Grade per cell for the MF1, MF2 and MF3 configurations

The MF1 configuration displayed the highest initial grades, although the lowest final recovery was also achieved. The effect of the regrind can be seen in the increase in grade for the MF2 circuit in cell 7; and for the MF3 circuit in cells 7 and 10 (Figure 4.12).

4.6 Flotation by size

The data was normalised to account for the slight differences in PGM head grade between the three circuits. The PGM's produced by size fraction (Figure 4.13) was calculated by adding the PGM's in tailing and total concentrate for each size fraction. PGM losses per size fraction are shown in Figure 4.14, and the recovery per size fraction is shown in Figure 4.15:

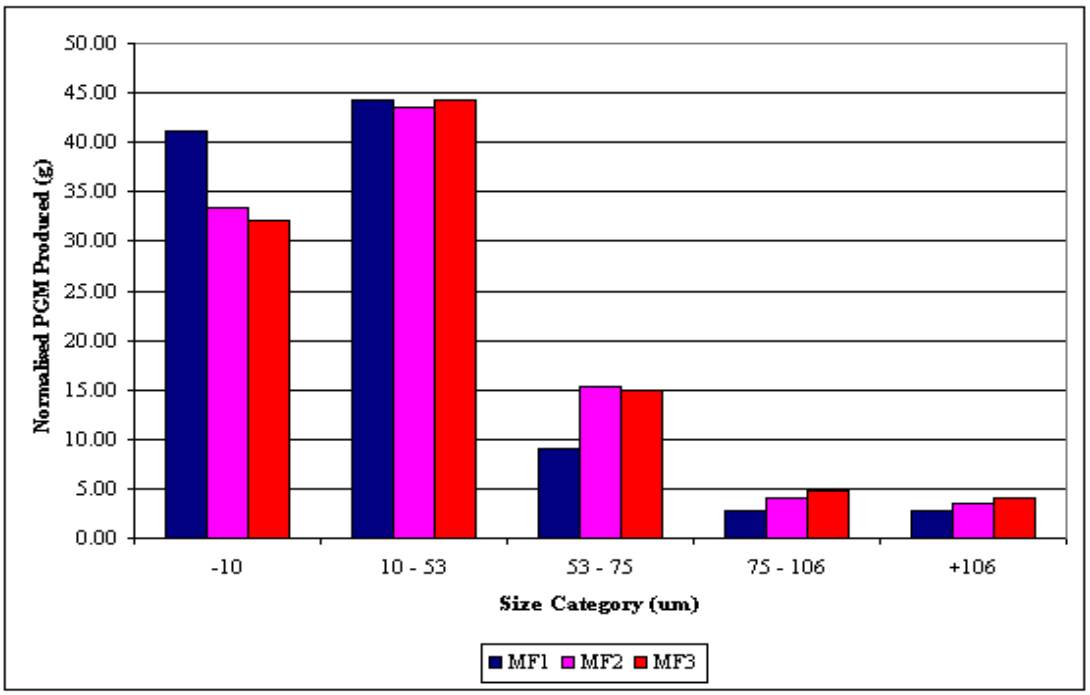

Figure 4.13 PGM units produced per size fraction for the MF1, MF2 and MF3 circuits

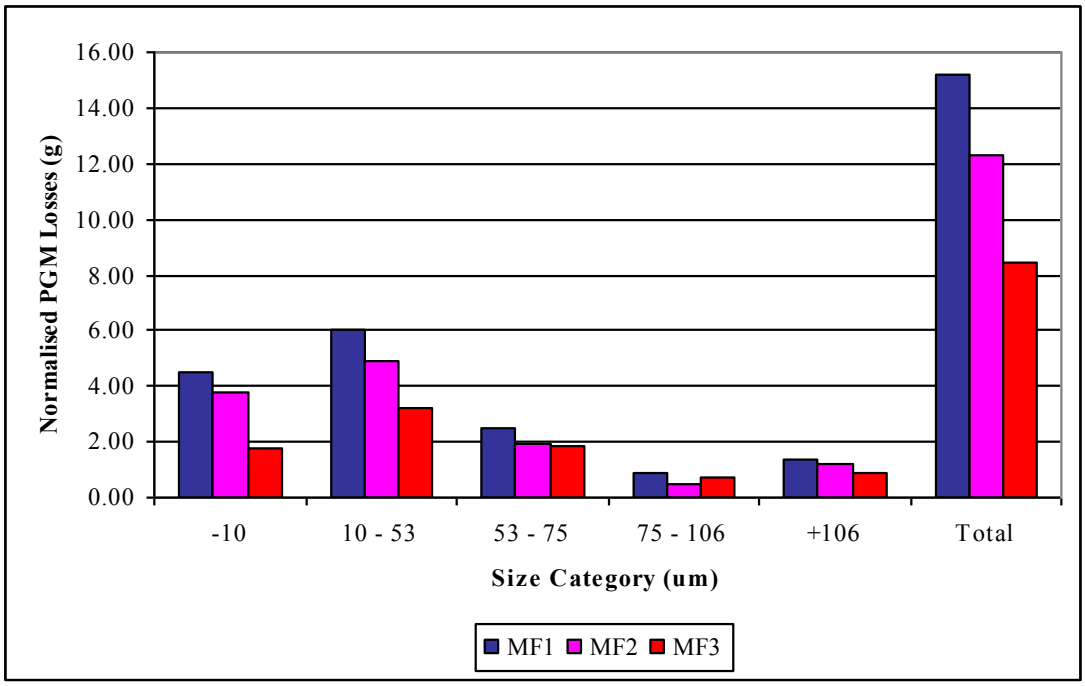

Figure 4.14 PGM losses per size fraction for the MF1, MF2 and MF3 circuits

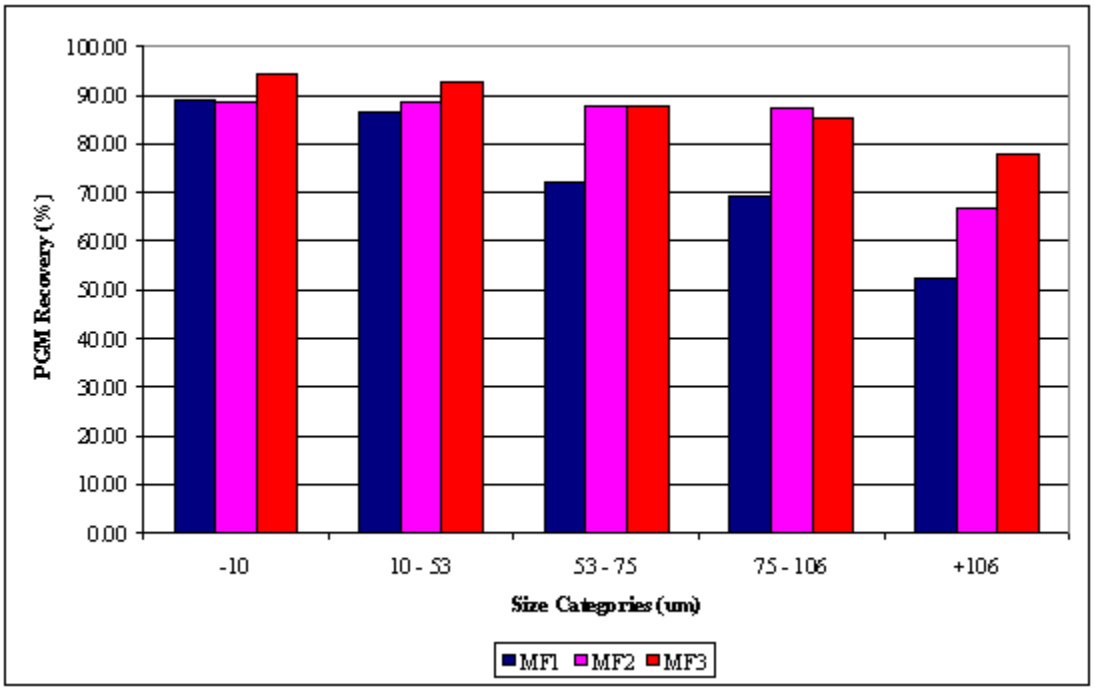

Figure 4.15 PGM recovery by size fraction for the MF1, MF2 and MF3 circuits

Figure 4.13 shows that the MF1 circuit produced more PGM particles in the –10µm size fraction than the other configurations, and reported the highest losses in that size fraction as well (Figure 4.14). The regrind configurations reduced the losses in all fractions coarser than 10µm as well. Of interest is that the PGM losses in the 10-53µm fraction were higher than the PGM losses in the –10µm fraction for all three circuits

From Figure 4.15 it can be observed that multiple grinding and flotation stages resulted in higher PGM recoveries in all size fractions. Also, the PGM recovery increased with decreasing size fraction for all three circuits, although the effect is more pronounced in the MF1 and MF3 circuits.

4.7 Discussion of flotation results

The overall recovery results seem to follow conventional wisdom – the improved recovery with regrind circuits can be explained by the stage-wise removal of floatable material to minimise over-grinding. However, the significant improvement in PGM grade observed with the MF1 circuits cannot be explained by a casual examination of the data. In addition, the results by size show an improvement in recovery for all size fractions with multiple stage circuits, and that the highest recoveries were obtained in the -10μm fraction. These observations can also not be explained without in-depth analysis of the results.

Part of the reason for the difficulty in analysing the results lie in the complexity of the ore. PGM's and BMS liberate at different sizes, and thus liberated PGM's and those associated with BMS would display different flotation characteristics. The milling devices also complicate matters, as both the breakage mechanisms and the milling environment differ between the ball mill and stirred mills.

In order to gain a better understanding of these issues, the flotation results were fitted to the EFC-model described in the Literature Review. Analysis of the floatability distribution of PGM's with different circuits, in different size classes and with different milling devices should assist in isolating the effect of these factors.

4.8 Mineralogy of primary flotation feed

For the primary flotation feeds, the general mineralogy, as well as the relative proportion of PGE minerals is the same as for the crushed ore sample. Results for PGE mineral grain size distribution and mode of occurrence are presented in Tables 4.6 and 4.7 respectively. The values are based upon the number of grains in each class.

Table 4.6 PGE mineral grain size distribution of primary flotation feed

Size (μm)	MF1 (%)	MF2 (%)	MF3 (%)
0-2	41.7	35.6	32.0
2-4	39.6	34.9	42.9
4-6	11.5	15.4	11.8
6-8	3.6	6.9	7.6
8-10	1.4	1.1	3.6
>10	2.2	6.1	2.1

Table 4.7 PGE mineral mode of occurrence

	MF1 (%)	MF2 (%)	MF3 (%)
Lib	38.1	31.9	26.8
Lock BMS	6.2	14.9	18.3
GB BMS-Si/Cr	40.3	22.2	26.6
Lock Si	7.6	19.5	17.0
GB Si-Si/Cr	2.6	3.1	5.1
Lock Cr	5.2	8.4	6.2

These results will be discussed in more detail in Chapters 9 and 10, along with the effect of milling devices and circuit configuration.

CHAPTER 5
RESULTS FROM SECOND PILOT PLANT CAMPAIGN

5.1 Introduction

The aim of the second campaign was twofold. The first was to validate the general findings from the first campaign regarding the effects of multiple grind-float circuits on the overall and size-by-size grade-recovery performance. Secondly, the flotation and milling residence times were shortened to provide a new data set from which to evaluate the performance of the various circuit components. To summarise, different feed size distributions and flotation residence times will ensure the analysis of multi-stage circuits over a wider operational range. However, it should still be possible to confirm general trends from the first campaign. Results of the second pilot plant campaign are presented in this chapter. The full data set is presented in Appendix B.

5.2 Milling

The particle size distributions for the MF1 and MF2 circuits are shown in Figures 5.1:

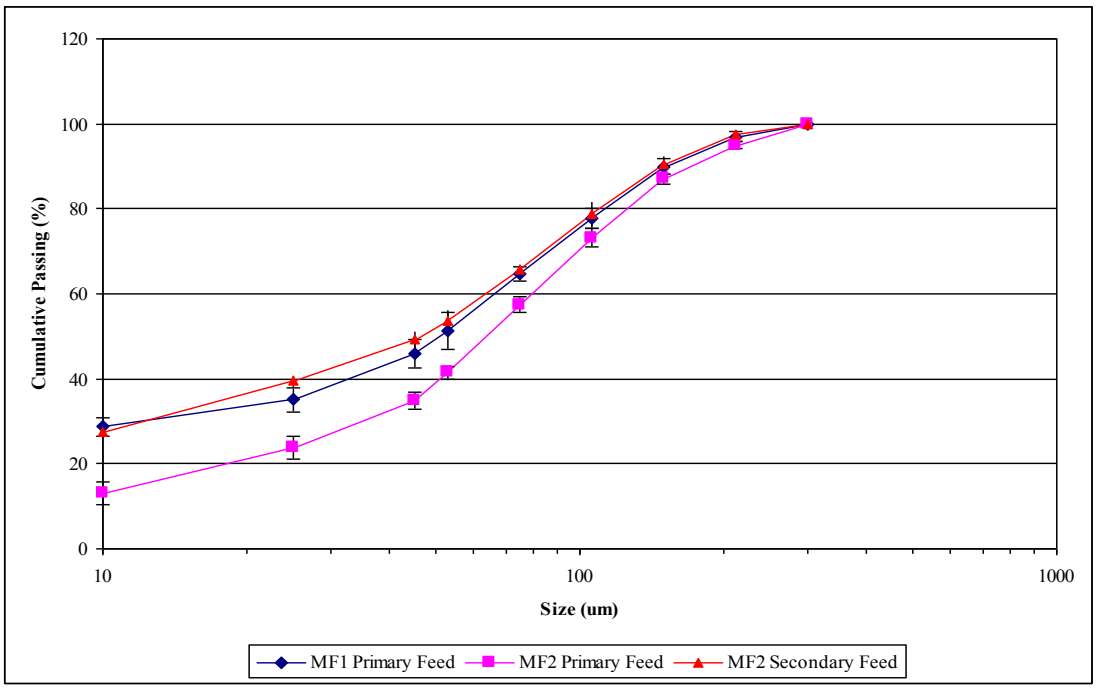

Figure 5.1 MF1 and MF2 Particle Size Distributions

Figure 5.1 shows that a similar final grind was achieved for the two configurations. The grind for each milling stage in the two circuits is summarised in Table 5.1

Table 5.1 Cumulative % -75µm achieved by each milling stage

	MF1	**MF2**
Primary	64.8	57.4
Secondary	-	65.6

5.3 Mass balancing and data integrity

Mass balancing for the circuit, fractional analysis and batch flotation was done using the same procedure as described for the first campaign. In order to determine the validity of the mass balances, each data set will be analysed by comparing the raw data set with the calculated values. Finally, the different raw data sets will be compared to each other to determine consistency between data sets.

5.3.1 Circuit mass balance

All flotation feed, tails and concentrate streams were sampled and analysed for PGM grade and % solids. The mass balances were done by simultaneously balancing experimental data for mass flows, PGM grades and % solids. The balanced values are compared graphically to the raw data for PGM's in Figure 5.2 and for % solids in Figure 5.3:

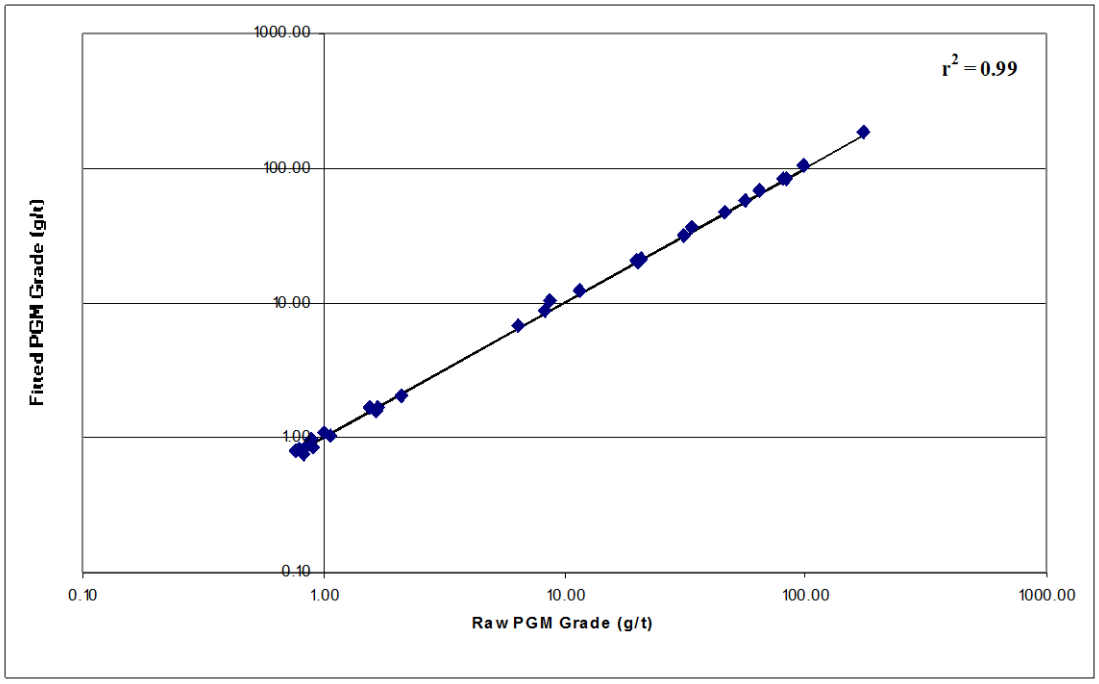

Figure 5.2 Balanced vs. Raw PGM grades for the MF1 and MF2 mass balances

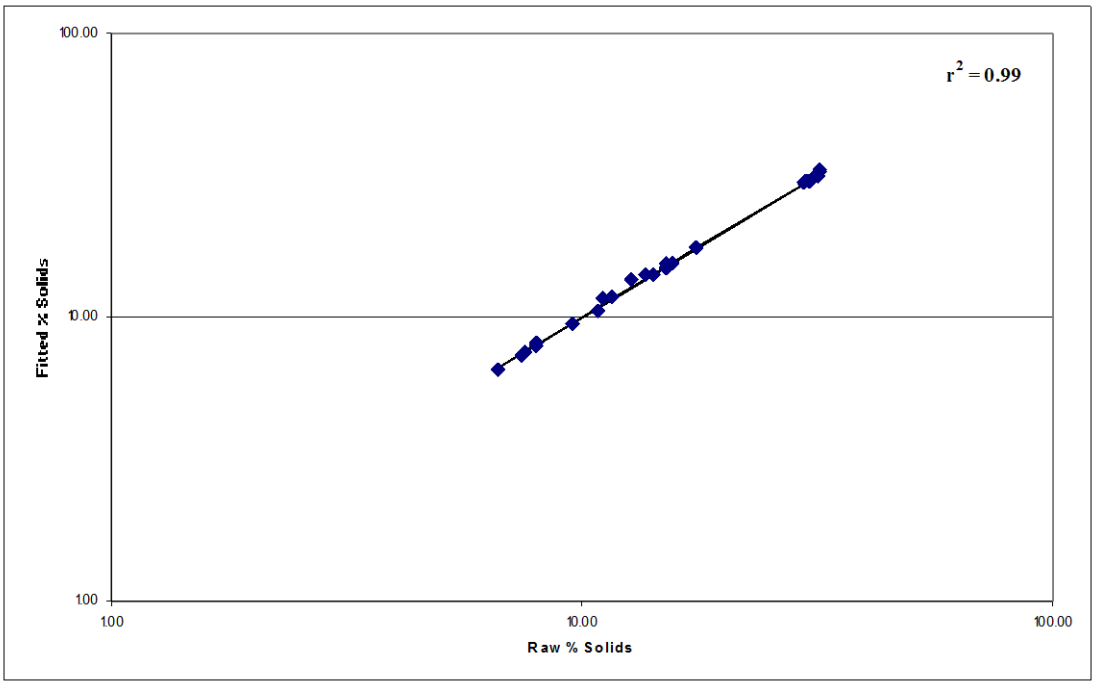

Figure 5.3 Balanced vs. Raw % solids for the MF1 and MF2 mass balances

A visual inspection of Figures 5.2 and 5.3 indicate that the raw and balanced data are very similar. This suggests that no major manipulation of the data was required to obtain the mass balances. Also, fitting a 45^{o} line through the data is an indication of how much the raw data had to be manipulated to achieve a mass balance. For both graphs the correlation coefficient is above 0.99, confirming that only minor changes were made to the raw data.

5.3.2 Fractional analysis

For the fractional analysis, the mass fractions and PGM grades were adjusted simultaneously to balance the feed, tails and concentrate in each size fraction. The combined PGM grade for each stream also had to correspond with the value balanced for the circuit. The balanced PGM grades and mass percentages versus raw data for both circuits are shown in Figures 5.4 and 5.5 respectively:

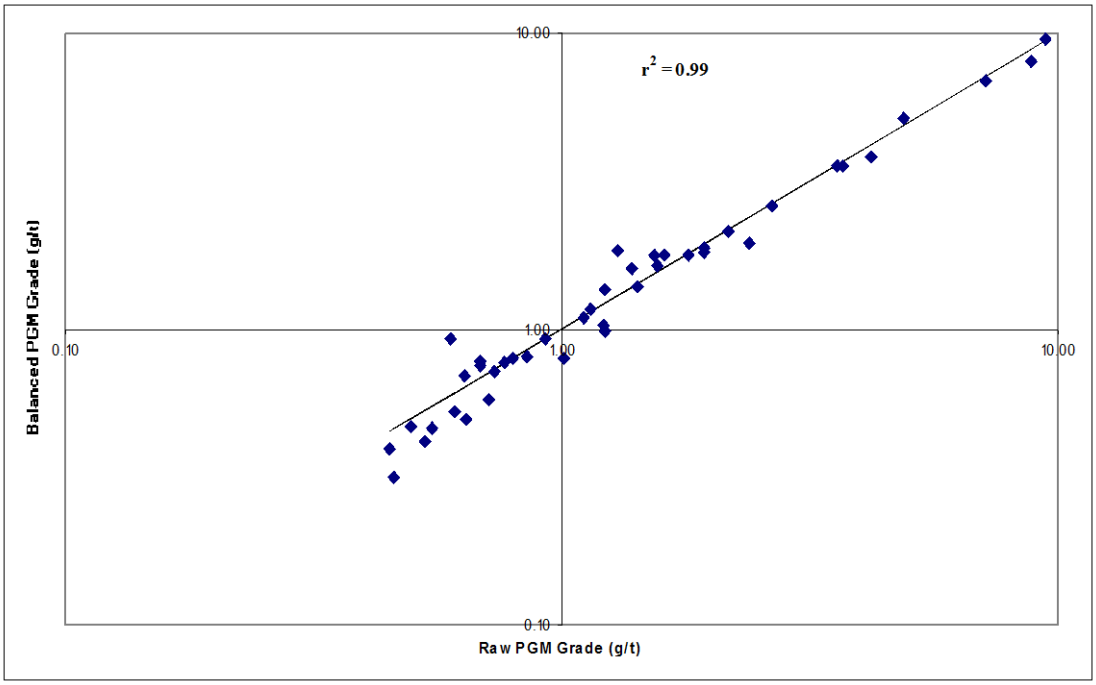

Figure 5.4 Balanced vs. Raw PGM Grades for MF1 and MF2 fractional analysis

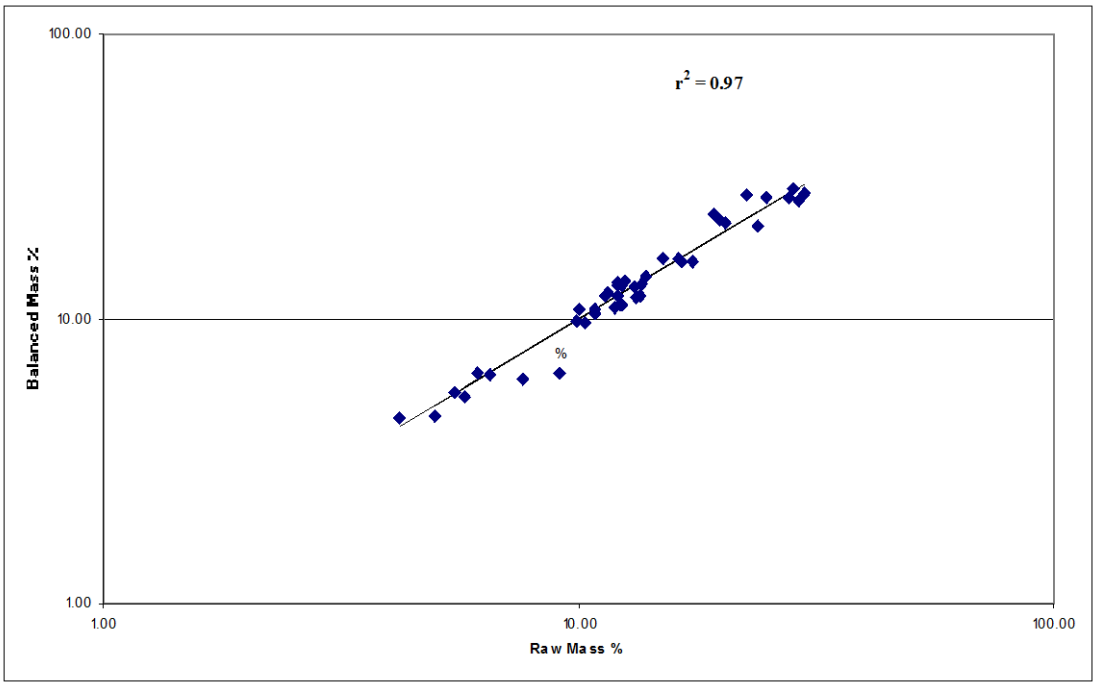

Figure 5.5 Balanced vs. Raw mass percentages for MF1 and MF2 fractional analysis

Figures 5.4 and 5.5 show that more manipulation of the raw data was required to achieve a mass balance for the fractional analysis than for the circuit balances. Because of the difficulty in achieving sufficient amount of sample for analysis by size fraction, it was not possible to do repeats on these samples. The lack of repeats, combined with the difficulties in mass balancing across size fractions resulted in the relatively large changes. However, because of the large number of data points, the correlation between raw and balanced data is still greater than 0.97.

5.3.3 Batch flotation

For each batch flotation test, the mass and PGM grades were balanced so that the build-up head grade corresponded with the value determined by the circuit balance. The balanced PGM grades and mass percentages versus raw data for both circuits are shown in Figures 5.6 and 5.7 respectively:

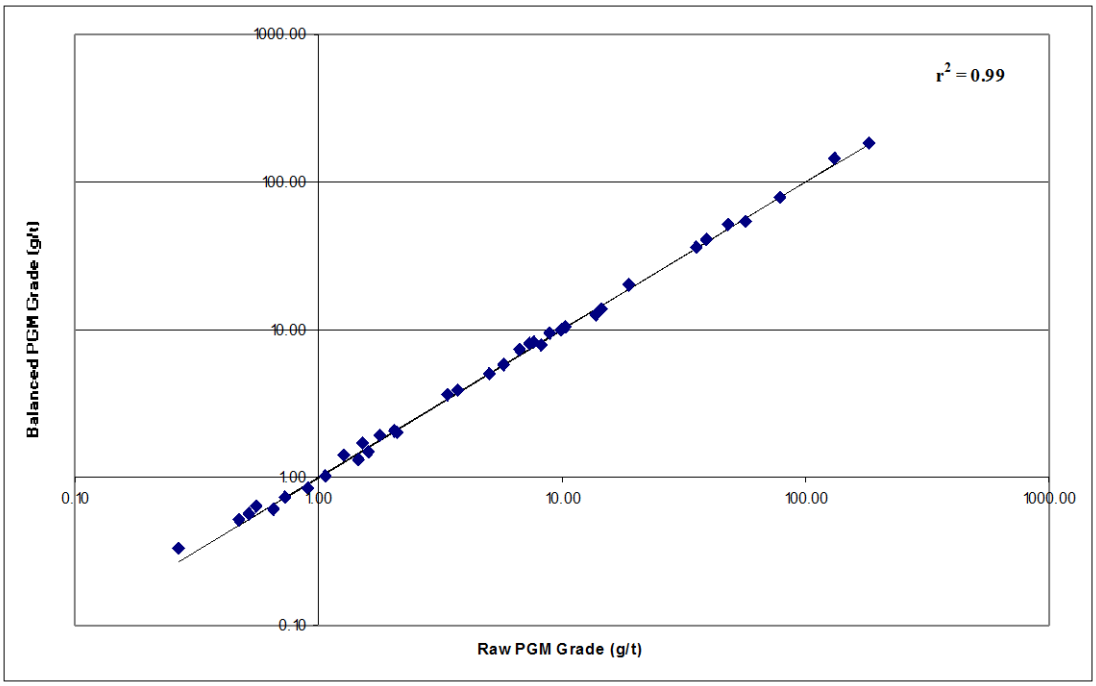

Figure 5.6 Balanced vs. Raw PGM Grades for MF1 and MF2 batch floats

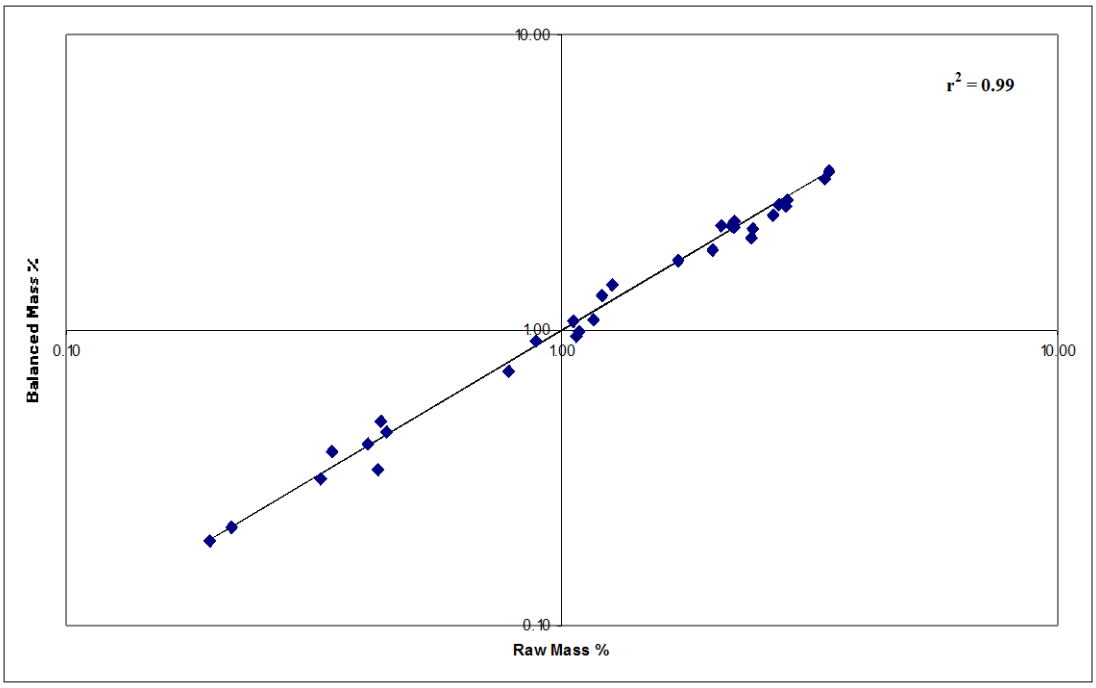

Figure 5.7 Balanced vs. Raw mass percentages for MF1 and MF2 batch floats

The graphs show that little manipulation of the raw data was required to obtain batch flotation balances that agree with the circuit balance. The correlation coefficient between raw and balanced data is also higher than 0.99 for PGM grades and mass percentages.

5.3.4 Comparing feed and tails values between data sets

Feed and tail PGM assays have the largest impact on recovery. Therefore, the validity of any conclusions concerning recovery will be determined by the accuracy of these values. Comparing raw data from the circuit sampling campaigns with the raw build-up head grades from the batch flotation and fractional analysis can give an indication of the consistency of these numbers. These grades are shown in Table 5.2:

Table 5.2 Feed and tail PGM grades (g/t) for the two configurations tested

	Raw Circuit	Build-up from Raw Fractional	Build-up from Raw Batch	Fitted
MF1 Primary Feed	3.80	3.94	3.72	3.81
MF1 Primary Tail	0.77	0.77	0.79	0.81
MF2 Primary Feed	3.80	3.90	3.84	3.80
MF2 Primary Tail	1.64	1.55	1.70	1.60
MF2 Secondary Feed	1.57	1.50	1.74	1.60
MF2 Secondary Tail	0.83	0.80	0.70	0.76

From Table 5.2 it can be seen that the raw data from the circuit compares favourably with the build-up values from the raw fractional analysis and batch flotation data. These numbers are also similar to the values that were determined by mass balancing. When considering that the circuit, batch flotation and fractional analysis samples were taken separately during the sampling campaigns, the consistency in the assays suggest that the values were representative of the plant performance.

5.4 Flotation

The PGM recovery versus residence time curves for the two configurations are displayed in Figure 5.8.

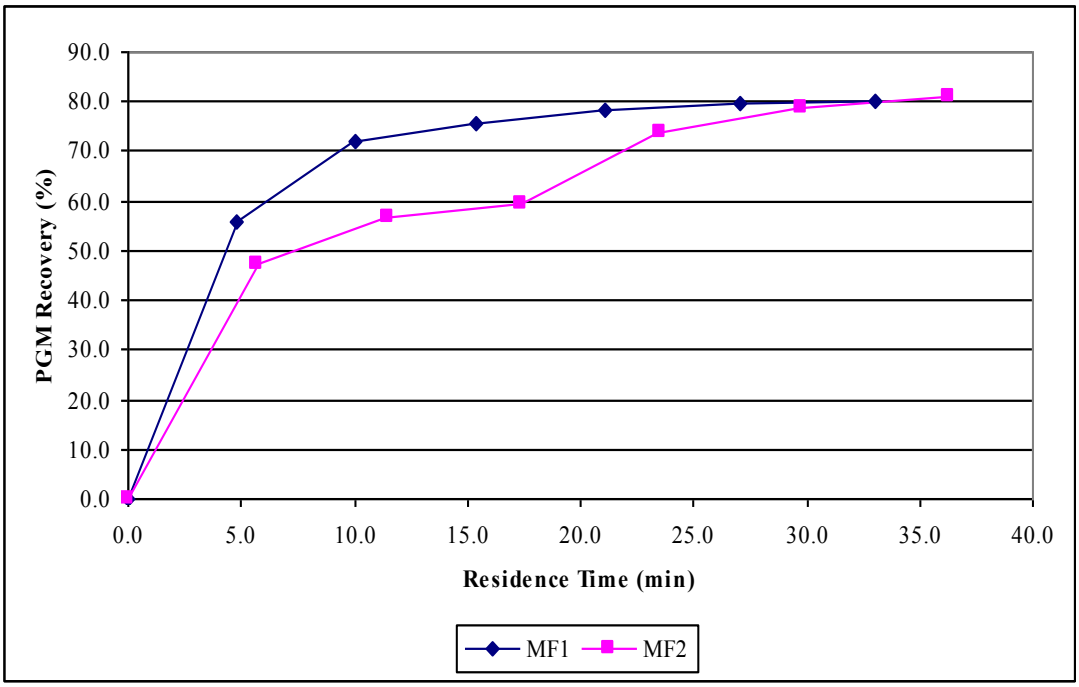

Figure 5.8 PGM Recovery vs. Residence Time curves for the MF1 and MF2 circuits

As was the case with the first campaign, the MF1 configuration displayed the fastest initial rate of PGM recovery. The MF2 secondary milling stage also increased the flotation rate, resulting in a higher overall PGM recovery.

Figure 5.9 shows the PGM recovery versus PGM grade curves, while the PGM grade for each cell is displayed in Figure 5.10:

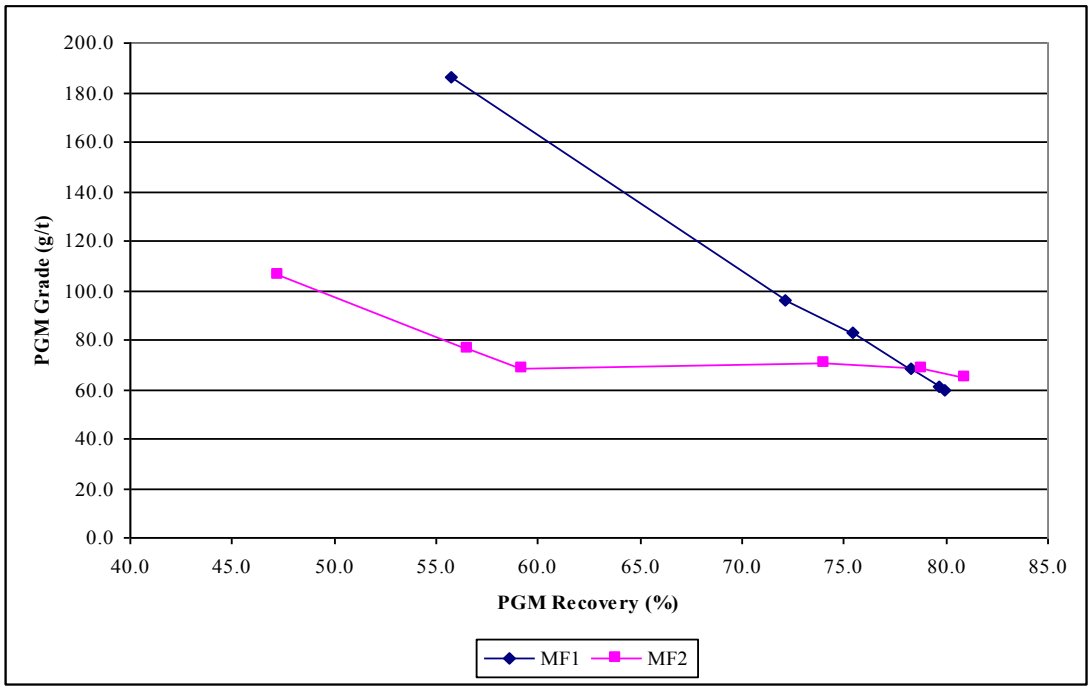

Figure 5.9 PGM Recovery vs. PGM Grade for the MF1 and MF2 circuits

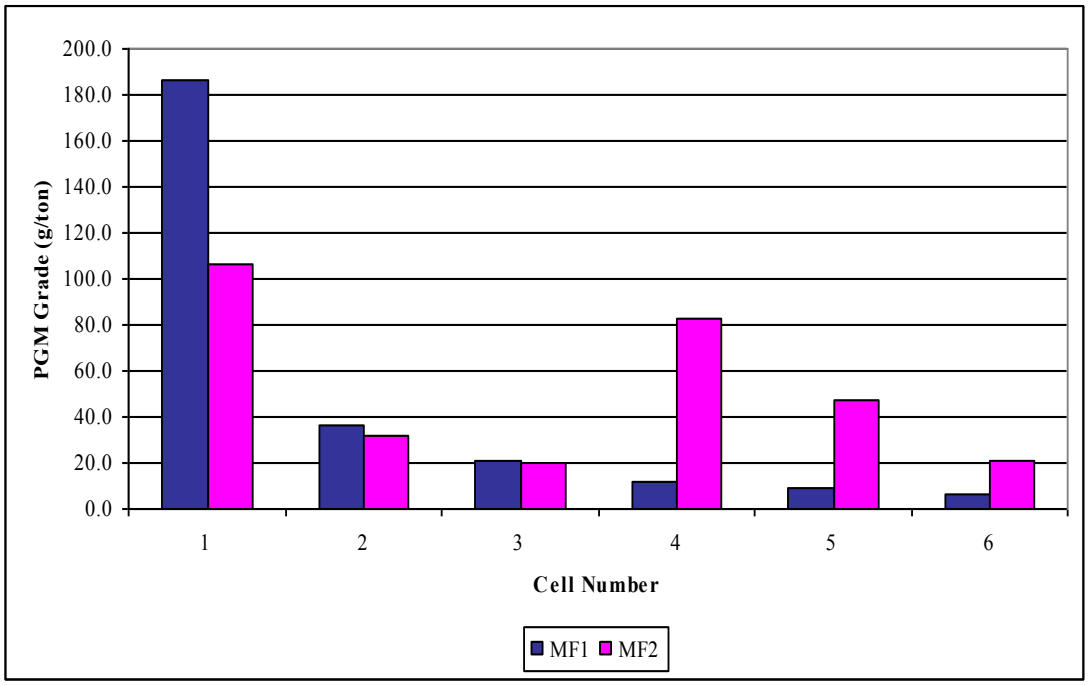

Figure 5.10 PGM Grade per cell for the MF1 and MF2 circuits

As was the case for the first campaign, the MF1 circuit achieved the highest initial grades – also shown in the grade-by-cell analysis. Once again the regrind resulted in an increase in grade at Cell 4.

5.5 Flotation by size

The PGM units produced per size fraction for the two configurations are displayed in Figure 5.11. Note that the data was normalised to account for differences in PGM feed grade.

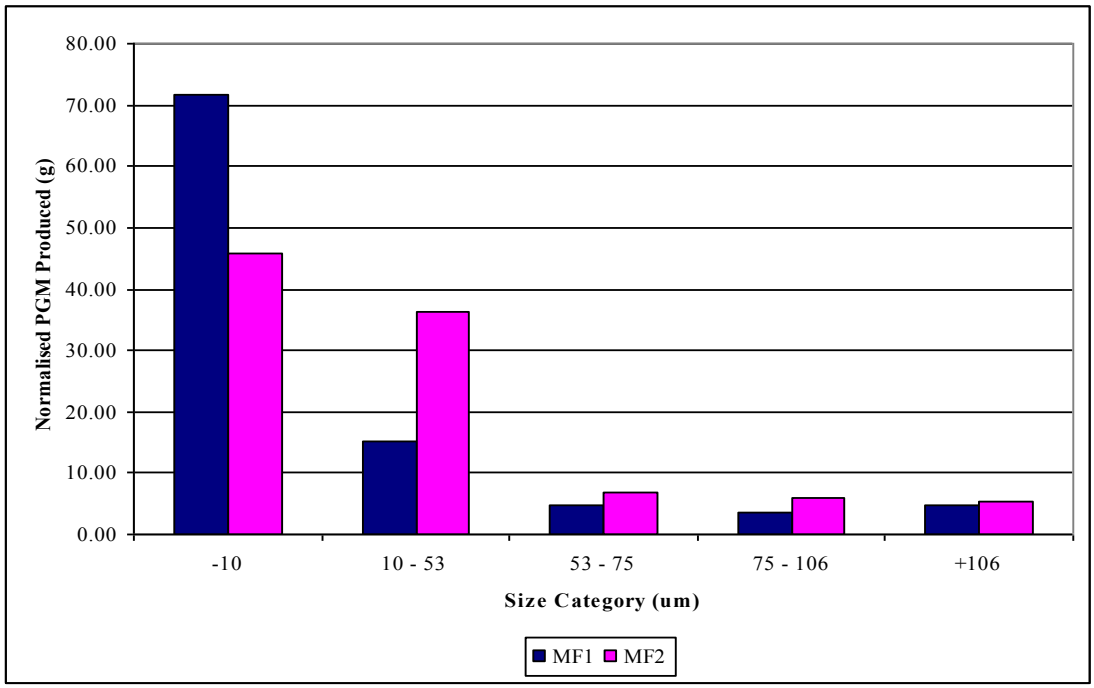

Figure 5.11 PGM units produced per size fraction for the MF1 andMF2 circuits

The PGM losses per size fraction are shown in Figure 5.12, and the recovery per size fraction in Figure 5.13:

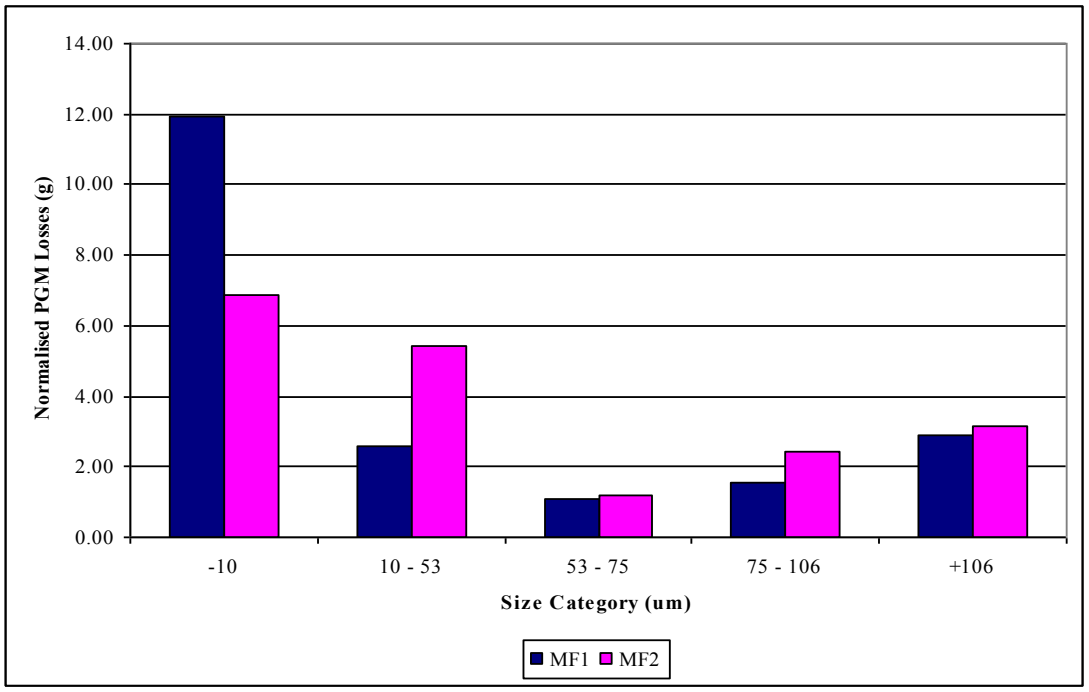

Figure 5.12 PGM losses per size fraction for the MF1 and MF2 circuits

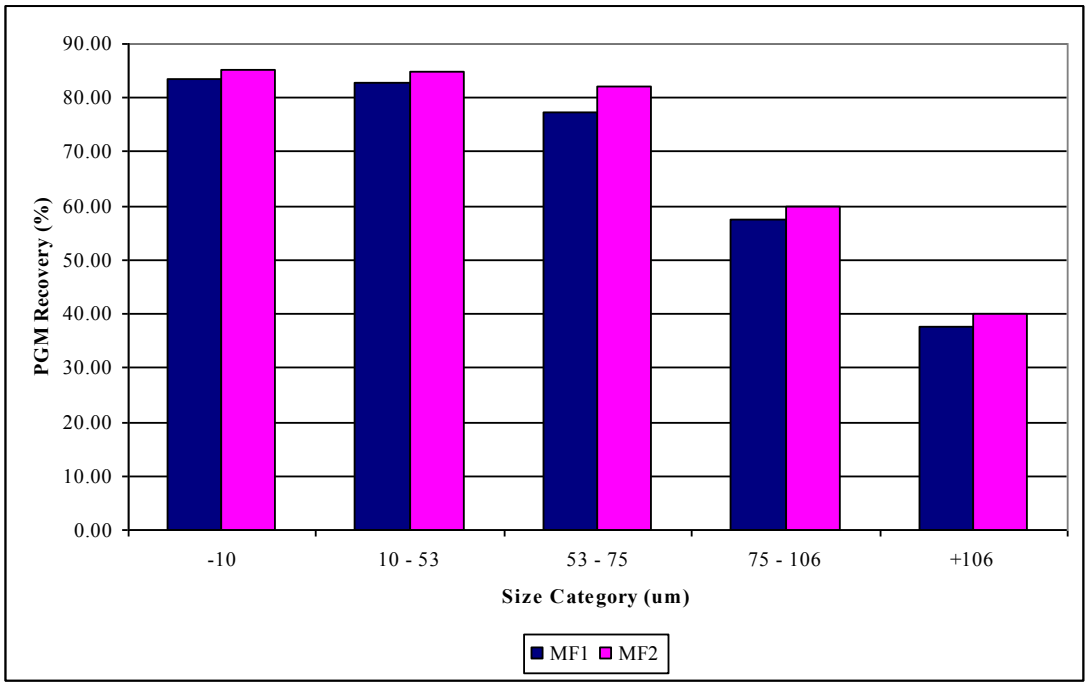

Figure 5.13 PGM recovery by size fraction for the MF1and MF2 circuits

The PGM's produced by size fraction (Figure 5.11) shows that the MF1 circuit produced the most PGM particles in the –10µm size fraction, while in Figure 5.12 it can be seen that the losses in the -10µm fraction was also highest for that circuit. The recovery by size graph reveals that the MF2 circuit produced higher PGM recoveries in all size fractions, and that PGM recovery increased with a decrease in size fraction for both circuits.

As was discussed in Chapter 4.6, modelling of the flotation results for each circuit should assist in separating the effects of milling device, liberation characteristics and the circuit configuration.

5.6 Mineralogy of flotation feed

The general mineralogy and relative proportion of PGE minerals of the primary flotation feeds are the same as for the crushed ore sample. Results for PGE mineral grain size distribution and mode of occurrence are presented in Tables 5.3 and 5.4 respectively. The numbers represent the number of grains in each class.

Table 5.3 PGE mineral grain size distribution of primary flotation feed

Size (μm)	MF1 (%)	MF2 (%)
0-2	42.4	27.5
2-4	34.2	41.8
4-6	13.6	11.5
6-8	7.3	12.5
8-10	1.7	1.8
>10	0.8	4.9

Table 5.4 PGE mineral mode of occurrence

	MF1 (%)	MF2 (%)
Lib	35.1	24.3
Lock BMS	8.9	16.8
GB BMS-Si/Cr	35.3	18.8
Lock Si	7.1	22.4
GB Si-Si/Cr	2.7	5.9
Lock Cr	10.9	11.8

These results will be discussed in more detail in Chapter 9 and 10, along with the effect of milling devices and circuit configuration.

CHAPTER 6
DATA ANALYSIS METHODOLOGY AND MODEL DEVELOPMENT

6.1 Introduction

In order to support the analysis of results, the empirical floatability component (EFC) flotation model discussed in the Literature Review was applied to experimental results on a size-by-size basis. However, it was not possible to collect sized batch flotation data for the campaigns. As a result, it was problematic to link the sized circuit model parameters with unsized parameters for the batch tests. This caused difficulty in applying the model as currently defined in the literature. In this chapter, a methodology is proposed to take account of information provided by un-sized batch data in a size-by-size circuit model.

6.2 Modelling methodology

From the Literature Review, the general form of the EFC model that was selected to determine the floatability components of the ore is shown in Equation 2.23:

$$R_i = \frac{P_i S_b \tau R_{f,i}(1-R_w) + R_w ENT_i}{(1+P_i S_b \tau R_{f,i})(1-R_w) + R_w ENT_i} \qquad (2.23)$$

The overall recovery can then be expressed as follows:

$$R = \sum_{i=1}^{n} m_i R_i \qquad (2.24)$$

While some of the model parameters could be measured or calculated, the following had to be determined by a model fitting exercise:

β - determines froth recovery via Equation 2.19

ENT_i - classification function that determines entrainment

P_i - floatability in floatability class i

m_i - mass in floatability class i

Fitting Equation 2.24 with such a large number of parameters will generally not yield a robust solution - in other words, a number of equally good solutions can present themselves without a clear way of distinguishing between these solutions. Batch flotation tests on selected streams in the circuit can be used to provide the additional information required to find a robust solution to the model. In order to achieve this, the circuit and batch data have to be fitted simultaneously to the respective models using common parameters that could be reasonably expected to be independent of the differences in flow and scale of the two systems. To model the batch flotation results, a modified version of Equation 2.8 was used that incorporates the non-floatable fraction via entrainment:

$$R = \sum_{i=1}^{n} x_i (1 - e^{-k_i t}) + f(ENT_i, R_{w,batch}) \qquad (6.1)$$

where:

x_i = mass fraction in floatability class i

k_i = rate constant of floatability class i

$R_{w,batch}$ = water recovery in the batch cell

Application of Equation 6.1 requires that the batch mass fraction parameters (x_i) be related to the circuit mass fraction parameters (m_i).

The form of the equation to calculate entrainment in the batch flotation tests had to be developed for this thesis, and is discussed later in the chapter. Since entrainability (ENT_i) is a function of the ore and independent of equipment, it can therefore be applied to calculate entrainment in both the circuit and batch flotation tests.

The procedure described above can be summarised in the following diagram:

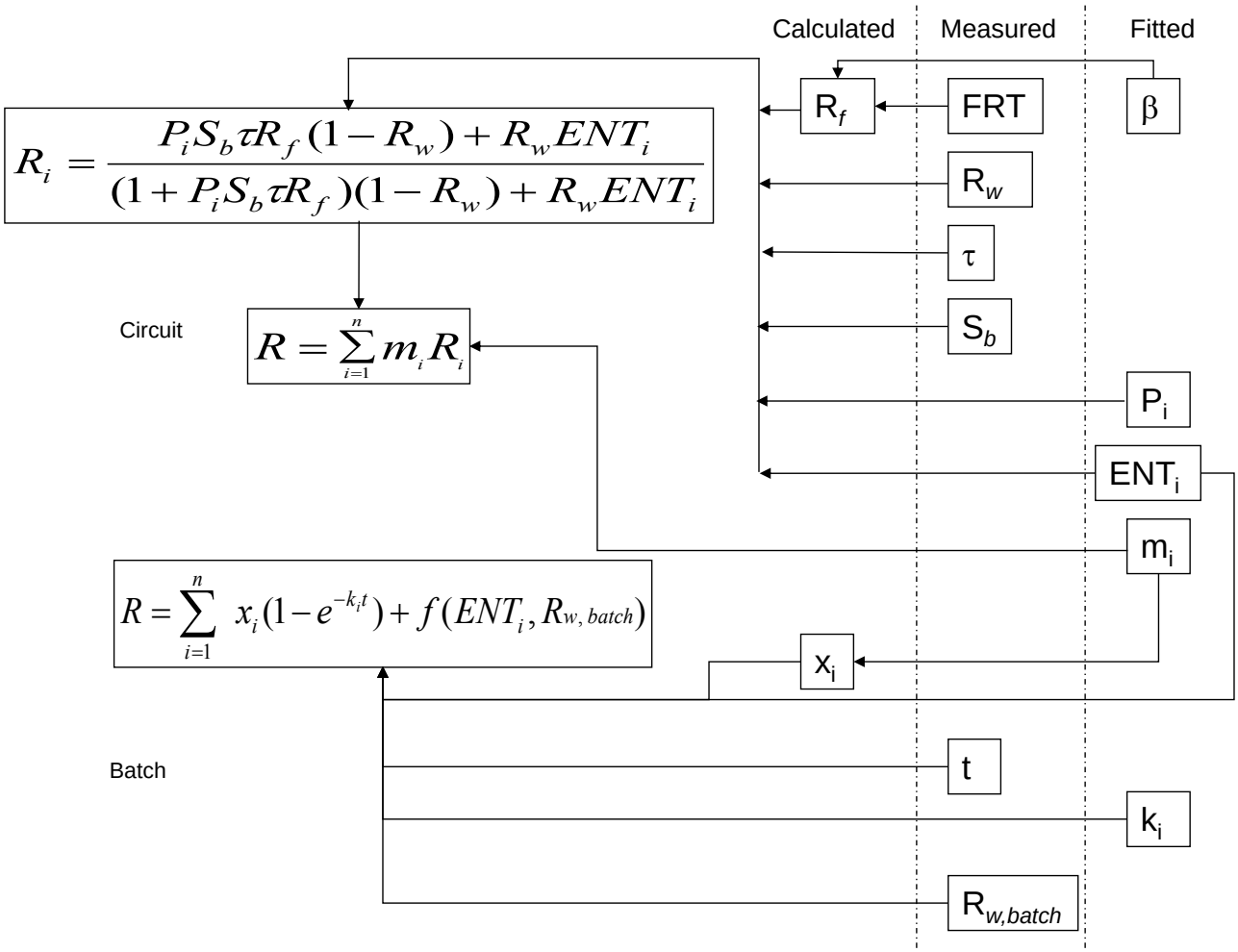

Figure 6.1 EFC modelling methodology

Figure 6.1 shows that the mass in floatability class i (m_i) and entrainability (ENT_i) are common to both the batch and continuous models. Therefore, these values can be used to link the two sets of data, thereby providing a route to finding a more robust solution of the model, provided the floatability numbers and rate constants (P_i, k_i and m_i) are calculated on the same size-by-size basis.

However, because of mass requirements for size-by-size PGM analysis, it was not possible to gather sized elemental data for the batch flotation tests in this project. Therefore, the unsized batch flotation data could not be used directly in conjunction with the sized circuit data. For example, the fastest floating material in a coarse size fraction might have different kinetics from the fastest floating fraction in the optimum size range, and both might be different from the fastest floating fraction in the unsized flotation feed. Therefore, the masses of these floatability classes could not be associated with each other, since each would refer to

different P and k values. Consequently, a new procedure had to be developed to allow the unsized batch data to be used in conjunction with the sized circuit data. This new methodology is summarised in Figure 6.2. Note that since ENT is dependent on size and water recovery and not on the floatability of the material, ENT_i for floatability class i had been replaced by ENT_{size}:

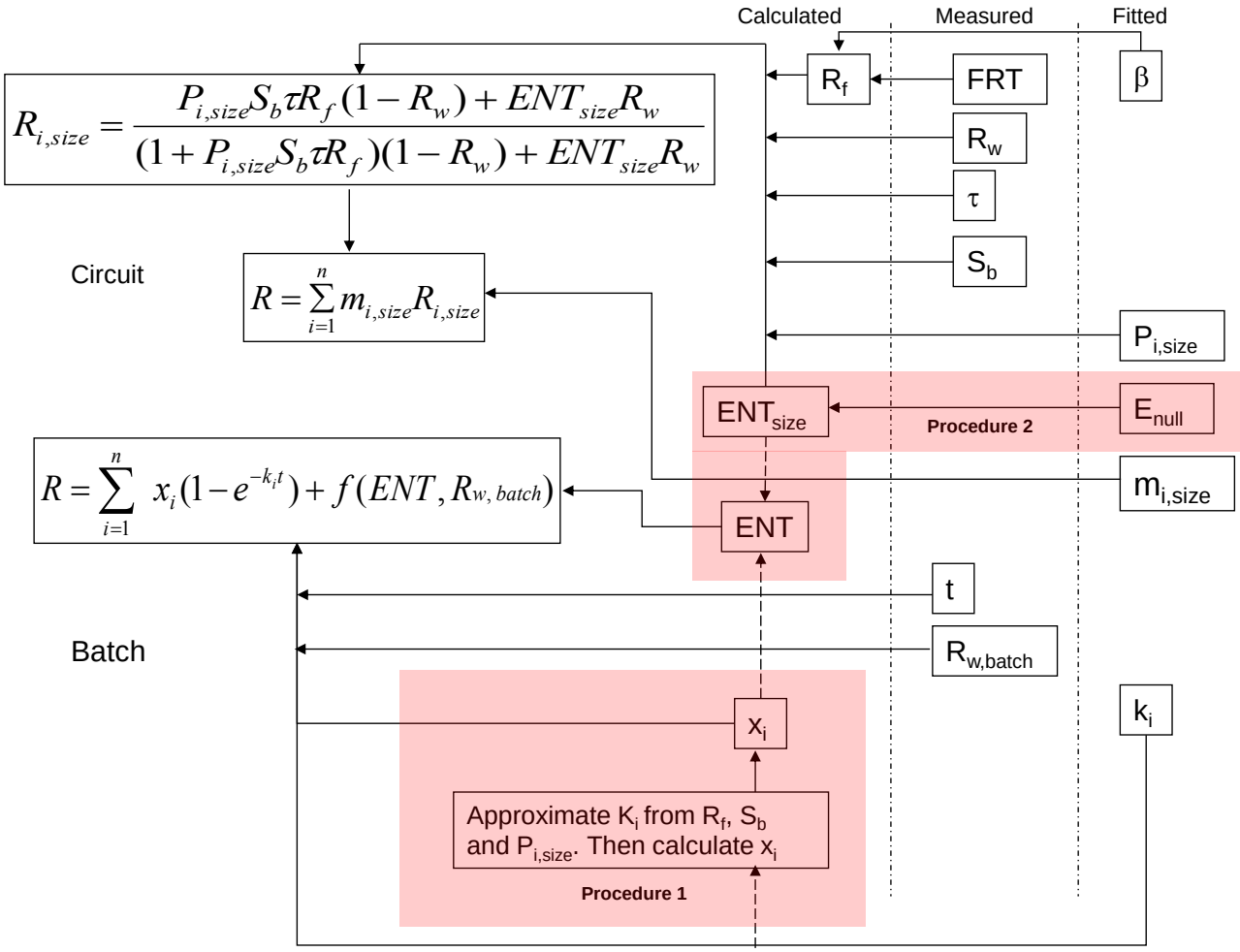

Figure 6.2 Modified EFC modelling methodology for disparate data sets

In Figure 6.2, the new procedures are highlighted by shading. Firstly, the link between m_i and x_i has been replaced with a methodology to calculate x_i from $P_{i,size}$, S_b and $R_{f,}$ (Procedure 1). Also, instead of fitting ENT for each size fraction, a single parameter ENT_{null} was fitted to calculate ENT per size fraction (Procedure 2). ENT_{null} refers to the maximum size above which entrainment becomes negligible. ENT for the batch flotation model was calculated from ENT_{size} and x_i, providing another link between the batch and circuit models. These methods will now be described in more detail, along with a detailed description of how all the modelling parameters were determined.

6.2.1 Procedure 1 – Determine x_i from $P_{i,size}$, S_b and R_f

As discussed in the precious section, a robust solution for the circuit model is achieved by fitting parameters that are common with the batch flotation model. Usually, these common parameters are Entrainability (ENT) and the amount of floatable material in each floatability class (m_i).

However, in this project the circuit model had to be fitted for different size fractions, with only unsized batch flotation data to assist in finding a robust modelling solution. Since the flotation kinetics in the size fractions are different from the kinetics of the unsized ore, the masses in the floatability classes would also differ. Therefore these masses are no longer common parameters that can be used to find a robust model solution. Instead, a new procedure was developed to calculate the unsized fast floating fraction from common parameters in the batch and circuit models.

The unsized fast floating fraction is a characteristic of the ore, and should be the same for the batch tests and the circuit. Although fast floating masses are fitted for each size class in the circuit ($m_{i,size}$), it would be incorrect to simply add these masses to get the overall amount of fast floating material (because of differences in kinetics between the size classes). For instance, if the fast floating rate constant in the +75μm fraction is significantly slower than the fast floating rate constant in the +10μm fraction, it would be incorrect to add the masses in these two "fast" floating fractions. Conversely, it is possible that some of the slow floating material in the +10μm size class would be considered fast floating in the context of the overall circuit. Therefore, a procedure was developed to calculate the amount of unsized, fast floating material from each size and floatability class. In order to accomplish this, firstly the rate constants for each floatability class (i) and size fraction in the circuit ($K_{i,size}$) was calculated from the following equation:

$$K_{i,size} = P_{i,size} \cdot R_f \cdot S_b \qquad (6.2)$$

These sized rate constants were then compared to the unsized rate constants that were fitted for the batch flotation tests to determine the contribution in each size class to the overall, unsized fast floating fraction (Figure 6.3):

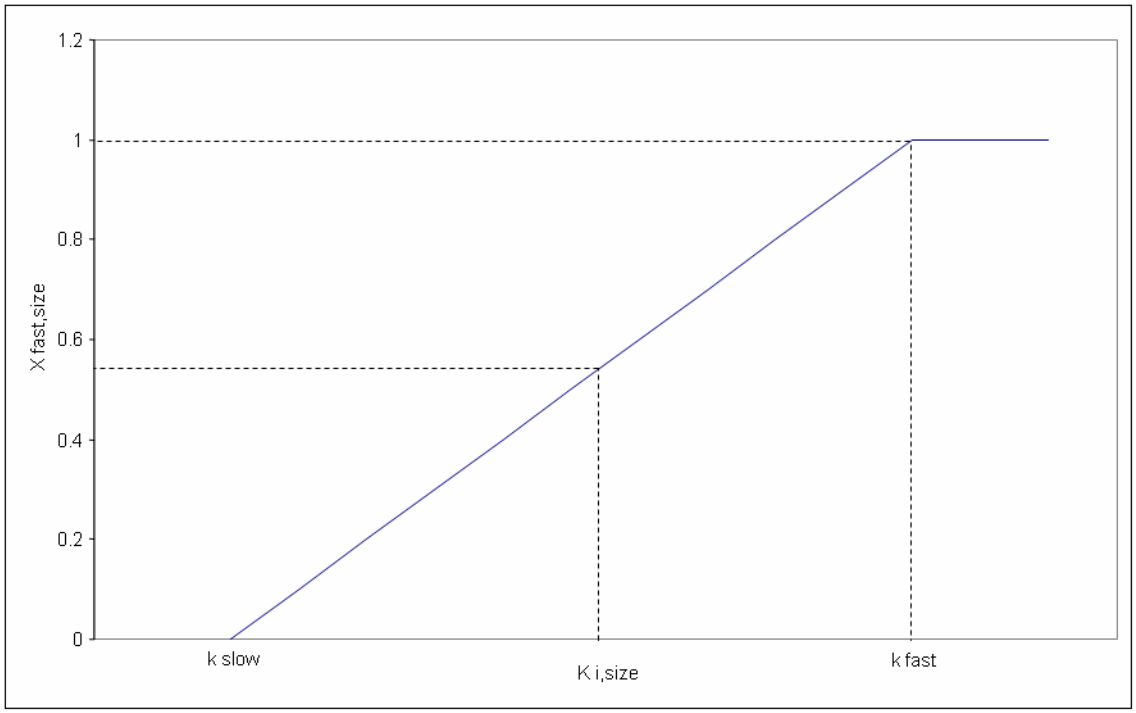

Figure 6.3 Relationship between $x_{i,fast}$ and $K_{i,size}$

In Figure 6.3, k_{fast} and k_{slow} were the fitted rate constants for the batch flotation tests, while $K_{i,size}$ was calculated for each size and floatability class (i) in the circuit from Equation 6.2. It was assumed that all material in a size class is fast floating when $K_{i,size}$ is equal to or greater than k_{fast}, and no material is fast floating when $K_{i,size}$ is equal to or smaller than k_{slow}. If $K_{i,size}$ falls between k_{fast} and k_{slow}, the fast floating fraction in the size fraction was calculated from a linear relationship as shown in Figure 6.3. The amount of fast floating material in each size and floatability class was added to get the total fast floating fraction in a stream (x_{fast}).

The linear relationship shown in Figure 6.3 was not investigated in detail, but was found to be a plausible approximation that fitted the data well. It is also important to note that this procedure does not imply that the rate constants in the circuit and batch flotation tests are the same. It only seeks to estimate the amount of unsized fast floating material from sized circuit kinetics and unsized batch kinetics, thereby providing a common link between the two models.

6.2.2 Procedure 2 – Entrainment by size fraction

Entrainability (ENT) is a function of size and density, thus different ENT values are required for each size class. However, in order to minimise the number of fitted parameters it was decided to describe entrainability with a size dependent function. Various functions were tested, and it was found that an exponential decay of ENT with size was both very simple and able to describe the data very well. Only one parameter was fitted: ENT_{null}, which represents the size above which entrainment becomes insignificant. ENT_{null} was selected because it allows for comparison with the value found by Robertson (2002) for UG2 ore. Figure 6.4 shows a graphical representation of ENT versus size:

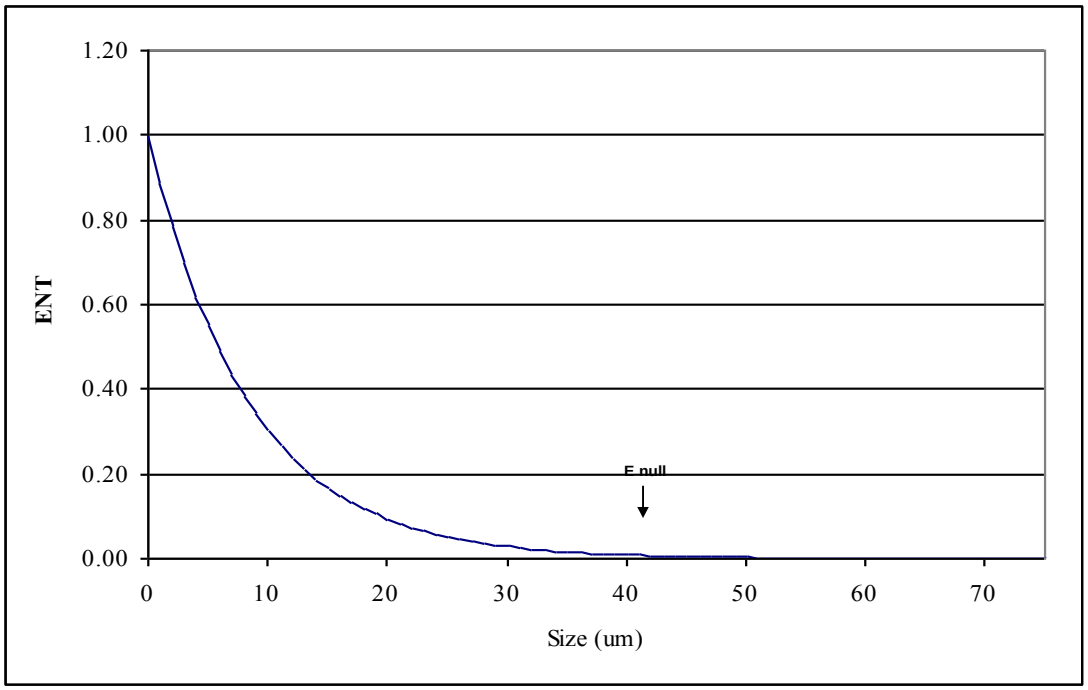

Figure 6.4 ENT versus Size

Although it is likely that a two parameter equation would provide a better estimation of ENT_{size}, it was not the aim of this thesis to investigate this relationship in detail. A more accurate function would likely add to the number of fitted parameters, which was contrary to the objective of this procedure. As stated earlier, it was found that a one-parameter exponential decay function with ENT_{null} described the data very well.

6.2.3 Measured parameters

As shown in Figure 6.2, residence times for the froth phase, batch flotation tests and circuit were measured, as well as all water recoveries. Although S_b was not a direct measurement, it was calculated from direct measurements only - as described in the Literature Review (section 2.3.2.1).

6.2.4 Calculated parameters

From Figure 6.2, the following modelling parameters were calculated: floatability mass fractions for the batch flotation tests (x_i), entrainability by size (E_{size}) and froth recovery (R_f). The procedures to calculate x_i and E_{size} were discussed in 6.2.1 (Procedure 1) and 6.2.2 (Procedure 2) respectively. Equation 2.19 from the Literature Review was used to calculate froth recovery:

$$R_f = e^{-\beta.FRT} \qquad (6.4)$$

β is a fitted parameter, and only one value was calculated for all size fractions. Although R_f is dependant on size, this effect is most prominent in the larger size classes. In the system that was investigated, virtually all the particles in the froth are very fine (sub 50μm). Under these conditions, the assumption that R_f is constant is a reasonable approximation that described the data well with minimal modelling parameters.

6.2.5 Fitted parameters

The model was developed on a size basis for the following three size fractions: +75μm, +10μm-75μm and -10μm. Two floatability classes were fitted for each size class. The following model parameters were fitted for the full circuit and associated batch flotation tests.

$P_{fast,size}$:	Floatability of fast floating particles in each size class
$P_{slow,size}$:	Floatability of slow floating particles in each size class
$m_{fast,size}$:	Mass of fast floating material in each size
$m_{slow,size}$:	Mass of slow floating material in each size

k_{fast}:	Batch flotation rate constant for unsized fast floating material
k_{slow}:	Batch flotation rate constant for unsized slow floating material
ENT_{null}:	Size above which entrainment becomes insignificant
β:	Froth recovery constant

Note that the floatability classes for each size fraction are relative to that size fraction only. It is often found that the fast floatability in a coarse size class is less than the slow floatability in another, more optimal size class. Therefore the terms fast and slow is only applicable to the same size class. As discussed earlier, this necessitated the development of Procedure 1 to reconcile the sized floatability classes with the unsized fast and slow floatability classes.

6.2.6 Entrainability relationship for batch flotation tests

A procedure to account for entrainment in the batch tests is particularly important, owing to the relatively high recovery of water to the concentrate in this type of test. A batch flotation experiment exhibits a response equivalent to that which is obtained from a plug flow reaction system. The plug flow system can be well approximated by a line of sequential steady state continuous stirred tank reactors, and it is this principle that was used to derive a suitable relationship for batch flotation entrainment. The batch flotation system was divided into different stages based upon the timed concentrate samples that were collected. For these tests the first stage would be from 0 – 1 minute (as per Experimental Procedure), and the recovery via entrainment for this stage can be summarized in the following diagram:

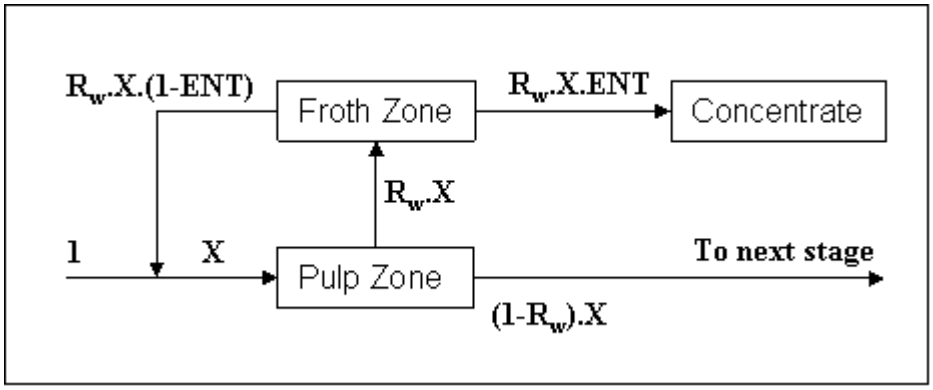

Figure 6.5 Recovery via entrainment for the first stage in a batch flotation system

In Figure 6.5, ENT represents the entrainability value and R_w the water recovery. The feed to the stage is defined as 1, and the feed to the pulp zone as an unknown (X). The first step is to construct a mass balance across the stage and solving for X:

$$1 = R_w X.ENT + (1 - R_w)X \qquad (6.5)$$

$$X = \frac{1}{1 - R_w + R_w ENT} \qquad (6.6)$$

The recovery (R) is equal to R_w.X.ENT – substituting for X yields the following equation:

$$R = \frac{R_w ENT}{1 - R_w + R_w ENT} \qquad (6.7)$$

Following the principle of sequential steady state continuous stirred tank reactors, the tails from the first stage is now fed to the second stage in the batch flotation test (1 - 2.5 minutes) – this stage is depicted as follows:

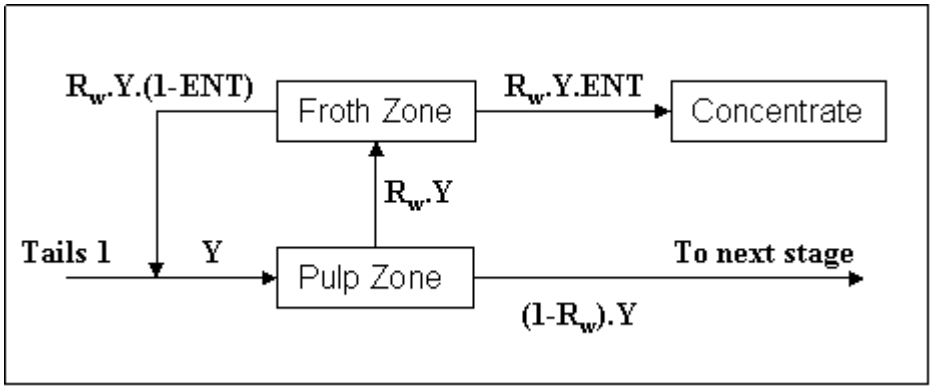

Figure 6.6 Recovery via entrainment for the second stage in a batch flotation system

In this instance, Y can be solved for as follows by constructing a mass balance across the stage:

$$\text{Tails}\,1 = R_w Y.ENT + (1 - R_w)Y \qquad (6.8)$$

$$Y = \frac{\text{Tails}\,1}{1 - R_w + R_w ENT} \qquad (6.9)$$

Recovery (R) over the second stage is equal to the following:

$$R = \frac{R_w Y.ENT}{\text{Tails } 1} \qquad (6.10)$$

substitute Y:

$$R = \frac{R_w ENT}{1 - R_w + R_w ENT} \qquad (6.11)$$

The equation for recovery via entrainment for the first and second stages in the batch flotation test has exactly the same form (Equations 6.7 and 6.11). This will be true for any number of stages defined for a batch flotation system. It is important to note that the equation is based upon the feed *into the stage*, and not the original feed into the batch flotation cell. Therefore, to apply this formula to calculate entrainment in a batch flotation cell, it must also be based upon the feed into the relevant stage. For this project, the amount of material recovered via entrainment for each stage in the batch flotation test was calculated from Equation 6.11, and added to the material recovered via true flotation (Equation 6.3).

6.3 Gangue modelling

The entrainability and froth recovery values (ENT_{null} and β) fitted for the PGM model were also used in the gangue model. Therefore, only the following parameters were fitted for gangue:

$P_{fast,size}$:	Floatability of fast floating particles in each size class.
$P_{slow,size}$:	Floatability of slow floating particles in each size class.
$m_{fast,size}$:	Mass fraction of fast floating material in each size.
$m_{slow,size}$:	Mass fraction of slow floating material in each size.
k_{fast}:	Batch flotation rate constant for unsized fast floating material
k_{slow}:	Batch flotation rate constant for unsized slow floating material

6.4 Model Evaluation

The decoupled kinetic model used in this thesis to assist with data analysis has been described in a lot of detail in the Literature Review. Although the actual model has been well established, some of the methods used to determine the modelling parameters are new. This requires an assessment of these methods after modelling has been completed, and will be done at the end of Chapter 7. The following methods will be evaluated:

- Procedure 1 - Consolidation of unsized batch flotation data and sized circuit data by calculating a sized circuit rate constant $K_{i,size}$ from $P_{i,size}$, S_b and R_f, and calculating x_{fast} for the stream by comparing circuit and batch rate constants.
- Procedure 2 - Determining entrainability by size from an exponential decay function and ENT_{null}

CHAPTER 7
DATA ANALYSIS WITH RESPECT TO THE USE OF STEEL MEDIA

7.1 Introduction

Both the literature and operating experience suggest that a ball mill with steel media would be expected to produce a different floatability profile to that obtained in a stirred mill with inert media. Therefore, it was hypothesised that a different set of floatability numbers would be produced in a ball mill and a stirred mill. To test this premise, in this chapter the results from circuits with a ball mill before flotation (steel circuits) were fitted to the flotation model presented in the previous chapter. In the next chapter, these floatability values are applied to circuits with a stirred mill before flotation (inert circuits). Finally, an independent set of floatability values are fitted for the inert circuits to determine which floatability set is best able to describe the inert data.

Model fitting followed the procedure discussed in the previous chapter to calculate modelling parameters. The steel circuits modelled in this chapter were Campaign 1 MF2 primary, Campaign 1 MF3 primary and Campaign 2 MF2 primary circuits.

7.2 PGM Modelling

7.2.1 PGM modelling parameters

The revised EFC modelling methodology described in Chapter 6 were applied to the raw data for steel circuits. An evaluation of the new methodologies will be conducted at the end of the chapter.

Floatability

The floatabilities determined for each size fraction are shown in Table 7.1, and the mass fractions in Table 7.2:

Table 7.1 PGM floatability numbers

	P_{fast} x10^{-4}	P_{slow} x10^{-4}
+75µm	5.85	0.77
+10µm-75µm	9.78	4.81
-10µm	5.37	0.77

Table 7.2 PGM mass fractions in feed

	Campaign 1 MF2 Primary	**Campaign 1 MF3 Primary**	**Campaign 2 MF2 Primary**
+75µm fast	0.07	0.06	0.12
+75µm slow	0.23	0.21	0.14
+75µm non	0.70	0.73	0.74
+10µm fast	0.58	0.64	0.56
+10µm slow	0.15	0.14	0.09
+10µm non	0.27	0.22	0.35
-10µm fast	0.58	0.63	0.59
-10µm slow	0.39	0.35	0.33
-10µm non	0.03	0.02	0.08

Campaign 1 MF2 and MF3 primary circuits had similar mass fractions in all floatability classes, which was to be expected since the two circuits had virtually the same grind. For campaign 2 the MF2 primary circuit grind was coarser, as shown by the higher amount of non-floating values in the -10µm and +10µm fractions. In order to analyse the efficiency of the flotation section, the mass fractions that were fitted for the tails are shown in Table 7.3:

Table 7.3 PGM mass fractions in tails for the steel circuits

	Campaign 1 MF2 Primary	**Campaign 1 MF3 Primary**	**Campaign 2 MF2 Primary**
+75µm fast	0.00	0.00	0.00
+75µm slow	0.06	0.07	0.07
+75µm non	0.94	0.93	0.93
+10µm fast	0.00	0.00	0.01
+10µm slow	0.00	0.00	0.01
+10µm non	1.00	1.00	0.98
-10µm fast	0.01	0.01	0.08
-10µm slow	0.70	0.88	0.59
-10µm non	0.29	0.11	0.33

All three circuits displayed similar trends. Almost all fast floating material were removed from all size fractions, while some slow floating material remained in the +75µm and -10µm fractions. These observations will be discussed in more detail in Chapters 9 and 10.

Froth recovery and entrainability

Fitted values for threshold entrainability and the froth recovery rate constant are shown in Table 7.4:

Table 7.4 ENT_{null} and β

ENT_{null}	44.9µm
β	0.07

ENT_{null} indicates that 44.9µm is the maximum particle size where significant entrainment occurred. This value was not constrained, and corresponds well with the literature (Robertson, 2002). From ENT_{null}, the following entrainability values were calculated for each circuit and size fraction (Table 7.5):

Table 7.5 Entrainability for each circuit by size

	+75µm	+10µm	-10µm
Campaign 1 MF2 Primary	0.00	0.07	0.72
Campaign 1 MF3 Primary	0.00	0.07	0.72
Campaign 2 MF2 Primary	0.00	0.07	0.75

7.2.2 PGM model fit

In order to evaluate the adequacy of the model fit, PGM modelling versus experimental results for the three circuits are shown in Figures 7.1 to 7.3. Included are the PGM flow rates in individual rougher concentrates and tails, as well as the PGM content per size fraction for the combined rougher concentrate and rougher tails:

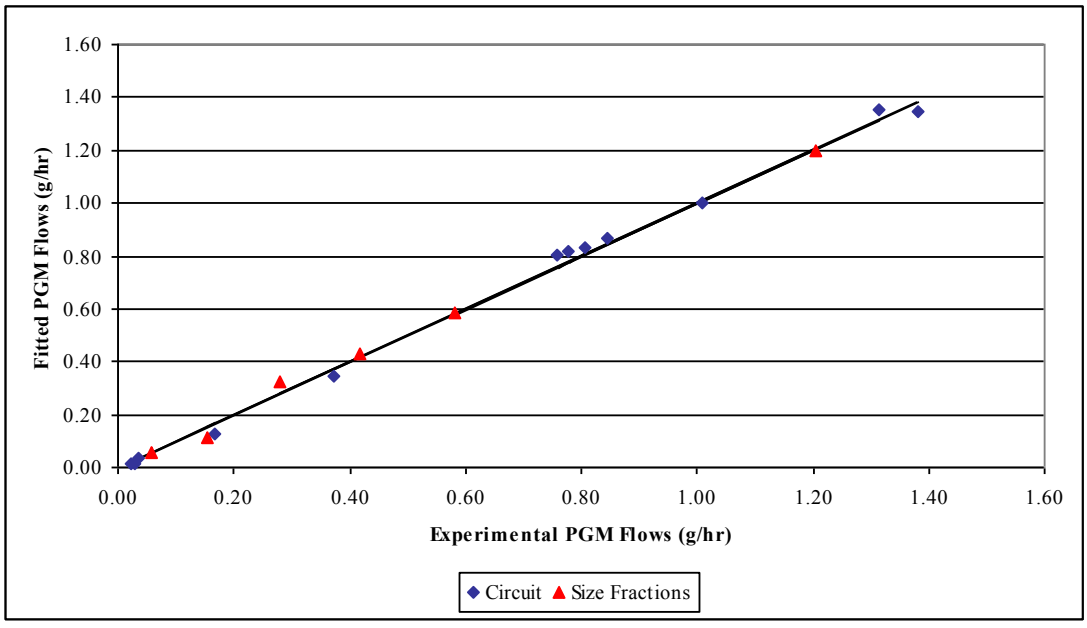

Figure 7.1 PGM modelling results for campaign 1 MF2 primary circuit

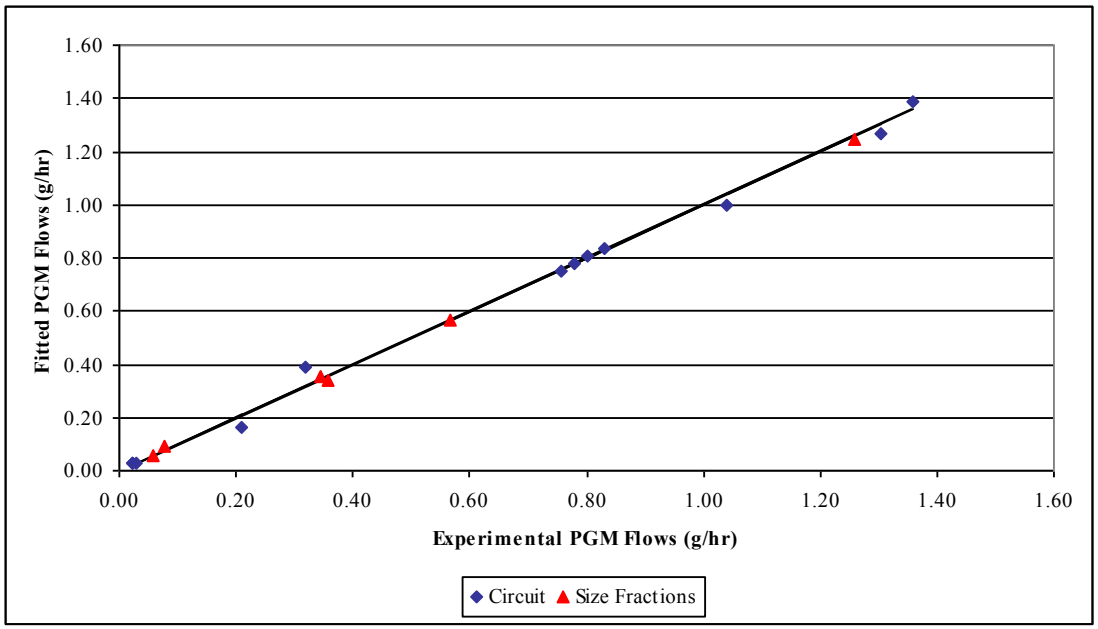

Figure 7.2 PGM modelling results for campaign 1 MF3 primary circuit

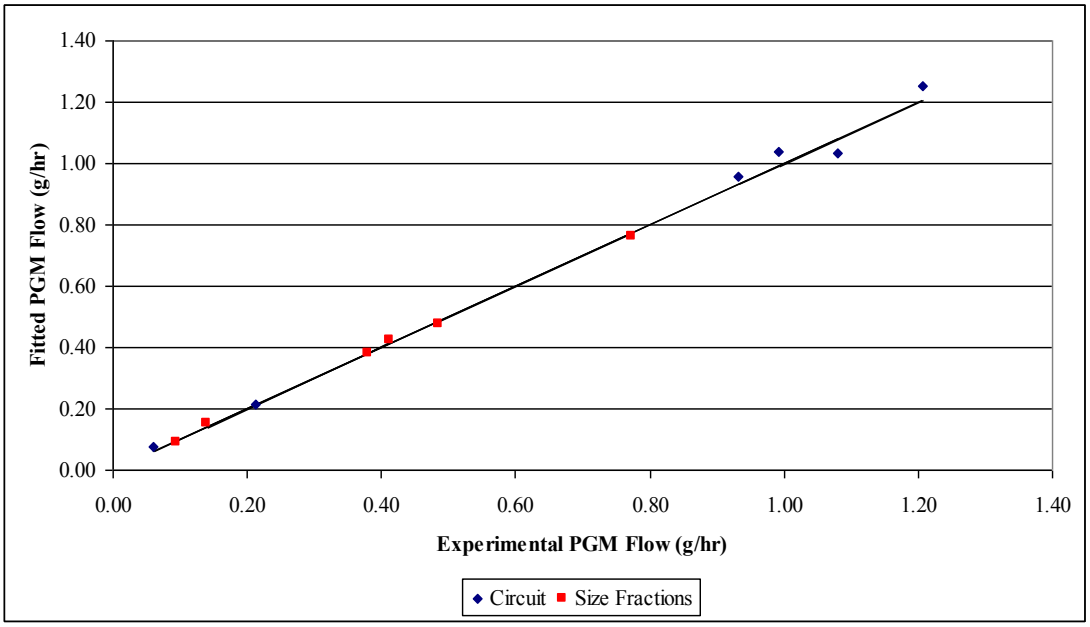

Figure 7.3 PGM modelling results for campaign 2 MF2 primary circuit

Figures 7.1 to 7.3 show that good model fits were achieved by applying the modified EFC model to the circuit data.

PGM modelling results for the batch flotation tests are shown in Figures 7.4 to 7.6. Experimental results are shown as data points, while the modelling results are shown as dotted lines:

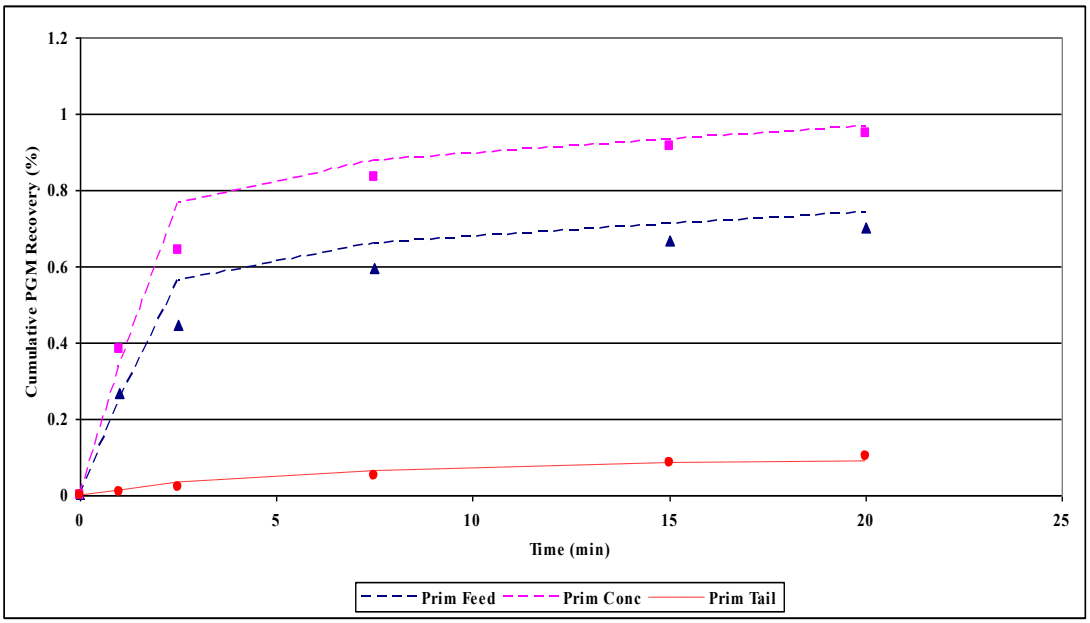

Figure 7.4 PGM batch flotation modelling results for campaign 1 MF2 primary circuit

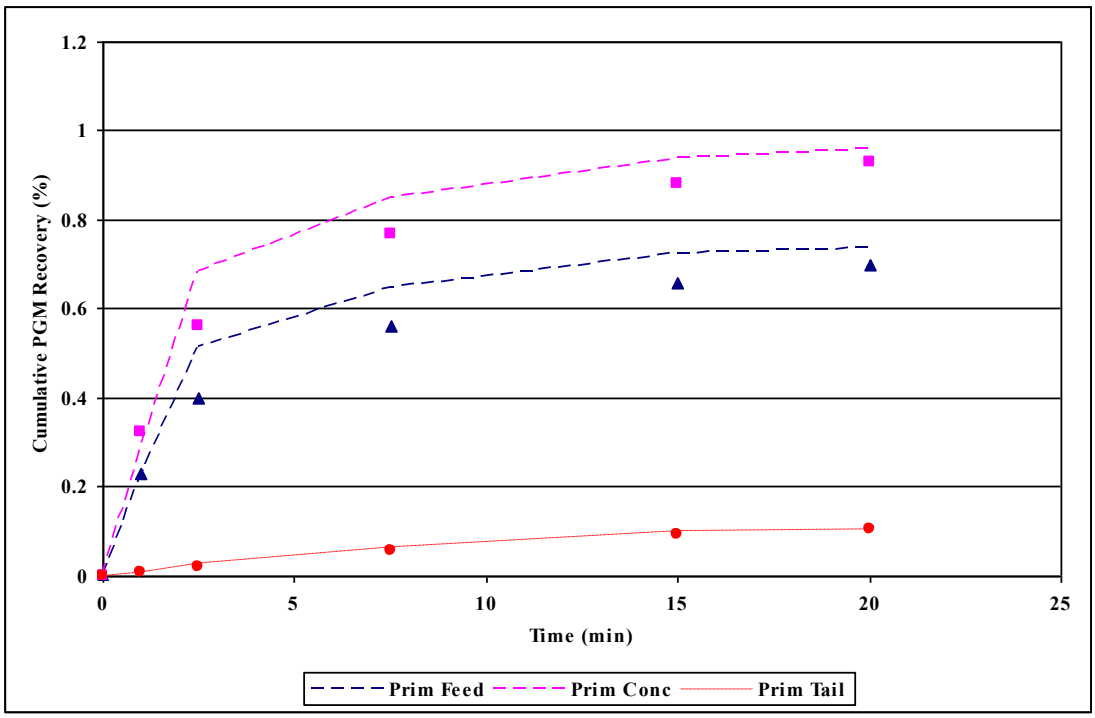

Figure 7.5 PGM batch flotation modelling results for campaign 1 MF3 primary circuit

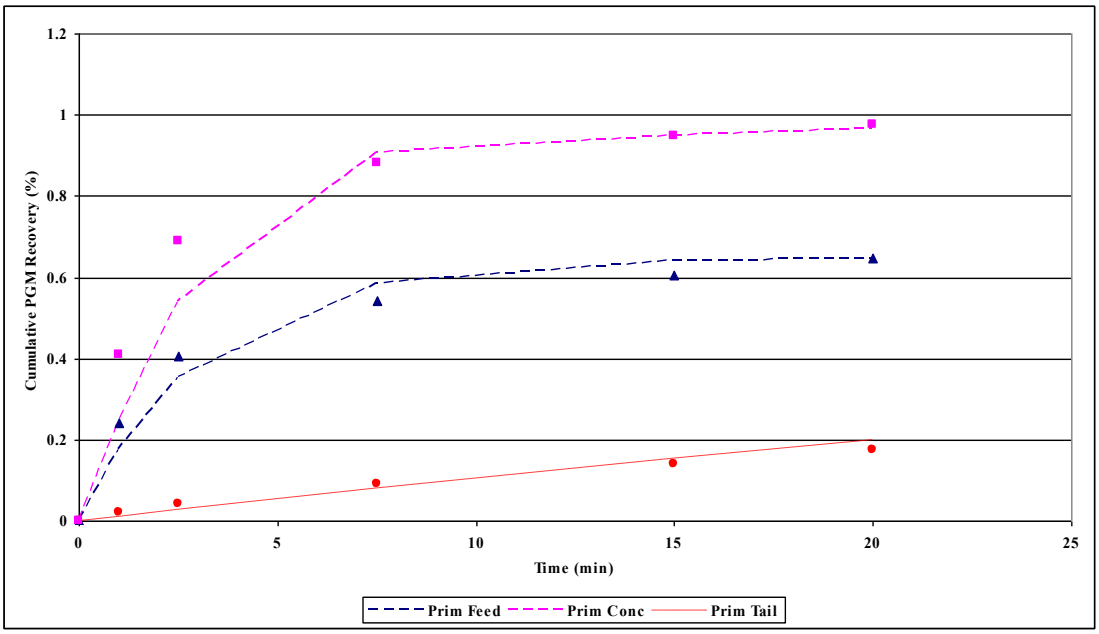

Figure 7.6 PGM batch flotation modelling results for campaign 2 MF2 primary circuit

Batch flotation modelling was less accurate than modelling for the circuit, especially for rougher concentrates. This is almost certainly because of the difficulty in controlling batch flotation mass pulls with highly floatable material. However, since these results were only used to constrain the model and not for data analysis, an accurate model fit was not essential.

7.3 Gangue modelling

For the gangue, only floatabilities and mass fractions were fitted; the same ENT_{null} and β values were used that were fitted for the PGM model.

7.3.1 Gangue modelling parameters

The gangue floatability values and mass fractions are shown in Tables 7.6 and 7.7:

Table 7.6 Gangue floatability values

	P_{fast} x10^{-4}	P_{slow} x10^{-4}
+75µm	0.58	0.04
+10µm-75µm	2.23	1.91
-10µm	0.58	0.23

Table 7.7 Gangue mass fractions

	Campaign 1 MF2 Primary	Campaign 1 MF3 Primary	Campaign 2 MF2 Primary
+75µm fast	0.02	0.02	0.01
+75µm slow	0.01	0.01	0.02
+75µm non	0.97	0.97	0.97
+10µm fast	0.05	0.05	0.04
+10µm slow	0.00	0.00	0.01
+10µm non	0.95	0.95	0.95
-10µm fast	0.08	0.09	0.06
-10µm slow	0.00	0.00	0.00
-10µm non	0.92	0.91	0.94

All three circuits had very similar gangue floatability mass fractions. The total floatable gangue in the feed was within the range that was determined by other researchers for PGM ore (Becker *et al*, 2006).

7.3.2 Gangue model fit

Gangue modelling versus experimental results for the three circuits is shown in Figures 7.7 to 7.9:

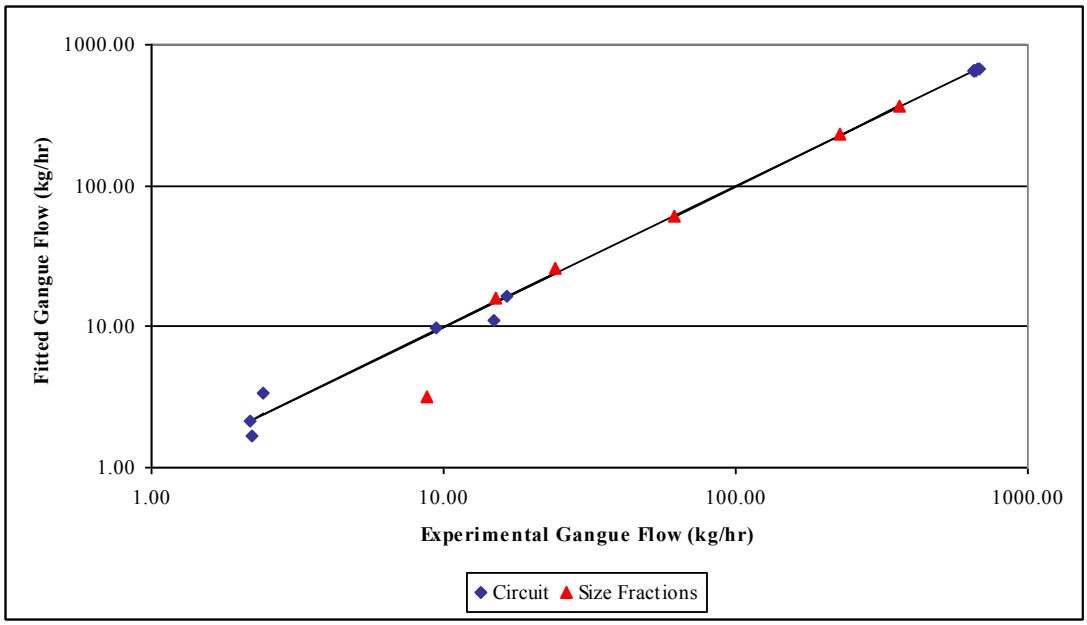

Figure 7.7 Gangue modelling results for campaign 1 MF2 primary circuit

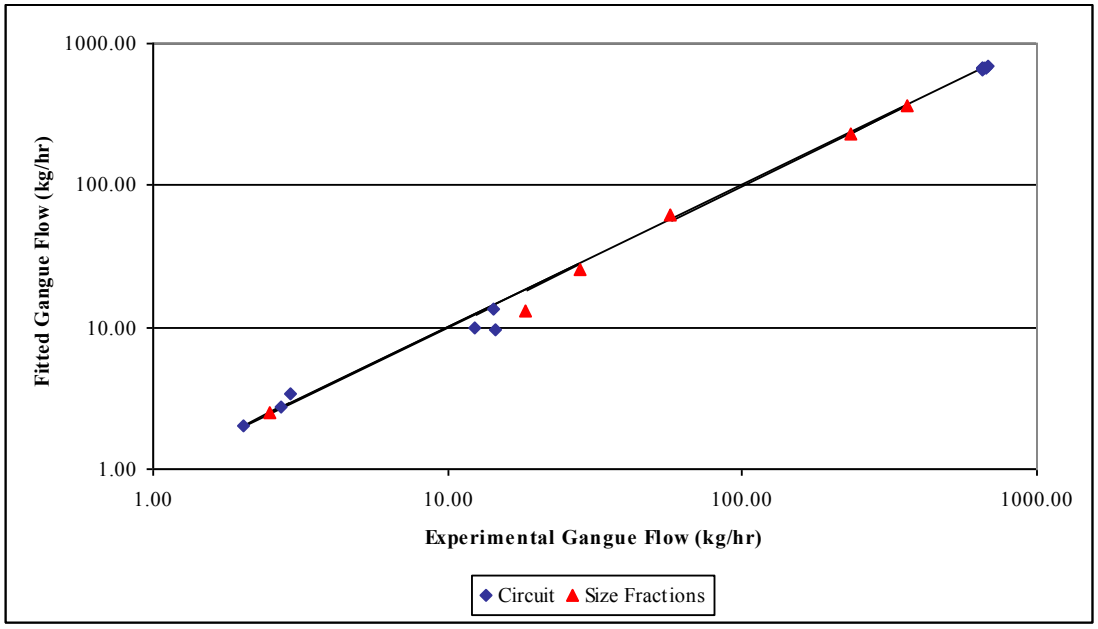

Figure 7.8 Gangue modelling results for campaign 1 MF3 primary circuit

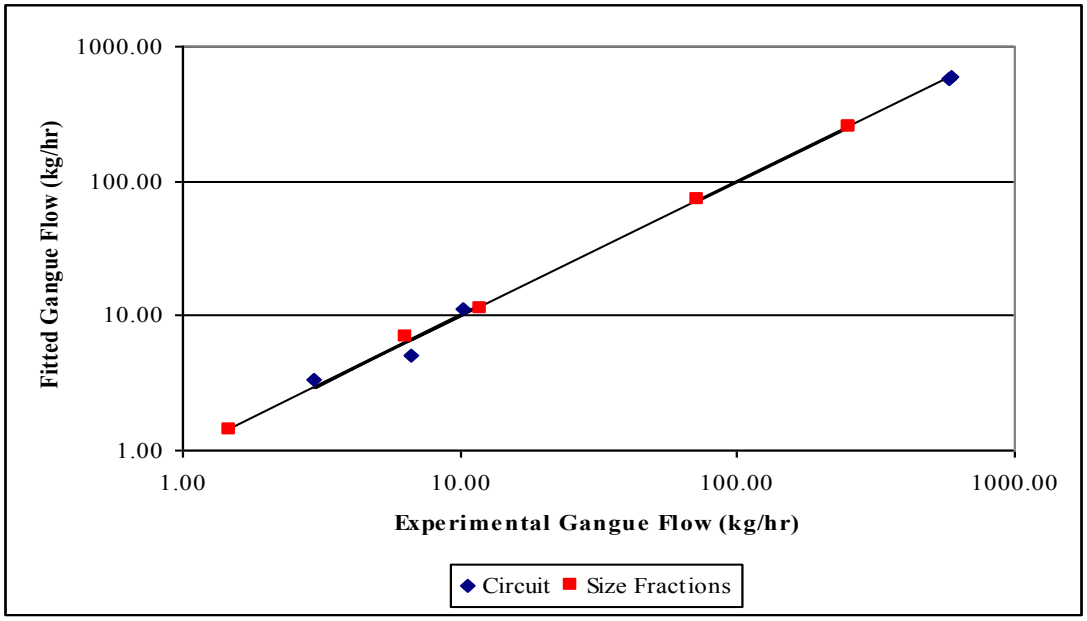

Figure 7.9 Gangue modelling results for campaign 2 MF2 primary circuit

Figures 7.7 to 7.9 show that good model fits were achieved for the gangue.

7.4 Model methodology evaluation

In Chapter 6 an approach was proposed to find a unique, well-constrained EFC modelling solution from un-sized batch flotation and sized circuit data. The outcome of these new methodologies will now be discussed.

7.4.1 Procedure 1 - Consolidating sized circuit and unsized batch data

For the unsized batch flotation data, a couple of rate constants were fitted for the feed (fast and slow), while the sized circuit data was described by a floatability profile by size, as well as S_b and R_f. It was therefore difficult finding a link between these disparate data sets, which was especially problematic as the purpose of the batch flotation tests were to constrain the parameter search for the circuit data. The aim of the methodology described in Procedure 1 (6.2.1) was to determine an unsized rate constant from the P, S_b and R_f in each size fraction. This value was then compared to the batch flotation rate constants to determine the amount of fast floating material (as defined by the batch rate constant) in each size fraction for the circuit data. In this way it was possible to constrain the model by using batch flotation data. It should be noted that without a method to relate unsized batch flotation and sized circuit data, the model would be very poorly constrained – in fact, the batch flotation data would add

nothing to the circuit model. It was also found during the modelling exercise that it was not possible to fit the model without this method.

7.4.2 Procedure 2 - Entrainability by size function

The fitted value ENT_{null} is defined as the size above which entrainment becomes negligible. The value of 44.9μm that was fitted for ENT_{null} corresponds well with the literature (Robertson, 2002). This is especially significant since ENT_{null} was not constrained by the model fit. The entrainability values that were determined for each size fraction from ENT_{null} and the exponential decay function are shown in Table 7.7, and also correspond well with values found by Robertson (2002).

CHAPTER 8
DATA ANALYSIS WITH RESPECT TO THE USE OF INERT MEDIA

8.1 Introduction

To test the hypothesis that steel and inert circuits produce different floatability numbers, two modelling methodologies were compared in this chapter for the inert circuits. Firstly, an attempt was made to model the inert circuits by using the floatability numbers from the steel circuit model fit, while the second approach was to fit an independent set of floatability parameters. For both methodologies the same froth recovery and entrainability values were used that were fitted for the steel circuits. Note that no attempt was made to model the MF3 tertiary circuit, owing to the very low PGM flows in that circuit.

8.2 Method 1

For this methodology it was assumed that floatability, froth recovery and entrainability values determined for the steel circuits were also valid for the inert circuits. Therefore, only the floatability mass fractions were fitted (shown in Table 8.1 for PGM's):

Table 8.1 PGM floatability mass fractions for the inert circuits (method 1)

	Campaign 1 MF1 Primary	Campaign 1 MF2 Secondary	Campaign 1 MF3 Secondary	Campaign 2 MF1 Primary	Campaign 2 MF2 Secondary
+75µm fast	0.08	0.28	0.19	0.05	0.21
+75µm slow	0.57	0.00	0.00	0.35	0.00
+75µm non	0.35	0.72	0.81	0.60	0.79
+10µm fast	0.00	0.00	0.00	0.00	0.00
+10µm slow	0.81	0.38	0.38	0.71	0.27
+10µm non	0.19	0.62	0.62	0.29	0.73
-10µm fast	0.90	0.00	0.55	0.90	0.41
-10µm slow	0.03	0.87	0.37	0.02	0.46
-10µm non	0.07	0.13	0.08	0.08	0.13

When using the steel circuit floatability values, a number of floatability classes were allocated zero mass when applied to the inert data. This indicates that either the inert mills liberate material within a smaller floatability range, or that the floatability values fitted for the steel circuits were not suitable to provide an adequate description of the inert circuits. A comparison between Methods 1 and 2 should reveal which of these statements is valid. The modelling results are shown in Figures 8.1 to 8.5:

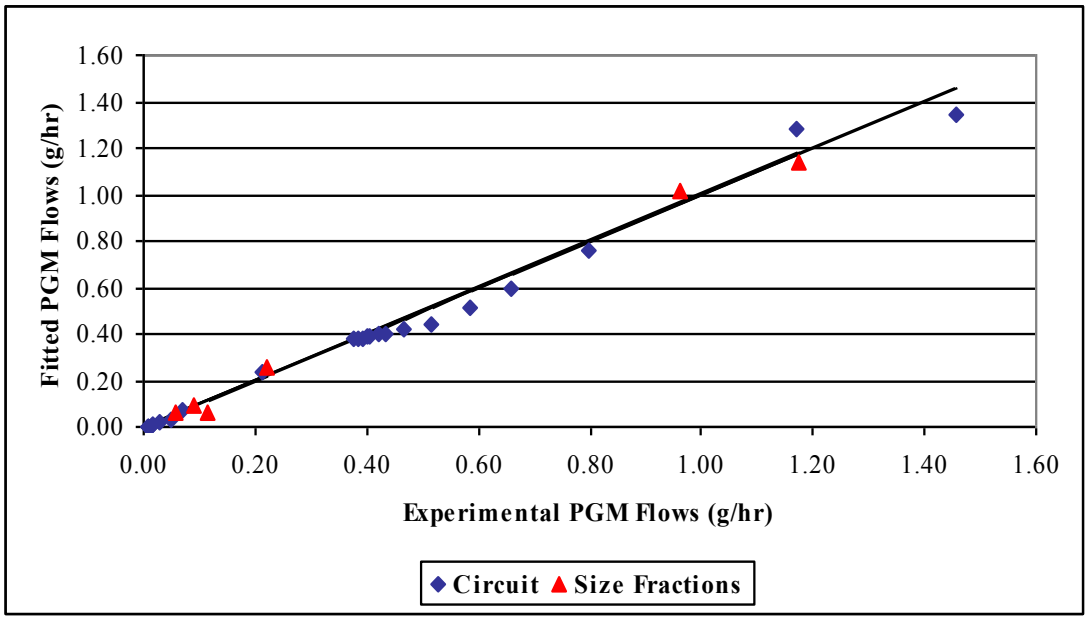

Figure 8.1 PGM modelling results for campaign 1 MF1 primary circuit (Method 1)

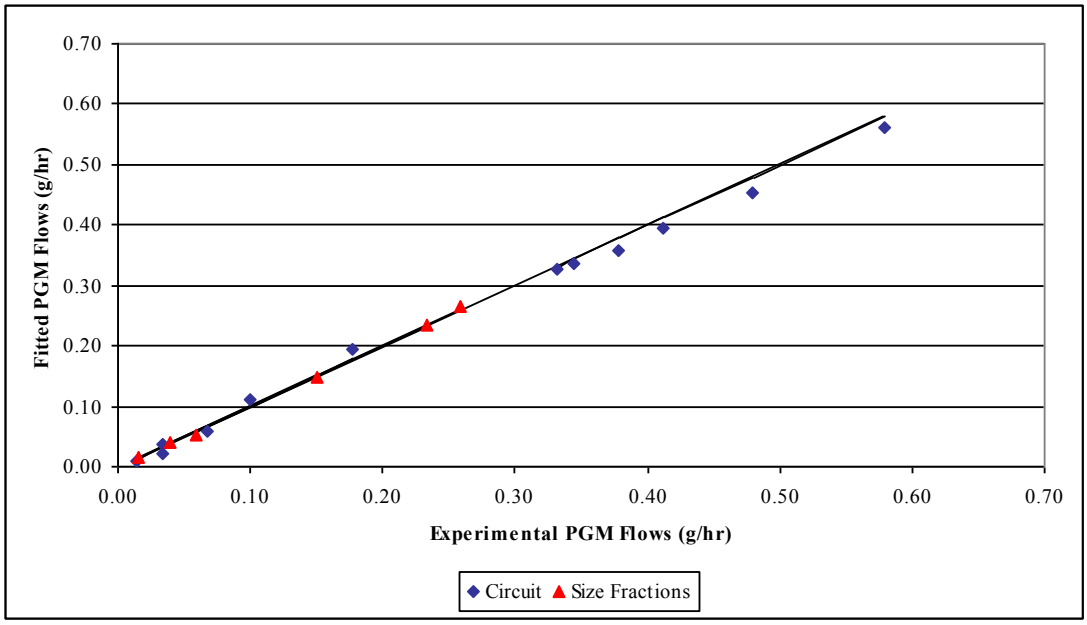

Figure 8.2 PGM modelling results for campaign 1 MF2 secondary circuit (Method 1)

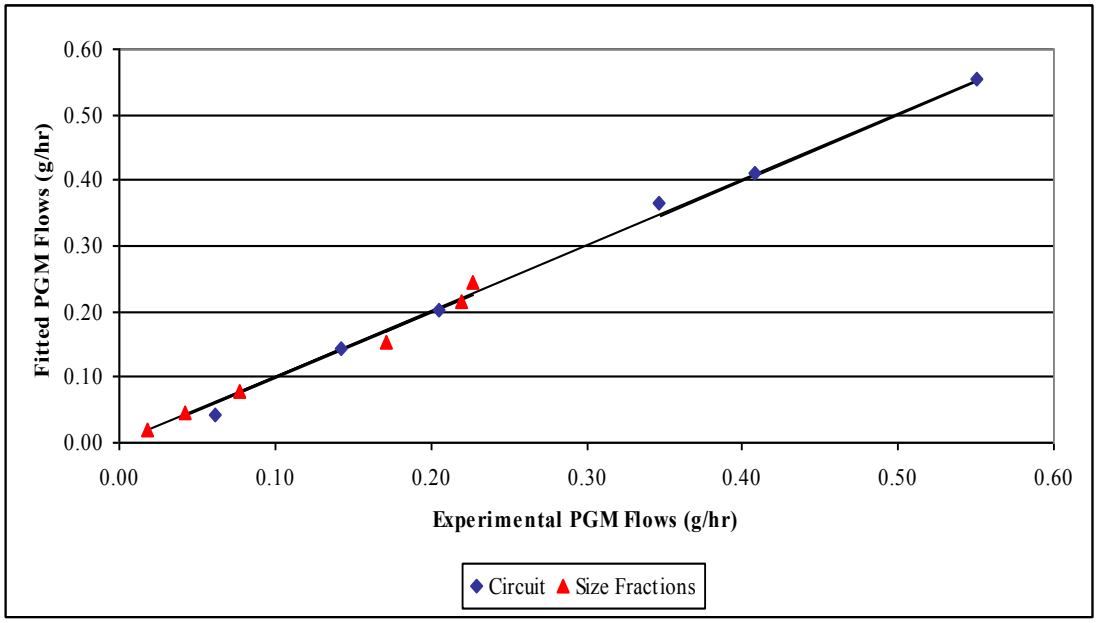

Figure 8.3 PGM modelling results for campaign 1 MF3 secondary circuit (Method 1)

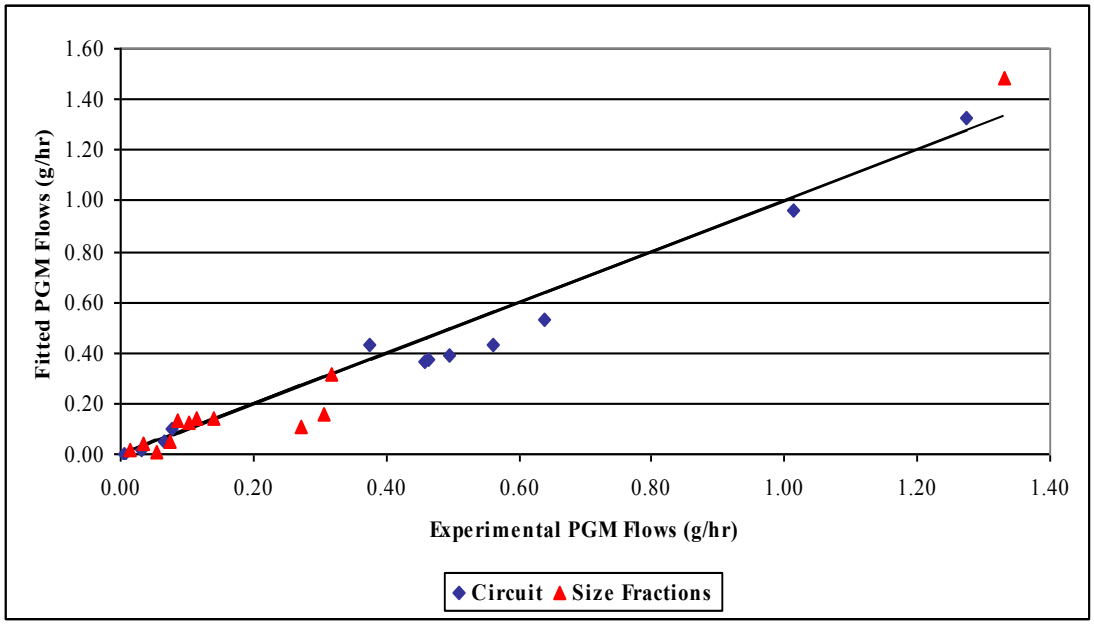

Figure 8.4 PGM modelling results for campaign 2 MF1 primary circuit (Method 1)

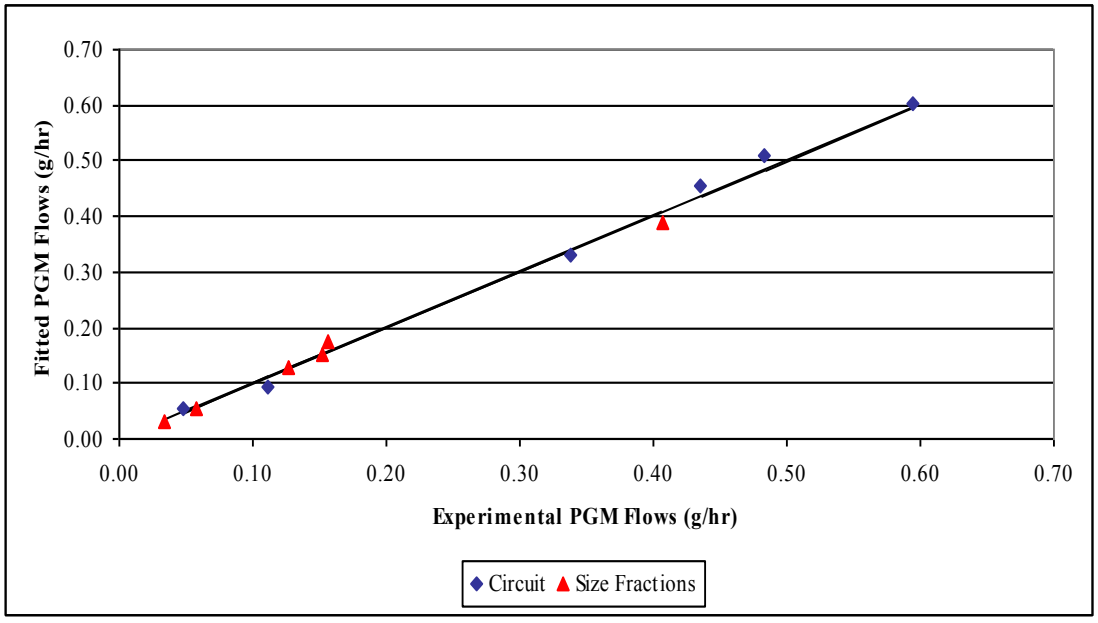

Figure 8.5 PGM modelling results for campaign 2 MF2 secondary circuit (Method 1)

From the graphs it can be seen that the secondary circuits achieved better model fits than the primary circuits. For the inert primary circuits (MF1), the relatively poor fit, combined with the use of only one floatability parameter in a number of size fractions seems to indicate that the floatability numbers derived from the steel circuits were not appropriate. The regrind circuits achieved better model fits by using one floatability class, which seems to indicate that the issue with the MF1 circuits was with respect to the easily (or quickly) liberated material. This material would have been removed by the primary circuit, and thus would not affect the regrind circuits to any great extent. However, from the primary circuit results it seems as

though the floatabilities did change in the inert mills - this is addressed in the assessment of the second model fit methodology.

For the gangue, it was not possible to achieve a model fit by only adjusting floatability mass fractions. The mass fractions all iterated to zero, indicating that the relative floatability of gangue was significantly less after the inert mills. This is investigated in the next section.

8.3 Method 2

In this method, the data for two primary inert circuits (Campaign 1 MF1 and Campaign 2 MF1) were used to fit floatabilities and floatability mass fractions. Entrainability and froth recovery parameters were kept constant from the steel circuit model fit. The floatability values determined in this way were then used to fit the secondary circuits, adjusting only the floatability mass fractions. The PGM floatabilities and mass fractions for the MF1 circuits are shown in Table 8.2:

Table 8.2 PGM floatability and mass fractions fitted for the MF1 circuits

	P x10^{-4}	**x (Campaign 1 MF1)**	**x (Campaign 2 MF1)**
+75µm fast	4.11	0.20	0.25
+75µm slow	0.25	0.74	0.46
+75µm non	-	0.06	0.29
+10µm fast	8.66	0.16	0.10
+10µm slow	3.96	0.68	0.69
+10µm non	-	0.16	0.21
-10µm fast	6.10	0.81	0.79
-10µm slow	0.68	0.05	0.03
-10µm non	-	0.14	0.18

No zero values were fitted for mass fractions, suggesting that these floatabilities were able to describe the process better than Method 1. The model fits achieved are shown in Figures 8.6 and 8.7:

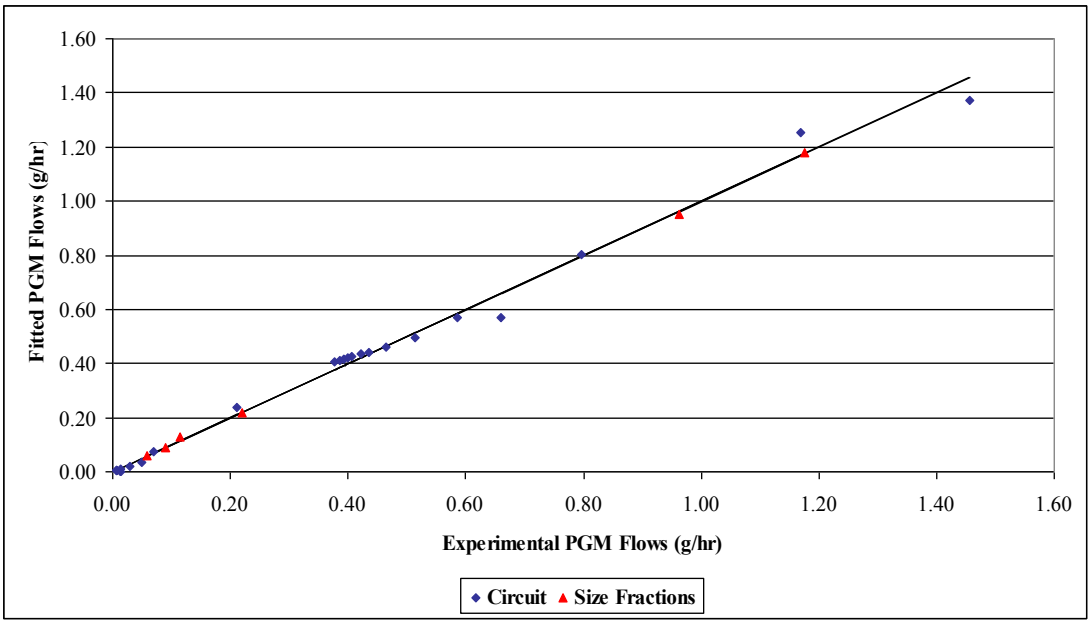

Figure 8.6 PGM modelling results for campaign 1 MF1 primary circuit (Method 2)

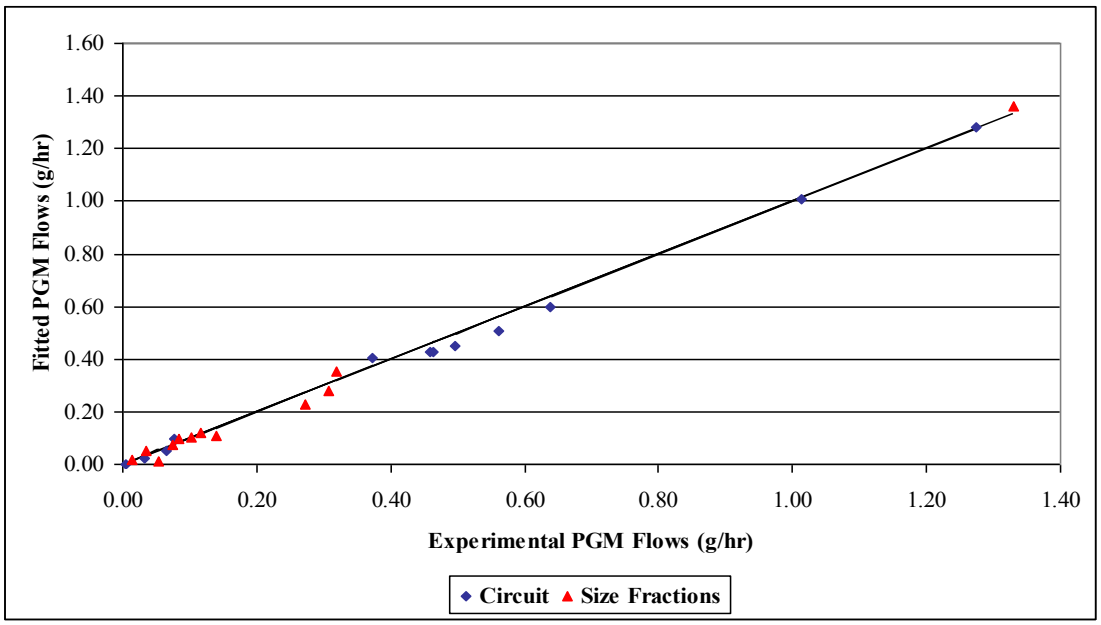

Figure 8.7 PGM modelling results for campaign 2 MF1 primary circuit (Method 2)

A visual comparison between Figures 8.1 and 8.6, and especially Figures 8.4 and 8.7 shows that the additional fitted parameters used in Method 2 (floatabilities and batch rate constants) did result in a better fit of the experimental data for the primary circuits. Also, Method 2 fitted non-zero values for all the floatability classes, whereas a number of floatability classes were fitted as zero with Method 1. These observations indicate that the experimental data is better described by using Method 2 for model fitting. This implies that inert circuits did produce a different floatability profile than steel circuits.

Using the floatabilities fitted for the MF1 circuits (Method 2), the floatability mass fractions were model fitted for the secondary circuits. These are shown in Table 8.3:

Table 8.3 PGM floatability mass fractions for the inert regrind circuits (method 2)

	Campaign 1 MF2 Secondary	Campaign 1 MF3 Secondary	Campaign 2 MF2 Secondary
+75µm fast	0.09	0.12	0.23
+75µm slow	0.32	0.23	0.14
+75µm non	0.59	0.65	0.63
+10µm fast	0.20	0.21	0.13
+10µm slow	0.22	0.29	0.23
+10µm non	0.58	0.50	0.64
-10µm fast	0.34	0.45	0.30
-10µm slow	0.47	0.48	0.66
-10µm non	0.19	0.07	0.04

Once again no zero values were fitted to describe the secondary circuits. The predicted versus experimental results for the regrind circuits are shown in Figures 8.8 to 8.10:

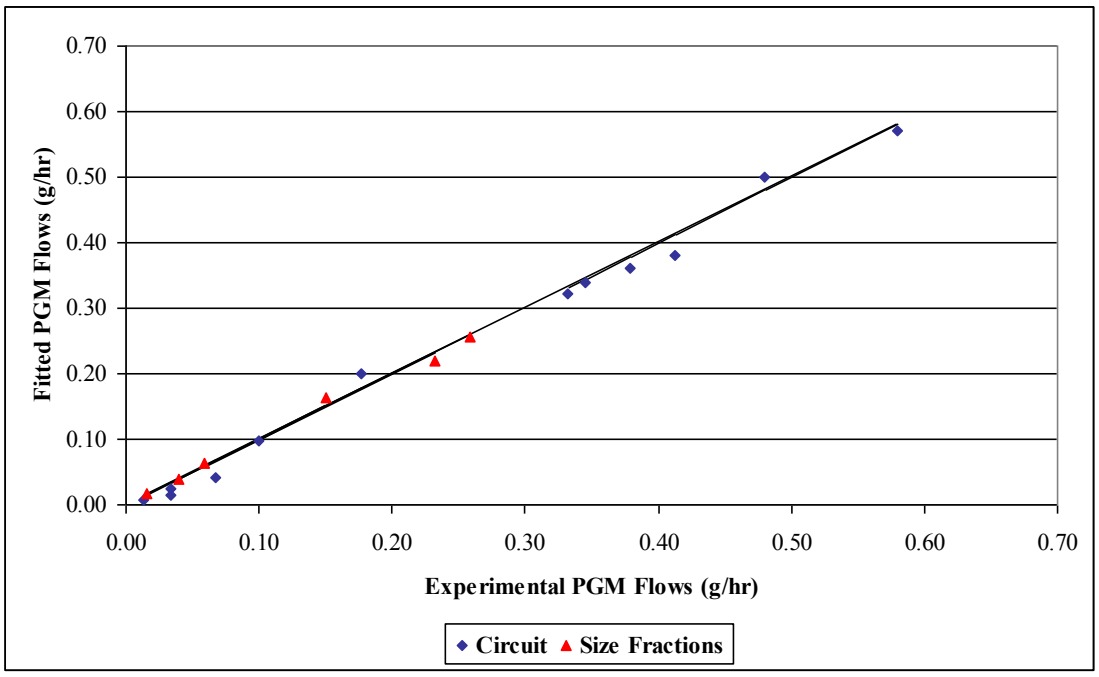

Figure 8.8 PGM modelling results for campaign 1 MF2 secondary circuit (Method 2)

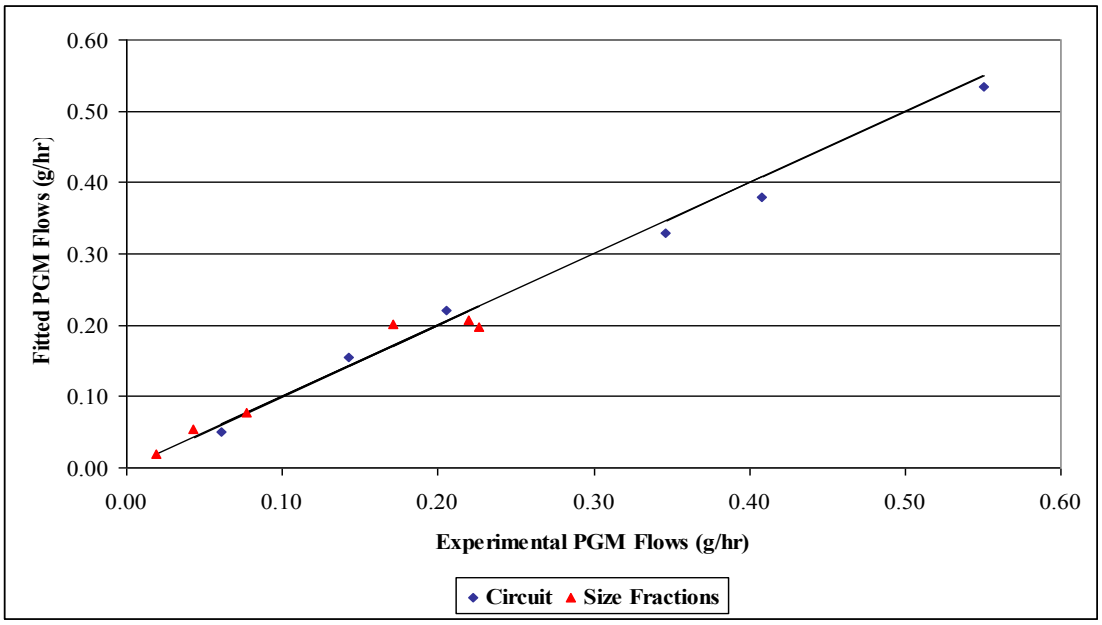

Figure 8.9 PGM modelling results for campaign 1 MF3 secondary circuit (Method 2)

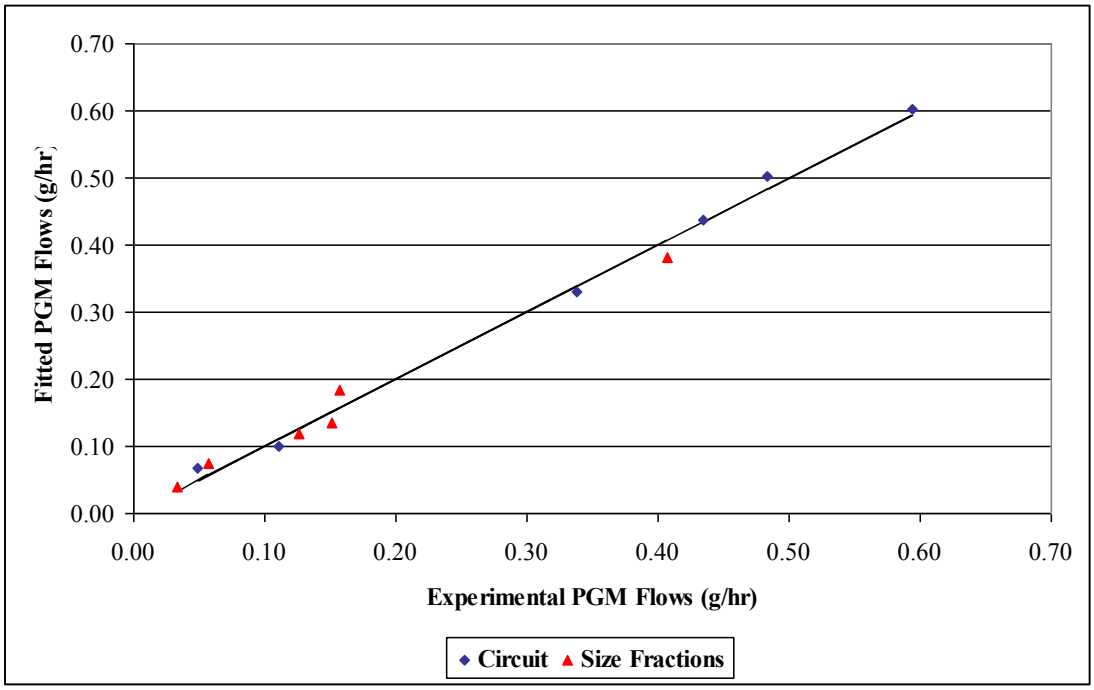

Figure 8.10 PGM modelling results for campaign 2 MF2 secondary circuit (Method 2)

Good model fits were achieved for all three regrind circuits, indicating that the floatability values fitted for the MF1 circuits were also valid for the regrind circuits.

From the modelling results achieved with Method 2 it appears as though the inert circuits were better described by using a different set of floatability numbers. Therefore, the modelling results produced by Method 2 will be used when analysing the performance of the inert circuits.

The PGM mass fractions in tails for all the inert circuits are shown in Table 8.4:

Table 8.4 PGM mass fractions in tails for all the inert circuits

	Campaign 1 MF1 Primary	**Campaign 1 MF2 Secondary**	**Campaign 1 MF3 Secondary**	**Campaign 2 MF1 Primary**	**Campaign 2 MF2 Secondary**
+75µm fast	0.00	0.00	0.00	0.00	0.01
+75µm slow	0.84	0.15	0.18	0.44	0.14
+75µm non	0.16	0.85	0.82	0.56	0.85
+10µm fast	0.00	0.00	0.00	0.00	0.00
+10µm slow	0.00	0.00	0.02	0.01	0.02
+10µm non	1.00	1.00	0.98	0.99	0.98
-10µm fast	0.00	0.00	0.02	0.00	0.02
-10µm slow	0.04	0.16	0.68	0.04	0.87
-10µm non	0.96	0.84	0.30	0.96	0.11

Almost all fast material was recovered from all size classes and circuits. For the MF1 circuits, a significant amount of slow material was not recovered in the +75µm fraction. It is also noticeable that a lot of slow floating -10µm material was left unrecovered by the two circuits with the shortest residence time (Campaign 1 MF3 Secondary and Campaign 2 MF2 Secondary). This suggests that additional residence time in UG2 flotation targets mainly fine, slow floating material.

Applying the second methodology to the gangue did not result in a model fit. It appears as though the floatability and/or entrainability and/or froth recovery of the gangue was significantly different in the inert circuits than in the steel circuits. However, the gangue model was not sufficiently constrained to determine these values in isolation. The reasons for the significant difference in gangue flotation performance will be discussed in more detail in the next chapter.

CHAPTER 9
ANALYSIS OF MILLING DEVICES

9.1 Introduction

The milling devices used in these tests break particles in different ways. The ball mill utilises large, high chrome steel balls that grinds via impact breakage and attritioning. The SMD and IsaMill are stirred devices, which grind exclusively via an attritioning action. In addition, the chemical environment under which grinding occurs also varies between ball and stirred mills. These effects result in different flotation responses as a result of the type of milling device used. Therefore, before analysing the effect of circuit configuration on flotation, it is necessary to first determine flotation response as a result of the type of milling device used.

9.2 Milling properties

The properties of the two types of milling devices used in the tests are shown in Table 9.1:

Table 9.1 Properties of grinding devices

	Tumbling Mill	**Stirred Mill**
Mill	Ball Mill	IsaMill and SMD
Predominant Grinding Mechanism	Impact	Attritioning
Grinding Media	Steel	Inert
Grinding Media Size	40 – 70mm	2 – 4mm

The type of milling device can affect flotation in a number of ways. Firstly, the chemical environment under which breakage occurs could be detrimental, as hydroxide species can attach to fresh surfaces in a steel mill. Fine grinding media in an attritioning environment can also clean mineral surfaces, removing ultra-fine gangue particles attached to the surface. Finally, the grinding action also plays a role - ball mills break particles predominantly via impact, while stirred mills grind through an attritioning action. The size of the grinding media can also affect liberation in different size classes. Coarse grinding media will be more efficient at liberating valuables from coarse sizes, while the opposite is true for fine grinding media.

In order to investigate these effects, the size distributions and breakage characteristics of each mill type will be compared. The flotation response of the primary and secondary circuits will be analysed separately. Analysis will be performed on a size basis, which should compensate to some extent for different size distributions in the various circuits.

9.3 Breakage characteristics

The size distribution achieved by each circuit's primary milling stage is shown in Table 9.2:

Table 9.2 Cumulative size distribution (% passing) produced by primary milling

	Campaign 1 - MF1	**Campaign 1 - MF2**	**Campaign 1 - MF3**	**Campaign 2 - MF1**	**Campaign 2 - MF2**
Final Mill	ISA	Ball	Ball	SMD	Ball
Media Type	Inert	Steel	Steel	Inert	Steel
106um	90.1	78.1	77.7	77.7	73.2
75um	81.5	66.4	66.2	64.8	57.4
53um	61.9	44.5	44.5	51.3	41.4
10um	17.3	10.9	10.7	28.7	13.0

In order to analyse the breakage characteristics of each milling stage, the size reduction achieved was normalised to compensate for feed size variation. This was done by calculating the cumulative amount of new mass in each size fraction, and normalising this to 100 units in the coarsest measured fraction (106µm). The result shows the mass change in each size fraction relative to milling 100 units from the coarsest fraction. The same procedure was applied to the PGM's. An example of the application of this procedure is included in Appendix C.

For the first campaign, mass results are shown in Table 9.3 and PGM results in Table 9.4. Note that the MF3 tertiary stage was not investigated, owing to the very low fractional PGM grades in this test.

Table 9.3 Normalised mass change in each size fraction for first campaign

	MF1 Primary	MF2 Primary	MF2 Secondary	MF3 Primary	MF3 Secondary
Final Mill	ISA	Ball	ISA	Ball	SMD
Media Type	Inert	Steel	Inert	Steel	Inert
+106um	-100.0	-100.0	-100.0	-100.0	-100.0
+75um	3.5	9.1	-32.2	8.8	-17.8
+53um	23.1	31.5	-26.8	31.4	-23.2
+10um	53.3	45.6	93.0	46.4	79.7
-10µm	20.2	13.7	65.9	13.5	61.3

Table 9.4 Normalised PGM mass change in each size fraction for first campaign

	MF1 Primary	MF2 Primary	MF2 Secondary	MF3 Primary	MF3 Secondary
Final Mill	ISA	Ball	ISA	Ball	SMD
Media Type	Inert	Steel	Inert	Steel	Inert
+106um	-100.0	-100.0	-100.0	-100.0	-100.0
+75um	-5.4	0.5	-13.6	0.4	-45.0
+53um	9.3	31.4	-36.8	31.7	-38.8
+10um	47.4	50.9	19.1	51.2	69.2
-10µm	48.7	17.2	131.3	16.7	114.5

From Table 9.3 it can be seen that the stirred inert mills generated more mass in the -10µm fraction relative to the ball mill. This is especially noticeable in the secondary circuits, which comprised of stirred mills only. For the MF1 circuit (consisting of a ball mill and stirred mills) the effect is still present, but not as pronounced. The same trend is detected for the PGM's in Table 9.4. For the stirred mills, PGM's report predominantly to the finer size fractions, whereas the PGM's are more distributed across all the size fractions by the ball mill.

When comparing the results in Table 9.3 with Table 9.4, it is clear that more PGM's accumulated in the -10µm fraction than the bulk of the mass. This indicates that preferential

liberation is occurring, and this effect is more pronounced with stirred mills, especially in the secondary circuits.

Note that these results do not indicate that stirred mills are efficient at grinding coarse material. What is suggested is that stirred mils are more efficient at grinding fine material relative to coarse material. Thus, it is a combination of slow grinding of material from coarse size fractions and efficient grinding of fine material.

The normalised mass and PGM results for the second campaign are shown in Tables 9.5 and 9.6:

Table 9.5 Normalised mass change in each size fraction for second campaign

	MF1 Primary	**MF2 Primary**	**MF2 Secondary**
Final Mill	SMD	Ball	SMD
Media Type	Inert	Steel	Inert
+106um	-100.0	-100.0	-100.0
+75um	11.2	17.3	-49.9
+53um	17.8	23.7	-68.4
+10um	28.0	40.4	-20.7
-10µm	43.0	18.6	238.9

Table 9.6 Normalised PGM mass change in each size fraction for second campaign

	MF1 Primary	**MF2 Primary**	**MF2 Secondary**
Final Mill	SMD	Ball	SMD
Media Type	Inert	Steel	Inert
+106um	-100.0	-100.0	-100.0
+75um	-3.9	4.5	-17.9
+53um	1.3	16.6	-52.8
+10um	-9.8	51.4	-57.1
-10µm	112.4	27.6	227.8

The same trends were observed as for the first campaign, with the stirred mills being much more efficient at generating fine material. Results for the primary mills seem to follow the same trend as for the first campaign, although the preferential deportment of material was much more pronounced in the secondary mill. This may be a function of the coarser primary grind in the second campaign, as more PGM's would have been locked in coarser sizes. This would result in an increased potential for the secondary mill to deport material to the finer sizes.

9.4 Flotation performance

In this section, the flotation performance is analysed in relation to mill type, in order to evaluate the effect of breakage mechanism, grinding media and chemical environment on flotation. For the primary circuits, the recovery by size is evaluated in a coarse size fraction for flotation (+75μm), the ideal flotation size range (-75μm to +10μm) and the finest size fraction measured (-10μm). Only the performance of the primary circuits was analysed, as the efficiency of these primary circuits render any analysis of the regrind circuits problematic.

9.4.1 Primary circuit recovery – coarse fraction

The recovery for each primary circuit in the +75μm fraction is shown in Figure 9.1:

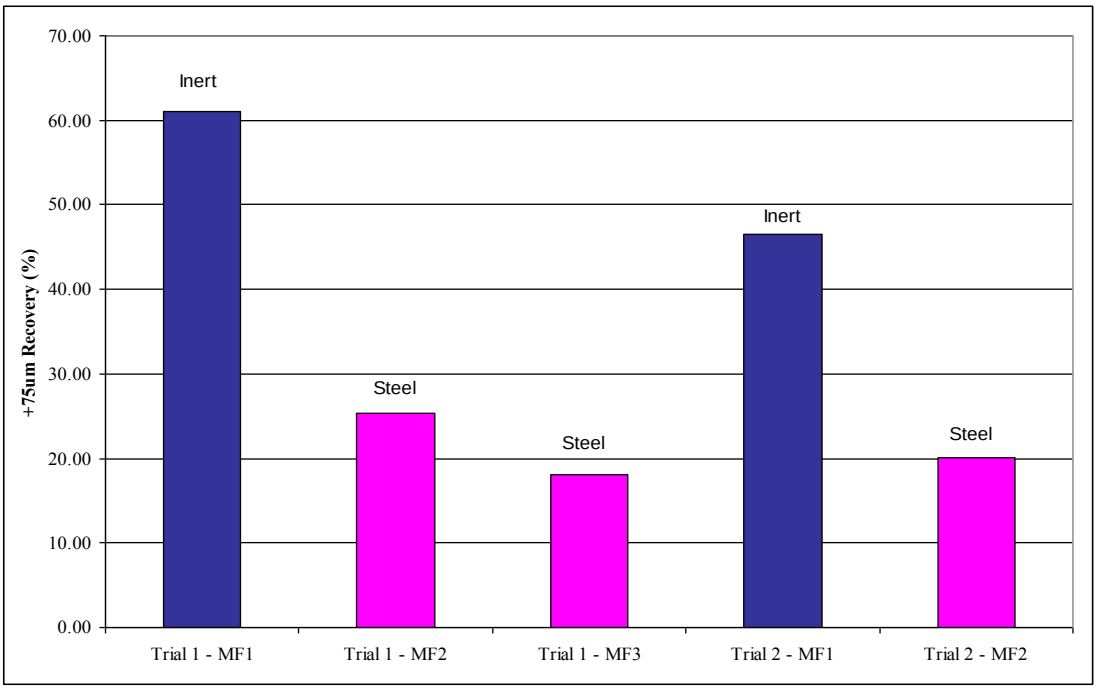

Figure 9.1 Primary stage PGM recovery in the +75µm fraction

Modelling results for the +75µm fraction are used to evaluate the recovery of coarse material. The PGM mass fractions and floatabilities that were modelled in campaigns 1 and 2 are shown in Tables 9.7 and 9.8 respectively.

Table 9.7 +75µm Floatability and PGM mass fractions for campaign 1 primary circuits

	Inert Floatability x10^{-4}	**Steel Floatability x10^{-4}**	**x MF1**	**x MF2**	**x MF3**
+75µm fast	4.11	5.85	0.20	0.07	0.06
+75µm slow	0.25	0.77	0.74	0.23	0.21
+75µm non	-	-	0.06	0.70	0.73

Table 9.8 +75µm Floatability and PGM mass fractions for campaign 2 primary circuits

	Inert Floatability x10^{-4}	**Steel Floatability x10^{-4}**	**x MF1**	**x MF2**
+75µm fast	4.11	5.85	0.25	0.12
+75µm slow	0.25	0.77	0.46	0.14
+75µm non	-	-	0.29	0.74

From Figure 9.1, it can be seen that the primary circuits with an inert stage before flotation achieved significantly higher recoveries in the coarse fraction. Especially noteworthy is the recoveries of Campaign 1 MF2 and MF3 when compared to Campaign 2 MF1, as these circuits were operated with similar amounts of +75µm material in the feed (see Table 9.2), as well as very similar residence times (6 cells).

From Tables 9.7 and 9.8 it can be seen that the stirred mills generated more floatable material in the coarse size fraction, as illustrated by the significant reduction in non-floating material when a stirred mill was used as final milling device. This can be explained by the predominant breakage mechanism of the different milling devices. With the predominance of impact breakage in ball mills, particles are typically broken apart, and PGM's are liberated to smaller size fractions. However, the attrition action of the stirred mills appears to transform a significant portion of non-floatable material into floatable material in the same size fraction. Liberation of locked particles in the stirred mills seems to be a gradual process, and hence some of these particles may well still be poorly liberated (i.e. have small floatable surfaces) after milling. This is shown by the reduction in floatabilities with stirred mills. However, the reduction in non-floating material with stirred mills seems to have a bigger impact on recovery than the reduction in floatability, as shown by the significant increase in PGM recovery with stirred mills in the coarse sizes. The influence of surface cleaning and the chemical environment does not seem to play a particularly significant role in the coarse size fractions. These effects are most likely present, but dominated by the increase in floatable material. Thus, it appears as if changes to the liberation profile dominate the other factors, such as the environment under which flotation occurs.

9.4.2 Primary circuit recovery – middling fraction

The recovery by size for each primary circuit in what could be considered to be the ideal flotation range (-75µm to +10µm) is shown in Figure 9.2:

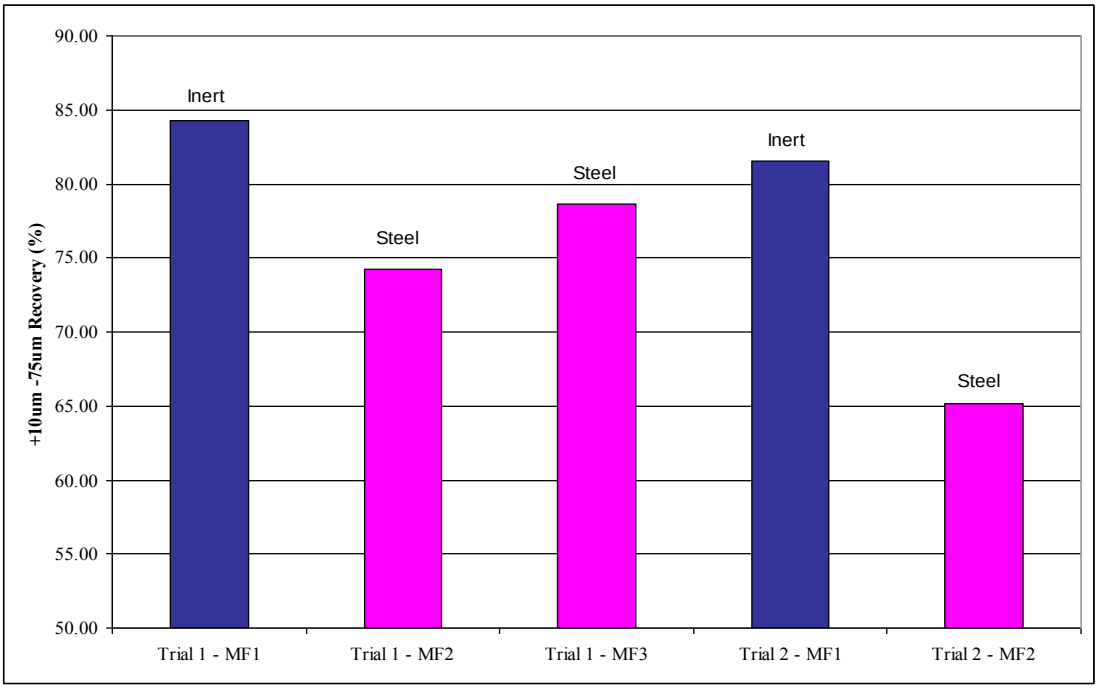

Figure 9.2 Primary stage PGM recovery in the +10µm -75µm fraction

The PGM mass fractions and floatabilities are shown in Tables 9.9 and 9.10:

Table 9.9 +10µm Floatability and PGM mass fractions for campaign 1 primary circuits

	Inert Floatability x10^{-4}	**Steel Floatability x10^{-4}**	**x MF1**	**x MF2**	**x MF3**
+10µm fast	8.66	9.78	0.16	0.58	0.64
+10µm slow	3.96	4.81	0.68	0.15	0.14
+10µm non	-	-	0.16	0.27	0.22

Table 9.10 +10µm Floatability and PGM mass fractions for campaign 2 primary circuits

	Inert Floatability x10^{-4}	**Steel Floatability x10^{-4}**	**x MF1**	**x MF2**
+10µm fast	8.66	9.78	0.10	0.56
+10µm slow	3.96	4.81	0.69	0.09
+10µm non	-	-	0.21	0.35

Figure 9.2 shows the same trend that was observed in Figure 9.1 – circuits with an inert stage before flotation achieved higher PGM recoveries. However, the effect was not as pronounced as for the coarser fraction. Once again, this is emphasised by observing the circuits with a similar residence time – the MF1 circuit in the second campaign achieved higher recoveries than the MF2 and MF3 circuits in the first campaign.

From Tables 9.9 and 9.10, the inert circuits produced less non-floatable material in the +10µm size fraction. However, most of the floatable PGM's generated by the inert circuits were slow floating, whereas the floatable PGM's generated by the steel circuits were predominantly fast floating. Since the recovery for the stirred circuits (with less non-floatable material) was higher than for the steel circuits (with more fast floating material), this indicates that recovery was dominated by the amount of non-liberated particles, rather than the degree of liberation.

In the previous section it was argued that impact breakage liberate PGM's and BMS to finer size fractions predominantly. Thus, for the ball mill a significant portion of the fast floating PGM's found in the +10µm fraction were probably liberated from the coarser sizes. Any further impact breakage would probably break the particle apart, once again liberating PGM's to a finer size. However, because the ball mill is less efficient at finer sizes, it is also less likely to liberate non-floatable PGM's from the +10µm size fraction.

For the stirred mills, a significant portion of the PGM's that were transported from the coarser sizes were probably partially liberated or locked in gangue. As was the case with the coarse fraction, attrition type grinding will result in the gradual liberation of this material, resulting in more partially liberated material. The floatable surface area of this material would

often be relatively small, as indicated by the lower floatabilities in stirred mills (Tables 9.9 and 9.10). Also, because of the higher efficiency of stirred mills in smaller size fractions, these mills are more likely to liberate PGM's from BMS, thus reducing the amount as well as the floatability of fast floating material. The overall effect in the +10µm fraction with stirred mills would be less non- and fast floating material, and more slow floating material.

9.4.3 Primary circuit recovery – fine fraction

The recovery by size for each primary circuit in the finest size fraction measured (-10µm) is shown in Figure 9.3:

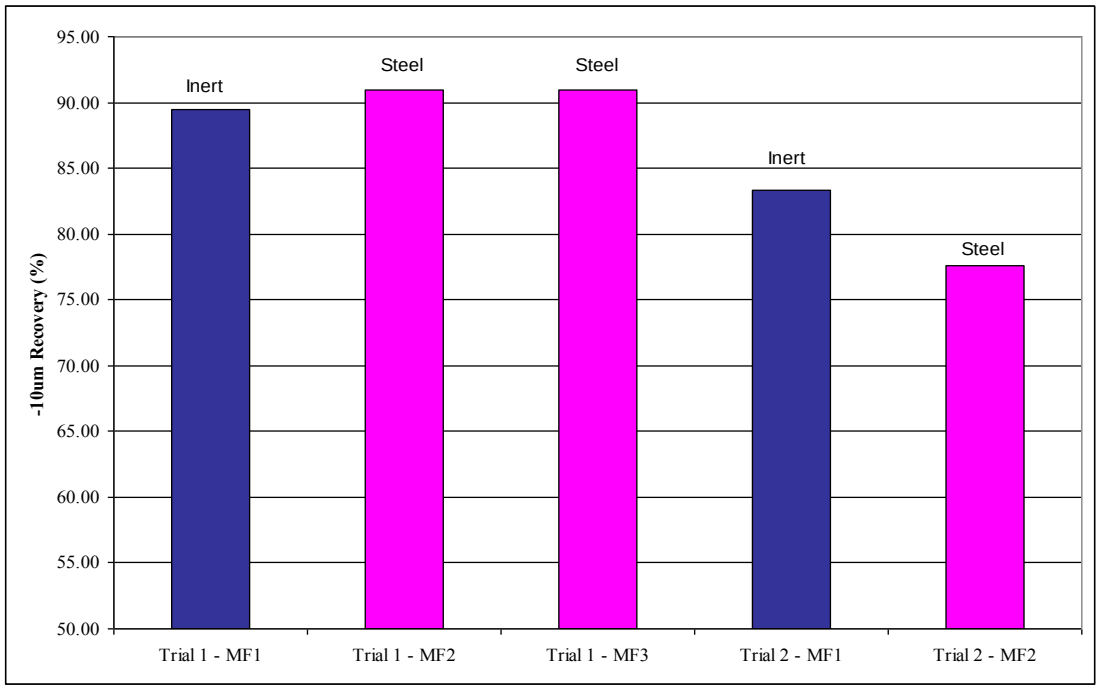

Figure 9.3 Primary stage PGM recovery in the -10µm fraction

The PGM mass fractions and floatabilities are shown in Tables 9.11 and 9.12:

Table 9.11 -10µm Floatability and PGM mass fractions for campaign 1 primary circuits

	Inert Floatability x10^{-4}	**Steel Floatability x10^{-4}**	**x MF1**	**x MF2**	**x MF3**
-10µm fast	6.10	5.37	0.81	0.58	0.63
-10µm slow	0.68	0.77	0.05	0.39	0.35
-10µm non	-	-	0.14	0.03	0.02

Table 9.12 -10µm Floatability and PGM mass fractions for campaign 2 primary circuits

	Inert Floatability x10^{-4}	**Steel Floatability x10^{-4}**	**x MF1**	**x MF2**
-10µm fast	6.1	5.4	0.79	0.59
-10µm slow	0.68	0.77	0.03	0.33
-10µm non	-	-	0.18	0.08

In the -10µm fraction, the effect of mill type on recovery was less pronounced (Figure 9.3). However, for the -10µm fraction it does appear as though the inert circuits performed better at coarser grinds (Campaign 2), while the steel circuits performed better at finer grinds (Campaign 1).

Regarding the floatability profiles, Tables 9.11 and 9.12 show the opposite of the +10µm fraction, with the inert circuits generating more non- and fast floating material. The fast floatability was also higher than with the steel circuits. This increase in fast floatability and mass fractions with inert mills were probably caused by two factors: The first is the higher efficiency of the stirred mills at smaller sizes – more locked material will be liberated in the -10µm fraction with stirred mills. Secondly, because of the relatively small surface areas, surface cleaning effects and the chemical environment should become prominent in the -10µm fraction.

However, the higher efficiency of the stirred mills in the fine fraction could also result in floatable material being milled too fine for efficient flotation (this would be expected to occur somewhere in the 2 to 4 micron range, but measurement difficulties at these sizes make an

exact determination difficult), which would explain the increase in non-floatable material observed with the inert circuit.

9.5 Mineralogy

From the previous discussions, the effect of the different breakage mechanisms on the floatability profiles in the various mills are summarised in Table 9.13:

Table 9.13 Summary of milling devices and proposed breakage mechanisms

	Predominant breakage mechanism	**Parent Particle**	**Liberation**
Ball Mill	Impact – particle shatter	Destroyed	Instantaneous liberation – not selective to a liberation type. Usually to smaller particle size class than parent
Stirred Mill	Attritioning – particle chipped away	Intact	Gradual liberation – selective towards partial liberation as particle size class increases. Often in same particle size class as parent

In order to fully evaluate these proposed mechanisms, a full size-by-size mineralogical evaluation would be required. However, the cost constraints and the large amount of sample required for tailings analysis made such an exercise impractical. Instead, a general mineralogical evaluation and PGE mineral search was conducted on the flotation feed of the primary circuits. These results were presented in Chapters 4 and 5, and only the relevant data will be discussed here. The grain size distribution of PGE minerals are shown in Figure 9.4:

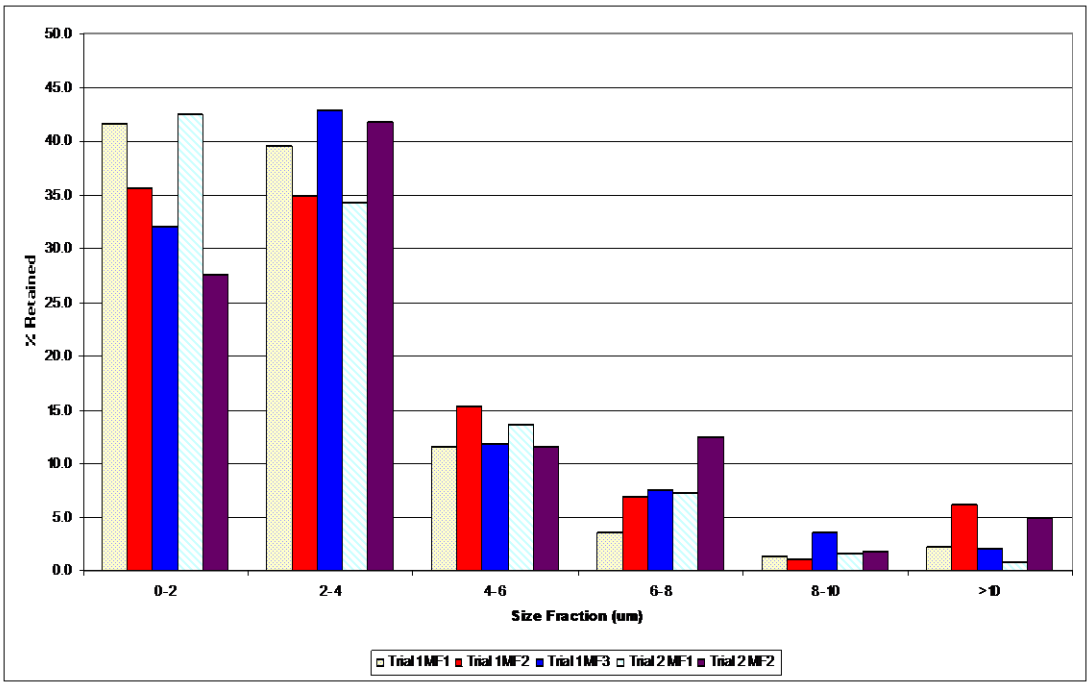

Figure 9.4 PGE mineral grain size distribution for all primary circuits

Although insufficient grains were found to meet any formal requirements for statistically significance (which is a common problem for the mineralogical evaluation of very sparse minerals such as PGM's), it does appear as though the MF1 circuits (stirred mill as final milling device) produced more ultra-fine material (<2μm) than the ball mill circuits. This supports the conclusion that stirred mills are more efficient at grinding fine material, and more likely to over-grind fine, liberated particles. However, in order to evaluate the effect of the different milling devices, the PGE mineral mode of occurrence is more significant (Figure 9.5):

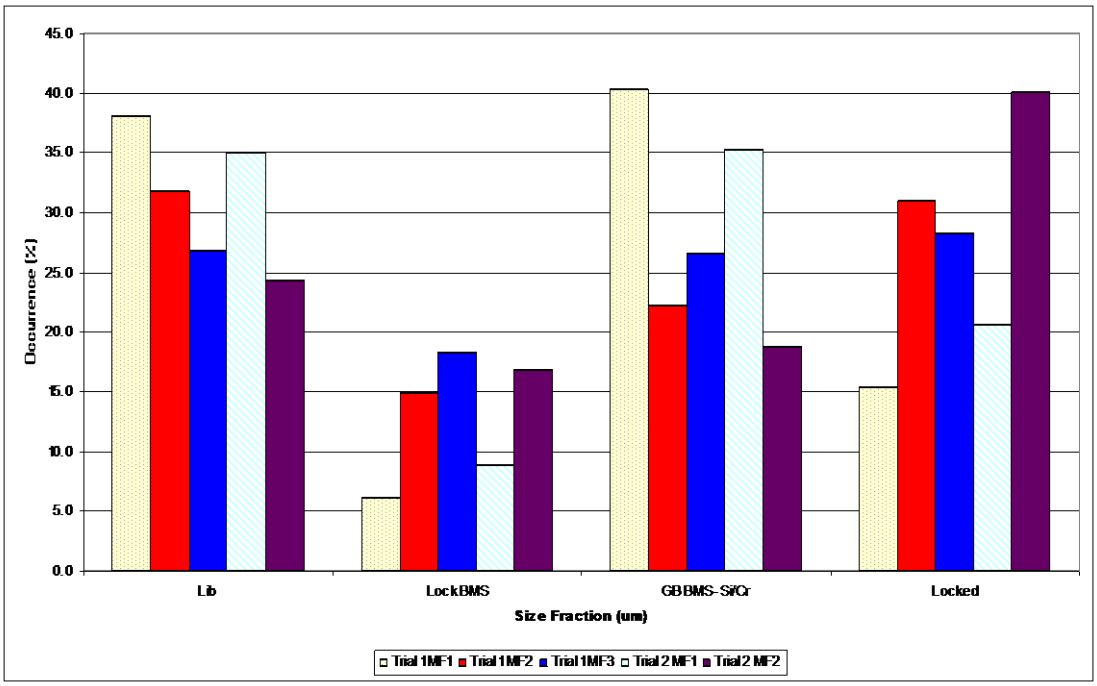

Figure 9.5 PGE mineral mode of occurrence for all primary circuits

From Figure 9.5 it can be seen that the two circuits with stirred mills (MF1) produced less locked PGM particles than the steel circuits. The partially liberated material is also a lot higher with stirred mills. This supports the suggestion made earlier in this chapter that attrition grinding is more likely to transform locked into partially liberated particles, especially in coarse size fractions. Another observation from the graph is that considerably less PGM's in the MF1 circuits are locked in BMS. Once again this supports the conclusion that the stirred mills liberate PGM's from BMS, resulting in a decrease in fast floating material in the optimum size fraction for flotation and an increase in liberated material in the smallest size fraction. These effects are especially significant when comparing the primary circuits of Campaign 1 MF2 and MF3 with Campaign 2 MF1, as these circuits had similar amounts of -75µm material in the feed.

9.6 Effect of breakage mechanism on grade

It was not possible to fit a model that could adequately describe the behaviour of gangue in the inert circuits. However, it was found that the inert primary circuits produced significantly higher grades than steel circuits. This can be seen from Figures 4.11 and 5.9, where the circuits with an inert mill before flotation (MF1) produced much higher grades than circuits with a combination of steel and inert mills before flotation. In the absence of an inert gangue

model, it was possible to investigate this increase in grade after an inert mill by investigating two circuits with similar grinds. The size distributions of campaign 1 MF3 primary circuit (steel) and campaign 2 MF1 circuit (inert) were similar, thus any difference in the grade profile is most likely a result of the mills, rather than overall size distribution. Firstly, consider the grade responses for both circuits in Figure 9.6:

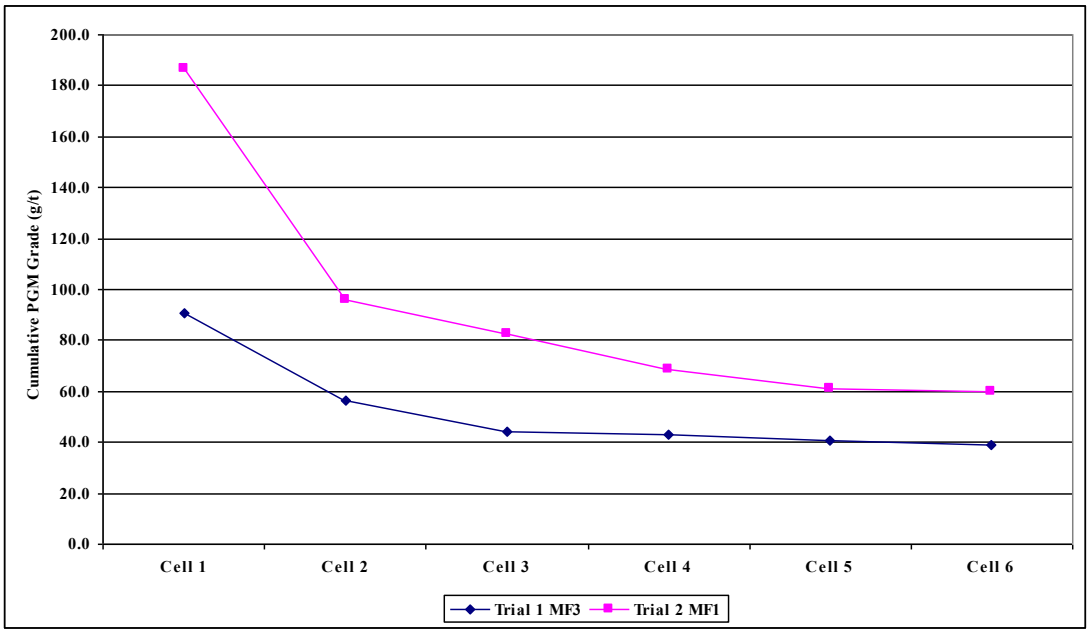

Figure 9.6 Cumulative PGM grade profiles for campaign 1 MF3 primary and campaign 2 MF1

From Figure 9.6, it can be seen that the MF1 circuit with an inert mill produced a significantly higher grade profile than the MF3 circuit with a steel mill, even though the grinds of these two circuits were similar. The flotation responses of the fast floating fraction for both circuits are shown next in Figure 9.7:

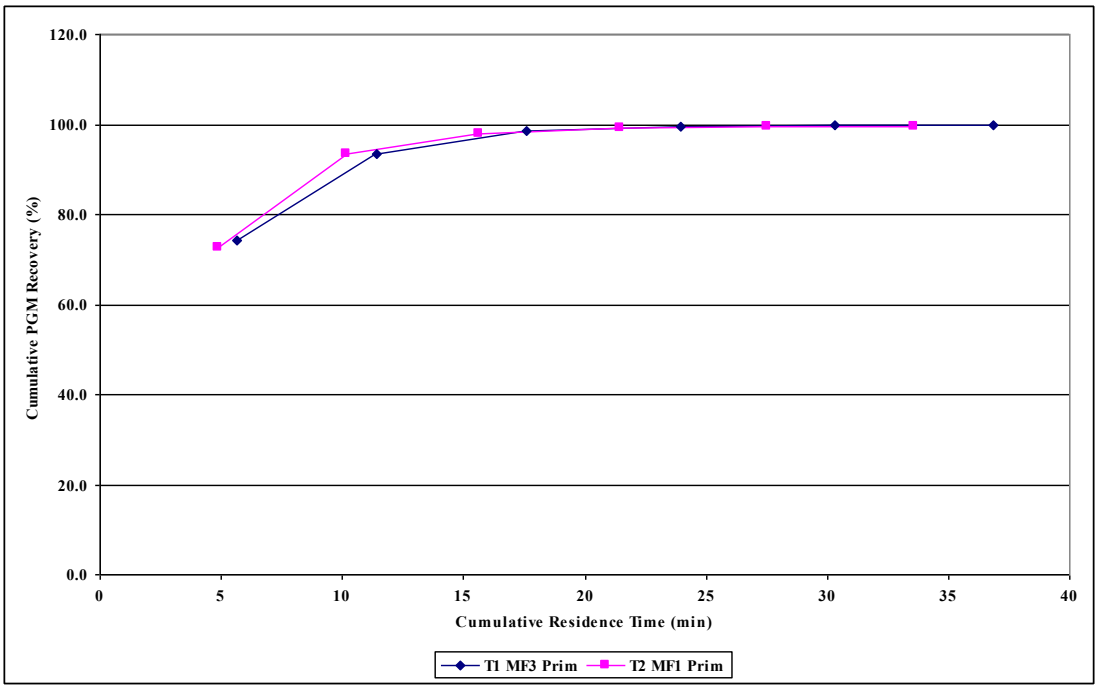

Figure 9.7 Cumulative fast floating PGM recovery for campaign 1 MF3 primary and campaign 2 MF1

Figure 9.7 shows that the fast floating PGM fraction for both circuits had a similar response, suggesting that this is not the reason for the higher grades observed with the inert circuit. However, when analysing the fast floating fraction by size (Table 9.14), some significant differences emerge between the two circuits:

Table 9.14 Fast floating PGM distribution by size for campaign 1 MF3 primary and campaign 2 MF1

	Fast floating PGM distribution (%)		
	+75mm	**+10mm**	**-10mm**
Campaign 1 MF3	2.13	80.61	17.26
Campaign 2 MF1	3.38	3.23	93.39

Although the fast floating response for both circuits were similar (Figure 9.7), Table 9.14 shows that most of the fast floating material for the steel circuit (Campaign 1 MF3) was in the +10µm fraction, compared to the -10µm fraction for the inert circuit. In the +10µm fraction, fast floating PGM's would typically be associated with BMS, while in the -10µm fraction the fast floating PGM's would usually occur as free, liberated PGM's. As was discussed in Section 9.4.2 and Section 9.5, it appears as though the attrition grinding in the inert mill was liberating PGM's from BMS in the +10µm fraction, while also grinding the

BMS finer (possibly to the extent that the BMS would be over-ground and not recovered). This would explain a grade increase with inert mills, since free, ultra-fine PGM's would display a higher grade than those associated with relatively large BMS. This liberation of PGM's from BMS is confirmed by the mineralogical associations of PGM's in the feed (as shown in Figure 9.5) – this clearly shows more liberated PGM's and less association with BMS for the MF1 (inert) circuits.

It is possible that other factors also played a role in the higher PGM's grades experienced with inert circuits. These include a change in entrainability and froth recovery for gangue, as well as surface cleaning of gangue from valuables with attrition grinding. However, these could not be quantified without a gangue model, and from the data is seems as if liberation from BMS played a significant role in the higher PGM grades with inert circuits.

CHAPTER 10
ANALYSIS OF CIRCUIT CONFIGURATION

10.1 Introduction

This chapter investigates the effect of staged grinding and flotation on the floatability of platinum-bearing UG2 ore. Final results obtained from the circuits under investigation will be analysed qualitatively with respect to the recovery and transportation of PGM-bearing particles through the different size classes.

10.2 Mineralogy and floatability

PGM's that are liberated or associated with BMS can usually be recovered relatively easily during flotation, and the majority of this material can be classified as fast floating. Exceptions are very coarse BMS particles, as well as very fine PGM and BMS particles, which are recovered at a slower rate. PGM's locked in gangue would normally be considered non-floatable. Floatability of partially liberated PGM's can range from very slow floating to fast floating, depending on size and degree of liberation.

The difference in size between the BMS and PGM grains has implications on the optimum flotation size range for this ore. From the ore mineralogy in Chapter 4, BMS liberate above 10µm, whereas the PGM grains require a grind appreciably finer than 10µm in order to achieve full liberation. These observations will be discussed in more detail once the flotation by size results is discussed.

10.3 Milling results

The final milling stage of each configuration achieved a similar size distribution with the same type of mills. Therefore, an assumption is made that any difference in flotation performance is the result of circuit configuration, rather than size distribution. Note however, that the overall size distribution does not imply that the PGM size distribution is also the same between the circuits.

10.4 Flotation

For campaign 1, Figure 4.10 shows that PGM recovery increased with additional milling and flotation stages, while the single mill-float circuit displayed a higher initial rate of recovery and higher grades. Similar trends were observed for the second campaign (Figure 5.8), although the increase in recovery with the MF2 circuit was not as pronounced. However, Table 8.4 shows that a significant amount of fine, slow floating material was left unrecovered in the final tails of the campaign 2 MF2 circuit. This was the result of the shorter flotation residence time in the second campaign, an intentional choice to generate data at these sub-optimum conditions to assist with the design framework. However, the potential recovery for the regrind circuit was also much higher in campaign 2.

The improvement in recovery with multiple grind-float circuits is usually attributed to a reduction in over-grinding. However, from Figure 4.15 it can be seen that the regrind circuits outperformed the single stage circuit in all size fractions. Therefore, the over-grinding of fine, floatable material cannot be the only explanation for the improved recovery with multiple stages. This is analysed in more detail in the next section with respect to the flotation by size results.

The higher initial rates observed with single stage configurations can be explained by the finer primary grinds. This is illustrated by Table 10.1, which shows the amount of non-floating material in the feed of the various circuits:

Table 10.1 Non-floating PGM fraction in primary feed for the different circuits

	Non-floating fraction in primary feed
Campaign 1 MF1 Primary	0.39
Campaign 1 MF2 Primary	0.76
Campaign 1 MF3 Primary	0.69
Campaign 2 MF1 Primary	0.44
Campaign 2 MF2 Primary	0.82

The table shows that the single-stage circuits (highlighted), produced significantly less non-floatable PGM's in the primary feed. This would result in higher rates and recoveries in the

primary circuit. The higher grades observed with inert circuits was discussed in more detail in Chapter 9.

For a more detailed analysis of each circuit, the flotation performance will now be analysed on a size-by-size basis.

10.5 Flotation by size

For the first campaign, Figure 4.15 shows that the regrind circuits outperformed the single stage circuit in all size fractions. This result was confirmed by the second campaign, shown in Figure 5.13. Three main conclusions were drawn from these findings:

(a) All the circuits achieved the highest recovery in the -10µm fraction. Because of screening limitations, it was difficult to detect a size below which flotation becomes inefficient (although, clearly there is a minimum size, as discussed below)
(b) The regrind circuits outperformed the MF1 circuit in the -10µm size fraction.
(c) The regrind circuits also outperformed the MF1 circuit in the size fractions coarser than 10µm.

These observations will now be discussed in more detail.

10.5.1 Minimum flotation size

Figure 4.15 shows that PGM recovery increased with decreasing size for all the size fractions that were measured. Therefore, a minimum size for optimum flotation could not be determined. The mineralogical associations of the PGM's in this ore complicate analysis of the data. For instance, BMS would readily liberate in the 10-53µm fraction. These liberated BMS and associated PGM's fall within the optimum flotation size range for BMS, and can therefore be considered fast floating. However, PGM's locked in gangue, as well as partially liberated BMS are also present in the 10-53µm fraction, effectively lowering the overall floatability of PGM's in that size fraction. Milling finer than 10µm would greatly reduce these locked and partially liberated PGM's. Therefore, it appears as though liberation plays a bigger role than particle size in recovery of UG2 ore, resulting in higher PGM recoveries in

the -10µm size fraction. The same conclusion was reached by Pease *et al* (2006), who found that ultra-fine particles can readily be recovered by flotation, provided these particles are liberated.

Although the PGM recovery was highest in the -10µm size fraction, the improvement in recovery that was realised by stage-wise removal does suggest that over-grinding can occur. However, limitations on screening smaller than 10µm complicate further analysis of this effect.

10.5.2 Lower MF1 recovery in –10µm fraction

The inferior PGM recovery achieved in the –10µm fraction by the MF1 circuits when compare to the regrind circuits is most likely a result of over-grinding of PGM and BMS particles. Ideally, BMS particles should be floated as soon as they are liberated, since the majority of these particles will be in the optimum flotation size range. Any grinding after liberation of BMS increases the risk of over-grinding. In particular, PGM grains locked in overground BMS are likely to be lost, especially if those grains are ultra-fine (smaller than 4µm), or comprised of PGM minerals that are known to be characterised by poor floatability (such as PGM sulfarsenides or PGM alloys). Those minerals are likely to be lost even if they are subsequently liberated in a further milling stage. The same argument holds for the PGM particles associated with gangue material. The majority of PGM's only liberate below 10µm, and are therefore even more susceptible to over-grinding. Although the sub -10µm liberated PGM's should have a higher floatability than a larger non-liberated PGM particle, any subsequent grinding after liberation would likely have a detrimental effect on floatability. Therefore, stage-wise removal of liberated particles should minimise the impact of over-grinding on PGM recovery.

10.5.3 Lower MF1 recovery in +10µm fractions

The improved PGM recovery achieved with the MF3 circuit in the size fractions coarser than 10µm indicates that over-grinding is not the only factor affecting PGM recovery. Otherwise PGM recoveries in the optimum flotation size range would have been similar for all three configurations. Two possible explanations present themselves: Firstly, partially liberated

PGM's grind at a faster rate than PGM's locked in gangue, and secondly impact and attrition type breakage have different effects on coarse, locked particles.

Preferential liberation on +10µm recovery

Consider Figure 10.1:

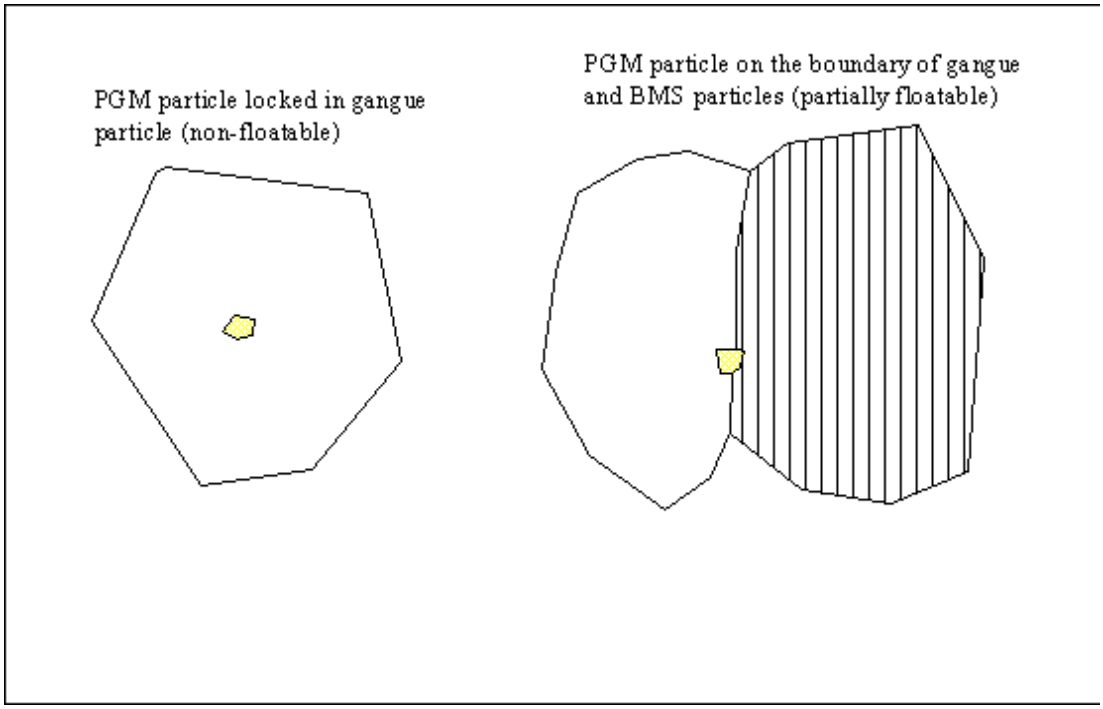

Figure 10.1 Schematic representation comparing a PGM particle locked in gangue with a PGM particle on the boundary of a gangue and BMS particle

It is plausible to suggest that breakage will occur preferentially on the grain boundaries, since more energy would be required to break single grains than composite grains. Therefore, the partially liberated particle in Figure 10.1 requires less energy to break than the gangue particle. Any breakage of the ore would therefore preferentially grind floatable PGM-bearing particles over non-floatable PGM-bearing particles. This would result in a gradual decrease of the average floatability in all the +10µm size fractions. The effect would be most pronounced in coarser size fractions, where most of the PGM's occur either as locked or partially liberated BMS particles. Since grinding decreases the average floatability in the coarser size fractions, stage-wise milling and removal of floatable material would result in higher recoveries in these sizes.

The claim that preferential grinding occurs is supported by the fractional PGM analysis performed on the ore sample used in these tests (Figure 10.2). Standard run-of-mine ore, crushed to 100% passing 6mm was used as feed for all three configurations.

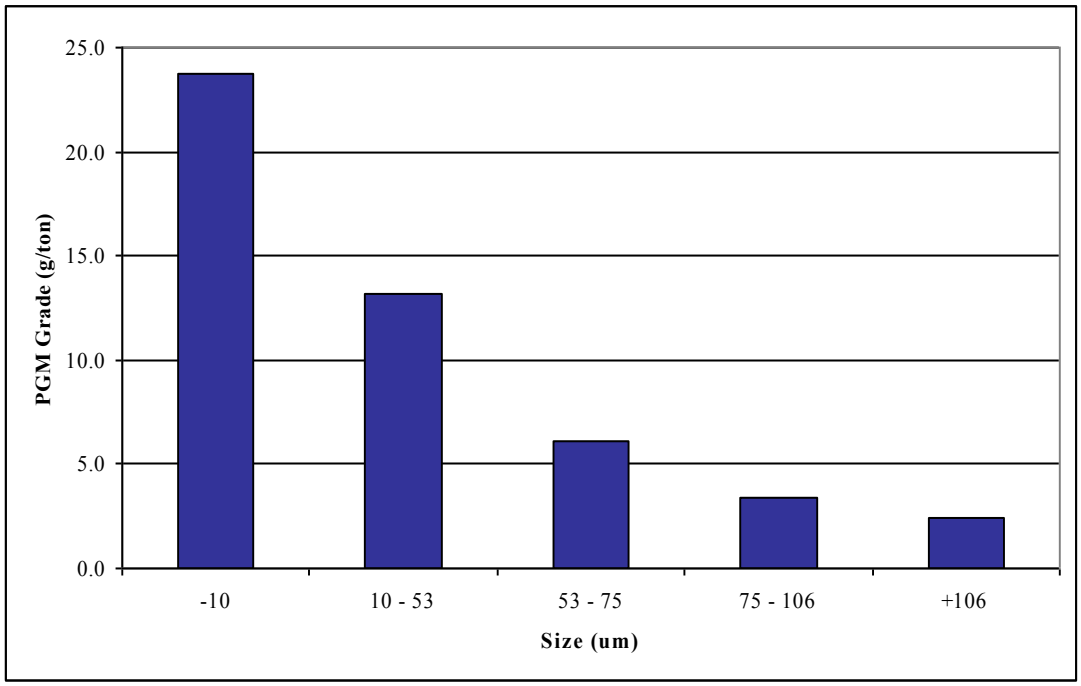

Figure 10.2 Fractional PGM analysis of the crushed ore sample used in the test work

From Figure 10.2, it can be seen that blasting of the ore and subsequent crushing to –6mm resulted in an exponential increase in PGM grade with decrease in size.

This feed sample (10% passing 75µm) was milled to 83% passing 75µm for the MF1 configuration. The change in total units of mass is compared to the change in PGM units for each size fraction in Table 10.2:

Table 10.2 Changes to total mass and PGM units by milling to 80% -75µm

Size Fraction (µm)	Normalised Mass Units Change	Normalised PGM Units Change
+106	-100.0	-100.0
106 - 75	3.5	-5.4
75 - 53	23.1	9.3
53 - 10	53.3	47.4
-10	20.2	48.7

The units were normalised to reflect the change in each size fraction by depleting the +106µm fraction by 100 units. It shows that 20% of the total mass depleted from the +106µm reported to the –10µm fraction, whereas 49% of the PGM's depleted from the +106µm reported to the –10µm fraction. Together with Figure 10.2, this clearly indicates preferential grinding of PGM's. Since Table 10.2 shows that the rate of PGM size reduction is much greater than that of the bulk of the ore, it is plausible to assume that the preferential grinding refers to PGM's on grain boundaries, rather than PGM's locked in gangue. This would result in a decrease in floatability of the coarser size fractions with extended milling circuits such as found in the MF1 configuration.

Milling mechanism on +10µm recovery

A second reason for the increase in recovery with size fractions coarser than 10µm is the effect of attrition type grinding on locked particles. In the previous chapter, it was shown that attrition grinding generates significant amounts of partially liberated material in coarser size fractions. Floating these particles in stages would result in a higher recovery in a specific coarse size, as any subsequent grinding increases the chance that the particle would be liberated to a finer size fraction.

10.6 Circuit design considerations

Three important parameters need to be determined when designing the main milling and rougher circuits. Firstly how fine to grind the ore, secondly at which grinding intervals to introduce a flotation stage and finally how much residence time to allow for each flotation stage.

10.6.1 Target grind and number of mill-float stages

The final size distribution and the number of mill-float stages in a circuit are determined by the balance between liberation of minerals and over-grinding of those liberated minerals. One extreme would be to liberate all valuable minerals before flotation, but this approach would result in considerable losses due to over-grinding. The other extreme would be to float each valuable particle as it becomes liberated, but this is not practically feasible. Therefore, the

circuit designer attempts to optimise return on investment by maximising recovery and minimising capital expenditure, and this is done by balancing liberation and over-grinding.

In order to establish optimum grind and the number of mill-float stages, information is required on the liberation characteristics of the ore. The ideal method would be to measure liberation at different size distributions. However, this is usually not feasible due to cost and the amount of sample needed for mineralogy. Therefore, the degree of liberation is usually inferred from batch flotation tests at different grinds. These tests will establish a recovery-grind relationship such as shown in Figure 10.3:

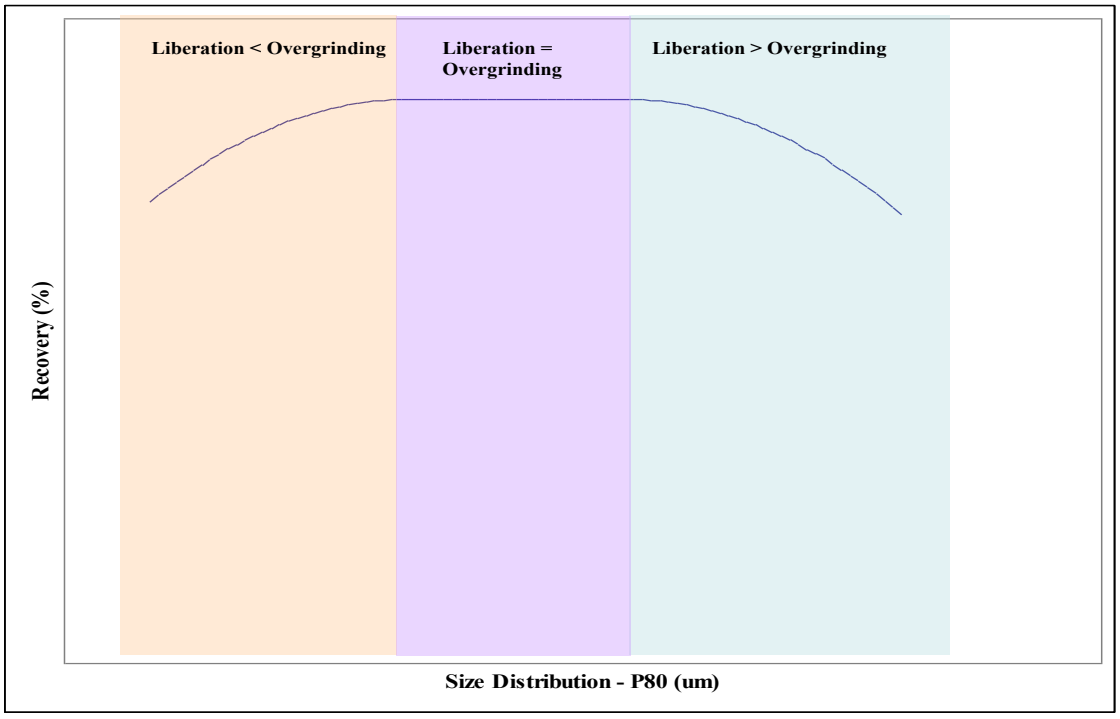

Figure 10.3 Recovery vs. grind relationship

All ore types will display the general shape of the curve shown in Figure 10.3, although the position and extent of the various zones will differ. There will be a zone at the coarse end where recovery increases as the grind becomes finer (liberation dominates), a zone in the middle where the recovery does not change with grind (liberation and over-grinding in balance) and a zone at the fine end where recovery decreases as grind becomes finer (over-grinding dominates). The ideal target grind will be at the coarse end of the zone where liberation and over-grinding is in balance. This is the point where the degree of liberation is maximised and the amount of over-grinding minimised. Introducing flotation stages at incremental intervals during the grinding process will result in the overall exposure of the ore

to the curve shown in Figure 10.3 to move to the left. In other words, since over-grinding is minimised by stage-wise removal of valuable material, liberation will dominate for longer and therefore the recovery would also be higher. This method could be refined by analysing the flotation response in different size fractions as the overall grind changes. This would be more effective at revealing signs of over-grinding, especially at or below the optimum size for flotation. To illustrate this, consider the first cell recovery for three of the primary circuits under investigation in this project (Table 10.3). The circuits were selected to represent the widest size range from the primary circuits that were tested.

Table 10.3 Sized PGM recovery in the first rougher cell

	% passing 75µm	**PGM Recovery in the First Cell (%)**		
		+75µm	**+10µm**	**-10µm**
Campaign 2 MF2 Primary	57.4	13.4	53.5	54.0
Campaign 1 MF2 Primary	66.4	11.5	59.0	53.8
Campaign 1 MF1 Primary	81.5	15.8	47.4	52.6

The first cell recoveries shown in Table 10.3 serve as a proxy for the initial rate of recovery. It can be seen that there is little difference in these initial "rates" for the +75µm and -10µm fractions, whereas a drop in rate was observed for the +10µm fraction at the finest grind. This suggests that some over-grinding is occurring in the +10µm fraction. For this size fraction, the optimum is reached where the liberation of BMS particles (with associated PGM's) is balanced by the over-grinding of these minerals. The decrease in rate that was observed for the +10µm suggests that over-grinding of BMS is starting to dominate at the finest grind (81.5% -75µm). From this data, an ideal grind to introduce an intermediate flotation stage would be between 57.4% and 66.4% -75µm, before the over-grinding of BMS dominates liberation.

10.6.2 Flotation residence time

Ideally the flotation residence time in each stage should be long enough to recover all liberated particles. However, this is not practical for two reasons – the first is that the cost of installing additional flotation capacity might not be covered by the recovery of extremely slow floating particles. The second reason is that most concentrators operate under some sort of concentrate quality constraint – whether it be grade, mass pull or the rejection of some undesired by-product (such as Cr_2O_3 in the case of UG2 ore). These constraints establish a hurdle that some slow floating particles cannot overcome – even if these particles would be recovered in roughers, they would be rejected in the cleaning stages in order to achieve concentrate targets. Since grade is such an important consideration when deciding on flotation residence time, it is necessary to determine the flotation response of the valuable mineral relative to the gangue. This can be done by conducting laboratory or pilot plant flotation tests, and calculating the response of fast and slow floating gangue and valuable minerals. To illustrate, consider Figures 10.4 to 10.6, showing these responses for the steel circuits (the steel circuits were selected since it was possible to derive a gangue model for them):

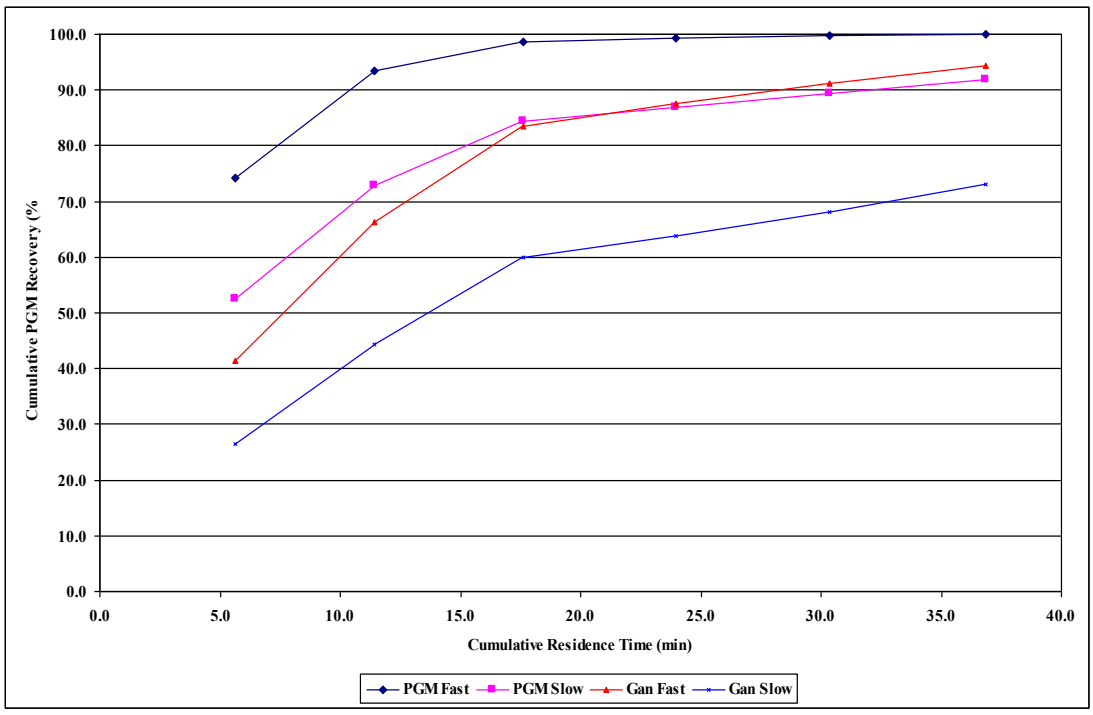

Figure 10.4 Campaign 1 MF3 primary circuit PGM's and gangue fast and slow flotation response

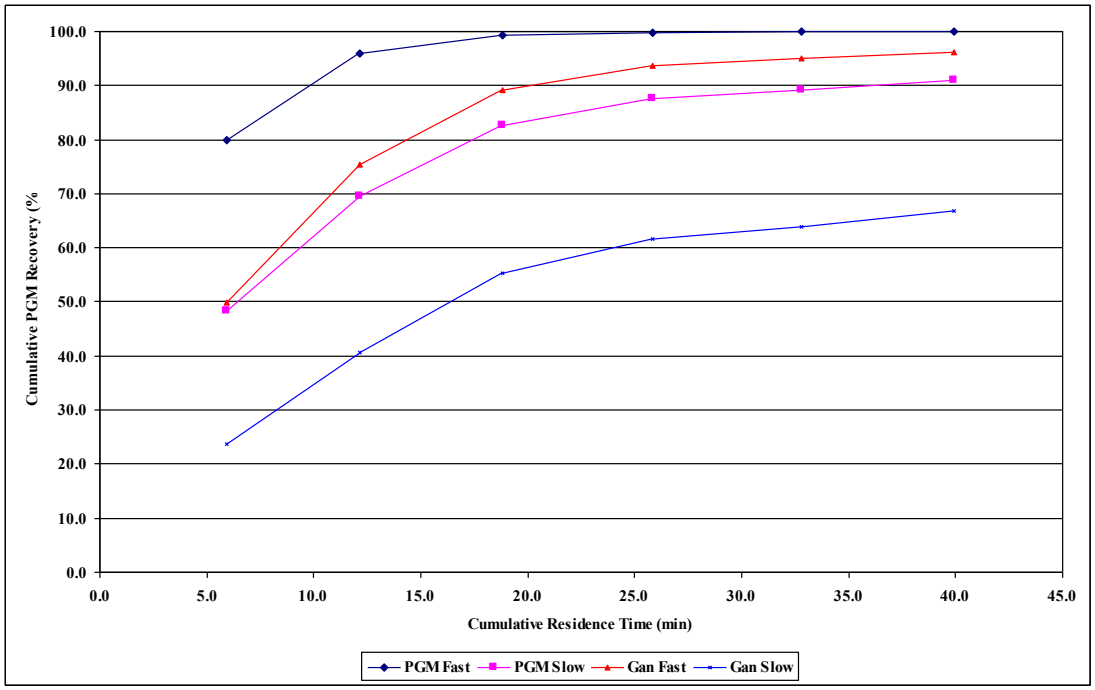

Figure 10.5 Campaign 1 MF2 primary circuit PGM's and gangue fast and slow flotation response

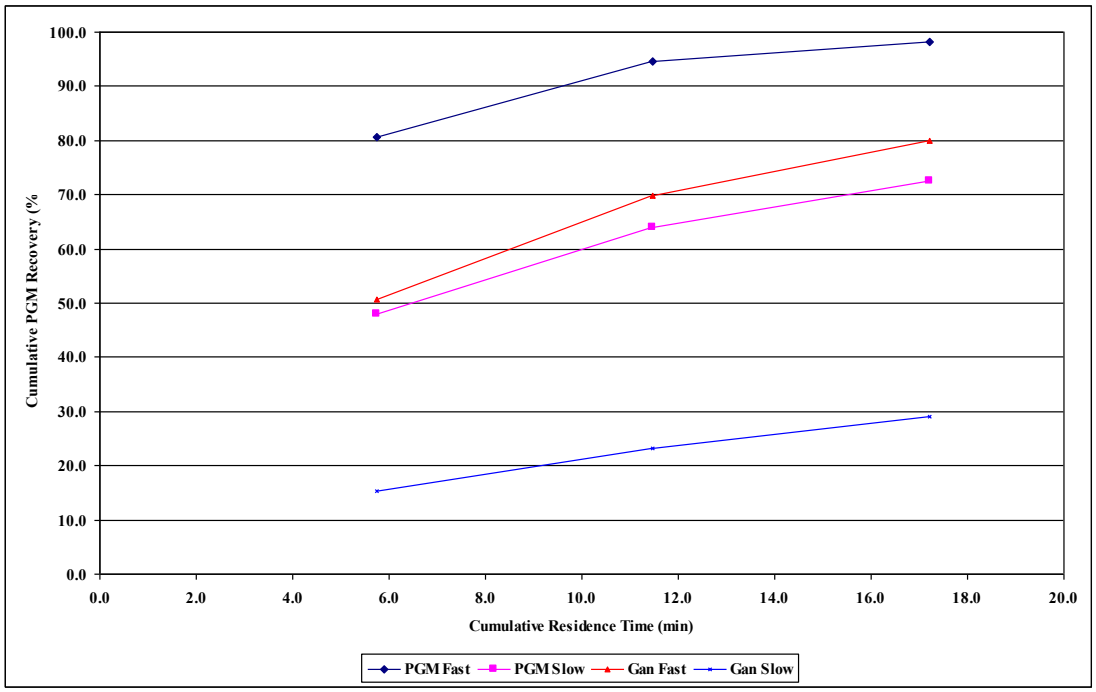

Figure 10.6 Campaign 2 MF2 primary circuit PGM's and gangue fast and slow flotation response

The flotation responses for all three circuits displayed similar trends, with almost all fast floating PGM's recovered between 15 and 20 minutes. The flotation response of the slow floating PGM's were comparable to that of fast floating gangue, suggesting that a significant portion of these particles were partially liberated PGM's with associated gangue. The slow floating gangue was probably not associated with faster floating sulphides. The kinetics of the

fast floating PGM's should ensure that the majority would be recovered under any cleaning regime, and therefore the minimum rougher residence time should ensure that all fast floating valuables are recovered. Depressant addition and multiple cleaning stages should reject most of the free, slow floating gangue – thus rougher residence time is determined by the amount of slow floating valuables to allow into the cleaning circuit. This partially liberated material can be influenced by depressant, and it is not sensible to recover material in the roughers that cannot overcome the grade hurdle set by the cleaning regime. Test work on rougher concentrate should reveal the flotation kinetics of the slow floating PGM's in the cleaning circuit. By combining this response in the cleaning circuit with the desired final concentrate grade, it should be possible to determine the amount of slow floating valuables that can be recovered in the roughers. From Figures 10.4 to 10.6 the rougher residence time can then be calculated.

It is not always possible to derive a model for floatable gangue, as was experienced with the inert circuits in this project. In such a case grade can also be used in conjunction with fast and slow floating valuables to evaluate rougher residence time. Figure 10.7 shows the fast and slow floating PGM's, together with the cumulative grade for the Campaign 1 MF1 circuit:

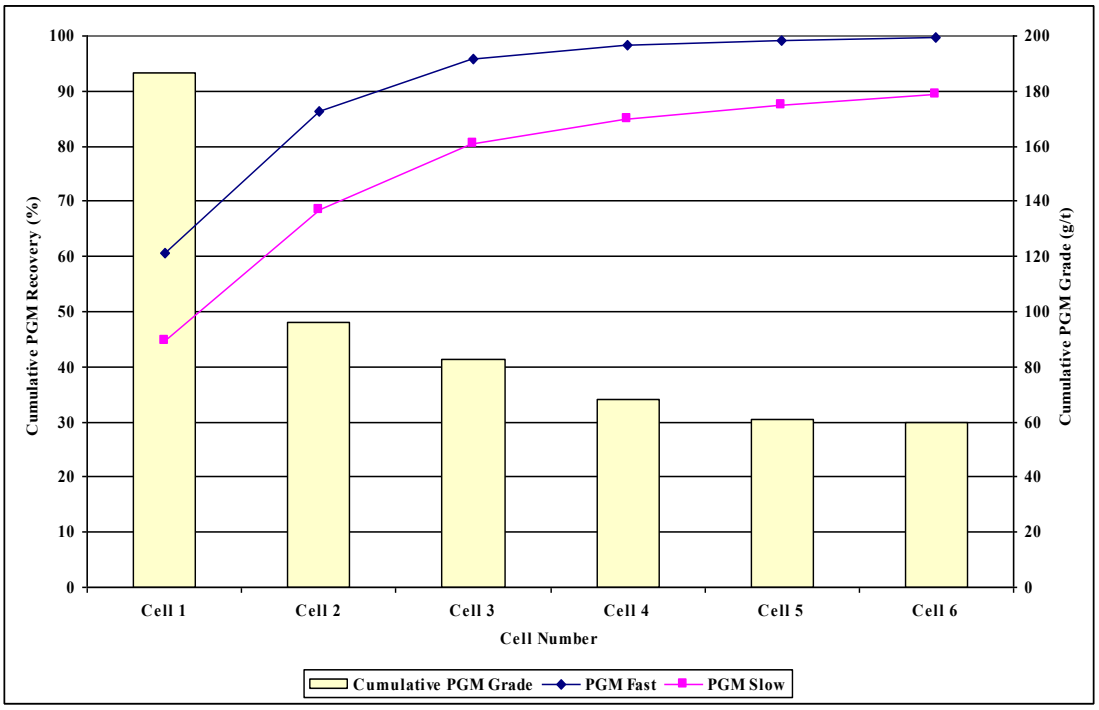

Figure 10.7 Campaign 1 MF1 PGM fast and slow flotation response and cumulative PGM grade

As was the case for the steel circuits, almost all fast floating PGM's were recovered between cells 3 and 4, which correspond to between 15 and 20 minutes residence time. It can also be seen that the grade stabilises once most of the fast floating material was recovered, indicating that the recovery of slow floating PGM's and gangue are in balance. This is also consistent with the findings for the steel circuits, which showed that slow floating PGM's and fast floating gangue display similar flotation rates. Once again, from this information and some laboratory flotation work on rougher concentrate it should be possible to determine the optimum flotation residence time.

To summarize, the number of cleaning stages and depressant dosage in the cleaning circuit sets a grade hurdle that some slow floating valuables cannot overcome. The rougher residence time should therefore be set to recover all fast floating valuables, and only the slow floating material that could potentially be recovered in the cleaners while achieving the final concentrate quality target.

CHAPTER 11
CIRCUIT DESIGN FRAMEWORK

11.1 Introduction

Every ore type has unique challenges that are often solved with unique, ore specific solutions. Therefore, it is not possible to develop a circuit design methodology that will cater for all ore types. For example, the issues with chromite in UG2 ore have been addressed with solutions that are ore specific: In order to prevent reverse classification, and the subsequent over-grinding and recovery of chromite, UG2 circuits have evolved to open circuit classification with extended cleaner banks.

Despite this caveat, in this chapter an attempt will be made to identify some general considerations regarding circuit configuration and milling devices. This will be done from the discussions in the previous chapters about multiple mill-float stages and the type of milling device. However, it is worth considering that the best theoretical circuit is often not the most advantageous in financial terms. A simple, sub-optimal circuit will often return a better yield on investment than a more complicated circuit with a theoretically superior design. These financial considerations are implied in all discussions in this chapter, although not always mentioned explicitly.

11.2 Liberation and size distribution

Circuit design methodology is driven to a large extent by the liberation characteristics of the ore. Therefore, the development of a design framework will usually focus on the liberation of valuable particles. However, because of time and cost constraints the direct measurement of milling performance is usually not liberation, but size distribution. Section 10.6 showed a methodology to determine the target size distribution of an ore from a series of laboratory flotation tests at different grinds, and using the recovery as a substitute for liberation. This method could be refined by analysing the flotation response by size, as it should be easier to detect over-grinding at or finer than the optimum size for flotation. This would also reveal at which grind to introduce intermediate flotation stages.

Although the target size distribution and number of mill-float stages could be determined by this method, mineralogy should still be performed on the ore. This will determine general mineralogical trends such as the size and associations of the valuable minerals. Furthermore, breakage tests should be performed to characterise the hardness and breakage characteristics of the ore. Therefore, the information needed for efficient circuit design is a flotation response per size in each size fraction, ore hardness and breakage characteristics and the size and associations of the valuable minerals. From this information the number of communition devices can be selected, as well as number of mill-float stages. It should also be possible to estimate the target grind in each milling stage.

11.3 Type of milling devices

The main function of the primary communition stage in any circuit is to reduce the top size of the ore, to allow for efficient materials handling through the rest of the circuit. The most energy efficient way to break run-of-mine (ROM) ore is still through a crusher plant. Crusher product could be fed to a rod mill, which would allow for flotation with minimal over-grinding. However, despite these advantages, new installations almost exclusively favour ROM type mills. This is because the overall capital cost, maintenance cost and operability of a ROM mill overshadow the advantages of a crusher plant. The relatively new HPGR technology in minerals processing may revive the crusher plant, but currently the primary comminution device in any new circuit would most likely be a traditional mill – autogenous (AG), semi-autogenous (SAG) or ROM ball mill, depending on the ore type. An exception would be if the ore is exceptionally competent, in which case a crusher plant would be used to reduce the top size. Currently such a crusher plant would most likely include a HPGR. The need for subsequent milling devices is usually a function of the quantity and deportment of the valuable minerals (the mineralogy of the ore).

If additional milling stages are necessary, the types of milling devices required for these additional communition stages will depend on the target size distribution, which is driven by the size distributions of the valuable minerals. If a relatively fine grind is required to achieve liberation, the primary mill would not be able to provide the attrition type grinding necessary for fine milling. In this case a traditional ball mill, or even a stirred mill for finer grinds (typically less than 10μm) would be required.

11.4 Number of stages and flotation residence time

The two most important factors when considering additional milling stages is the size distribution of the valuable minerals and the minimum size for optimal flotation. When the mineral grain size is relatively coarse, it is often possible to achieve sufficient liberation via impact breakage in the primary mill. However, even if the mineral is coarse, if a significant amount of material is finer than the minimum size for optimal flotation, a second mill becomes an option to allow for stage-wise flotation. Therefore, a second milling device might be required if a significant amount of mineral is finer than the minimum size for optimal flotation, and/or if it is not possible to achieve sufficient mineral liberation in the primary mill. The methodology described in Chapter 10.6.1 should confirm whether over-grinding is an issue and at what size distribution to introduce an intermediate flotation stage. Flotation residence time for each stage can be determined from the procedure in Chapter 10.6.2, by evaluating the fast and slow flotation responses of the valuable minerals against the response for gangue or the grade profile.

It is possible that the ore characteristics demand more than one milling device to achieve the target grind, although the mineralogy and flotation characteristics don't require additional flotation stages. Note that it should always be beneficial from a minerals recovery point of view to have a flotation stage after a milling device, even if this is a flash cell in the milling circuit. However, if the risk of over-grinding is slim, it is often not financially beneficial to include the additional flotation stages. In addition, process instability can become more problematic with increased circuit complexity, which can easily override any improvement in recovery potential. The driving factor in the number of flotation stages is the risk of over-grinding. When the mineral being liberated is significantly coarser than the minimum size for optimal flotation, and the mills are sized correctly, only one flotation stage is required, irrespective of the number of milling stages. However, when the mineral is close to or finer than the minimum size for optimum flotation, multiple mill-float stages will always be beneficial for recovery.

From the discussions in this chapter, a decision path to determine the number of communition stages, the milling type and the number of rougher stages is proposed in Figure 11.1:

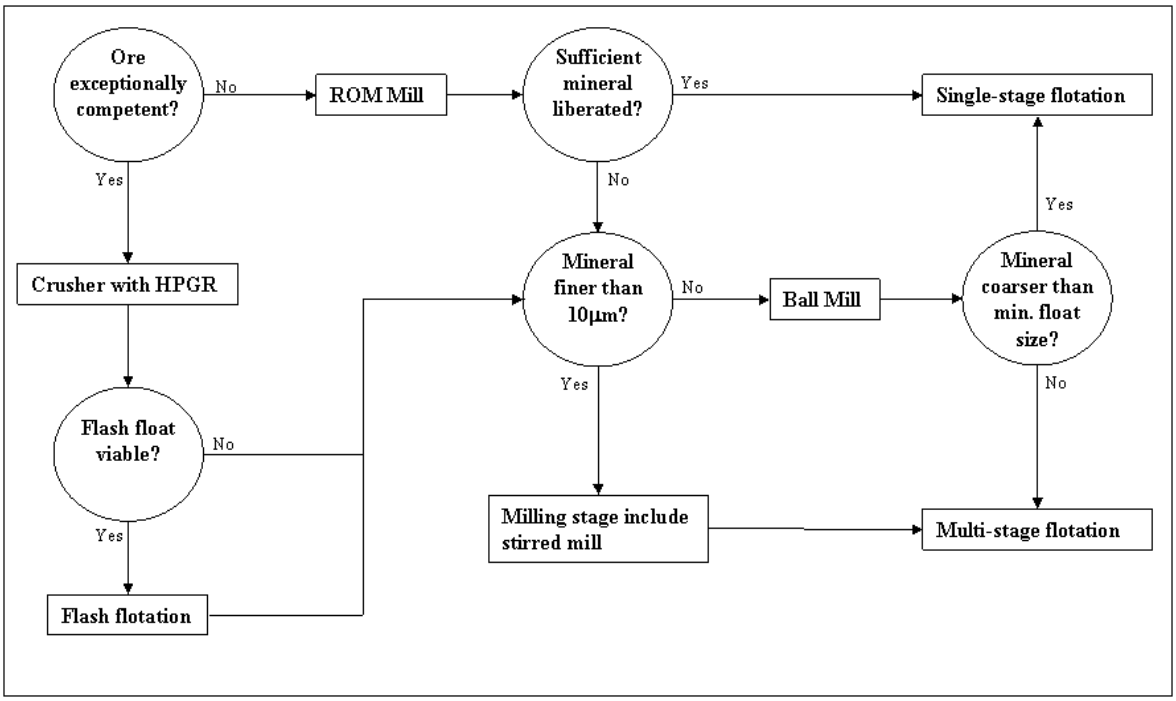

Figure 11.1 Proposed decision tree for circuit selection

Note that the ROM mill in the diagram refers to any run-of-mine milling device, whether it is an autogenous, semi-autogenous or ROM ball mill. Mineral refers to mineral grains in the host rock. Multi-stage flotation in the diagram refers to multiple milling and rougher flotation stages.

In the section that follows, the decision tree shown in Figure 11.1 is used to evaluate the mill and circuit selection for three platinum-bearing ore types found within Lonmin.

11.5 Case studies – platinum bearing ore types

11.5.1 Merensky ore

The decision tree for Merensky ore is shown in Figure 11.2:

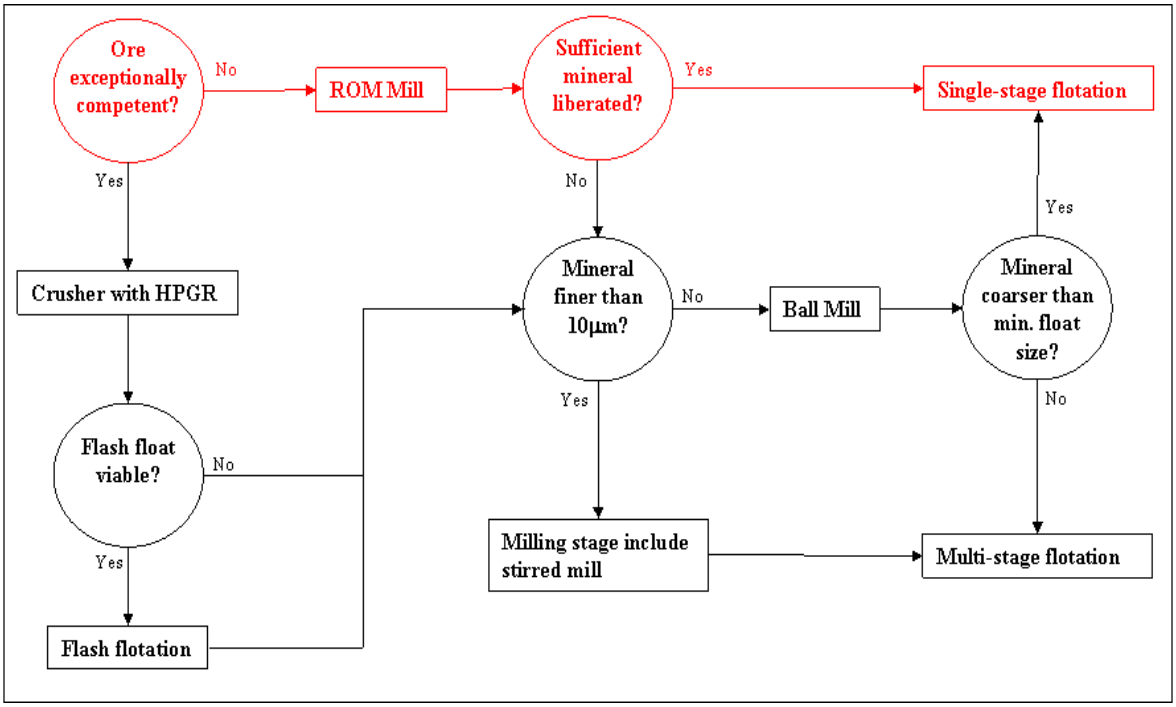

Figure 11.2 Decision tree for Merensky ore

The red path shows the typical decision tree for Merensky ore. In the Merensky ore found at Lonmin, the vast majority of PGM's are associated with BMS. Therefore this decision tree looks similar to a bulk BMS float. Typically, most of the BMS can be liberated in a ROM mill – for Merensky a ROM ball mill is usually used. Since most of the BMS have been liberated, and most of the PGM's are associated with these BMS, only a single flotation stage is required. Note that a subsequent milling and flotation stage will almost certainly liberate and recover additional valuable minerals. However, for Merensky ore this improvement is usually not sufficient to cover the capital and operation expenditure of the additional mill-float stage.

11.5.2 UG2 ore

The decision tree for UG2 ore is shown in figure 11.3:

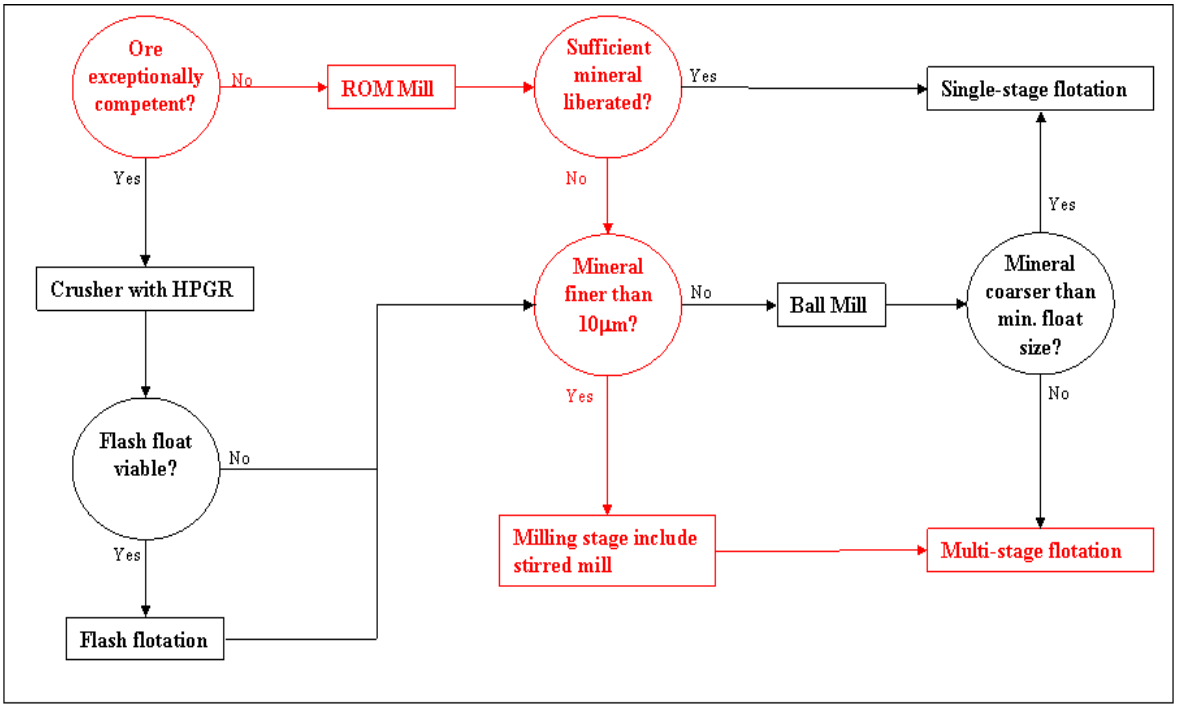

Figure 11.3 Decision tree for UG2 ore

The mineralogy of Lonmin's UG2 ore has been discussed in Chapter 4. Since the ore is not exceptionally competent, a ROM mill (ROM ball mill in this case) can be used as the primary communition device. However, because a significant amount of ultra-fine (-10µm) PGM minerals are associated with gangue minerals, the impact breakage in the primary mill cannot efficiently liberate these particles. Also, since these particles are ultra-fine, a stirred mill would be required for efficient liberation. Any circuit that uses a stirred mill would have a significant risk of over-grinding, and therefore multi-stage flotation would be beneficial. It should also be noted here that stirred mills allow for a lot of flexibility in circuit design. For instance, it might be beneficial to split the fine and coarse fractions after the primary milling stage, and treat only the fine fraction in a stirred mill and the coarse fraction in a ball mill. Also, care should be taken with the classification of UG2 ore, especially in a stirred milling application. Reverse classification of fine chromite to the cyclone underflow can result in inefficient liberation of valuable particles and/or the accumulation of the chromite in the mill, which can lead to equipment failure. Finally, the fine nature of the PGM minerals in UG2 ore creates the potential for much higher concentrate grades than with Merensky ore. Although a finer grind usually results in higher entrainment of gangue minerals, the disassociation of PGM minerals from BMS in UG2 ore results in much higher grades. The effect of more entrainment at finer grinds is completely overshadowed by the effect of recovering finer PGMs with less association with other minerals. This can be exploited in the cleaning circuit

with the addition of a stirred mill, to liberate ultra-fine, partially liberated PGM minerals from gangue and to clean PGM mineral surfaces.

11.5.3 Platreef ore

The decision tree for Platreef ore is shown in figure 11.4:

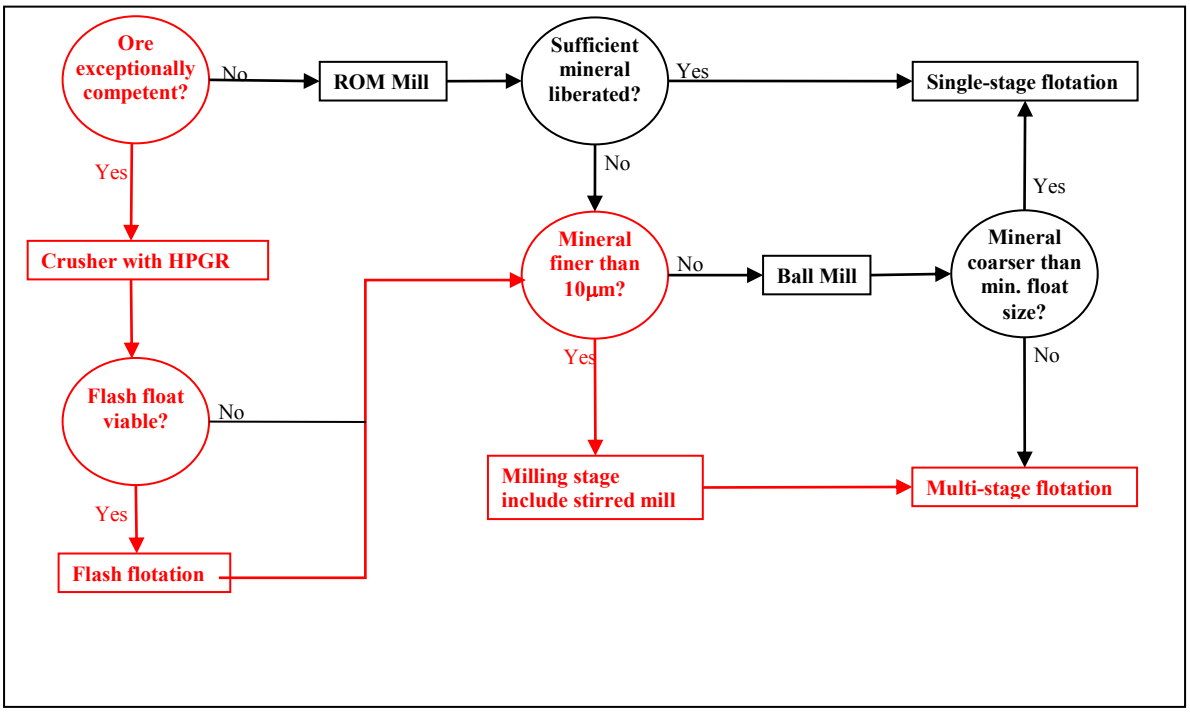

Figure 11.4 Decision tree for Platreef ore

Lonmin's Akanani deposit is classified as Platreef ore. This ore type is exceptionally competent, and requires pre-crushing. This allows for the use of a HPGR with flash flotation. Since a significant proportion of the PGE's occur as free sulphide minerals (finer than 10µm), a stirred mill is required to provide the attrition grinding to liberate these minerals. Any circuit with a stirred mill has a significant risk of over-grinding, which necessitates more than one flotation stage. Note that in this instance the flash float is the first stage, followed by an additional stage after every mill in the circuit.

These three examples illustrate the basic decision making philosophy for the main stream milling and flotation circuits and milling devices. Additional considerations will typically include classification and grade control. Efficient classification has the potential to significantly improve the efficiency of a milling circuit. However, the extent of this impact is

often ore dependent. In general, the more homogeneous the ore, and the narrower the valuable mineral size distribution, the more efficient classification should be.

Although grade control is usually determined by the cleaner circuit design, the milling and rougher circuits can also play a role. A prominent example from this study is the significant improvement in grade that was realised with stirred mills. Results suggest that higher grades could be achieved when stirred or inert mills were used. Therefore, it is a possibility to include stirred mills for grade considerations, especially when the risk of over-grinding is minimal.

CHAPTER 12
CONCLUSIONS

12.1 Introduction

The aim of this work was to establish a framework for the design of milling and flotation circuits to treat platinum bearing ore from the UG2 reef, to extend these rules to other platinum bearing ores in particular, and as far as possible, to complex ores in general. The primary focus of the work was on main stream milling and rougher design. In order to establish the design framework, firstly it was necessary to evaluate the effect of the breakage mechanism of particles on the resultant floatability profile, and secondly to assess the behaviour of these particles in a multi-stage milling and flotation circuit. For a PGM-bearing UG2 ore, these effects were analysed at different size fractions for both the valuable and gangue minerals.

Tests were conducted on circuits in a variety of configurations (MF1, MF2 and MF3) each incorporating a ball mill (where impact breakage would be dominant) and two stirred mills (where attrition breakage would be dominant). The test work was also repeated at different grinds and flotation residence times. Where possible, data was gathered with respect to size, assay and mineralogy. However, some characteristics of the response of the ore could not be measured directly, and these had to be inferred (or estimated from the measured data) by fitting an appropriate model. The most important characteristic determined in this way was the floatability distribution of the ore through the different circuits.

In order to evaluate the effect of the breakage mechanism on the floatability distribution of the product, account needed to be taken of effects related to the chemical environment of the particles in the different milling devices. This is owing to the fact that the milling devices that were used paired impact-dominant breakage with steel media, and attrition-dominant breakage with ceramic media. A qualitative attempt was made to decouple these factors by considering the response of the different size fractions, as it was considered that the effect of surface phenomena on the floatability distribution would be most prevalent in the finer size fractions, while the effect of breakage on the floatability distribution would be most prevalent in the coarser size fractions.

12.2 Analysis methodology

For each circuit, a model was fitted to the mass balanced data to estimate the floatability distribution in each stream and size fraction. This information was then used to evaluate the milling devices and circuit configurations, using the mineralogical analysis of selected streams to support the analysis.

It was not the objective of this project to develop a new flotation model, and so the most suitable model for the required purpose was selected from the literature. However, the nature of the data obtained in this study made it necessary to develop some novel methods with respect to the application of the model. In particular, methods were developed with respect to (Chapter 6):

- Using unsized batch flotation data in combination with the size-by-size data provided by the circuit mass balance to constrain the model parameter search
- A robust procedure to estimate the size-by-size entrainment response of the ore.
- A formula that was derived to determine the entrainment contribution in a batch flotation system.

12.3 Circuit design framework

The main factors that were investigated to provide insight into a design framework were the effect of the type of breakage, as well as the number of milling and flotation stages. It was found that the effect of the breakage mechanism appeared to be dominant over the effect of the chemical environment in most size fractions for UG2 ore, which is most likely a result of the sparse sulphide mineral content of this ore type (< 0.01 %). The effect of the breakage type, as well as the number of milling and flotation stages (circuit configuration) are discussed in the sections that follow.

12.3.1 Breakage mechanism

Findings and discussion

(a) Figures 9.1 and 9.2 shows that circuits with a stirred mill as final milling stage achieved higher recoveries than the ball mill in both the +75μm and +10μm size fractions. This could be attributed to the breakage mechanism, since particles in a stirred mill are subjected to surface attrition, usually exposing mineral surfaces without destroying the host particle. By contrast, a significant proportion of particles in a ball mill are shattered by massive impact, resulting in material being liberated to smaller size fractions. The result is higher recoveries with a stirred mill circuits in the coarsest size fraction (+75μm in this study). The effect was less pronounced in the middling sizes (+10μm -75μm in this study), as it becomes more likely that attritioning results in liberation of the minerals into the finest size fraction.

(b) The floatability profile of the -10μm fraction (Tables 9.11 and 9.12) shows that inert attrition grinding generated more fast and non-floating material than impact breakage, suggesting that stirred mill circuits were more efficient at liberating particles in the finest size fraction. However, it also indicates that stirred mill circuits were more likely to over-grind liberated particles.

(c) The results of the stirred mill circuits in the +75μm and +10μm size fractions could be fully explained from breakage mechanism only, suggesting that the effects of the chemical environment in the mill and surface cleaning was not prominent. However, the floatability increase in the -10μm with stirred mills suggests that these effects could well have played a role in the finest size fraction.

(d) Throughout these campaigns, higher grades were measured with inert mills as final grinding stage than steel mills. In Section 9.6, a comparison of the fast floating material in the +10μm and -10μm fractions suggests that PGM's are liberated from BMS through attrition grinding in inert mills, a process which is also likely to overgrind the BMS. Ultra-fine, free PGM's would produce a higher grade than PGM's associated with relatively coarse BMS.

Implications for circuit design

(a) While the attrition action in a stirred mill produced higher recoveries in the coarser size fractions, the ball mill was still more efficient at liberating particles from the coarse size fractions; although the liberated material was recovered in finer size fractions. The ball mill is also more efficient at top size reduction, which is an important consideration since one of the main objectives of any communition circuit is to produce a size distribution that can be handled by the rest of the circuit.

(b) Stirred mills are more efficient than a ball mill at grinding and liberating minerals from fine material. Therefore, stirred mills should be considered when a significant amount of valuable material is locked in the finer size fractions. Although stirred mills will also grind and liberate material in the coarse sizes, this liberation and size reduction will be a slow and energy inefficient process.

(c) Since stirred mills are prone to over-grinding of fine, liberated minerals, multi-stage mill-rougher circuits should be considered when utilising these devices.

12.3.2 Circuit configuration

Findings and discussion

(a) It was reported in Chapters 4 and 5 that regrind circuits achieved higher PGM recoveries than single-stage circuits, although the single stage circuits produced better concentrate grades. These observations will be analysed in more detail under further findings in this section. The results were reported in Chapters 4 and 5, while the data was analysed and discussed in Chapter 10.

(b) Stage-wise milling and flotation resulted in a recovery increase in the finest size fraction measured (-10μm). Both theory and operating experience suggest that stage-wise milling and flotation should improve recovery by minimising over-grinding. The results of this study support this conclusion, as it was found that more non- or slow floating particles were generated in the -10μm size fraction with single stage circuits.

(c) No minimum to the optimum flotation size range was detected: This indicates that floatability is determined firstly by liberation, and then by the size of the particle. While this may seem obvious, it is nonetheless interesting to see this principle extend

into a size range which for many years was considered highly problematic. For UG2 ore, a significant amount of PGE minerals are smaller than 10μm and locked in gangue. These locked particles will be non-floatable in the coarser size fractions (also in the optimum size range), and only becomes liberated and thus floatable in the finest measurable size fraction. It also showed that the majority of PGM particles in the -10μm size range were still floatable, probably aided to some degree by the high density of these minerals. It is important to note that even PGM minerals will stop floating below a certain size, but it was not possible to screen fine enough to determine that size. Finally, since PGM minerals liberate at such fine grinds, the risk of over-grinding is higher and multi-stage circuits should be more efficient at preventing over-milling and thereby increasing recovery.

(d) Stage-wise milling and flotation also benefits the recovery of coarse particles: Two reasons were proposed to explain this result. The first is connected to the different grinding mechanisms of the mills that were used. It was found that attrition grinding generated partially liberated particles in the coarser size fractions. The more grinding is done, the more likely it becomes that these particles will be milled to a finer size fraction. Therefore, the results of this study suggest that stage-wise removal should increase the recovery in the coarser size fractions where stirred mills are employed. The second mechanism that was proposed is that valuable minerals are milled preferentially over the host gangue matrix. The reason for this is that PGE-bearing minerals are often found on grain boundaries between gangue and BMS. These particles will be floatable, but also more likely to break than a competent, non-floatable gangue particle with a PGE mineral locked inside. Thus, the more grinding is done the more partially floatable PGM's will be milled to smaller size fractions relative to the non-floatable PGM's. Stage-wise flotation will recover more of these partially liberated PGM's before such preferential breakage occurs, and thus increase recovery in the coarse size fractions.

(e) By evaluating the recovery by size in the first flotation cell at different grinds (Table 10.3), signs of over-grinding were detected for the +10μm fraction but not for the -10μm fraction. This was shown by the decrease in the initial recovery for the +10μm fraction at finer grinds, while the initial recovery for the -10μm fraction stayed constant for all the grinds that were tested. This suggests that over-grinding of BMS particles (with associated PGM's) became more important than liberation at the finest

grind that was tested. It also shows that liberation of PGM particles in the -10μm fraction was still the dominant mechanism at the finest grind, rather than over-grinding.

(f) Figures 10.4 to 10.6 shows that for all the steel circuits, most of the fast floating PGM's were recovered at between 15 and 20 minutes of flotation residence time. It was also observed that slow floating PGM's and fast floating gangue displayed similar flotation kinetics. This suggests that a significant portion of slow floating PGM's are partially liberated particles associated with gangue, and therefore recovered at similar rates. By contrast, the slow floating gangue appears to be recovered independent from PGM's, and probably represents naturally floatable free gangue particles, comprised of or associated with altered silicates such as talc.

Implications for circuit design

(a) The introduction of multiple mill-float stages has the potential to increase recovery in both the fine and coarse size fractions. In the fine fractions, multiple mill-float circuits recover liberated particles at incremental intervals, and thereby reduce losses due to over-grinding. Recovery in the coarse size fractions can also be increased by multiple mill-float circuits, especially if preferential breakage of valuable minerals is significant. This mechanism is similar to the minimisation of over-grinding, as partially liberated valuables are removed in the coarse size fractions by intermediate flotation stages before they are broken to finer size fractions.

(b) It was found that the highest PGE recovery was achieved in the finest size fraction measured. This indicates that fine, liberated particles have a higher floatability than locked or partially liberated particles in the optimum size range. The implication for design is that liberation of particles should take preference over generating particles in the optimum size range for flotation.

(c) In general, ore types where the minerals liberate at the fine end of the optimum size range for flotation should benefit from multiple mill-float stages. Also, if the ore contains a range of minerals which liberates at different sizes, multi-stage circuits would be beneficial.

(d) Ideally, the target size distribution of a circuit should be determined by a liberation analysis at different grinds. However, this is both costly and sample intensive, and

therefore the optimum size distribution is usually established by evaluating the flotation kinetics by size at different grinds. As the grind becomes finer, the kinetics in a finer than the optimum size range should start decreasing, which would indicate the size distribution where over-grinding could become dominant. Depending on economics, this size distribution would either be the target final grind for the circuit, or the grind at which to introduce an intermediate flotation stage.

(e) The rougher residence time of a circuit can be determined by evaluating the flotation kinetics of the valuable and gangue minerals (or the grade response in the absence of gangue kinetics). This residence time is closely linked to the target final concentrate quality. The minimum rougher residence time should be selected to recover the maximum amount of fast floating valuables, as these particles are usually independent of gangue and could be recovered without a grade penalty in the cleaning circuit. After the maximum amount of fast floating particles have been recovered, the rougher residence time is driven by the amount of slow floating valuables to allow into the cleaning circuit, and this can be established from an evaluation of the kinetics of the slow floating valuables under cleaning conditions.

12.3.3 Design framework

The aim of circuit design is to maximise return on investment, and that should be the primary driver behind any design framework. The rules and theories on circuit design expressed in this chapter and elsewhere in this thesis should always be weighed against financial benefit. Design decisions should therefore not be based on the theoretically correct design, but on whether it would be the most advantageous financially. However, this design framework should establish the basis for efficient circuit design, against which the financial drivers of the circuit are measured.

From the conclusions that were drawn regarding breakage mechanism and the circuit configuration, it was possible to develop a rule based framework for the design of UG2 circuits (Chapter 11). This framework is general enough to apply to most ore types, although it would add more benefit to complex ores requiring difficult design decisions. The basic information needed for the framework is as follows:

- Ore hardness and breakage characteristics
- Flotation response in each size fraction
- The size and associations of the valuable minerals
- The flotation kinetics of the valuable and gangue minerals

From this information the basic flow sheet, types of milling devices, target grinds in different stages and flotation residence time can be determined. The design framework for the basic circuit layout is shown in Figure 12.1:

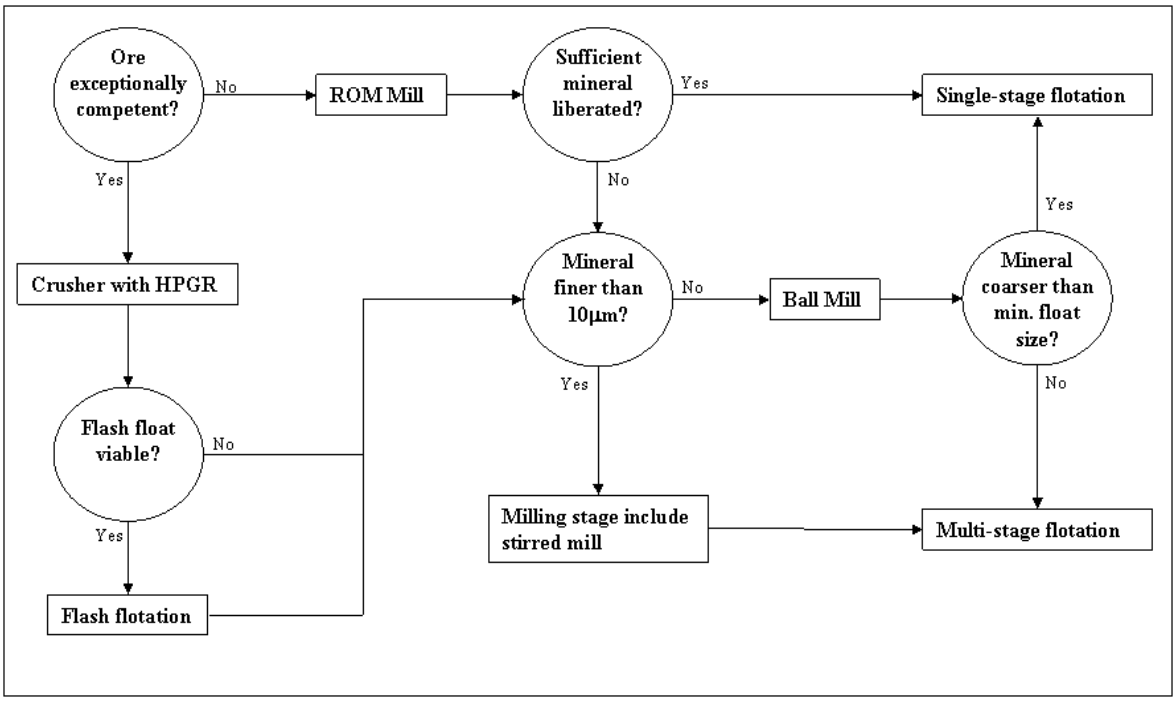

Figure 12.1 Design framework for basic circuit layout

The various design decisions will now be summarised briefly, while showing how the basic design information is used to guide decision making.

Primary comminution

Information required: ore hardness and breakage characteristics

The main purpose of the primary comminution stage is to reduce the top size of the ore for efficient materials handling through the rest of the circuit. If the ore is particularly hard, this stage will often include a crusher section followed by a ball mill, while softer and friable ore

would be treated in a ROM ball mill. Although this framework was developed for UG2 ore in particular and platinum ores in general, for many ore types the ROM ball mill could be replaced by an AG or SAG mill.

Number of milling stages

Information required: ore hardness and breakage characteristics
size and associations of valuable minerals

If insufficient minerals are liberated by the primary comminution stage, a second or even third milling stage is required. Note that this does not necessarily imply additional flotation stages – if the mineral is sufficiently coarse it is perfectly reasonable to design a primary mill followed by a ball mill and a single flotation stage.

Number of mill- float stages

Information required: size and associations of valuable minerals
flotation response in each size fraction

If the minerals in the ore liberate at different sizes, multiple mill-float stages would allow for the recovery of the coarser minerals before targeting the finer minerals. Also, if any of the minerals liberate close to their optimum size for flotation, multiple mill-float stages would minimise over-grinding of this mineral. Even in the absence of mineralogical data, the size-by-size flotation response at different grinds should indicate whether over-grinding is an issue, and if intermittent flotation stages would add benefit.

Type of milling device

Information required: ore hardness and breakage characteristics
size and associations of valuable minerals

Stirred mills were shown to be more efficient than ball mill at liberating ultra-fine minerals (sub 10μm). Therefore, if the ore contains a significant amount of valuable material in the -

10μm range, a stirred mill should be included in the circuit. Since the mineral is so fine, this would automatically invoke a multi-stage circuit from the previous design decision. However, at coarser sizes the traditional ball mill becomes more efficient than the stirred mill. Ore hardness and breakage characteristics could also influence whether to use a stirred or ball mill.

Target size distribution for each milling stage

Information required: flotation response per size in each size fraction

Conducting laboratory flotation tests at different grinds and evaluating the flotation kinetics in different size fractions should reveal when over-grinding of minerals becomes an issue. Of special importance is the flotation rate in the size fraction just finer than the minimum size for optimum flotation. If this rate starts decreasing it is an indication that over-grinding is becoming dominant, and a flotation stage should be introduced.

Flotation residence time

Information required: flotation kinetics of the valuable and gangue minerals

Once the target size distribution(s) has been established, a series of laboratory flotation tests should be conducted at those grinds to separate the valuable and gangue minerals into fast and slow floating fractions. Evaluating the response of each of these, in conjunction with the target quality of final concentrate, should reveal the optimum flotation residence time. It was established that the residence time should at least be long enough to recover all fast floating valuable material. The amount of slow floating material, and thus the final flotation residence time, is determined by the final concentrate grade target as well as the response of the slow floating valuables under cleaning conditions.

CHAPTER 13
FUTURE WORK

13.1 Model Development

Although it was not the objective of this thesis to develop a new flotation model, the nature of the data collected necessitated the development of novel methods with respect to the application of the model. These methods should be verified and expanded upon by future test programmes.

In particular, the methodology to reconcile unsized batch flotation data and sized circuit data in the model framework should be verified (Procedure 1 in this thesis). This could be done by collecting and fitting sized circuit and batch data, and comparing the results with an exercise where the sized batch data is replaced with unsized data and Procedure 1.

In Procedure 1, the amount of fast floating material in the unsized stream is approximated from an unsized rate constant that is calculated from sized kinetic data, and comparing this value to the unsized batch flotation rate constants. A linear relationship is assumed to determine the fast floating fraction, and although this assumption fitted the data very well, more work needs to be done to determine the actual relationship.

In a similar vein, entrainability by size was calculated from a one-parameter exponential decay function. The parameter used was ENT_{null}, the maximum size above which entrainment becomes insignificant. Once again, although this approach describes the data well, the correct form of this relationship should be established by future test work.

An equation was derived to calculate entrainment in a batch flotation cell. This formula could be verified by performing batch flotation tests with a non-floatable tracer mineral (such as MnO_2), and comparing the actual amount of entrained material with the amount predicted by the equation. This test could potentially also shed light upon the relationship between entrainability and size that was mentioned under the previous point.

13.2 Circuit Design Framework

The experiments in this thesis were designed around size distribution with regards to optimal circuit layout, without detailed analysis of the energy consideration in the various mills. Designing a set of experiments to investigate the energy considerations in the different mills would be an excellent topic for future work. This would incorporate energy efficiency into the design framework that was laid down in this thesis.

Establishing a design framework for cleaning circuits would be a valuable addition to the work done in this thesis. Cleaning circuits usually consist of multiple flotation stages, sometimes incorporating re-grind mills as well. Therefore, the same experimental design that was used for this thesis could also be applied to an investigation into cleaner circuit design. Section 10.6.2 touch upon the type of analysis that could be performed with regards to fast and slow floating valuables and gangue, and how that could drive a decision making tree for the design of a cleaner circuit.

13.3 General

The flotation performance of the +75μm and +10μm material was explained fully from the breakage characteristics in the various milling devices. Therefore it was concluded that the breakage mechanism was more important for flotation than chemical environment in coarse size fractions. This conclusion could be tested by designing an experiment where the breakage mechanism and chemical environment is controlled explicitly, and analysing the flotation performance in coarse the size fractions.

The improvement in recovery observed in the coarse size fractions with attrition breakage was attributed to the gradual liberation of valuable particles, as opposed to the shattering of a particle into smaller sizes via impact breakage. Therefore, with attrition breakage a mineral is often recovered as a partially liberated particle in a coarser size fraction. This could be tested by comparing the mineralogical profile of a stirred mill product with a ball mill product.

BIBLIOGRAPHY

Apling, A. and Bwalya, M.
Evaluating high pressure milling for liberation enhancement and energy saving
Minerals Engineering, Vol. 10, September, 1997, pp. 1013-1022

Arbiter, N. and Harris, C.C.
Flotation Kinetics
In: D.W. Fuerstenau (Ed.) Froth Flotation, 50th Anniversary Volume, AIME, 1962, New York, Chapter 8

Austin, L.G.
A treatment of impact breakage of particles
Powder Technology, Vol. 126, 2002, pp. 85-90

Becker, M., Harris, P., Wiese, J. and Bradshaw, D.
The use of quantitative mineralogical data to interpret the behaviour of gangue minerals in the flotation of Merensky Reef ores
Proceedings of Automated Mineralogy, 2006, Brisbane, Australia

Becker, M., Mainza, A.N., Powell, M.S., Bradshaw, D.J. and Knopjes, B.
Quantifying the influence of classification with the 3 product cyclone on liberation and recovery of PGMs in UG2 ore
Minerals Engineering, Vol. 21, 2008, pp. 549-558

Bryson, M.A.W.
New Technologies in the concentration of PGM values from UG-2 ores
Journal of the South African Institute of Mining and Metallurgy, 2004, pp. 311-314

Chen, F., Gomez, C.O. and Finch, J.A.
Technical note: bubble size measurements in flotation machines
Minerals Engineering, Vol. 14, April, 2001, pp. 427-432

Contini, N.J., Wilson, S.W. and Dobby, G.S.
Measurement of the rate data in flotation columns
Column flotation ’88 Proceedings, Phoenix, USA, 1988, pp.81-89

Corrans, I.J., Brugman, C.F., Overbeek, P.W. and McRae, L.B.
The recovery of platinum group metals from ore of the UG-2 reef in the Bushveld Complex
Proceedings of the 12th CMMI congress, Johannesburg, South Africa, 1982, pp. 629-634

Cullinan, V.J., Grano, S.R., Greet, C.J., Johnson, N.W. and Ralston, J.
Investigating fine galena recovery problems in the lead circuit of Mount ISA mines Lead/Zinc Concentrator, Part 1: Grinding media effects
Minerals Engineering, Vol. 12, Edition 2, 1999, pp. 147-163

Deglon, D.A., Egya-Mensah, D. and Franzidis, J.P.
Review of hydrodynamic and gas dispersion in flotation cells on South African platinum concentrators
Minerals Engineering, Vol. 13, March, 2000, pp. 235-244

Ekmekçi, Z., Bradshaw, D.J., Allison, S.A. and Harris, P.J.
Effects of frother type and froth height on the flotation behaviour of chromite in UG2 ore
Minerals Engineering, Vol. 16, 2003, pp. 941-949

Falutsu, M. and Dobby, G.S.
Direct measurement of froth drop back and collection zone recovery in a laboratory flotation column
Minerals Engineering, Vol. 2, 1989, pp. 377-386

Feng, D. and Aldrich, C.
Effect of particle size on flotation performance of complex sulphide ores
Minerals Engineering, Vol. 12, July, 1999, pp. 721-731

Finch, J.A. and Dobby, G.S.
Column Flotation, Pergamon Press, Oxford, 1990, Chapter 3

FLSmidth, 2010, *World's Largest Flotation Cells*, FLSmidth [online],
http://www.flsmidth.com/en-US/Services+and+Capabilities/Case+Stories/Flotation+Cells

Gaudin, A.M., Groh, J.O. and Henderson, H.B.
Effect of particle size on flotation
American Institute of Mining and Metallurgical Engineering, Technical Publication No. 414, 1931, pp. 3-23

Goodall, C.M.
Milling and flotation circuits for the processing of platinum group metals in Southern Africa
Presented at the SAIMM and Mintek conference, Randburg, South Africa, 1995

Gorain, B.K., Franzidis, J-P and Manlapig, E.V.
Studies on impeller type, impeller speed and air flow rate in an industrial scale flotation cell. Part 1: Effect on bubble size distribution
Minerals Engineering, Vol. 8, June, 1995, pp. 615-635

Gorain, B.K., Franzidis, J-P and Manlapig, E.V.
Studies on impeller type, impeller speed and air flow rate in an industrial scale flotation cell. Part 2: Effect on gas holdup
Minerals Engineering, Vol. 8, December, 1995, pp. 1557-1570

Gorain, B.K., Franzidis, J-P and Manlapig, E.V.
Studies on impeller type, impeller speed and air flow rate in an industrial scale flotation cell. Part 3: Effect on superficial gas velocity
Minerals Engineering, Vol. 9, June, 1996, pp. 639-654

Gorain, B.K., Franzidis, J-P and Manlapig, E.V.
Studies on impeller type, impeller speed and air flow rate in an industrial scale flotation cell. Part 4: Effect of bubble surface area flux on flotation performance
Minerals Engineering, Vol. 10, April, 1997, pp. 367-379

Gorain, B.K., Harris, M.C., Franzidis, J-P. and Manlapig, E.V.
The effect of froth residence time on the kinetics of flotation
Minerals Engineering, Vol. 11, July, 1998, pp. 627-638

Gorain, B.K., Napier-Munn, T.J., Franzidis, J-P and Manlapig, E.V.
Studies on impeller type, impeller speed and air flow rate in an industrial scale flotation cell. Part 5: Validation of k-S_b relationship and effect on froth depth
Minerals Engineering, Vol. 11, July, 1998, pp. 615-626

Grano, S.R., Wong, P., Skinner, W., Johnson, N.W. and Ralston, J.
The effect of autogenous and ball mill grinding on the chemical environment and flotation of the copper ore of Mount ISA Mines Ltd.
Proceedings of the III Latin-American Congress on Froth Flotation, Chile, 1994, pp. 351-388

Greet, C.J.
The significance of grinding environment on the flotation of UG2 ores
Third International Platinum Conference, SAIMM, 2008, pp. 29-35

Harris, M.C.
The use of flotation plant data to simulate flotation circuits
Proceedings of the SAIMM Mineral Processing Design School, Johannesburg, South Africa, 1998, pp. 1-27

Harris, M.C, Runge, K.C., Whiten, W.J and Morrison, R.D.
JKSimFloat as a practical tool for flotation process design and optimisation
Proceedings of the SME Mineral Processing Plant Design, Practice and Control Conference, Vancouver, Canada, 2002, pp. 461-478

Hochreiter, R.C., Kennedy, D.C., Muir, W. and Woods, A.I.
Platinum in South Africa
Journal of the SAIMM, Vol. 85, 1985, pp. 165-185

Hogg, R.
Breakage mechanism and mill performance in ultrafine grinding
Powder Technology, Vol. 105, 1999, pp. 135-140

Imaizumi, T. and Inoue, T.
Kinetic considerations of froth flotation
Proceedings of the Sixth International Mineral Processing Congress, Cannes, 1965, pp. 581-593

Iwasaki, I., Reid, K.J., Lex, H.A. and Smith, K.A.
Effect of autogenous and ball mill grinding on sulphide flotation
Mining Engineering, Vol. 35, 1983, pp. 1184-1190

Johnson, N.W.
The flotation behaviour of some chalcopyrite ores
PhD Thesis, University of Queensland, 1972

Johnson, N.W.
Practical aspects of the effect of electrochemical conditions in grinding mills on the flotation process
Proceedings of Flotation and Flocculation – from Fundamentals to Application, Hawaii, 2002

Kapur, P.C., Pande, D. and Fuerstenau, D.W.
Analysis of single-particle breakage by impact grinding
International Journal of Mineral Processing, Volume 49, 1997, pp. 223-236

King, R.P.
A pilot-plant investigation of a kinetic model for flotation
Journal of the SAIMM, July, 1978, pp. 325-338

Kelsall, D.F.
Application of probability assessment of flotation systems
Transactions, American Society of Mining and Metallurgical Engineers, Vol. 70, 1961, pp. 191–204

Klimpel, R.R.
Selection of chemical reagents for flotation
In Mineral Processing Plant Design 2nd Edition, Ed. Mular, A. and Bhappu, R., SME, Littleton, 1980, pp. 907-934

Knights, B.D.H. and Bryson, M.A.W.
Current challenges in PGM flotation of South African ores
In Advances in minerals processing, Eds. Gomez, C.O., Nesset, J.E. and Rao S.R., 2009, pp. 385-396

Lanham, A.
Cracking the chrome conundrum
Modern Mining, Vol. 4, December, 2008, pp. 20-25

Laplante, A.R., Toguri, J.M. and Smith, H.W.
The effect of air flow rate on the kinetics of flotation. Part 1: The transfer of material from slurry to the froth
International Journal of Mineral Processing, Vol. 11, 1983a, pp. 203-220

Laplante, A.R., Toguri, J.M. and Smith, H.W.
The effect of air flow rate on the kinetics of flotation. Part 2: The transfer of material from froth over the cell lip
International Journal of Mineral Processing, Vol. 11, 1983b, pp. 221-234

Liddell, K.S., McRae, L.B. and Dunne, R.C.
Process routes for beneficiation of noble metals from the Merensky and UG-2 ores
Extraction Metallurgy ’85, IMM, London, UK, 1985, pp. 789-816

Loveday, B.K. and Raghubir, S.
Design and optimisation of flotation circuits using simulation
Proceedings of the SAIMM Colloquium on interactions between Comminution and Downstream processing, Mintek, South Africa, 1995, pp. 1-10

Lynch, A.J., Johnson, N.W., Manlapig, E.V. and Thorne, C.G.
Mineral and Coal Flotation Circuits, Elsevier, Amsterdam, 1981

Mainza, A., Narasimha, M., Powell, M.S., Holtham, P.N. and Brennan, M.
Study of flow behaviour in a three-product cyclone using computational fluid dynamics
Minerals Engineering, Vol. 19, 2006, pp. 1048-1058

Mankosa, M.J. and Yoon, R.H.,
Design and scale-up criteria for column flotation
AusIMM – XVIII International Mineral Processing Congress, Sydney, Australia, 1993, pp. 785-792

Mathe, Z.T., Harris, M.C. and O'Connor, C.T.
A review of methods to model the froth phase in non-steady state flotation systems
Minerals Engineering, Vol. 13, 2000, pp. 127-140

Merkle, R.K.W. and McKenzie, A.D.
The mining and beneficiation of South African PGE ores – an overview
Canadian Institute of Mining, Metallurgy and Petroleum, Special Volume 54, Ed: Cabri, L.J., 2002, pp. 793-810

Mular, A.L. and Musara, W.T.
Batch column flotation: Rate data measurements
Proceeding of an International Conference on Column Flotation, Sudbury, Canada, Vol. 1, 1991, pp. 63-74

Nel, E., Valenta, M. and Naude, N.
Influence of open circuit regrind milling on UG2 ore composition and mineralogy at Impala's UG2 concentrator
Minerals Engineering, Vol. 18, 2005, pp. 785-790

Pease, J.D., Curry, D.C. and Young, M.F.
Designing flotation circuits for high fines recovery
Minerals Engineering, Vol. 19, 2006, pp. 831-840

Powell, M.S., Govender, I. and McBride, A.T.
Applying DEM outputs to the unified comminution model
Minerals Engineering, Vol. 21, 2008, pp. 744-750

Rahal, K.R., Manlapig, E.V. and Franzidis, J.P.
Flotation plant modelling and simulation using the Floatability Characterisation Test Rig (FCTR)
Proceedings of the International Congress on Mineral Processing and Extractive Metallurgy (MINPREX 2000), AusIMM, Melbourne, September, 2000, pp. 339-344.

Robertson, C.
Decoupling dispersion and depression effects in batch flotation of a PGM ore
MSc Thesis, University of Cape Town, 2002

Ross, V.E.
Mass transport in flotation froths
PhD Thesis, University of Stellenbosch, South Africa, 1988

Rule, C.M.
Energy considerations in the current PGM processing flowsheet utilizing new technologies
Third International Platinum Conference, SAIMM, 2008, pp. 45-52

Runge, K.C., Harris, M.C., Frew, J.A. and Manlapig, E.V.
Floatability of streams around the Cominco Red Dog Lead cleaning circuit
Proceedings of the Sixth Mill Operators Conference, Madang, Papua New Guinea, 1997, pp.157-163

Savassi, O.N.
Direct estimation of the degree of entrainment and the froth recovery of attached particles in industrial flotation cells
PhD Thesis, JKMRC, University of Queensland, Australia, 1998

Savassi, O.N., Alexander, D.J., Franzidis, J.P. and Manlapig, E.V.
An empirical model for entrainment in industrial flotation plants
Minerals Engineering, Vol. 11, March, 1998, pp. 243-256

Schubert, H. and Bischofberger, C.
On the hydrodynamics of flotation machines
International Journal of Mineral Processing, Vol. 5, 1978, pp. 131-142

Schwarz, S. and Alexander, D.
Gas dispersion measurements in industrial flotation cells
Minerals Engineering, Vol. 19, 2006, pp. 554-560

Trahar, W.J.
A rational interpretation of the role of particle size in flotation
International Journal of Mineral Processing, Vol. 8, 1981, pp. 289-327

Tavares, L.M. and King, R.P.
Single-particle fracture under impact loading
International Journal of Mineral Processing, Vol. 54, 1998, pp. 1-28

Tucker, J.P., Deglon, D.A., Franzides, J-P., Harris, M.C. and O'Connor, C.T.
Evaluation of a direct method of bubble size distribution measurement in a laboratory batch flotation cell
Minerals Engineering, Vol. 7, 1994, pp. 667-680

Valenta, M.M.
Balancing the reagent suite to optimise grade and recovery
Minerals Engineering, Vol. 20, 2007, pp. 979-985

Vera, M.A.
The determination of collection zone rate constant and froth zone recovery by column flotation
MSc Thesis, JKMRC, University of Queensland, Australia, 1995

Vogel, L. and Peukert, W.
Determination of material properties relevant to grinding by practicable labscale milling tests
International Journal of Mineral Processing, Vol. 74, 2004, pp. 329-338

Wesseldijk, Q.I., Reuter, M.A., Bradshaw, D.J. and Harris, P.J.
Flotation behaviour of chromite with respect to beneficiation of UG2 ore
Minerals Engineering, Vol. 12, 1999, pp. 1177-1184

Wiese, J.G., Harris, P.J. and Bradshaw, D.J.
The effect of increased frother dosage on froth stability at high depressant dosages
Minerals Engineering, Vol. 23, 2010, pp. 1010-1017

Wills, B.A. and Atkinson, K.
Some observations on the fracture and liberation of mineral assemblies
Minerals Engineering, Vol. 6, 1993, pp. 697-706

Yelloji Rao, M.K. and Natarajan, K.A.
Effect of electrochemical interactions among sulphide minerals and grinding media on chalcopyrite flotation
Minerals and Metallurgical Processing. 1989, pp. 146-151

Yianatos, J.B., Henríquez, F.H. and Oroz, A.G.
Characterization of large size flotation cells
Minerals Engineering, Vol. 19, 2006, pp. 531-538

APPENDIX A

DATA FIRST CAMPAIGN

A1 First campaign float feed size distributions (% passing)

	MF1	MF2		MF3		
Size (um)	**Primary Feed**	**Primary Feed**	**Secondary Feed**	**Primary Feed**	**Secondary Feed**	**Tertiary Feed**
300	100.0	100.0	100.0	100.0	100.0	100.0
212	97.9	94.9	98.0	94.5	96.0	97.9
150	95.2	88.3	95.5	87.7	91.8	95.5
106	90.1	78.1	90.9	77.7	84.9	90.6
75	81.5	66.4	83.6	66.2	74.3	82.8
53	61.9	44.5	64.6	44.5	53.7	61.2
25	31.3	24.1	33.4	23.6	27.8	38.2
10	17.3	10.9	18.6	10.7	14.0	21.2

A2 First campaign MF1 raw and balanced data

	PGM Grade (ppm)		% Solids		Cr_2O_3 (%)		Mass (kg/hr)
	Raw	**Balanced**	**Raw**	**Balanced**	**Raw**	**Balanced**	**Balanced**
Feed	3.75	3.75	32.17	32.17	28.81	29.80	700.00
Primary Conc 1	385.61	338.25	10.28	9.10	7.26	7.11	3.46
Primary Conc 2	134.49	154.59	8.89	8.98	8.71	7.50	4.27
Primary Conc 3	56.28	50.25	6.46	6.33	8.29	7.90	4.20
Primary Conc 4	30.79	32.75	6.65	6.10	10.70	8.90	2.15
Primary Conc 5	21.43	18.32	5.92	5.86	9.44	9.80	2.72
Primary Conc 6	10.43	11.59	5.98	5.81	12.59	10.90	2.50
Primary Conc 7	22.14	24.07	5.29	5.09	11.11	11.30	0.58
Primary Conc 8	8.37	9.40	5.07	4.78	15.34	13.70	1.55
Primary Conc 9	8.04	7.81	5.35	4.82	15.49	14.60	0.94
Primary Conc 10	8.47	9.73	5.00	4.63	16.25	15.40	0.74
Primary Conc 11	8.37	8.54	5.02	4.92	17.83	16.80	0.85
Primary Conc 12	8.41	7.44	4.37	4.80	16.88	17.30	0.98
Primary Tail 1	1.96	2.09	32.77	32.58	31.06	29.91	696.54
Primary Tail 2	1.18	1.15	33.58	33.12	28.14	30.05	692.28
Primary Tail 3	0.88	0.85	34.02	34.00	29.80	30.19	688.07
Primary Tail 4	0.77	0.75	34.39	34.49	32.43	30.25	685.92
Primary Tail 5	0.70	0.68	34.85	35.17	33.49	30.33	683.20
Primary Tail 6	0.65	0.64	35.54	35.84	32.36	30.41	680.70
Primary Tail 7	0.62	0.62	36.11	36.02	30.98	30.42	680.12
Primary Tail 8	0.61	0.60	36.70	36.57	30.11	30.46	678.58
Primary Tail 9	0.60	0.59	37.01	36.91	31.39	30.48	677.64

Primary Tail 10	0.59	0.58	37.35	37.19	29.53	30.50	676.90
Primary Tail 11	0.57	0.57	37.68	37.50	30.90	30.52	676.05
Primary Tail 12	0.56	0.56	38.11	37.87	30.54	30.53	675.07
Primary Conc 1-6	115.73	113.46	7.40	6.98	7.93	8.44	19.30
Primary Conc 7-12	9.71	10.22	4.68	4.82	13.92	14.92	5.64

A3 First campaign MF2 raw and balanced data

	PGM Grade (ppm)		**% Solids**		**Cr_2O_3 (%)**		**Mass (kg/hr)**
	Raw	**Balanced**	**Raw**	**Balanced**	**Raw**	**Balanced**	**Balanced**
Feed	3.85	3.85	34.50	34.50	29.86	29.70	700.00
Primary Conc 1	68.00	79.80	22.63	20.48	7.12	6.98	16.47
Primary Conc 2	26.29	24.80	15.03	16.89	6.78	7.82	14.97
Primary Conc 3	20.51	17.53	8.71	9.30	7.66	7.94	9.46
Primary Conc 4	12.94	14.87	7.72	7.50	6.98	8.52	2.42
Primary Conc 5	15.23	13.13	9.05	9.90	9.49	9.40	2.20
Primary Conc 6	11.42	10.20	6.87	7.70	9.06	9.84	2.17
Secondary Conc 1	132.08	124.60	3.41	3.10	10.29	9.99	1.42
Secondary Conc 2	37.74	33.40	3.56	3.80	10.41	11.15	2.99
Secondary Conc 3	18.89	18.70	4.18	4.00	13.34	13.63	3.59
Secondary Conc 4	11.89	14.50	3.15	3.70	12.69	14.34	2.32
Secondary Conc 5	12.99	11.10	4.58	4.50	14.53	15.83	3.04
Secondary Conc 6	7.52	8.00	3.80	3.90	16.15	16.97	1.71
Primary Tail 1	2.11	2.02	34.91	35.08	29.04	30.25	683.53
Primary Tail 2	1.58	1.51	35.21	35.95	32.13	30.75	668.56
Primary Tail 3	1.33	1.28	36.69	37.49	31.06	31.08	659.10
Primary Tail 4	1.25	1.23	37.35	38.05	29.29	31.16	656.68
Primary Tail 5	1.22	1.19	38.29	38.41	28.04	31.23	654.48
Primary Tail 6	1.10	1.16	38.92	38.93	29.14	31.30	652.31
Secondary Tail 1	0.91	0.89	39.57	39.94	30.00	31.35	650.89
Secondary Tail 2	0.72	0.74	40.99	41.77	31.35	31.44	647.90
Secondary Tail 3	0.64	0.64	41.25	44.09	30.15	31.54	644.31
Secondary Tail 4	0.61	0.59	43.94	45.90	32.39	31.61	642.00
Secondary Tail 5	0.55	0.54	46.90	48.00	31.37	31.68	638.96
Secondary Tail 6	0.53	0.52	48.07	49.50	31.85	31.72	637.25
Primary Conc	45.77	40.65	12.10	13.49	8.37	7.75	47.69
Secondary Conc	29.67	28.23	3.54	3.88	14.49	13.73	15.06

A4 First campaign MF3 raw and balanced data

	PGM Grade (ppm)		% Solids		Cr_2O_3 (%)		Mass (kg/hr)
	Raw	Balanced	Raw	Balanced	Raw	Balanced	Balanced
Feed	3.80	3.80	33.70	33.70	30.14	29.7	700.00
Primary Conc 1	88.89	90.70	23.59	25.10	6.92	6.86	14.36
Primary Conc 2	21.78	22.00	23.28	24.00	7.19	8.05	14.42
Primary Conc 3	15.07	16.93	14.52	13.20	8.29	8.18	12.42
Primary Conc 4	12.30	14.30	11.48	13.20	7.51	8.75	2.01
Primary Conc 5	9.58	8.40	8.55	9.40	9.78	9.30	2.73
Primary Conc 6	7.74	7.90	7.56	7.20	9.85	10.14	2.91
Secondary Conc 1	56.84	51.67	14.08	13.80	8.85	9.72	3.97
Secondary Conc 2	14.81	14.10	7.62	7.70	10.02	11.09	10.10
Secondary Conc 3	7.66	8.80	7.66	6.90	13.21	12.58	6.95
Tertiary Conc 1	32.72	30.30	4.42	4.60	12.31	12.48	2.11
Tertiary Conc 2	11.27	10.53	3.26	3.70	14.62	13.86	3.72
Tertiary Conc 3	9.04	8.53	4.37	3.90	15.80	15.40	2.29
Primary Tail 1	2.02	1.98	34.02	33.94	29.01	30.18	685.64
Primary Tail 2	1.63	1.55	34.33	34.25	31.17	30.65	671.22
Primary Tail 3	1.33	1.26	34.98	35.31	31.81	31.08	658.80
Primary Tail 4	1.25	1.22	35.26	35.49	30.30	31.15	656.79
Primary Tail 5	1.23	1.19	35.72	35.91	32.18	31.24	654.05
Primary Tail 6	1.17	1.16	36.01	36.56	30.94	31.33	651.14
Secondary Tail 1	0.86	0.85	37.52	36.93	32.68	31.46	647.17
Secondary Tail 2	0.71	0.64	38.99	39.30	31.20	31.79	637.07
Secondary Tail 3	0.59	0.55	39.51	41.45	32.48	32.00	630.12
Tertiary Tail 1	0.50	0.45	42.88	42.59	31.90	32.06	628.01
Tertiary Tail 2	0.45	0.39	44.90	45.44	31.76	32.17	624.30
Tertiary Tail 3	0.41	0.36	45.98	47.29	33.06	32.23	622.00
Primary Conc	43.66	38.98	17.65	16.50	7.60	7.96	48.86
Secondary Conc	18.55	19.45	7.42	8.06	12.05	11.32	21.02
Tertiary Conc	15.86	15.11	4.31	3.96	13.73	13.94	8.12

A5 First campaign fractional analysis raw and balanced data

		PGM Grade (ppm)		Mass Fraction (%)	
		Raw	**Balanced**	**Raw**	**Balanced**
MF1 Feed	**+106um**	1.05	1.07	10.08	9.88
	+75um	1.19	1.23	8.16	8.65
	+53um	1.75	1.73	19.73	19.53
	+10um	4.07	3.72	44.64	44.64
	-10um	8.93	8.91	17.39	17.30
MF1 Tail	**+106um**	0.53	0.52	10.30	9.99
	+75um	0.40	0.40	8.18	8.51
	+53um	0.50	0.49	19.31	19.69
	+10um	0.53	0.51	44.29	44.74
	-10um	1.00	0.99	17.92	17.07
MF2 Primary Feed	**+106um**	1.63	1.81	19.4	21.9
	+75um	1.69	1.91	10.4	11.7
	+53um	2.96	3.17	23.5	21.9
	+10um	5.29	4.84	32.0	33.6
	-10um	8.03	8.33	14.67	10.95
MF2 Primary Tail	**+106um**	1.43	1.56	22.9	22.9
	+75um	0.65	0.60	12.0	11.8
	+53um	1.00	1.02	22.8	22.8
	+10um	1.10	1.24	35.5	33.1
	-10um	1.00	0.93	6.72	9.45
MF2 Secondary Feed	**+106um**	0.59	0.60	9.2	9.1
	+75um	0.40	0.41	7.8	7.3
	+53um	0.60	0.64	19.7	19.1
	+10um	0.86	1.02	45.5	46.0
	-10um	2.47	2.62	17.81	18.59
MF2 Secondary Tail	**+106um**	0.72	0.47	8.9	9.1
	+75um	0.71	0.26	7.2	7.3
	+53um	0.78	0.23	18.5	19.1
	+10um	1.12	0.70	45.9	45.9
	-10um	0.78	0.50	19.48	18.60
MF3 Primary Feed	**+106um**	1.67	1.80	22.8	22.3
	+75um	1.74	1.91	10.7	11.5
	+53um	3.05	3.16	20.9	21.7
	+10um	5.41	4.74	31.0	33.8
	-10um	8.26	8.30	14.64	10.72
MF3 Primary Tail	**+106um**	1.23	1.56	22.0	23.8
	+75um	0.74	1.44	13.2	12.1
	+53um	1.07	0.97	25.7	22.6
	+10um	1.04	0.94	33.1	32.7

	-10um	1.10	1.00	5.99	8.70
MF3 Secondary Feed	**+106um**	0.57	0.64	14.4	15.1
	+75um	0.45	0.48	10.7	10.6
	+53um	0.47	0.55	21.1	20.6
	+10um	0.88	1.25	41.7	39.7
	-10um	2.60	2.87	12.13	14.02
MF3 Secondary Tail	**+106um**	0.70	0.54	16.4	15.6
	+75um	0.60	0.35	10.9	10.9
	+53um	0.40	0.39	20.2	21.2
	+10um	0.40	0.71	41.5	39.4
	-10um	0.60	0.52	11.09	12.98
MF3 Tertiary Feed	**+106um**	0.50	0.53	9.7	9.4
	+75um	0.40	0.42	7.0	7.9
	+53um	0.43	0.49	22.6	21.5
	+10um	0.48	0.63	40.0	40.0
	-10um	0.47	0.53	20.65	21.23
MF3 Tertiary Tail	**+106um**	0.42	0.40	8.7	9.5
	+75um	0.40	0.38	7.8	7.9
	+53um	0.40	0.36	20.9	21.7
	+10um	0.42	0.35	38.0	39.9
	-10um	0.40	0.36	24.62	20.94

A6 First campaign batch flotation raw and balanced data

		PGM Grade (ppm)		**Mass Fraction (%)**	
		Raw	**Balanced**	**Raw**	**Balanced**
MF1 Feed	**1 min**	151.26	149.74	0.59	0.66
	2.5 min	56.71	64.65	1.10	1.12
	7.5 min	39.49	37.52	3.22	2.96
	15 min	10.55	9.29	3.41	3.17
	20 min	6.84	6.15	1.75	1.87
	Tails	0.59	0.57	89.9	90.2
MF1 Tail	**1 min**	1.66	1.51	0.58	0.54
	2.5 min	1.38	1.49	0.92	0.98
	7.5 min	1.06	1.01	1.58	1.67
	15 min	0.81	0.87	1.93	1.87
	20 min	0.72	0.73	1.11	0.98
	Tails	0.52	0.53	93.9	94.0
MF2 Primary Feed	**1 min**	133.95	135.29	0.74	0.70
	2.5 min	104.17	110.42	1.09	1.10
	7.5 min	18.40	18.77	2.08	2.00
	15 min	8.96	9.23	2.36	2.12
	20 min	7.21	7.06	1.68	1.60

	Tails	1.14	1.09	92.0	92.5
MF2 Primary Tail	**1 min**	10.28	8.74	0.16	0.15
	2.5 min	4.54	3.90	0.62	0.70
	7.5 min	3.05	3.53	0.99	0.90
	15 min	2.93	2.55	1.01	1.10
	20 min	1.38	1.57	0.19	0.20
	Tails	1.10	1.09	97.0	97.0
MF2 Secondary Feed	**1 min**	40.92	40.10	0.69	0.64
	2.5 min	14.17	14.73	1.06	1.00
	7.5 min	6.11	5.99	2.08	2.41
	15 min	4.48	4.39	2.11	2.41
	20 min	2.67	2.70	1.24	1.20
	Tails	0.48	0.51	92.8	92.3
MF2 Secondary Tail	**1 min**	1.37	1.43	0.41	0.40
	2.5 min	1.37	1.30	1.19	1.30
	7.5 min	1.26	1.19	2.83	2.94
	15 min	1.15	1.01	2.67	2.46
	20 min	0.86	0.93	0.90	0.95
	Tails	0.45	0.47	92.0	92.0
MF3 Primary Feed	**1 min**	131.14	114.09	0.65	0.74
	2.5 min	75.26	78.27	1.33	1.41
	7.5 min	20.33	24.60	2.29	2.08
	15 min	16.68	15.68	2.07	1.80
	20 min	5.06	5.26	1.11	0.99
	Tails	1.13	1.08	92.5	93.0
MF3 Primary Tail	**1 min**	9.48	8.63	0.11	0.10
	2.5 min	5.55	5.33	0.51	0.48
	7.5 min	3.65	3.80	1.27	1.07
	15 min	3.49	3.59	1.04	1.15
	20 min	1.54	1.73	0.31	0.30
	Tails	1.01	1.07	96.8	96.9
MF3 Secondary Feed	**1 min**	12.21	13.92	0.88	0.85
	2.5 min	16.03	15.39	1.21	1.09
	7.5 min	6.00	5.70	2.82	2.51
	15 min	3.61	3.76	2.13	2.04
	20 min	1.91	1.80	0.80	0.90
	Tails	0.71	0.69	92.2	92.6
MF3 Secondary Tail	**1 min**	2.39	2.08	0.66	0.74
	2.5 min	1.81	1.72	0.94	1.05
	7.5 min	0.96	0.82	2.19	2.37
	15 min	0.62	0.64	3.43	3.74
	20 min	0.69	0.61	0.69	0.70

	Tails	0.47	0.51	92.1	91.4
MF3 Tertiary Feed	**1 min**	6.26	5.51	0.66	0.70
	2.5 min	3.99	4.07	1.58	1.39
	7.5 min	2.29	2.42	2.65	2.60
	15 min	1.02	1.29	2.50	2.78
	20 min	1.79	1.61	0.71	0.65
	Tails	0.37	0.38	91.9	91.9
MF3 Tertiary Tail	**1 min**	1.84	1.69	0.56	0.45
	2.5 min	1.09	1.18	0.83	0.73
	7.5 min	1.12	1.28	2.47	2.74
	15 min	1.27	1.18	2.95	3.22
	20 min	0.80	0.70	1.44	1.50
	Tails	0.28	0.28	91.7	91.4

APPENDIX B

DATA SECOND CAMPAIGN

B1 Second campaign float feed size distributions (% passing)

	MF1	MF2	
Size (um)	**Primary Feed**	**Primary Feed**	**Secondary Feed**
106	77.7	73.2	78.7
75	64.8	57.4	65.6
53	51.3	41.4	53.6
45	46.0	35.0	49.1
25	35.1	23.8	39.4
10	28.7	13.0	27.4

B2 Second campaign MF1 raw and balanced data

	PGM Grade (ppm)		% Solids		Cr_2O_3 (%)		Mass (kg/hr)
	Raw	**Balanced**	**Raw**	**Balanced**	**Raw**	**Balanced**	**Balanced**
Feed	3.80	3.81	26.80	26.41	29.4	29.58	600.19
Primary Conc 1	174.98	186.51	9.07	9.00	8.0	8.13	6.84
Primary Conc 2	33.60	36.13	6.66	6.55	11.1	11.61	10.35
Primary Conc 3	19.91	20.90	6.91	6.87	11.6	11.80	3.68
Primary Conc 4	11.60	12.25	6.42	6.10	13.6	14.16	5.33
Primary Conc 5	8.24	8.69	6.07	5.86	15.1	15.58	3.67
Primary Conc 6	6.45	6.77	7.33	7.29	17.5	17.64	0.78
Primary Tail 1	1.55	1.71	27.40	27.01	29.6	29.82	593.35
Primary Tail 2	1.01	1.10	28.17	28.59	29.8	30.15	583.00
Primary Tail 3	0.89	0.97	29.12	29.18	30.4	30.26	579.32
Primary Tail 4	0.85	0.86	30.30	30.24	30.6	30.41	574.00
Primary Tail 5	0.79	0.81	30.89	31.07	30.7	30.51	570.33
Primary Tail 6	0.77	0.81	31.05	31.21	30.8	30.53	569.54
Primary Conc 1-3	82.87	82.71	7.44	7.26	10.3	10.50	20.86
Primary Conc 4-6	8.68	10.48	6.39	6.09	15.4	14.97	9.78

B3 Second campaign MF2 raw and balanced data

	PGM Grade (ppm)		% Solids		Cr_2O_3 (%)		Mass (kg/hr)
	Raw	Balanced	Raw	Balanced	Raw	Balanced	Balanced
Feed	3.80	3.80	31.60	30.13	30.1	29.22	601.57
Primary Conc 1	97.56	106.16	14.17	14.16	6.79	6.29	10.18
Primary Conc 2	30.98	31.88	15.52	15.50	7.55	7.09	6.70
Primary Conc 3	20.10	20.26	9.53	9.52	9.75	9.41	2.94
Secondary Conc 1	80.38	82.62	7.58	7.49	9.02	9.13	4.10
Secondary Conc 2	46.13	47.34	8.01	7.96	10.55	10.62	2.34
Secondary Conc 3	20.72	21.15	6.62	6.57	15.5	15.68	2.29
Primary Tail 1	2.11	2.04	30.68	30.73	29.9	29.62	591.39
Primary Tail 2	1.68	1.70	31.00	31.08	29.7	29.88	584.69
Primary Tail 3	1.64	1.60	31.74	31.44	30.1	29.98	581.75
Secondary Tail 1	1.07	1.03	31.80	32.17	29.9	30.13	577.65
Secondary Tail 2	0.90	0.84	31.92	32.57	29.4	30.21	575.31
Secondary Tail 3	0.83	0.76	32.00	33.09	30.3	30.27	573.02
Primary Conc	64.45	68.30	12.68	13.57	7.6	7.02	19.82
Secondary Conc	56.47	57.04	7.47	7.34	12.6	11.25	8.73

B4 Second campaign fractional analysis raw and balanced data

		PGM Grade (ppm)		Mass Fraction (%)	
		Raw	Balanced	Raw	Balanced
MF1 Feed	**+106um**	1.01	0.79	19.76	22.31
	+75um	1.11	1.09	13.11	12.91
	+53um	1.42	1.39	12.09	13.44
	+45um	1.93	1.82	5.76	5.30
	+25um	2.16	2.14	11.89	10.94
	+10um	4.21	3.82	9.10	6.43
	-10um	9.45	9.52	28.28	28.66
MF1 Tail	**+106um**	0.64	0.50	19.32	23.46
	+75um	0.55	0.46	12.51	13.55
	+53um	0.46	0.31	13.84	14.08
	+45um	0.61	0.52	5.48	5.49
	+25um	0.53	0.42	12.21	11.19
	+10um	0.50	0.47	7.65	6.12
	-10um	1.30	1.83	28.99	26.11
MF2 Primary Feed	**+106um**	1.93	1.89	24.80	26.79
	+75um	1.80	1.78	16.47	15.84
	+53um	2.66	2.62	17.33	15.96

	+45um	3.60	3.57	6.12	6.43
	+25um	4.88	5.17	12.37	11.19
	+10um	7.16	6.93	10.80	10.76
	-10um	8.82	7.98	12.11	13.03
MF2 Primary Tail	**+106um**	1.54	1.78	29.86	27.58
	+75um	1.22	0.99	16.23	16.25
	+53um	1.38	1.61	15.06	16.23
	+45um	1.22	1.36	6.52	6.34
	+25um	1.61	1.78	10.00	10.85
	+10um	1.56	1.63	10.82	10.38
	-10um	2.39	1.95	11.50	12.37
MF2 Secondary Feed	**+106um**	0.85	0.81	23.86	21.31
	+75um	0.69	0.78	12.31	13.12
	+53um	0.77	0.77	13.24	11.95
	+45um	0.80	0.80	4.21	4.52
	+25um	0.92	0.93	10.29	9.69
	+10um	1.14	1.17	13.47	12.06
	-10um	3.68	3.54	22.63	27.36
MF2 Secondary Tail	**+106um**	0.71	0.58	20.40	21.62
	+75um	0.73	0.72	13.59	13.30
	+53um	0.45	0.39	12.09	12.11
	+45um	0.64	0.69	4.97	4.58
	+25um	0.69	0.75	9.90	9.81
	+10um	0.60	0.93	11.34	12.06
	-10um	1.21	1.03	27.72	26.53

B5 Second campaign batch flotation raw and balanced data

		PGM Grade (ppm)		**Mass Fraction (%)**	
		Raw	**Balanced**	**Raw**	**Balanced**
MF1 Feed	**1 min**	181.80	183.62	0.43	0.49
	2.5 min	78.95	78.16	1.16	1.09
	7.5 min	39.15	40.72	2.23	2.35
	15 min	5.01	5.01	3.38	3.25
	20 min	0.27	0.34	2.83	2.63
	Tails	1.07	1.02	89.97	90.20
MF1 Tail	**1 min**	2.12	2.01	0.3	0.4
	2.5 min	3.37	3.64	0.33	0.32
	7.5 min	1.78	1.94	2.01	1.87
	15 min	1.28	1.42	3.47	3.47
	20 min	1.52	1.72	1.72	1.72
	Tails	0.73	0.73	92.12	92.23
MF2 Primary Feed	**1 min**	131.40	147.17	0.44	0.45

	2.5 min	48.40	51.79	1.2	1.3
	7.5 min	35.63	35.99	2.67	2.46
	15 min	9.91	10.11	2.41	2.05
	20 min	0.66	0.61	2.85	2.77
	Tails	1.61	1.49	90.41	90.97
MF2 Primary Tail	**1 min**	8.90	9.52	0.19	0.19
	2.5 min	13.80	12.56	0.22	0.22
	7.5 min	8.19	7.94	1.1	1.1
	15 min	7.70	8.24	1.27	1.42
	20 min	6.68	7.42	1.07	0.95
	Tails	1.45	1.33	96.20	96.14
MF2 Secondary Feed	**1 min**	56.52	54.83	0.43	0.34
	2.5 min	18.80	20.31	1.08	0.99
	7.5 min	14.53	13.80	2.43	2.21
	15 min	10.38	10.59	0.9	0.9
	20 min	0.47	0.52	2.10	2.26
	Tails	0.90	0.86	93.08	93.28
MF2 Secondary Tail	**1 min**	7.40	8.14	0.41	0.41
	2.5 min	5.79	5.79	0.78	0.73
	7.5 min	3.73	3.95	2.20	2.25
	15 min	2.06	2.06	2.74	2.66
	20 min	0.56	0.64	2.2	2.2
	Tails	0.52	0.57	91.65	91.73

APPENDIX C
SIZE REDUCTION NORMALISATION

In chapter 9, the size reduction of each primary milling stage was normalised to compensate for feed size variation. This was done by calculating the cumulative amount of new mass (or PGM's) in each size fraction, and normalising this to 100 units in the coarsest measured fraction (106µm). This shows the mass change in each size fraction relative to milling 100 units from the coarsest fraction. This procedure will now be explained in a step-wise fashion for the first campaign MF1 circuit:

First consider the size and PGM distributions for the primary mill feed and final milling product:

C1 Size and PGM distributions for the first campaign MF1 milling circuit feed

Screen Sizes	Mass (%)	PGM (g/t)	PGM Flow (g/100t)
+106 µm	83.0	2.44	202.5
+75 µm	6.1	3.43	21.0
+53 µm	2.6	6.10	16.0
+10 µm	5.7	13.19	74.9
-10 µm	2.5	23.76	60.6
Combined	100.0	3.75	375.0

C2 Size and PGM distributions for the first campaign MF1 milling circuit product

Screen Sizes	Mass (%)	PGM (g/t)	PGM Flow (g/100t)
+106 µm	9.9	1.07	10.6
+75 µm	8.6	1.23	10.6
+53 µm	19.5	1.73	33.8
+10 µm	44.6	3.72	165.9
-10 µm	17.3	8.91	154.1
Combined	100.0	3.75	375.0

Since the mass in the feed to the milling circuit is the same as the product (no mass is added or removed), the size distribution in the feed can be subtracted from the size distribution in the product. This shows the change in mass for each size fraction in the milling circuit. The same was done for the PGM's (Table C3):

C3 Mass and PGM change in each size fraction for the first campaign MF1 circuit

Screen Sizes	Mass Change (based on 100 tons)	PGM Mass Change (g/100t)

+106 µm	-73.2	-191.9
+75 µm	2.5	-10.4
+53 µm	16.9	17.8
+10 µm	39.0	91.0
-10 µm	14.8	93.5

However, in order to compare results between different circuits, these numbers had to be normalised to a common standard. It was decided to normalise to -100 units in the coarsest size fraction. In this example, for overall mass this was done by simply multiplying the mass change in each size fraction by -100 and dividing by -73.2. The PGM's in each size fraction were multiplied by -100 and divided by -191.9. Therefore, the results reflect the accumulation of mass or PGM's in each size fraction by milling 100 units from the coarsest size. These results are shown in Table C4:

C4 Normalised mass and PGM change in each size fraction for the first campaign MF1 circuit

Screen Sizes	**Mass Change (based on 100 units from 106µm)**	**PGM Mass Change (based on 100 units from 106µm)**
+106 µm	-100.0	-100.0
+75 µm	3.5	-5.4
+53 µm	23.1	9.3
+10 µm	53.3	47.4
-10 µm	20.2	48.7